R-08-95

Bedrock hydrogeology Forsmark

Site descriptive modelling, SDM-Site Forsmark

Sven Follin
SF GeoLogic AB

December 2008

Svensk Kärnbränslehantering AB
Swedish Nuclear Fuel
and Waste Management Co

Box 250, SE-101 24 Stockholm
Phone +46 8 459 84 00

ISSN 1402-3091
SKB Rapport R-08-95
ID 1200489
Updated 2013-08

Bedrock hydrogeology Forsmark

Site descriptive modelling, SDM-Site Forsmark

Sven Follin
SF GeoLogic AB

December 2008

Keywords: Forsmark, Deformation zones, Fracture domains, Quaternary deposits, Hydraulic properties, Hydrogeology, Modelling, Verification, Confirmatory testing, Sensitivity, Uncertainty.

Update notice

The original report, dated December 2008, was found to contain both factual and editorial errors which have been corrected in this updated version. The corrected factual errors are presented below.

Updated 2009-05

Location	Original text	Corrected text
Page 161, Table C-1, column 4, rows 1, 2, 5	Wrong data in table	Table updated with correct data
Page 161, Table C-1, column 5	Wrong data in table	Table updated with correct data
Page 161, Table C-1, column 6, line 6	(–7.0, 1.2)	(–6.7, 1.2)
Page 162, Table C-2, column 5	Wrong data in table	Table updated with correct data
Page 162, Table C-3, column 5	Wrong data in table	Table updated with correct data

Updated 2013-08

Location	Original text	Corrected text
Page 161, Table C-1, column 3	Wrong data in table	Table updated with correct data
Page 161, Table C-1, column 6, last row	(–8.3, 1.0)	(–8.8, 1.0)
Page 161, footnote 3		Footnote deleted
Page 162, Table C-2, column 3	Wrong data in table	Table updated with correct data
Page 162, Table C-3, column 3	Wrong data in table	Table updated with correct data

The updated tables show what was actually used in the groundwater flow modelling for SDM-Site Forsmark.

Preface

The site descriptive modelling work at Forsmark was conducted by the Forsmark multi-disciplinary project group (PFM) in close collaboration with various discipline-specific working groups. All members of the hydrogeological modelling expert group (HydroNet) are gratefully acknowledged for excellent teamwork and contributions to the development of the bedrock hydrogeological model of Forsmark.

The present report is intended to summarise the hydrogeological conditions and the hydraulic properties of the bedrock at Forsmark and to give the information essential for demonstrating understanding. It relies heavily on numerous background reports concerning details in data analyses and modelling. The selected material from these reports is the responsibility of the author.

Abstract

The Swedish Nuclear Fuel and Waste Management Company (SKB) has conducted site investigations at two different locations, the Forsmark and Laxemar-Simpevarp areas, with the objective of siting a final repository for spent nuclear fuel according to the KBS-3 concept. Site characterisation should provide all data required for an integrated evaluation of the suitability of the investigated site and an important component in the characterisation work is the development of a hydrogeological model. The hydrogeological model is used by repository engineering to design the underground facility and to develop a repository layout adapted to the site. It also provides input to the safety assessment. Another important use of the hydrogeological model is in the environmental impact assessment.

This report presents the understanding of the hydrogeological conditions of the bedrock at Forsmark reached following the completion of the surface-based investigations and provides a summary of the bedrock hydrogeological model and the underlying data supporting its development. It constitutes the main reference on bedrock hydrogeology for the site descriptive model concluding the surface-based investigations at Forsmark, SDM-site, and is intended to describe the hydraulic properties and hydrogeological conditions of the bedrock at the site and to give the information essential for demonstrating understanding.

Contents

1 Introduction

1.1 Context

Radioactive waste from nuclear power plants is managed by the Swedish Nuclear Fuel and Waste Management Co., SKB. The Swedish programme for geological disposal of spent nuclear fuel is approaching major milestones in the form of permit applications for an encapsulation plant and a final repository. For siting of the repository, SKB has undertaken site characterisation at two different locations, Forsmark and Laxemar-Simpevarp (Figure 1-1). The site investigations have been conducted in campaigns, punctuated by data freezes. After each data freeze, the site data have been analysed and modelling has been carried out with the overall purpose to develop a site descriptive model (SDM). An SDM is an integrated model for geology, thermal properties, rock mechanics, hydrogeology, hydrogeochemistry, bedrock transport properties and a description of the surface system. The final site descriptive model, SDM-Site, presents the integrated understanding of the Forsmark site at the completion of the surface-based investigations and provides a summary of the models and the underlying data supporting the site understanding.

1.2 Scope and role of the hydrological model

Site characterisation should provide all data required for an integrated evaluation of the suitability of the investigated site for a deep geological repository and an important component of the site description is the development of a hydrogeological model.

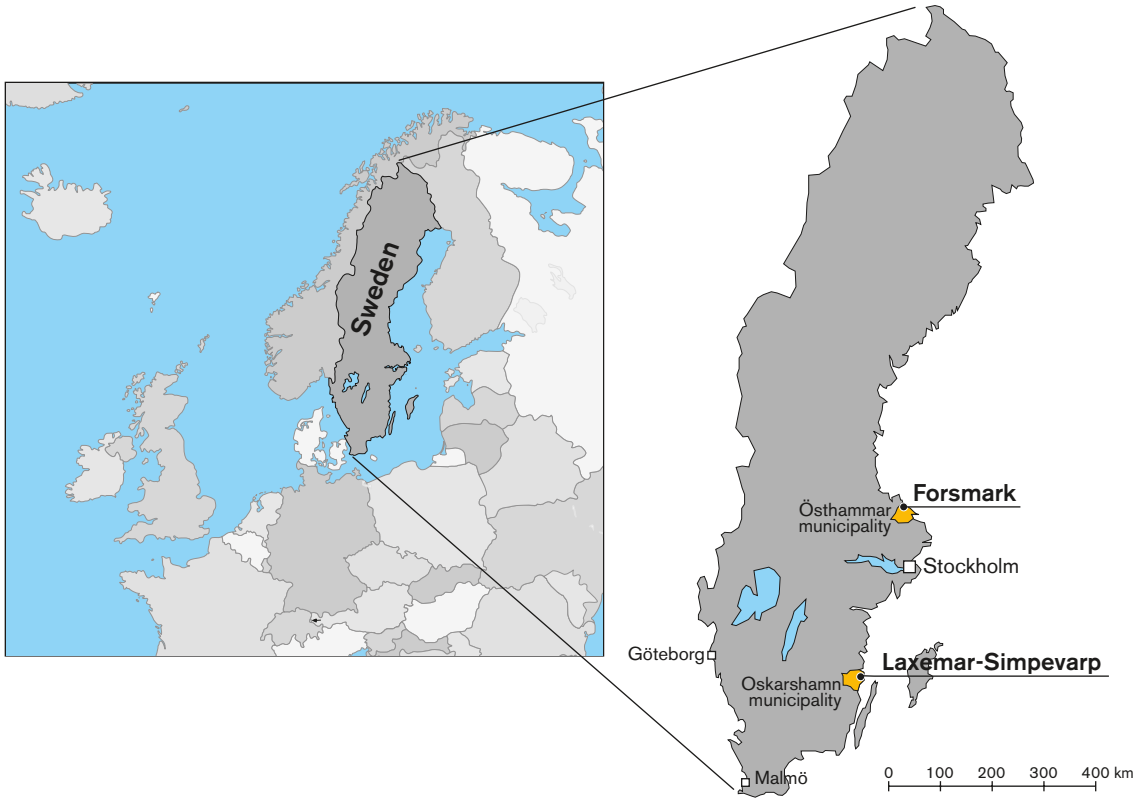

Figure 1-1. *Map of Sweden showing the location of the Forsmark and Laxemar-Simpevarp sites.*

Quality-assured hydrogeological data from site investigations, stored in the SKB database Sicada and the SKB geographic information system (GIS) are the input to hydrogeological modelling. The hydrogeological model is used by repository engineering to design the underground facility and to develop a repository layout adapted to the site. It also provides input to the safety assessment. Another important use of the hydrogeological model is in the environmental impact assessment.

The role of the hydrogeological model is to provide descriptions of the current state of the hydrologic cycle as well as descriptions of on-going natural processes that can affect its long-term evolution. However, it is not the task of the present-day hydrogeological modelling to make any predictions of the future evolution of site hydrogeological conditions. This is completed within safety assessment based on the understanding of the current conditions and of the past evolution as compiled in the site hydrogeological description. It is also not the task of the present-day hydrogeological modelling to evaluate the inflow rates or the impact on current site conditions of the excavation or the operation of a repository at the site. Such issues are analysed within the framework of safety assessment (SR-Site), repository engineering and environmental impact assessment, but again based on input from the site hydrogeological description.

1.3 Objectives and strategy

Primary objectives of the bedrock hydrogeological model are to provide a general conceptual understanding of the site and to determine and justify the assignment of hydraulic properties, boundary and initial conditions. The evaluations are based on primary data and a conceptual model is derived with the purpose to serve the needs of repository engineering, safety assessment and environmental impact assessment studies. Three-dimensional, large-scale numerical flow models are used to test and underpin the development of the bedrock hydrogeological model.

The work conducted to meet the primary objectives encompasses the following steps:

- analyse the primary data produced within the surface-based site investigation including data available for the first time at data freezes 2.2 and 2.3,
- describe evolutionary aspects of the groundwater system at the site during Holocene time (the last 10,000 years) to the current day,
- develop an integrated conceptual hydrogeological model covering key components of the geology, hydrogeochemistry and surface system at the site,
- build a three-dimensional numerical groundwater flow and solute transport model and test its representation of the site against different types of hydrogeological data as a means of approaching the need of confirmatory testing (cf. Step 4 in Figure 1-2), and
- perform a confidence assessment including systematic treatment of uncertainties and evaluation of alternative interpretations.

The strategy applied for achieving the stated objectives was to base the site descriptive model on the quality assured, geoscientific field data from Forsmark that were available in the SKB databases Sicada and GIS at the date defined for data freeze 2.2 (September 30, 2006). This data freeze contained all data planned to be collected from the target volume, i.e. the rock volume that has been selected as potentially suitable for hosting a final repository (see further section 1.4), except for data from borehole KFM08D (see further section 5.2), which was planned and drilled at a late stage in the site investigation. All new data that were available at the date defined for data freeze 2.3 (March 31, 2007), were used for complementary analyses and verification of the models. Since the site investigation has continued after data freeze 2.3, although to a very much smaller extent, additional data have also emerged after this data freeze. As far as possible, these “late” data have been assessed and commented upon in relation to the models established earlier.

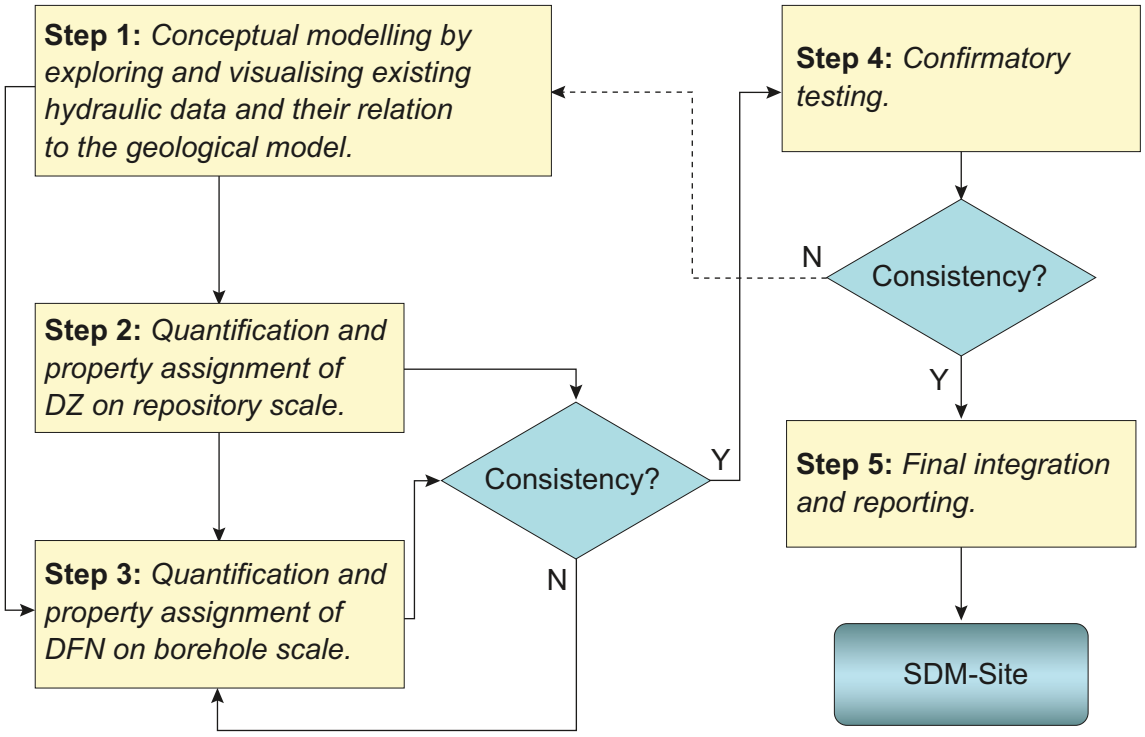

Figure 1-2. *Flow chart of the five steps suggested for the hydrogeological modelling during the complete site investigation (CSI) stage: DZ = deformation zone, DFN = discrete fracture network. (Modified after Figure 1-1 in /Follin et al. 2007a/.)*

The strategy outlined above implies that all discipline-specific modelling was completed on the basis of data available at data freeze 2.2. In order to achieve the specific objective of delivering documented models of hydrogeological properties to repository engineering, it was decided to compile the results of the modelling based on data freeze 2.2 into modelling stage 2.2 reports, prior to conducting and reporting the complementary analyses and verification activities using new data in data freeze 2.3. The reports on bedrock hydrogeology supporting the Forsmark SDM-Site are further described in section 1.6.

1.4 Handling of the hydrologic cycle

Figure 1-3 shows a cartoon of how the numerical modelling of the hydrologic cycle has been handled in the SDM. Two codes have been used in parallel, ConnectFlow /Hartley and Holton 2004, Hartley et al. 2004a, Hartley et al. 2004b, Hoch and Jackson 2004/ and MIKE SHE /DHI Software 2008/.

Flow modelling with ConnectFlow has been performed to support the description of the bedrock hydrogeological system at Forsmark /Follin et al. 2007bc, 2008a/. This modelling has been made with an emphasis on (*i*) applying the assignment of hydraulic properties to the identified deformation zones and fracture domains /Follin et al. 2007b/, and (*ii*) simulate variable-density flow and solute transport in an equivalent porous medium (ECPM) model of the fracture system and in the bedrock matrix over long time periods (thousands of years) /Follin et al. 2007c, 2008a/. The relation between *potentially flowing fractures vis-à-vis flowing fractures* and the upscaling of discrete fracture network (DFN) models to an ECPM are two examples of key assignments of the bedrock hydrogeological modelling.

Flow modelling with MIKE SHE has been performed to support the description of the interaction between the surface hydrology and the near-surface hydrogeology at Forsmark /Johansson 2008, Bosson et al. 2008/. This modelling has been made with an emphasis on understanding

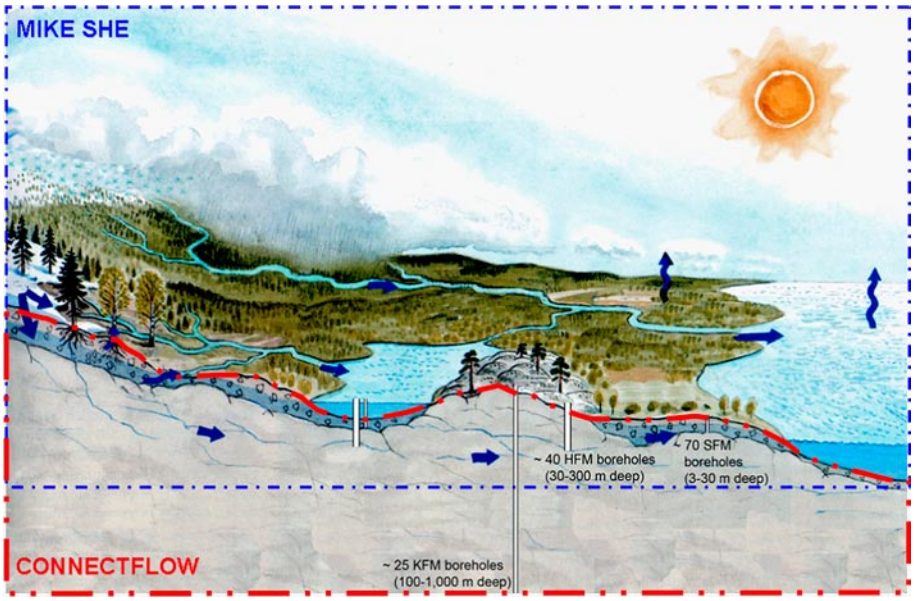

Figure 1-3. *Cartoon showing how the modelling of the hydrologic cycle is divided into a surface-based system and a bedrock-based system. The former is modelled with the MIKE SHE code and the latter with the ConnectFlow code. (Figure 2-2 in /Follin et al. 2007c/.)*

the recharge-discharge process and includes a calibration against surface water flow data and groundwater levels in the regolith and the superficial parts of the bedrock on a diurnal basis. In contrast to the bedrock hydrogeological modelling, the modelling with MIKE SHE has been performed for the present-day conditions only. Moreover, variable-density flow was not modelled with MIKE SHE.

The integration of the results from the different studies carried out has been essential for the development of the overall hydrogeological understanding of the site. However, it is emphasised that the present report focuses mainly on issues of particular importance for understanding the bedrock hydrogeology at the site and the derivation of hydraulic properties needed for groundwater flow and solute transport modelling with ConnectFlow.

1.5 Setting

The Forsmark area is located in northern Uppland within the municipality of Östhammar, about 120 km north of Stockholm (Figure 1-1 and Figure 1-4). The candidate area for site investigation is located along the shoreline of Öregrundsgrepen. It extends from the Forsmark nuclear power plant and the access road to the SFR-facility, a repository for low- and intermediate level radioactive waste, in the north-west to Kallrigafjärden in the south-east (Figure 1-4). It is approximately 6 km long and 2 km wide. The north-western part of the candidate area was selected as the target area for the complete site investigation work /SKB 2005c/ (Figure 1-5).

The Forsmark area consists of crystalline bedrock that belongs to the Fennoscandian Shield, one of the ancient continental nuclei on the Earth. The bedrock at Forsmark in the south-western part of this shield formed between 1.89 and 1.85 billion years ago during the Svecokarelian orogeny /SKB 2005a/. It has been affected by both ductile and brittle deformation. The ductile deformation has resulted in large-scale, ductile high-strain belts and more discrete high-strain zones. Tectonic lenses, in which the bedrock is less affected by ductile deformation, are enclosed between the ductile high strain belts. The candidate area is located in the north-westernmost part of one of these tectonic lenses. This lens extends from north-west of the nuclear power plant south-eastwards to the area around Öregrund (Figure 1-6). The brittle deformation has given rise to reactivation of the ductile zones in the colder, brittle regime and the formation of new fracture zones with variable size.

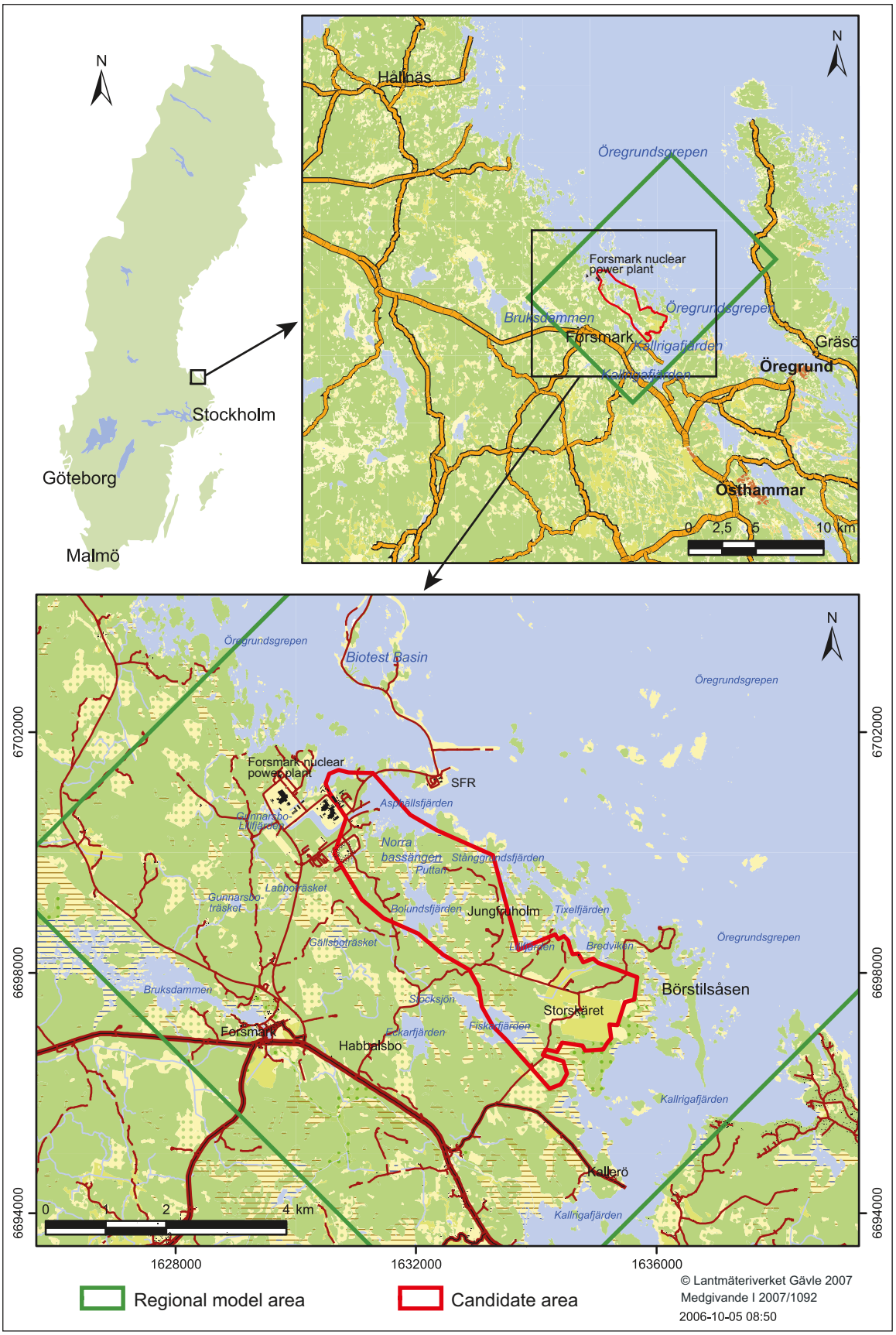

Figure 1-4. *Location of the Forsmark candidate area (red) for site investigation. Figure 1-8 and Figure 3-4 provide a fuller display of the regional model area).*

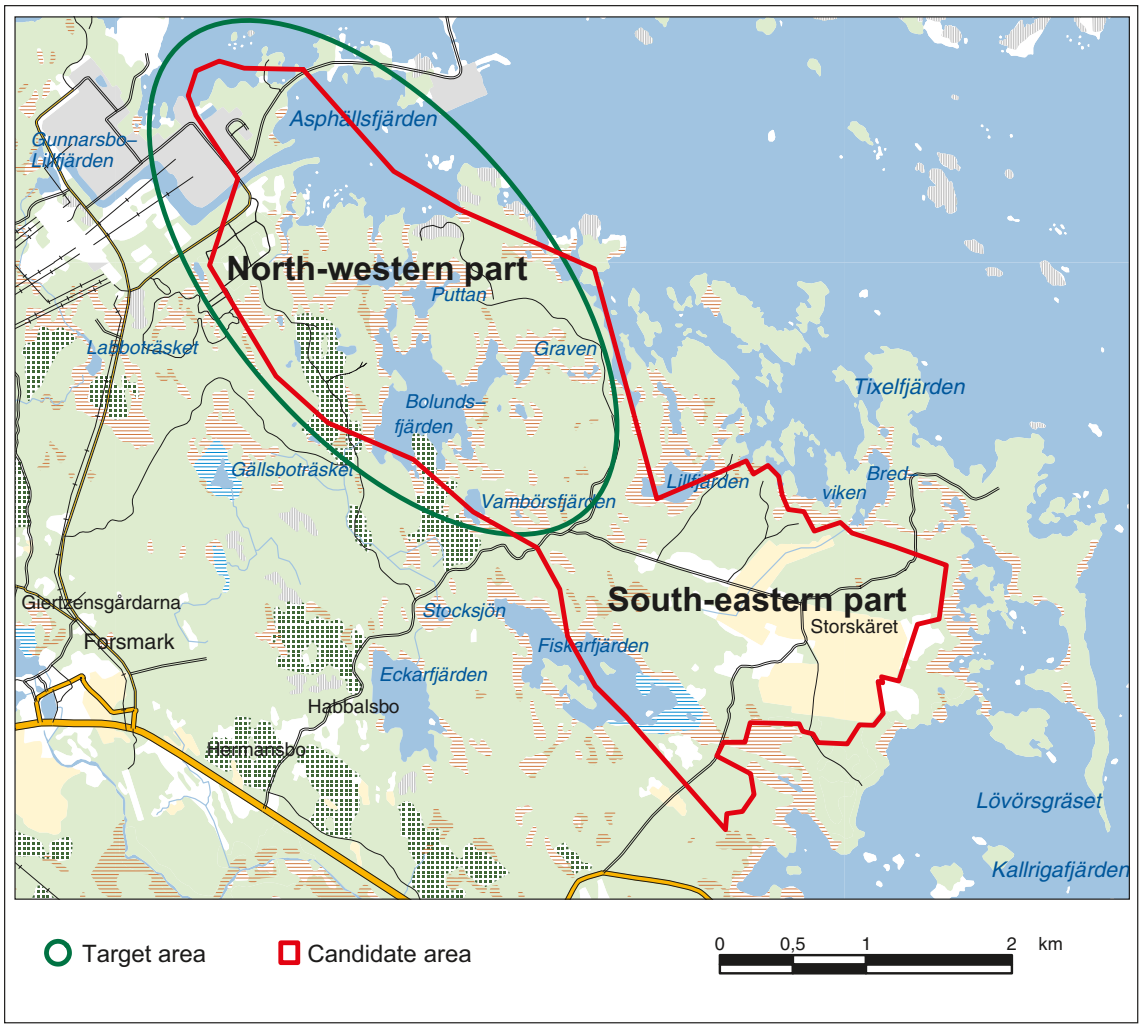

Figure 1-5. *The north-western part of the candidate area was selected as the target area for the complete site investigation work. (Modified after Figure 2-15 in /SKB 2005c/.)*

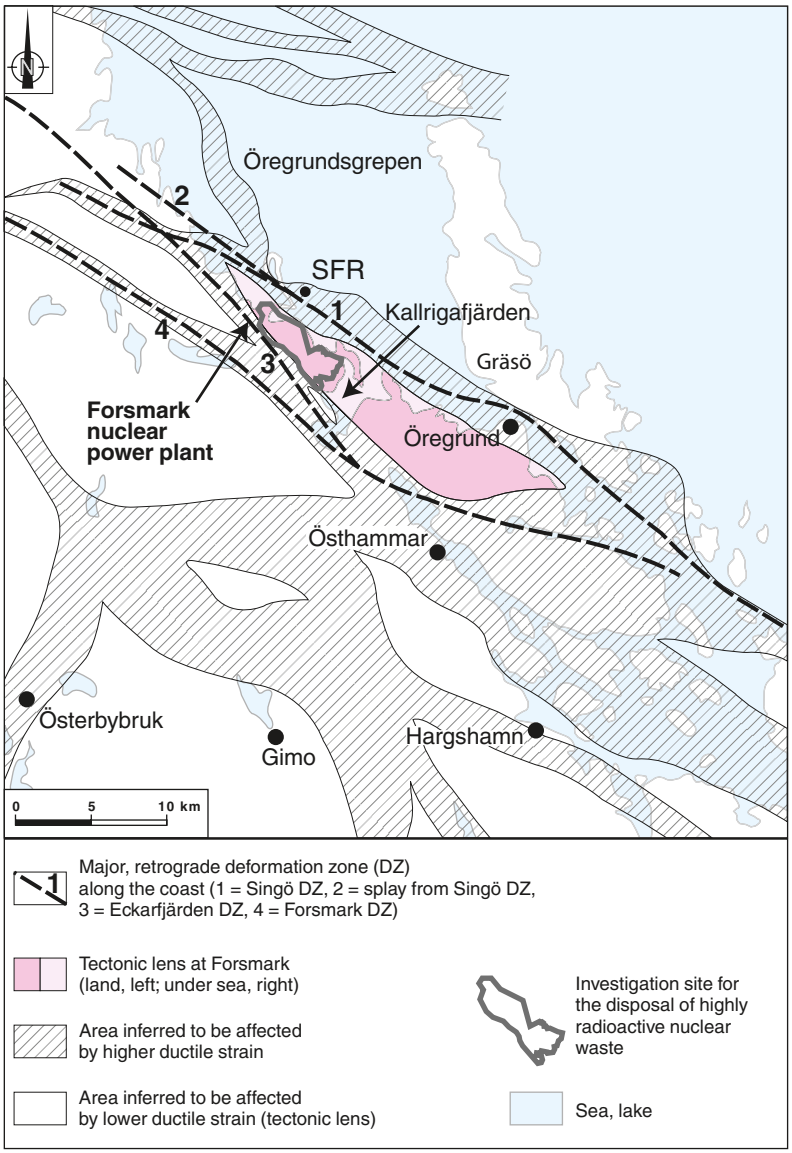

Figure 1-6. *Tectonic lens at Forsmark and areas affected by strong ductile deformation in the area close to Forsmark. (Figure 4-1 in /Stephens et al. 2007/.)*

The current ground surface in the Forsmark region forms a part of the sub-Cambrian peneplain in south-eastern Sweden. This peneplain represents a relatively flat topographic surface with a gentle dip towards the east that formed more than 540 million years ago. The candidate area at Forsmark is characterised by a small-scale topography at low altitude (Figure 1-7). The most elevated areas to the south-west of the candidate area are located at c 25 m above current sea level (datum RHB 70). The whole area is located below the highest coastline associated with the last glaciation, and large parts of the candidate area emerged from the Baltic Sea only during the last 2,000 years. Both the flat topography and the still ongoing shore level displacement of c 6 mm per year strongly influence the current landscape (Figure 1-7). Sea bottoms are continuously transformed into new terrestrial areas or freshwater lakes, and lakes and wetlands are successively covered by peat.

Figure 1-7. *Photos from Forsmark showing the flat topography and the low-gradient shoreline with recently isolated bays due to land uplift.*

1.6 Scales and volumes

The site descriptive modelling is performed using two different scales, a local scale and a regional. The local scale covers the volume within which the repository is expected to be placed, including accesses and the immediate environs. The regional scale covers a larger volume that places the description of the local volume in a larger context. In selecting the volumes of the two scales some rules of thumb have been applied, cf SKB's strategy document for integrated evaluation /Andersson 2003/. The motivation for the different model areas/volumes shown in Figure 1-8 and Table 1-1 are found in /SKB 2006a/. It is noted that the north-western part of the candidate area has been selected as the target area for the Complete Site Investigation phase /SKB 2005b/. This is the main reason why the local model area since stage 2.1 is smaller than the local model area up to version 1.2. It needs also to be understood that the distinct rectangular volumes shown in Table 1-1 concern primarily the development of the geological model in the SKB Rock Visualisation System, RVS.

For the groundwater flow and solute transport modelling with ConnectFlow in stage 2.2, topographic data were supplied as a digital elevation model (DEM) with a spatial resolution of 20m scale in the horizontal directions. The surface water divides visible in the digital elevation model were used to define the model area for the numerical modelling. Figure 1-9 shows the locations of the regional model area, the water divides visible in the digital elevation model, the chosen upstream boundary and the hydrogeological model area used in the flow modelling. The sensitivity of the groundwater flow within the target volume with regard to the location of the upstream boundary and the size of the hydrogeological model area was studied in version 1.2 /Follin et al. 2005/. In conclusion, the location of the upstream boundary and the model area shown in Figure 1-9 were considered appropriate for the site descriptive modelling.

In version 1.2, the elevation of the bottom of the hydrogeological model volume was set to –2,300 m based on the *a priori* assumptions made in the geological modelling. In stage 2.2, this elevation was changed to –1,200 m in the hydrogeological modelling as a result of the large amount of low transmissivities acquired down to 1,000 m depth in 25 core-drilled boreholes.

1.7 This report

This report presents the understanding of the hydrogeological conditions of the bedrock at Forsmark at the completion of the surface-based investigations and provides a summary of the bedrock hydrogeological model and the underlying data supporting its development. It constitutes the main reference on bedrock hydrogeology for the final site descriptive model, SDM-Site, and is intended to summarise the hydraulic properties and hydrogeological conditions of the bedrock at the site and to give the information essential for demonstrating understanding. However, it relies heavily on a number of background reports concerning details in data analyses and modelling. The report numbers of the background reports are listed in Table 1-2.

Chapter 2 in this report describes SKB's systems approach to groundwater flow and solute transport modelling in sparsely fractured crystalline bedrock as applied in the site descriptive modelling work. Chapter 3 provides a brief summary of the regolith geology and the bedrock geology at Forsmark. Chapter 4 provides an overview of the primary data and summarises the evaluation. In chapter 5, the general understanding (conceptual model) of the bedrock hydrogeology at Forsmark is described. Chapter 6 presents the suggested hydraulic parameterisation of the bedrock and the regolith. Chapter 7 presents the results of the flow model calibration (confirmatory testing). Chapter 8 visualises the capability of the resulting flow and transport model in terms of a few exploration simulations. Chapter 9 discusses the impact of various model uncertainties, in particular parameter heterogeneity. Chapter 10, finally, provides a summary of the conceptual and numerical modelling carried out. Chapter 10 also contains a discussion about model confidence and remaining uncertainties.

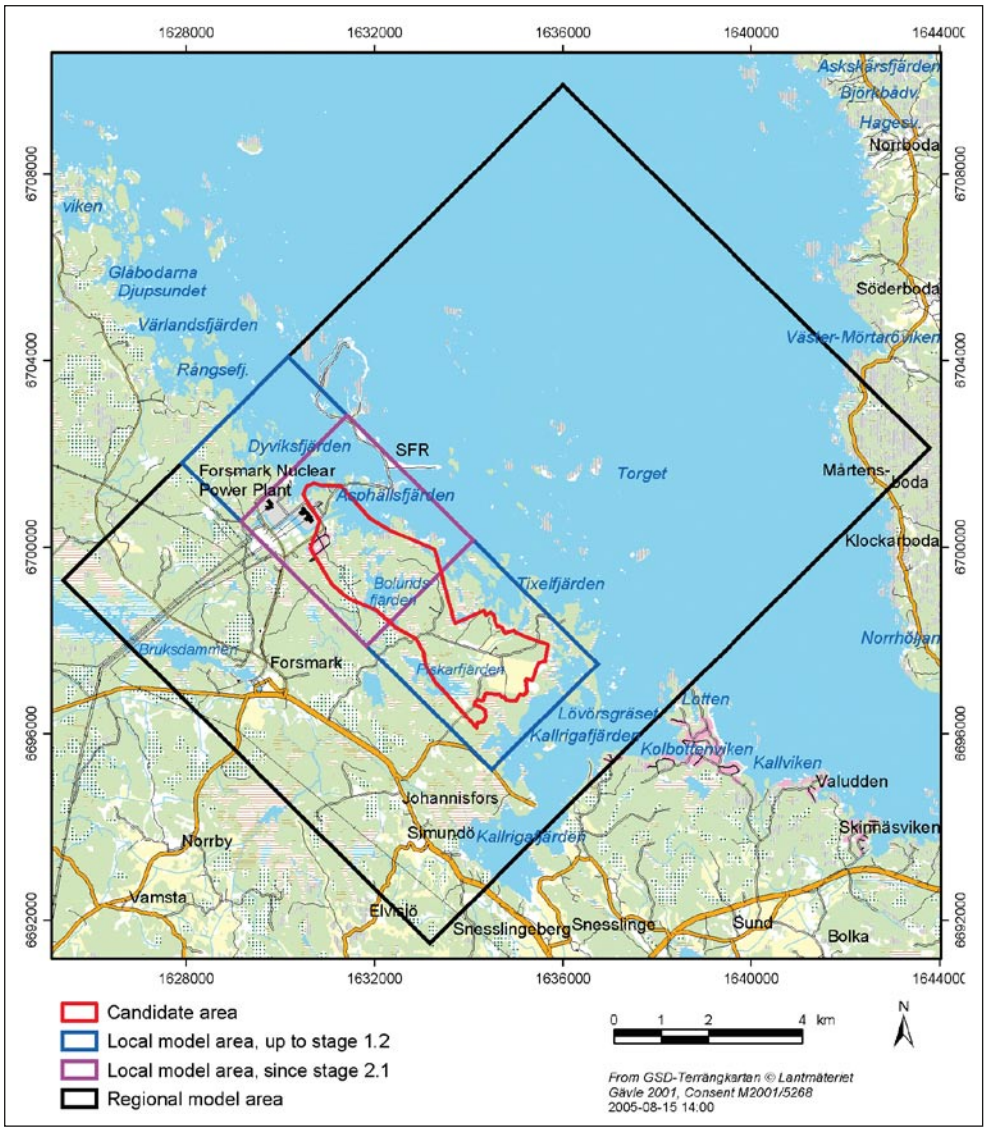

Figure 1-8. *Regional (black) and local (purple) model areas in stage 2.2. The regional model area is the same as in model versions 0, 1.1 and 1.2 and 2.1. The local model area in stage 2.2 is smaller than in version 1.2 (blue line) and covers the north-western part of the candidate area selected as target area for a potential repository /SKB 2005b/. (Figure 2-2 in /SKB 2006a/.)*

Table 1-1. Coordinates defining the regional and local model volumes (in metres).

Regional Model				
Vertex	1; 5	2; 6	3; 7	4; 8
RT 90* Easting	1625400	1636007	1643785	1633178
RT 90* Northing	6699300	6709907	6702129	6691522
RHB 70 elevation**	+100; –2,100	+100; –2,100	+100; –2,100	+100; –2,100
Local Model				
Vertex	1; 5	2; 6	3; 7	4; 8
RT 90 Easting	1629171	1631434	1634099	1631841
RT 90 Northing	6700562	6702824	6700159	6697892
RHB 70 elevation	+100; –1,100	+100; –1,100	+100; –1,100	+100; –1,100

* X/Y (N/E): the national 2.5 gon W 0:–15, RT 90 system (“RAK”)
** Z (elevation): the national RHB 70 levelling system

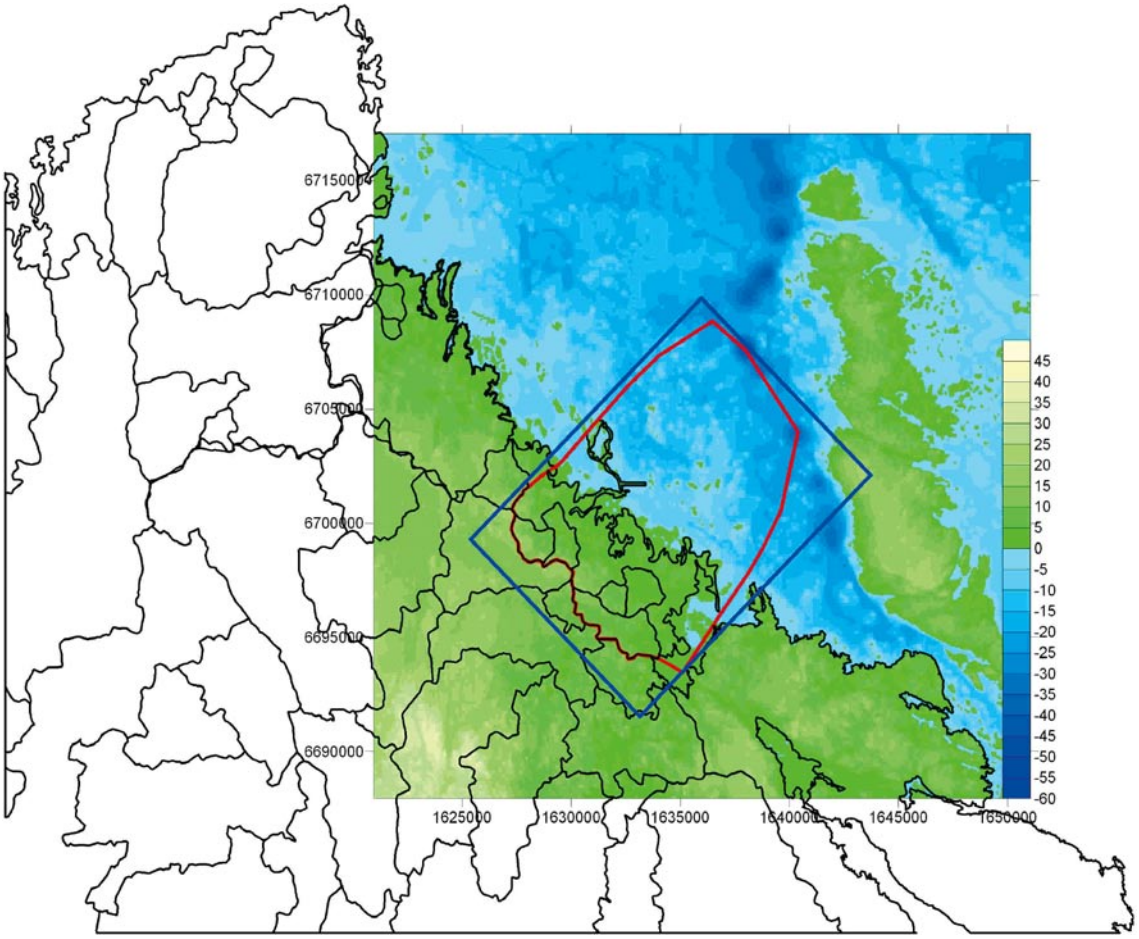

Figure 1-9. *Surface hydrology catchments used to define the hydrogeological model area (red line). The regional model domain used for the structural model is defined by the blue lines. (Figure 3-4 in /Follin et al. 2007c/. Geographic data ©Lantmäteriverket Gävle 2007. Consent I 2007/1092.*

1.7.1 Supporting documents and nomenclature

Three versions of a site descriptive model have been completed at Forsmark prior to the final site description, SDM-Site. Version 0 established the state of knowledge prior to the start of the site investigation programme. Version 1.1 was essentially a training exercise and was completed during 2004. Version 1.2 was a preliminary site description and concluded the initial site investigation work (ISI) in June 2005. The site descriptive modelling resulting in the final site description, SDM-Site, has involved three modelling stages. The first modelling stage, referred to as stage 2.1, included an updated geological model for Forsmark and aimed to provide a feedback from the modelling working group to the site investigation team to enable completion of the site investigation work. The two background reports reported in stage 2.2 are key to repository engineering, one documenting the hydraulic properties of deformation zones and fracture domains /Follin et al. 2007b/ and one the development of a conceptual flow model and the results of numerical implementation and calibration of the flow model /Follin et al. 2007c/. Since the flow model with its calibrated hydraulic properties is also an essential input to the safety assessment, the main findings of the flow modelling in stage 2.2 were revisited in stage 2.3. /Follin et al. 2008a/ addressed the impact of parameter heterogeneity on the flow modelling results as well as the impact of the new field data acquired in data freeze 2.3 on the conceptual model development.

Table 1-2 shows the cumulative number of boreholes providing hydraulic information about the bedrock at Forsmark (Appendix A shows the location of the boreholes). Table 1-2 also shows the reference numbers of the background reports on bedrock hydrogeology. This information is shown in relation to the three model versions and the three modelling stages carried out in preparation of this report and the SDM-Site.

Table 1-2. The cumulative number of boreholes providing hydraulic information about the bedrock at Forsmark at the end of each of the three model versions and three model stages carried out during the period 2002–2007 in preparation of the final version of the site descriptive model, SDM-Site. Here, KFM means core-drilled boreholes and HFM means percussion-drilled boreholes. The reports with reference numbers typed in italics describe the hydraulic data gathered and/or the hydrogeological modelling undertaken. The reports with underlined reference numbers summarise the development of the hydrogeological modelling along with the developments achieved within the other disciplines. (Table 1-1 in /Follin et al. 2007c/).

	Initial site investigation (ISI)		Complete site investigation (CSI)		
Desk top exercise	Training exercise	Preliminary SDM	Feedback and strategy	Hydrogeological model	Model verification and uncertainty assessment
Version 0	Version 1.1	Version 1.2	Stage 2.1	Stage 2.2	Stage 2.3
0 KFM (0%)	1 KFM (4%)	5 KFM (21%)	9 KFM (38%)	20 KFM (83%)	25 KFM (100%)
0 HFM (0%)	8 HFM (21%)	19 HFM (50%)	22 HFM(58%)	32 HFM (84%)	38 HFM (100%)
R-02-32	R-04-15	R-05-18	R-06-38	*R-07-48*	*R-08-23*
		R-05-32	*R-07-20*	*R-07-49*	
		R-05-60			

Table 1-3 provides definitions of some geological terms that are of importance for the bedrock hydrogeological modelling at Forsmark.

Table 1-3. Definitions of some geological terms that are of importance for the bedrock hydrogeological modelling at Forsmark. (Based on section 2.4 in /Stephens et al. 2007/.)

Term	Definition
Candidate area/volume	The candidate area refers to the area at the ground surface that was recognised as suitable for a site investigation, following the feasibility study work /SKB 2000/. The extension at depth is referred to as the candidate volume.
Target area/volume	The target area/volume refers to the north-western part of the candidate area and the rock volume beneath that was selected during the site investigation process as potentially suitable for hosting a final repository for spent nuclear fuel.
Rock unit	A rock unit is defined on the basis of the composition, grain size and inferred relative age of the dominant rock type. Other geological features including the degree of bedrock homogeneity, the degree and style of ductile deformation, the occurrence of early-stage alteration (albitisation) that affects the composition of the rock, and anomalous fracture frequency also help define and distinguish some rock units.
Rock domain	A rock domain refers to a rock volume in which rock units that show specifically similar composition, grain size, degree of bedrock homogeneity, and degree and style of ductile deformation have been combined and distinguished from each other. Different rock domains at Forsmark are referred to as RFMxxx.
Deformation zone	Deformation zone is a general term that refers to an essentially 2D structure along which there is a concentration of brittle, ductile or combined brittle and ductile deformation. Deformation zones at Forsmark are denoted ZFM followed by two to eight letters or digits. An indication of the orientation of the zone is included in the identification code.
Fracture zone	Fracture zone is a term used to denote a brittle deformation zone without any specification whether there has or has not been a shear sense of movement along the zone.
Fault zone	Fault zone is a term used for a fracture zone that shows a shear sense of movement along it.
Fracture domain	A fracture domain is a rock volume outside deformation zones in which rock units show similar fracture frequency characteristics. Fracture domains at Forsmark are denoted FFMxx.

2 Hydrogeological modelling in the SDM

2.1 Systems approach

Figure 2-1 illustrates schematically the division of the groundwater system into hydraulic domains used in the bedrock hydrogeological modelling for Forsmark. The bedrock hydrogeological model consists of three hydraulic domains, HSD, HCD and HRD, where (see Figure 2-1 for explanation):

- HSD (Hydraulic Soil Domain) represents the regolith (Quaternary deposits),
- HCD (Hydraulic Conductor Domain) represents deformation zones, and
- HRD (Hydraulic Rock mass Domain) represents the less fractured bedrock in between the deformation zones.

The division into hydraulic domains constitutes the basis for the conceptual modelling, the planning of the site investigations and the numerical modelling carried out using ConnectFlow and MIKE SHE. The variable-density flow modelling simulates the shore level displacement in the Fennoscandian Shield during Holocene time, i.e. between 8000 BC and 2000 AD, and the associated changes of the salinity in the different aquatic systems in the Baltic basin during this period.

Besides the three hydraulic domains shown in Figure 2-1, the groundwater flow and solute transport modelling with the ConnectFlow code consists of three additional elements:

- A solute transport model for the modelling of matrix diffusion.
- Initial conditions for groundwater flow and hydrochemistry.
- Boundary conditions for groundwater flow and hydrochemistry.

The parameterisation of the six elements is based on altogether 13 different submodels, see Table 2-1. /Follin et al. 2007c/ provide a detailed description of the 13 submodels and how they were merged in the numerical modelling.

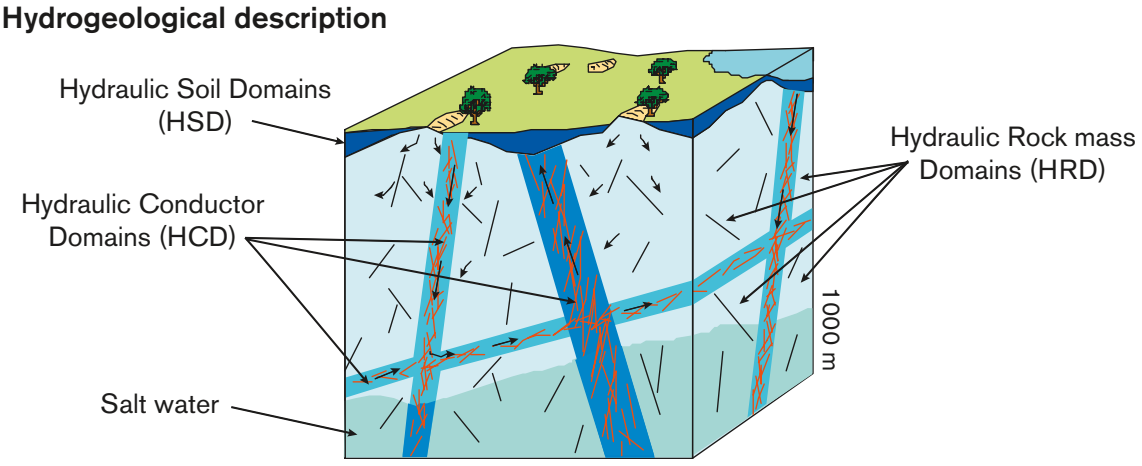

Figure 2-1. *Cartoon showing the division of the crystalline bedrock and the regolith above it (Quaternary deposits) into three hydraulic domains, HCD, HRD and HSD. (Figure 3-2 in /Rhén et al. 2003/.)*

Table 2-1. The groundwater flow and solute transport modelling with the ConnectFlow code is based on altogether 13 different submodels. The shaded fields show the key field/laboratory data used to conceptualise and parameterise the six elements listed in the top row. (Modified after Table 3-1 in /Follin et al. 2007c/.)

HCD, Hydraulic conductor domain model	HRD, Hydraulic rock mass domain model	HSD, Hydraulic soil domain model	Solute transport model	Initial conditions	Boundary conditions
2. Deformation zone model	1. Rock domain model	8. Regolith model	7. Hydro-DFN model	10. Palaeo-hydrological model	3. Digital elevation model
5. Bedrock hydrogeological model	4. Fracture domain model	3. Digital elevation model	13. Bedrock transport properties model		11. Shore level displacement model
	5. Bedrock hydrogeological model	9. Quaternary deposits hydrogeological model			12. Baltic Sea salinity model
	6. Geo-DFN model				
	7. Hydro-DFN model				
Single-hole hydraulic tests (PSS and PFL-f)	Single-hole hydraulic tests (PFL-f)	Slug-tests	Single-hole hydraulic tests (PFL-f)	Hydrochemical database	Hydrochemical database
		BAT tests	Resistivity logging		
Borehole core description	Borehole fracture data	Grain size distribution	Dilution tests SWIW tests Tracer tests Laboratory tests		Hydrological monitoring data

2.2 Confirmatory testing

The implementation of the HSD, HCD and HRD elements in ConnectFlow is based on the geological models of the regolith and the bedrock, respectively, and the hydraulic investigations conducted in the KFM, HFM and SFM boreholes. That is, the geometries of the hydraulic domains are coherent with the geometries of the geological features, and their hydraulic properties reflect the anisotropy and spatial variability observed in the hydraulic investigations. Table 1-2 shows the cumulative number of boreholes providing hydraulic information about the bedrock in the Forsmark area.

As a means of approaching the issue of confirmatory testing, a strategy was developed after version 1.2 /Follin et al. 2007a/, see Figure 1-2. In practice, four kinds of data were treated during stage 2.2 (Figure 2-2) /Follin et al. 2007bc/:

A. Hydraulic properties deduced from single-hole hydraulic tests (double-packer injection tests (PSS), difference flow logging pumping tests (PFL-f) and open-hole pumping tests combined with impeller flow logging (HTHB) /Follin et al. 2007b/.

B. Groundwater level responses (point water head drawdowns) in the bedrock in the depth interval 0 to c 700 m observed during large-scale interference (cross-hole) tests /Follin et al. 2007c/.

C. Present-day mean groundwater levels (point water heads) observed in the Quaternary deposits and the uppermost (c. 150 m) part of the bedrock /Follin et al. 2007c/.

D. Hydrochemical data (fracture water and matrix porewater) gathered from the bedrock investigations (primarily the core-drilled boreholes) /Laaksoharju et al. 2008/.

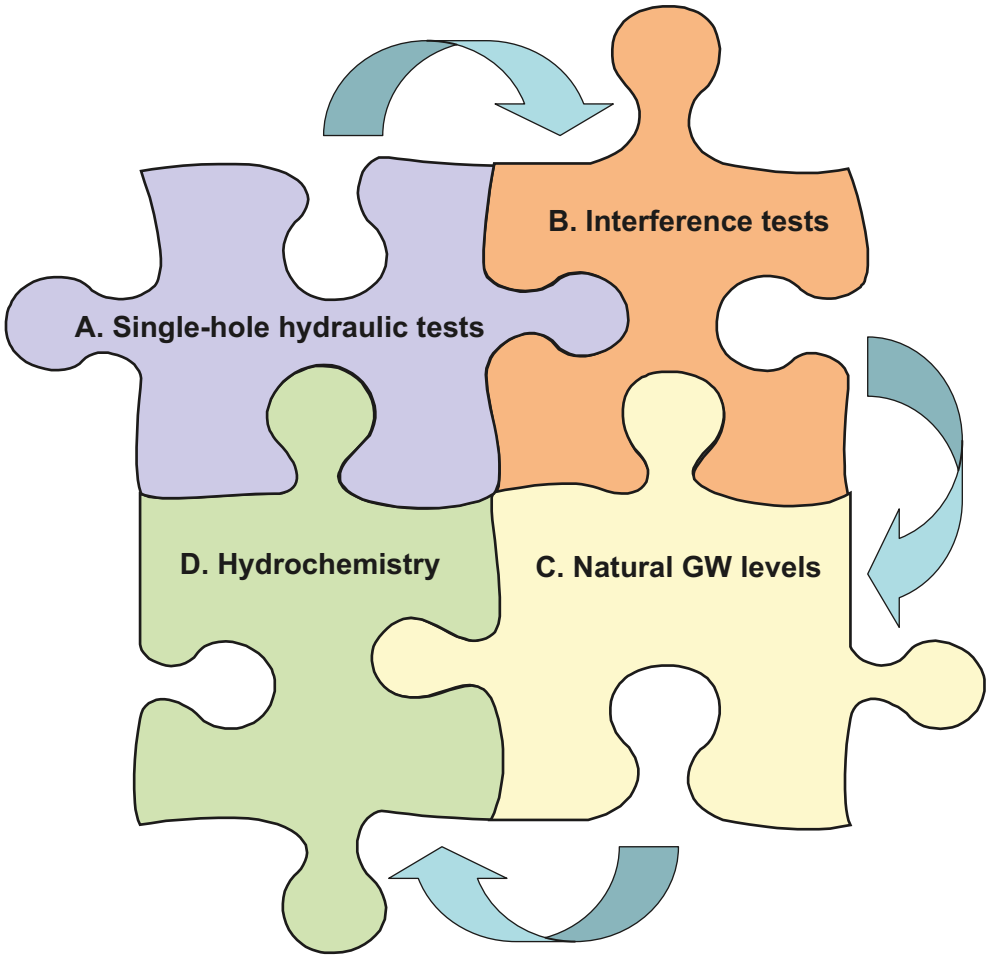

Figure 2-2. *Four kinds of data are used in the numerical modelling as a means of approaching the issue of confirmatory testing. A: Hydraulic properties of deformation zones and fracture domains as deduced from single-hole tests; B: Large-scale interference (cross-hole) tests; C: Natural groundwater levels in the bedrock and the Quaternary deposits; D: Hydrochemistry in deep boreholes. (Figure 1-2 in /Follin et al. 2007c/.)*

The general approach applied in the numerical modelling in stage 2.2 was to first parameterise the deformation zones and fracture domains hydraulically using fracture and inflow data from individual boreholes (A). Second, the confirmatory step relies on using essentially the same groundwater flow and solute transport model in terms of grid discretisation and parameter settings for matching three types of independent field data (B-D). Using the three types of data, a unified conceptual description of the groundwater system has been attempted.

The hydraulic properties of the HCD, HRD and HSD inferred during Task A were implemented in ConnectFlow and MIKE SHE as described in /Follin et al. 2007c/ and /Bosson et al. 2008/, respectively. The calibration of the hydrogeological model in MIKE SHE included Tasks B and C but did not include Task D.

It is noted that a primary idea of the confirmatory testing in ConnectFlow is that the same groundwater flow and solute transport model is used for each type of simulation to make it transparent that a single implementation of the conceptual model could be calibrated against all four types of field observations, although it may have been possible to improve the modelling of a particular data type by refining the model around a relevant observation borehole, for example.

2.3 Primary concepts and assumptions

2.3.1 Deterministic versus stochastic features

The hydraulic characterisation of the more intensely fractured deformation zones and the less fractured bedrock in between, the so-called fracture domains /Olofsson et al. 2007/, is a cornerstone of the bedrock hydrogeological description. The adopted modelling approach combines a deterministic geometrical representation of the HCD with a stochastic geometrical representation of the HRD using a discrete fracture network (DFN) approach and the tectonic continuum hypothesis, see Figure 2-3. Both domains were treated as hydraulically heterogeneous.

The tectonic continuum hypothesis is a working hypothesis. It invokes that the size and intensity of fractures on multiple scales can be approximated through the use of a *single* power-law relation ship, which by definition requires scale-invariant fracture orientation sets. However, the density functions may vary between the sets. The orientations of the fracture sets used in the hydrogeological DFN modelling work at Forsmark were assumed to be Fisher distributed.

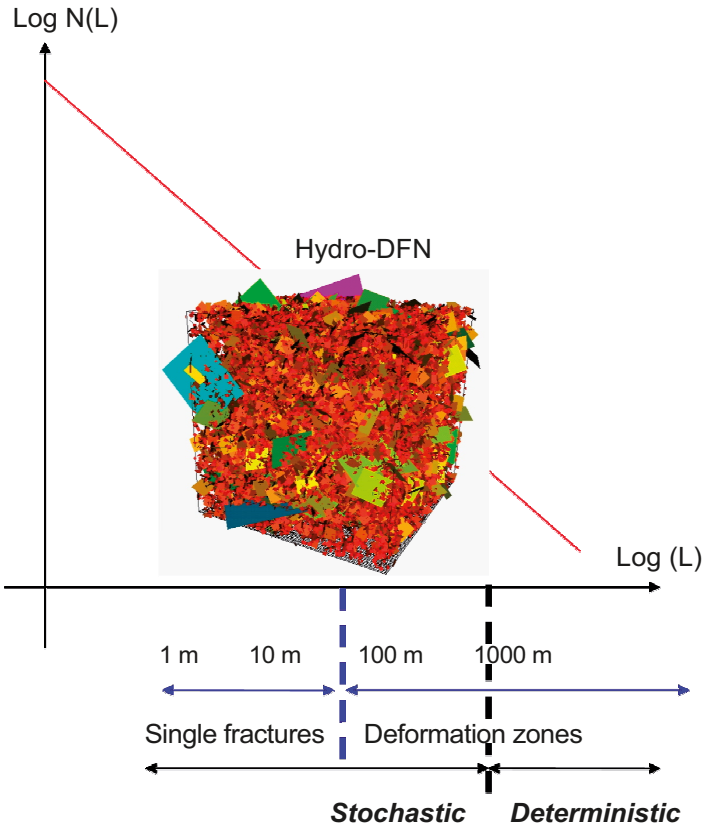

Figure 2-3. *The tectonic continuum hypothesis invokes that the frequency of fractures of different sizes can be approximated through the use of a single power-law density function. Features with trace lengths less than L = 1,000 m are regarded as uncertain in the SDM and treated stochastically using the DFN concept. In the geological single-hole interpretation, all borehole intervals with deformation zone type properties were called "possible deformation zones". The intervals that could not be tied to particular lineaments or geophysical anomalies remained non-deterministic in the geological modelling work, i.e. uncertain. The remaining possible deformation zones were regarded as minor deformation zones, i.e. stochastic, in the hydrogeological DFN modelling work, cf Table 3-2 (Figure 2-3 in /Follin et al. 2007b/.)*

Fracture intensity is closely connected to the spatial arrangement of the fractures. The hydrogeological DFN modelling was based on the assumption that the spatial distribution of fracture centres of each fracture set within each fracture domain follows a Poisson process, which in turn implies a Euclidean scaling[1].

The assumption of a tectonic continuum with a Euclidean scaling was tested in the geological DFN modelling in parallel with other assumptions (see section 4.2.3 and section 5.1.1 in /Fox et al. 2007/ for a brief description of the tested model variants). Of particular interest for the hydrogeological DFN modelling is the finding that the spatial correlation of the fractures observed on outcrops and in boreholes is weak or absent above a few tens of metres or less, indicating that the spatial pattern of the identified fracture clusters could be reasonably well approximated by a Poisson process and an Euclidean scaling (cf. p. 126–127 in /Fox et al. 2007/). In effect, the primary geometrical concepts and statistical assumptions of the global fracture sets defined in the geological DFN modelling are the same as those used in the hydrogeological DFN modelling:

- Fisher distributed fracture orientations
- Set-specific power-law size probability density functions
- Poissonian fracture locations

A key difference between the two DFN descriptions is in the data used to determine fracture size; the geological DFN modelling work considered primarily the geometrical properties of *surface data* (outcrop data and lineament data) representing *all features*, whereas the hydrogeological DFN modelling work focussed solely on the frequency of *borehole data* representing two different types (subsets) of features: (*i*) *potentially flowing features* (i.e., *open and partly open fractures*), and (*ii*) *continuously flowing features* detected by the Posiva Flow Log method (so-called *PFL-f* features) [2].

The differences between the geological and hydrogeological databases impacted on the how the DFN modelling was carried out. However, since the frequency of *potentially flowing features* indeed constitutes a fraction (subset) of the frequency of *all features*, the envisaged relationship between the associated power-law density functions has been as illustrated in Figure 2-4. Figure 2-4 implies that completely sealed fractures exist predominantly among the small features, whereas large features, i.e. deformation zones, are generally heterogeneous with regard to fracture aperture, i.e. open over at least some parts of their surface area.

Figure 2-4 shows also the conceived behaviour of the *continuously flowing fractures*. In the hydrogeological DFN modelling, the *PFL-f fractures* are imagined to be a subset of the latter category, see section 6.2.

[1] Euclidean scaling is a particular kind of a tectonic continuum where the number of features is linearly proportional to the dimensionality of the observation (length, area or volume). Thus, Euclidean scaling implies that doubling the scale (size) of observation, effectively doubles the number of features. That is, Euclidian intensity is scale invariant (constant) in contrast to fractal intensity which is scale dependent.

[2] In the context of the SDM, '*all features*' means that no distinction was made between fractures with regard to fracture aperture. Hence, *sealed* fractures were pooled with '*partly open*' and '*open fractures*' in the geological DFN modelling work. In contrast, the hydrogeological DFN modelling work focussed, to begin with, on the properties of the '*potentially flowing features*', which implies that the analysed fractures must be at least partly open. No distinction was made between open and partly open fractures; however. They were all called *open fractures* for the sake of simplicity. In order for an *open fracture* to be detected as a flowing feature with the PFL-f method it must be (*i*) connected to a positive hydraulic boundary (either directly or indirectly via a network of other flowing features) and (*ii*) have a sufficient transmissivity with regard to the measurement threshold of the test equipment used, cf section 2.3.2.

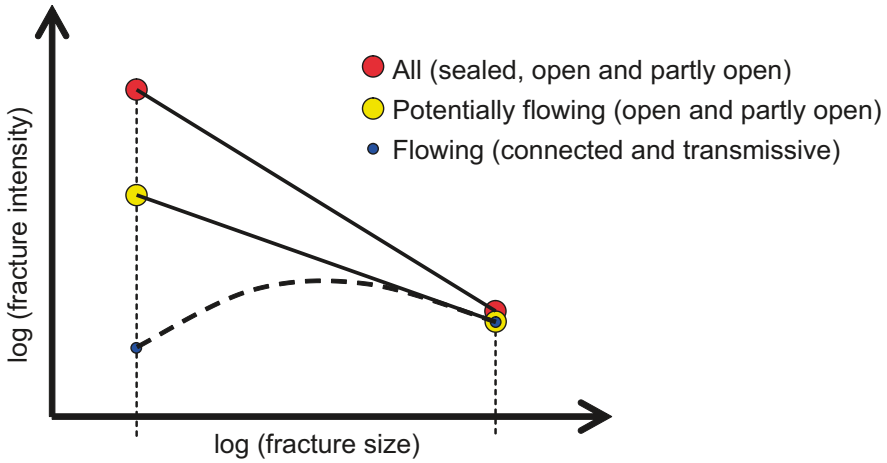

Figure 2-4. *Cartoon showing the envisaged relationship between the probability density functions of all, the potentially flowing and the flowing fractures.*

There is a clear variation in the occurrence of steeply dipping lineaments and deformation zones with WNW-ESE to NW-SE strike as well as in the occurrence of gently dipping deformation zones at Forsmark /Stephens et al. 2007/. For instance, the intensity of large, steeply-dipping structures with WNW-ESE to NW-SE strike is much higher in the bedrock outside relative to that inside the tectonic lens, which hosts the candidate and target areas, cf Figure 1-5 and Figure 1-6. The spatial variability in the intensity of large structures impacts on the geological DFN modelling work /Fox et al. 2008/. In summary, the fracture size models derived in the geological DFN modelling work /Fox et al. 2007/ are not readily compared with those derived in the hydrogeological DFN modelling work /Follin et al. 2007b/. The conditions at Forsmark are discussed in Appendix C, which also suggests an alternative approach to address the relevance of Figure 2-4.

2.3.2 Basic characteristics of single-hole tests

The hydraulic parameterisation of the deformation zones and fracture domains to become HCD and HRD models is based on single-hole tests in boreholes (Task A in Figure 2-2). Difference flow logging pumping tests (PFL-f) and double-packer injection tests (PSS) were used in the deep, core-drilled boreholes, whereas flow-logging pumping tests in open holes (HTHB) were used in the shallower, percussion-drilled boreholes. The lower measurement limits of the PFL-f and PSS test methods are superior to that of the HTHB test method, but they cannot be readily used in the percussion-drilled boreholes for technical reasons. Further, the PFL-f and PSS test methods have different advantages and disadvantages. For this reason, they were run in parallel, in order to quantify the consequences for the site characterisation, the hydrogeological discrete fracture network modelling and the groundwater flow modelling. /Follin et al. 2007b/ provide a description of the interpretations of the single-hole hydraulic tests conducted in the core-drilled boreholes (PFL-f and PSS) and the percussion-drilled boreholes (HTHB) along with an extensive interdisciplinary comparison between the interpretation of geological and hydraulic data.

The constituent parameters measured during the hydraulic tests are the flow rate, Q, and the pressure, p. Since these are correlated, the parameter studied is the specific capacity, $Q/\Delta p$, which has the same dimension as transmissivity, T. The envisaged test conditions in fractured rock are shown in Figure 2-5. The specific capacity is dependent on several important aspects, among which the following are particularly noted:

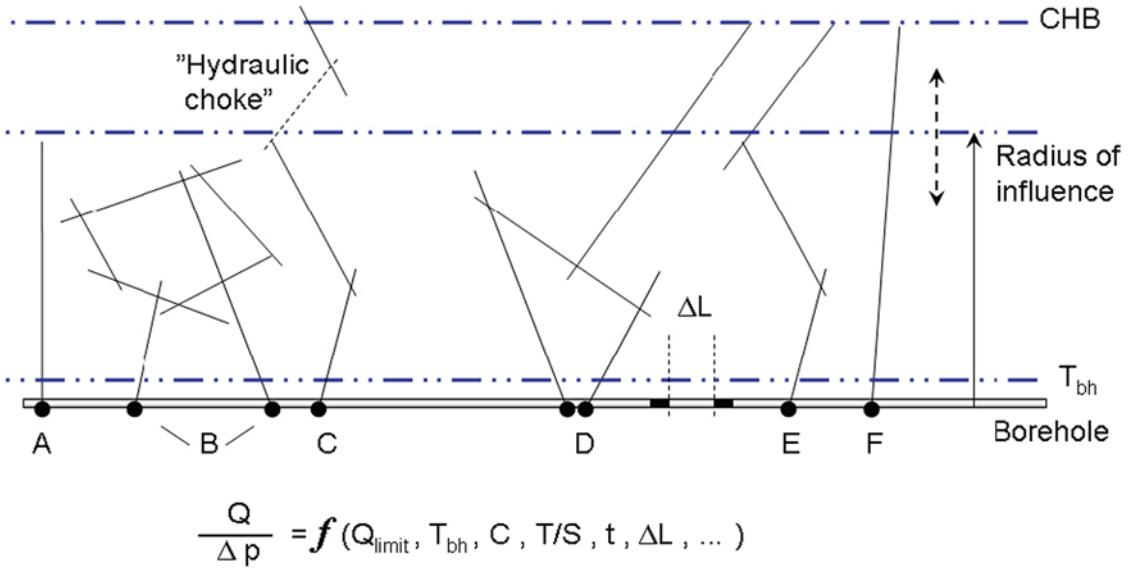

Figure 2-5. *Cartoon showing a borehole with six different symbolic fracture network situations, cases A–F. The specific capacity, Q/Δp, measured along the borehole is dependent on several factors, e.g. the measurement limit, Q_{limit}, of the test method, the transmissivity of the fracture intersecting the borehole, T_{bh}, the fracture connectivity, C, the hydraulic diffusivity, T/S, of the fracture network, the test time, t, the length of the test section, ΔL, etc. The hydraulic characterisation of the fracture system varies depending on the method used as well as on the in situ conditions, e.g. the occurrence of "hydraulic chokes". Cases A–C represent isolated fracture networks and cases D–F represent fracture networks connected to the overall hydrogeological system. The overall hydrogeological system is here indicated by a constant head boundary (CHB) suggesting a pseudo steady state flow regime at long test times. The cartoon is rotated 90° to improve the readability. (Modified after Figure 2-2 in /Follin et al. 2007b/.)*

- Q_{limit}; the lower measurement limit of the test method.
- T_{bh}; the transmissivity of the tested fracture intersecting the borehole. T_{bh} can be affected during the drilling operations. For instance, the fracture can be clogged (positive skin) or stimulated (negative skin).
- C; the connectivity of the tested fracture to other fractures away from the borehole. Some fractures are isolated, or are a part of an isolated cluster of fractures. Others are well connected and a part of the overall hydrological system.
- T/S; the hydraulic diffusivity of the fracture system within the radius of influence.
- t; the duration of the hydraulic testing, i.e. the test time.
- ΔL; the length of the test interval (test section).

The PFL-f method uses a short test interval and a long test time. Thus, the resolution of the PFL-f method is sufficient to study the specific capacity of individual fractures and the method can be used to evaluate the conductive fracture frequency (CFF) of continuously flowing networks, e.g. situations like cases D–F in Figure 2-5. However, the PFL-f method cannot identify situations with isolated fractures/clusters or "hydraulic chokes" such as in cases A–C.

The PSS method uses a longer test interval and a much shorter short test time. In effect, it has greater problems in distinguishing network situations like cases A–C from network situations like cases D–F, which means that using data from the PSS method alone for the hydrogeological DFN modelling could easily result in an over prediction of fracture connectivity in the sparsely fractured bedrock in between the deformation zones.

Due to these differences, the hydrogeological DFN modelling carried out was based on the information acquired by the PFL-f method. The typical lower threshold value of the PFL-f investigations at Forsmark is roughly $1 \cdot 10^{-9}$ m^2/s expressed in terms of modelled transmissivities. The corresponding value of the PSS investigations is about $6 \cdot 10^{-10}$ m^2/s /Follin et al. 2007b/.

2.3.3 Hydraulic conductor domain (HCD) model

The hydraulic parameterisation of a deformation zone is fairly straightforward. All fracture data and transmissivity data between the upper and lower bounds of a deformation zone interval, as determined in the single-hole geological interpretations, are integrated to form a single feature with a lumped in-plane transmissivity value for that interval. This approach implies that the hydraulic thickness is assumed to be equal to the geological. The heterogeneity in the in-plane transmissivity of a given deformation zone was studied by means of a combination of PSS/PFL-f single-hole tests at different locations in that zone. The assumptions are illustrated in Figure 2-6 and Figure 2-7.

2.3.4 Hydraulic rock domain (HRD) model

The hydraulic description of the fracture domains between the deformation zones is focused on the conductive fracture frequency, CFF, and the specific capacity, $Q/\Delta p$ (or Q/s, where Q denotes flow rate and s denotes "drawdown"), of continuously flowing fractures. This means that the connected fracture network situations such as cases D–F in Figure 2-5 were regarded as more important for the hydrogeological DFN modelling and the groundwater flow modelling in the SDM than disconnected (compartmentalised) network situations such as cases A–C. The role of compartmentalised networks, if any, needs to be addressed in the safety assessment.

It is important to recollect what is actually measured with the PFL-f tests. For each PFL-f transmissivity value identified, the change in flux (inflow) and head (drawdown) after several days of pumping relative to conditions prior to pumping are calculated. The specific capacity, $Q/\Delta p$, has the same dimension as transmissivity, T, and a transmissivity value is interpreted for each PFL-f test conducted based on Thiem's equation and an assumed value of the radius of influence to borehole radius ratio (R_0/r_w) = 500. The choice of 500 reflects that tests are performed over several days, and hence should represent an effective transmissivity of the whole fracture intersected, and possibly adjoining parts of the network, but the choice of 500 is otherwise arbitrary.

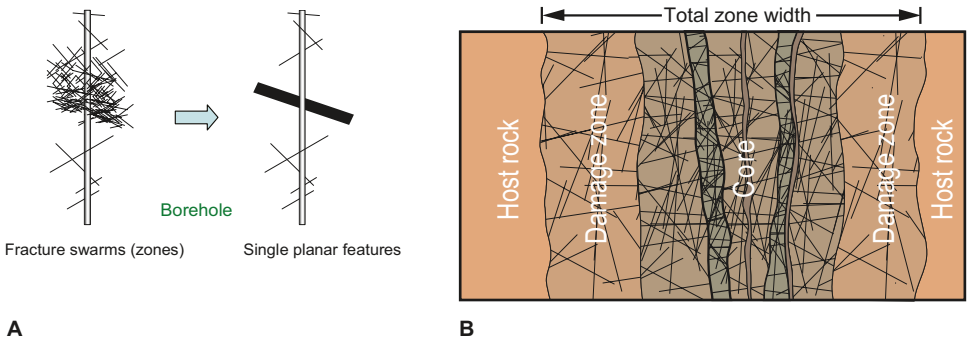

Figure 2-6. *A: The fracture data between the upper and lower bounds of a deformation zone interval are lumped together to form a single planar feature. In the same fashion, all hydraulic data in the interval are also lumped together in the hydrogeological modelling, to form a single in-plane transmissivity value. (Figure 2-3 in /Follin et al. 2007b/.). B: Cartoon of the typical fracturing associated with faults. The major deformation zones at Forsmark display various degrees of the fracturing shown in this illustration. (Modified after Figure 2-1 in /Munier et al. 2003/.)*

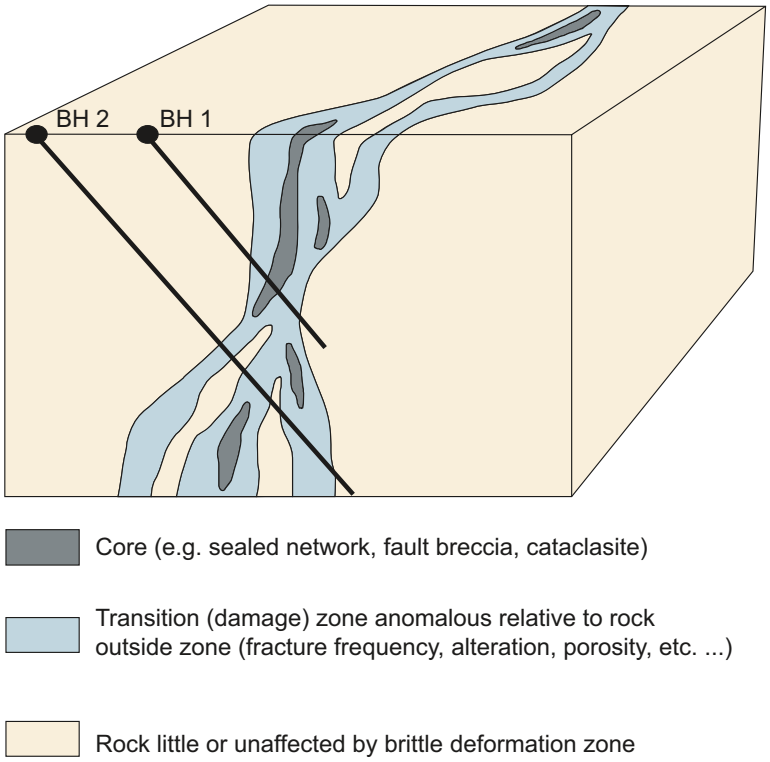

Figure 2-7. *Illustration of the typical fracturing associated with faults. The major deformation zones at Forsmark display various degrees of the fracturing shown in this illustration. The heterogeneity in the in-plane transmissivity of a given deformation zone was studied by means of single-hole tests at different locations in that zone. (Modified after Figure 5-1 in /Stephens et al. 2007/.)*

Consequently, the interpreted values of transmissivity should not be viewed as necessarily the transmissivity of individual fractures, or the transmissivity of the fracture local to the borehole intersect. They are more indicative of the effective transmissivity over a larger scale. This remark influences the way the PFL-f data were used in the hydrogeological DFN modelling. Before carrying out the regional groundwater flow simulations, the hydrogeological DFN model was calibrated by means of steady state pumping tests representing the measured values of $Q/\Delta p$ in each fracture. Three different kinds of correlations between fracture transmissivity and fracture size were used in the pumping test simulations, see Table 2-2. By semi-correlation, it was implied that the mean transmissivity of a fracture increases with its size, but there is some random component or spread of values for any given fracture size. This is perhaps the most realistic situation. Hence, in the flow calibration, the aim was to establish appropriate choices for the parameters for each relationship between fracture size and transmissivity that gives a match to the magnitude of the specific capacities in each fracture domain. To assess the 'goodness of fit', the following four statistics were calculated in the calibration process:

1. Arithmetic average total specific capacity, $\Sigma\, Q/s$, to the abstraction borehole over ten realisations.
2. Histogram of the distribution of the log specific capacities, log (Q/s), as an average (geometric mean) over ten realisations.
3. Bar and whisker plot of [minimum, mean minus one standard deviation, mean, mean plus one standard deviation, maximum] of the log specific capacities, log(Q/s), for the inflows within each fracture set taken over all realisations.
4. The average numbers of fractures within each set giving inflows to the abstraction borehole above the measurement limit for the PFL-f tests.

Table 2-2. Transmissivity-size parameters used for all sets when matching measured PFL-f flow distributions. 'log' refers to the common log. (Table 3-9 in /Follin et al. 2008a/.)

Type	Description	Relationship	Parameters
Correlated	Power-law relationship	$\log(T) = \log(a\, r^{b})$	a , b
Semi-correlated	Log-normal distribution about a power-law correlated mean	$\log(T) = \log(a\, r^{b}) + \sigma_{\log(T)}\, \mathbf{N}[0,1]$	a , b, $\sigma_{\log(T)} = 1$
Uncorrelated	Log-normal distribution about a specified mean	$\log(T) = \mu_{\log(T)} + \sigma_{\log(T)}\, \mathbf{N}[0,1]$	$\mu_{\log(T)}$, $\sigma_{\log(T)}$

The finest scale of heterogeneity in fracture transmissivity studied in the SDM was the variability in transmissivity between fractures of different sizes as defined by Table 2-2. The heterogeneity in fracture transmissivity within individual fractures was not modelled due to lack of data to support this scale of modelling. That is, individual fractures were assumed to be homogeneous. The adopted modelling approach is envisaged to render stronger channelling effects on the transport of radionuclides for the correlated and semi-correlated transmissivity-size models than for the uncorrelated transmissivity-size model, although this issue was not studied in the hydrogeological modelling. For the sake of the subject, it is noted that a number of different forms of flow channelling, including the role of intra-heterogeneity versus of inter-heterogeneity on field-scale transport, are discussed in detail in /Painter 2006/ and /Crawford (ed) 2008/ and will be addressed in the SR-Site safety assessment project.

Furthermore, it was assumed that the groundwater flow and solute transport within the network of fractures can be represented by an equivalent continuous porous medium (ECPM) by upscaling to an appropriate grid size, see Figure 2-8. Since each ECPM model is based on a particular underlying stochastic realisation, the ECPM models are also stochastic. Uncertainties relating to spatial variability in the geometrical and/or hydraulic properties was quantified by means of multiple realisations /Follin et al. 2008a/. The procedure used to upscale a DFN realisation to a heterogeneous and anisotropic continuum was to conduct permeameter tests in three orthogonal directions on the scale of each grid element /Jackson et al. 2000/. Grid elements were of size 20 m around the candidate area and 100 m on the regional scale.

For the HRD rock outside the mapped fracture domains, there is no fracture information available, and so a simplified property assignment is used to specify homogeneous continuum porous medium (CPM) properties. Approximate values for this rock are taken from hydraulic single-hole tests in deep boreholes at Finnsjön /Andersson et al. 1991/ using their results given for the geometric mean for 3 m PSS tests in the bedrock between deformation zones (Table 3-6 in /Follin et al. 2007c/). A depth dependency was suggested by the data, which was simplified to a step-wise model consistent with the same depth zonations as used within the candidate area, see Appendix C.

2.3.5 Hydraulic soil domain (HSD) model

The modelling approach used in ConnectFlow implies a considerable simplification of the detailed geometrical description of the near-surface system derived in /Hedenström and Sohlenius 2008/ and /Hedenström et al. 2008/. The thickness of the regolith (Quaternary deposits) within the model area varies from less than a decimetre to over 25 m, not all layers exist everywhere, and the thickness of individual layers varies significantly. In ConnectFlow, this complex stratigraphy was simplified in order to relax the computational constraints. The interpreted stratigraphy was substituted by four element layers each of a constant 1 m thickness. The same equivalent hydraulic conductivity tensor was specified for each vertical stack of four grid elements, but was varied horizontally from stack to stack, and was anisotropic between horizontal and vertical components. The horizontal component of the stack tensor was based on the arithmetic mean of the hydraulic properties of the original stratigraphy, whereas the vertical component was based on its harmonic mean. The upscaling is described in section 3.15 in /Follin et al. 2007c/.

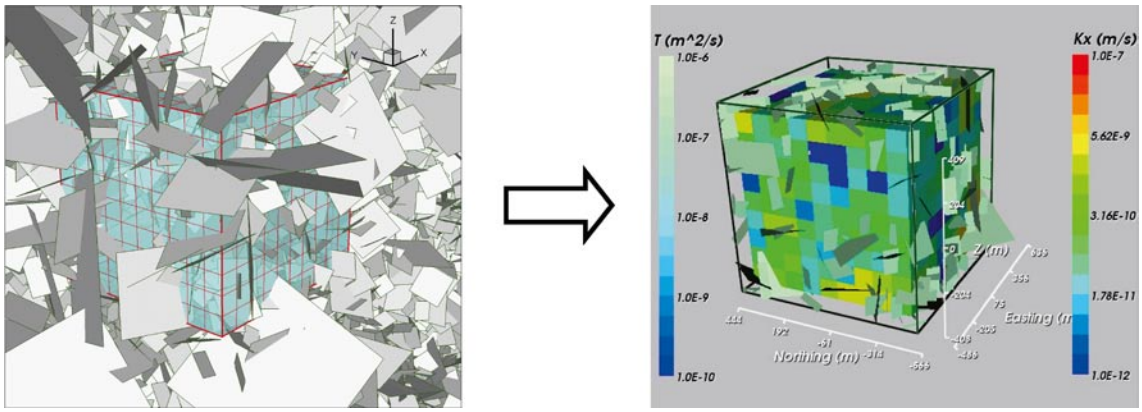

Figure 2-8. *Illustration showing the upscaling approach from a DFN to an ECPM in ConnectFlow. (Figure 2-4 in /Follin et al. 2007b/.)*

2.3.6 Solute transport model

The solute transport model applied in the hydrogeological modelling is based on the ECPM approach. It should be noted that in safety assessment calculations such as SR-Can /Hartley et al. 2006/ and the upcoming SR-Site safety assessment projects, the transport properties of the bedrock are calculated explicitly along migration pathways obtained from DFN flow simulations.

In the ECPM approach, the total connected pore space available to solutes is divided between a mobile pore space, known as the *kinematic porosity*, in which both groundwater flow and solute transport takes place, and an immobile pore space, referred to as *diffusion accessible porosity*, in which only solute transport through diffusive exchange with the mobile pore space is considered. For the sparsely fractured bedrock at Forsmark, the mobile pore space may be interpreted as the open fracture channels that are connected and responsible for the circulation of groundwater, and the immobile pore space is the rest of the total connected pore space including inter-granular pore space and micro-fractures. The immobile pore space may also include contributions from fractures in which there is negligible flow and from regions of nearly immobile water in the larger fractures (resulting from constrictions in fracture aperture or the presence of gouge material). In practice, it may be difficult to estimate either type of pore space accurately by direct measurement, and hence one purpose of the solute transport modelling of natural tracers in the SDM is to confirm the interpretation of transport properties.

In the mobile pore space, groundwater flow is modelled and solute transport takes place by advection, dispersion and diffusion through the kinematic porosity together with diffusion of solute between the mobile groundwater in the kinematic porosity and immobile groundwater in the diffusion accessible porosity. The process of diffusion between the mobile groundwater in the kinematic porosity and the immobile groundwater in the diffusion accessible porosity can lead to a significant retardation of solute migration relative to solute migration in the kinematic porosity alone. The rock matrix diffusion (RMD) model used in /Follin et al. 2007c/ represents the process in terms of a 1D model of diffusion between groundwater flowing in infinite, parallel, equidistant, constant-aperture, planar fractures and immobile groundwater in the intervening rock /Hoch an Jackson 2004/. The parameters used in the RMD model are:

- the effective (or intrinsic) diffusion coefficient (for diffusion in immobile water),
- the diffusion accessible porosity,
- the maximum distance available for diffusion into the diffusion accessible porosity,
- the flow-wetted fracture surface area per unit volume over which there may be diffusion between the groundwater flowing in the fractures and the diffusion accessible porosity, and
- the kinematic porosity.

Estimates of the effective diffusion coefficient and the diffusion accessible porosity are available from diffusion experiments. Parameters relating to the fracture spacing can be derived from information about the hydraulic fracture network (hydrogeological DFN). This may be derived based on the frequency of water conducting fractures mapped using the PFL-f method. Because this frequency can be biased by the relative orientation of fractures to the borehole trajectory, it is more appropriate to estimate the 'true' linear fracture intensity, $P_{10,corr}$, rather than the linear intensity, P_{10}, measured in the borehole. The maximum distance available for diffusion into the diffusion accessible porosity can be based on the spacing of the fractures (if it is considered that all of the rock between the fractures is potentially accessible) or based on the dimensions of alteration halos around fractures (if it is considered that only the rock within a limited distance of fractures is accessible). Similarly, the flow-wetted surface per unit volume can be estimated from the corrected linear fracture intensity, $P_{10,corr}$. The flow wetted fracture surface area per unit volume of rock, a_r, was derived from the corrected linear intensity of flowing features identified in PFL-f tests observed in boreholes, $P_{10,PFL,corr}$, and the approximation:

$$a_r = 2\ P_{10,PFL,corr} \tag{2-1}$$

It should be noted that in safety assessment calculations, flow wetted fracture surface area per unit volume of rock is calculated explicitly along migration pathways obtained from DFN flow simulations implemented in ConnectFlow.

Measurement of the kinematic porosity is difficult in fractured rocks. In practice, it may be necessary to infer the kinematic porosity on the basis of DFN models of the flowing fractures. For the sake of the SDM, the kinematic porosity, n_e, was derived based on the underlying hydrogeological DFN calculated element-by-element as the total connected volume divided by the element volume. The fracture volume for an individual fracture was calculated as the fracture area within an element multiplied by the transport aperture, and this is modelled based on Äspö Task Force 6c results /Dershowitz et al. 2003/, which assumes a direct correlation between the transport aperture e_t and the transmissivity T, such that:

$$e_t = 0.46\ \sqrt{T} \tag{2-2}$$

Although this approach provides a direct link between the assignment of kinematic porosity in the ECPM model and the underlying DFN model, it relies on several approximations, including that the full fracture surface area contributes to advection and that the contribution to porosity of fractures below the truncation of fracture sizes in the regional DFN model is not significant. Hence, the derived kinematic porosity using Eq. (2-2) was used as an initial guess to the calibration, and adjustments were made as part of the calibration to help inform the description of the fracture transport properties.

2.3.7 Boundary and initial conditions

Mixtures of several types of so-called reference waters (end-member waters) are imagined to be present in the bedrock at Forsmark /SKB 2005d, Laaksoharju et al. 2008/. The chemical compositions of the reference waters (or end-members) handled at Forsmark are summarised in Table 2-3.

Table 2-3. Compilation of reference water compositions for Forsmark. (Modified after Table 1-1 in /Laaksoharju et al. 2008/.)

Reference water	Na mg/L	K mg/L	Ca mg/L	Mg mg/L	HCO_3 mg/L	Cl mg/L	SO_4 mg/L	Br mg/L	δ^2H ‰SMOW	$\delta^{18}O$ ‰SMOW
Deep Saline Water (DS)	8,200	45.5	19,300	2.12	14.1	47,200	10	323	–44.9	–8.9
Holocene Glacial Melt Water (HGM)	0.17	0.4	0.18	0.1	0.12	0.5	0.5	0	–158	–21
Littorina Sea Water (LS)	3,674	134	151	448	92.5	6,500	890	22.2	–37.8	–4.7
Present-day Meteoric Water (PM)	274	5.6	41.1	7.5	466	181	85.1	0.6	–80.6	–11.1

The reference waters can be associated with past climatic events during the Pleistocene, including inter-glaciations, glaciations, deglaciations, and associated changes in the shore level in connection with transgressions and regressions /Söderbäck (ed) 2008/. Among these, the last glaciation and the post-glacial period (the Holocene) are the most important for the current status of the groundwater composition in the Fennoscandian Shield, especially in terms of land uplift and shore level displacement, as well as the development of the Baltic Sea, see Figure 2-9 and Figure 2-10, respectively.

The notion of mixtures of different reference waters in the bedrock was derived by the chemists by analysing the hydrochemical information gathered in fractures and in the matrix according to a multivariate mixing and mass balance method (M3) /Laaksoharju et al. 1999/. The analyses presented in / Laaksoharju et al. 2008/ suggest that there must have been old meteoric waters derived from both warm and cold climate events in the bedrock in the Forsmark area before the injection of glacial melt water during the last deglaciation just prior to the Holocene. The importance of this working hypothesis for the integrated geological-hydrogeological-hydrogeochemical understanding is discussed in /Follin et al. 2008b/.

In the hydrogeological model, the transport of solutes was modelled in terms of the infiltration and mixing of several different reference waters that were assumed to be transported conservatively, i.e. without reaction, but subject to advection, dispersion, and diffusion in both the fracture water and the porewater (i.e. rock matrix diffusion). The palaeohydrogological simulations were started at 8000 BC and the development of the hydrochemistry was calculated according to the changes in sea level azimuth and salinity shown in Figure 2-9 and Figure 2-10. The chemical compositions of the reference waters were fixed in time. Therefore, given the simulated mixture of references waters (defined by the mass fraction) at any point in space and time, the concentrations of the major ions or environmental isotopes were calculated by multiplying the reference water fraction by the concentration of the component in that reference water and then summing over the reference waters. Finally, the predicted concentrations, or isotope ratios, were compared with the measured data as a means to meet Task D in Figure 2-2. The reference waters as such were not used in the calibration process.

The chemical compositions were calculated both for the mobile water in the fractures and the immobile porewater in the matrix. For simplicity, the simulated values of the porewater were essentially an average within the matrix blocks, although ConnectFlow stores internally the spatial variation of reference water fractions within the matrix blocks, which could be analysed should such detail be required. The spatial variations of concentration in the porewater between connected fractures are likely to be large at Forsmark since the spacing between water conducting fractures is large, at least at depth. Hence, it should be borne in mind that there may be trends within the porewater data according to where a sample was taken relative to water-bearing fractures that are as important as trends with respect to the absolute elevation of the sample, for example.

The assignment of initial hydrochemical conditions at the start of the simulation period are a vital part of the palaeohydrogeological model and the motives for the working hypothesis used in the SDM are discussed in detail in /Follin et al. 2008b/. In short, it was envisaged that the groundwater at depth in the Forsmark area at 8000 BC, i.e. before the percolation of *Littorina Sea (LS) Water*, was a mixture of *Deep Saline (DS) Water*, *Holocene Glacial Melt (HGM) Water* and remnants of *Old Meteoric and Glacial (OMG) Waters*, i.e. pre-Weichselian waters. This hypothesis allows for an explanation of the observed differences between the fracture water and the porewater with regard to Cl and $\delta^{18}O$ /Laaksoharju et al. 2008/. In the hydrogeological model, the hydrochemical composition of the composition of the pre-Weichselian waters was assumed to be identical to that of *Present-day Meteoric Water* (*PM*) with one exception – the concentration of bicarbonate of the *Old Meteoric and Glacial Waters* was assumed to be the same as for the *Holocene Glacial Melt Water*, cf Table 2-3.

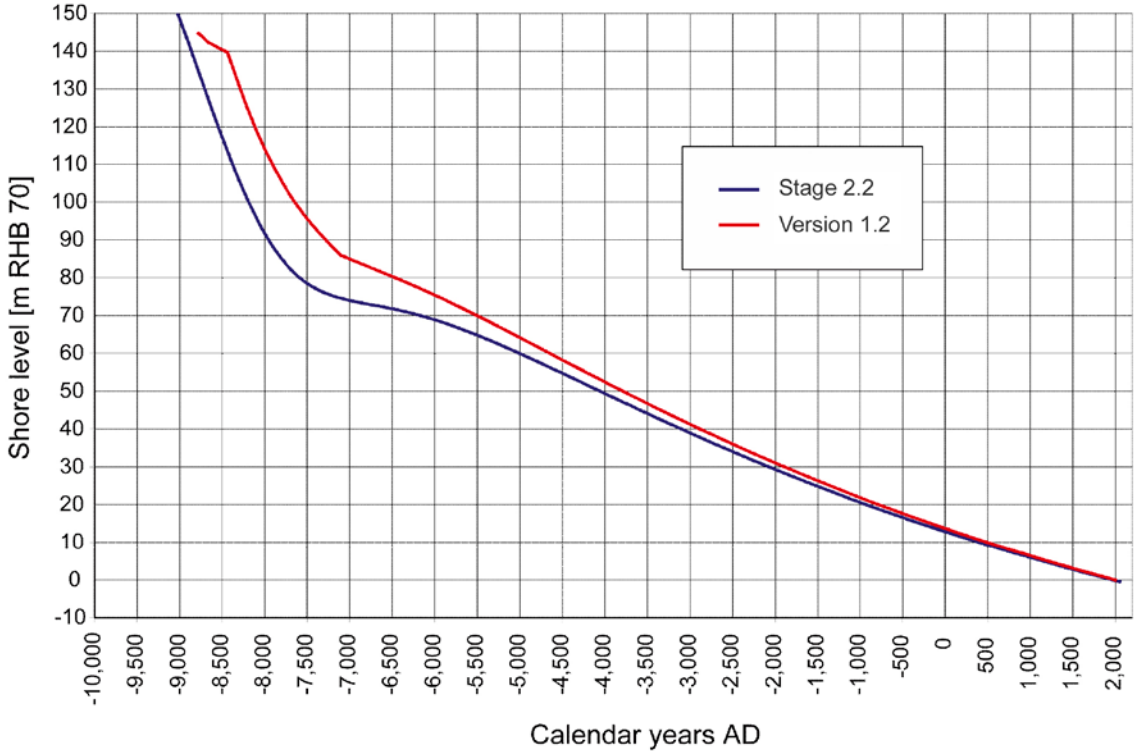

Figure 2-9. *Shore level displacement evolution close to Forsmark during Holocene time (8000 BC to 2000 AD). (Figure 3-55 in /Follin et al. 2007/). /*

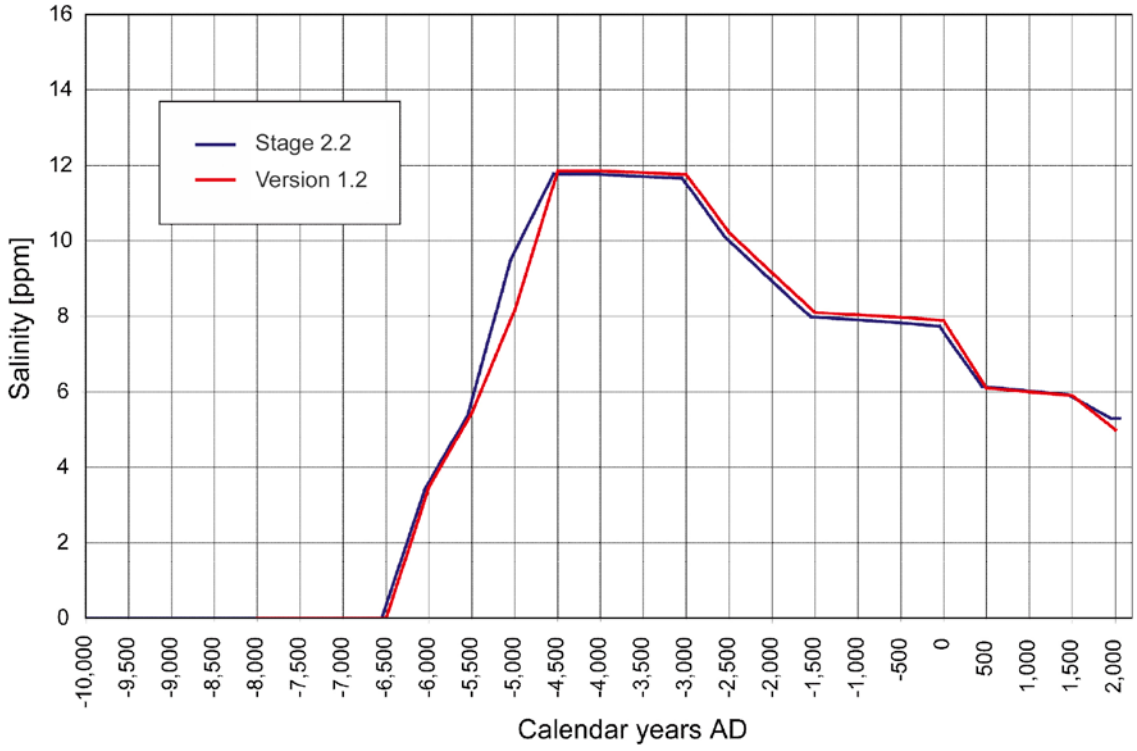

Figure 2-10. *Changes in the salinity of the Baltic Sea close to Forsmark during Holocene time (8000 BC to 2000 AD). (Figure 3-57 in /Follin et al. 2007/.)*

In summary, the transient conditions shown in Figure 2-9 and Figure 2-10 were used to specify the hydraulic and hydrochemical boundary conditions with time for those parts of the top boundary of the hydrogeological model that were covered by sea water. The terrestrial parts of the top boundary were assigned a specified flux that varied in space depending on the depth to the groundwater table, and a hydrochemical composition of the flux in the recharge areas according to suggested composition of the *Present-day Meteoric Water*, cf Table 2-3. A maximum value of the specified flux of 150 mm/y was used based on the results reported in /Johansson 2008/. All other sides of the hydrogeological model were assumed to be impervious (no-flow boundaries). However, on the bottom side of the hydrogeological model (elevation –1,200 m), the initial hydrochemical boundary conditions specified at 8000 BC were fixed at all times. It is noted that the initial hydrochemical conditions varied in space in relation to the variation in the geological and hydrogeological properties as inferred from the site investigations and the integrated modelling work, see Figure 2-11.

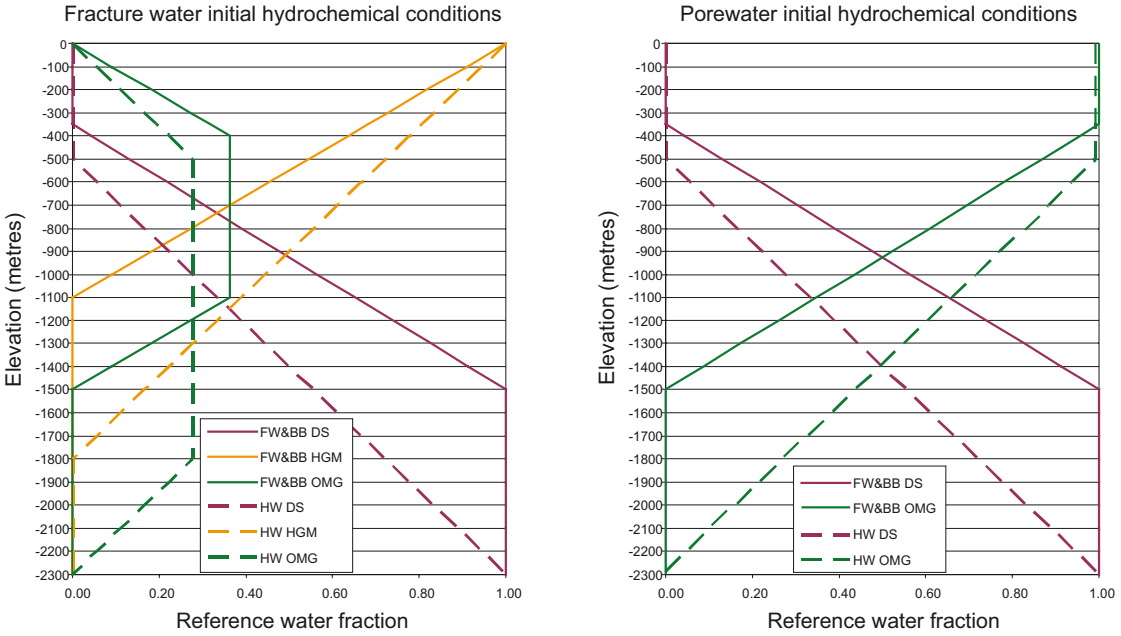

Figure 2-11. *Assumed initial hydrochemical conditions at 8000 BC. The elevation of the bottom boundary of the hydrogeological model in the SDM was set to –1,200 m. DS = Deep Saline Water, HGM = Holocene Glacial Melt Water, OMG = Old Meteoric-Glacial Waters. Different profiles were assumed for the footwall (FW) and bordering bedrock (BB) regions of deformation zone A2 compared to the hanging wall (HW) bedrock region of this zone, see chapters 3 and 1 for an explanation of these bedrock regions. (Modified after Figure 3-63 and Figure 3-67 in /Follin et al. 2007c/.)*

3 Geological conditions at Forsmark

3.1 Regolith geology

In the Forsmark area, all known regolith was deposited during the Quaternary period, thus generally referred to as Quaternary deposits. In addition, most of the Quaternary deposits at Forsmark were probably deposited during or after the latest deglaciation (Weichsel) /Hedenström and Sohlenius 2008/. Figure 3-1 shows the conceptual model of the stratigraphical distribution of the Quaternary deposits at Forsmark. The model consists of nine layers (L1–L3, Z1–Z6). Not all layers exist everywhere, and the thickness of individual layers varies significantly. The overall thickness of the Quaternary deposits varies from less than a decimetre to a maximum of 42 m /Hedenström et al. 2008/. The definition of the nine layers is shown in Table 3-1.

The conceptual model was developed for the area shown in Figure 3-2, which covers most of the site descriptive regional model area. The model was truncated in the south slightly more than in the regional-scale hydrogeological model. The interpreted thicknesses of the Quaternary deposits are also shown in Figure 3-2. The compilation of different kinds of data obtained from several types of investigations has produced this model. The accuracy of the map varies therefore and the most detailed information was obtained from the central part of the model area and in the near shore coastal area. The profile in Figure 3-2 shows the stratification of the Quaternary deposits layers beneath Lake Bolundsfjärden as an example.

3.2 Bedrock geology

3.2.1 Rock domain model

The bedrock in the Forsmark area is divided into rock domains referred to as RFM in SKB's 3D geometric modelling work and rock visualisation system (RVS). A rock domain refers to a rock volume in which rock units that show similar composition, grain size, degree of bedrock homogeneity, and degree and style of ductile deformation have been combined and distinguished from each other. Rock volumes that show early-stage alteration (albitisation) are also distinguished as separate rock domains. The modelling of the rock domains and their petrophysical properties, e.g. the porosity of fresh bedrock samples without visible fractures, are described in /Stephens et al. 2007/.

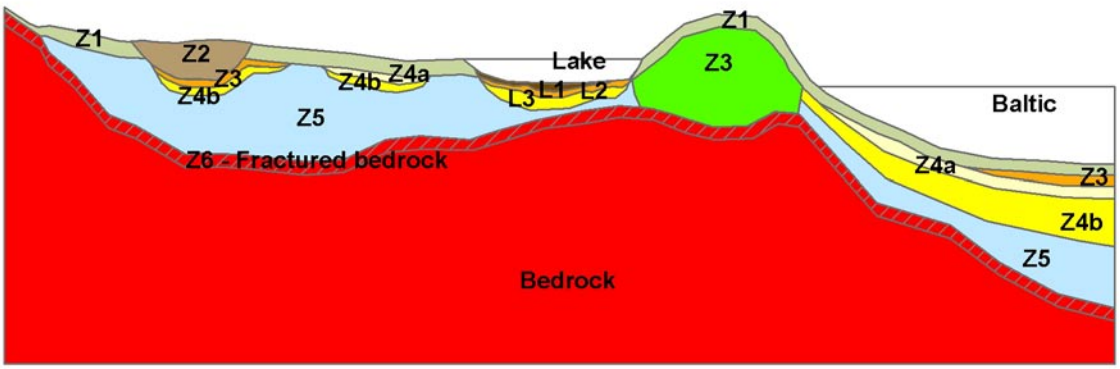

Figure 3-1. *Conceptual model for the layering of Quaternary deposits at Forsmark in stage 2.2. The different layers are explained in Table 3-1 (Figure 3-1 in /Hedenström et al. 2008/.)*

Table 3-1. Names and definition of Quaternary deposits layers. (Modified after Table 2-4 in /Hedenström et al. 2008/.)

Layer	Description and comments
L1	Layer consisting of different kinds of gyttja/mud/clay or peat. Is interpolated from input data, thickness will therefore vary.
L2	Layer consisting of sand and gravel. Is interpolated from input data, thickness will therefore vary.
L3	Layer consisting of different clay (glacial and postglacial). Is interpolated from input data, thickness will therefore vary.
Z1	Surface affected layer present all over the model, except where peat is found and under lakes with lenses. Thickness is 0.10 m on bedrock outcrops, 0.60 m elsewhere. If total regolith thickness is less than 0.60 m, Z1 will have the same thickness as the total, i.e. in those areas only Z1 will exist.
Z2	Surface layer consisting of peat. Zero thickness in the sea. Always followed by Z3.
Z3	Middle layer of sediments. Only found where surface layers are other than till, clay or peat.
Z4a	Middle layer consisting of postglacial clay. Always followed by Z4b.
Z4b	Middle layer of glacial clay.
Z5	Corresponds to a layer of till. No min or max range. The bottom of layer Z5 corresponds to the bedrock surface.
Z6	Upper part of the bedrock. Fractured rock. Constant thickness of 0.5 m. Calculated as an offset from Z5.

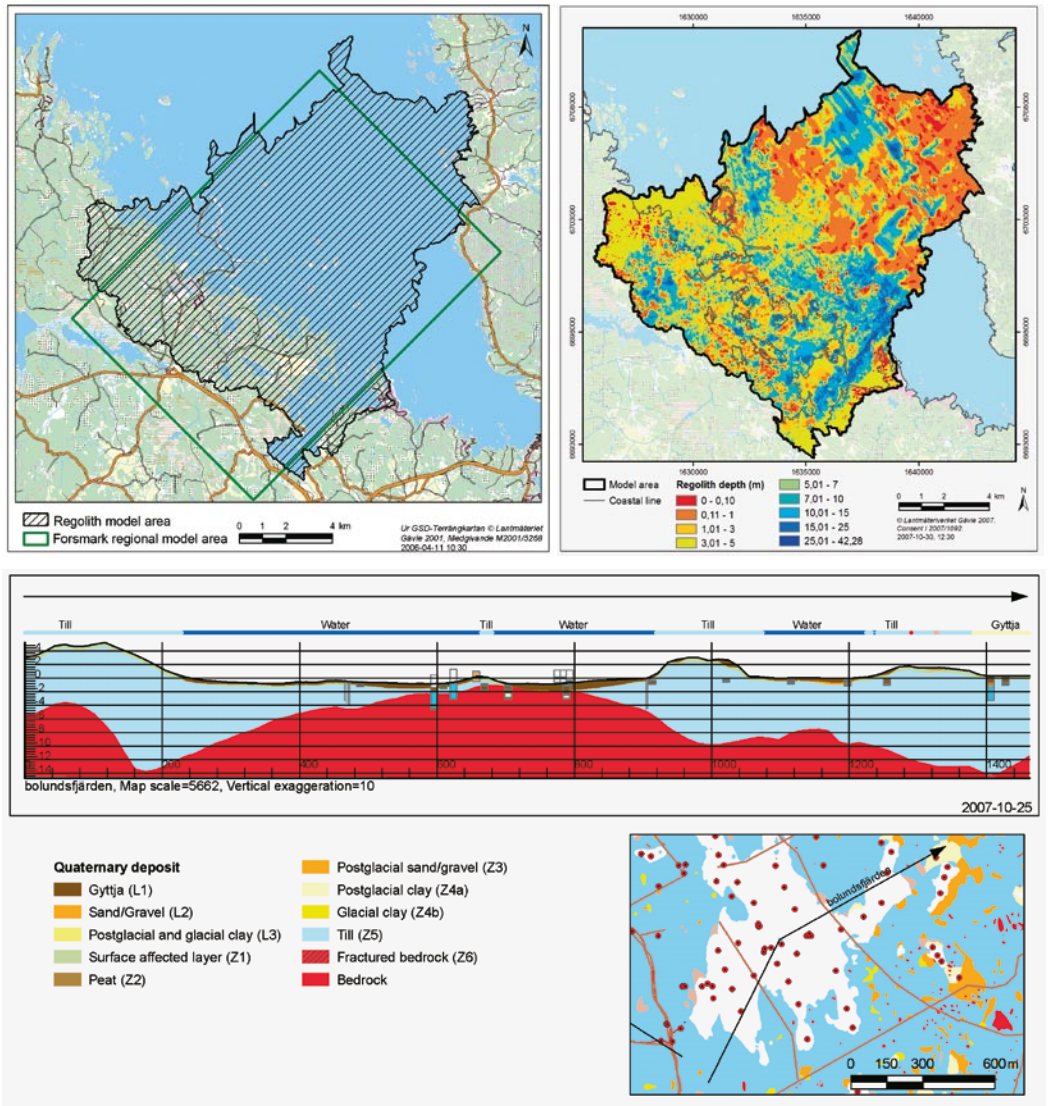

Figure 3-2. *Top left: Extent of the model of the Quaternary deposits in stage 2.2. Top right: Interpreted total thickness of the Quaternary deposits. Bottom: Example cross-section showing the interpreted stratification and thicknesses of the Quaternary deposits layers beneath Lake Bolundsfjärden. (Based on figures shown in Appendix 2 in /Hedenström et al. 2008/.)*

The candidate area at Forsmark is situated more or less exclusively inside a tectonic lens. Due to its internal homogeneity, most of the lens and, in particular, the north-western part can be described as two rock domains referred to as RFM029 and RFM045 (Figure 3-3). These are also the two domains that define the target volume (Figure 1-5).

3.2.2 Deformation zone model

A deformation zone is a general term referring to an essentially 2D structure along which there is a concentration of brittle, ductile or combined brittle and ductile deformation. The term fracture zone is used to denote a brittle deformation zone without any specification whether there has or has not been a shear sense of movement along the zone. A fracture zone that shows a shear sense of movement is referred to as a fault zone. Table 3-2 presents the terminology for brittle structures based on trace length and thickness.

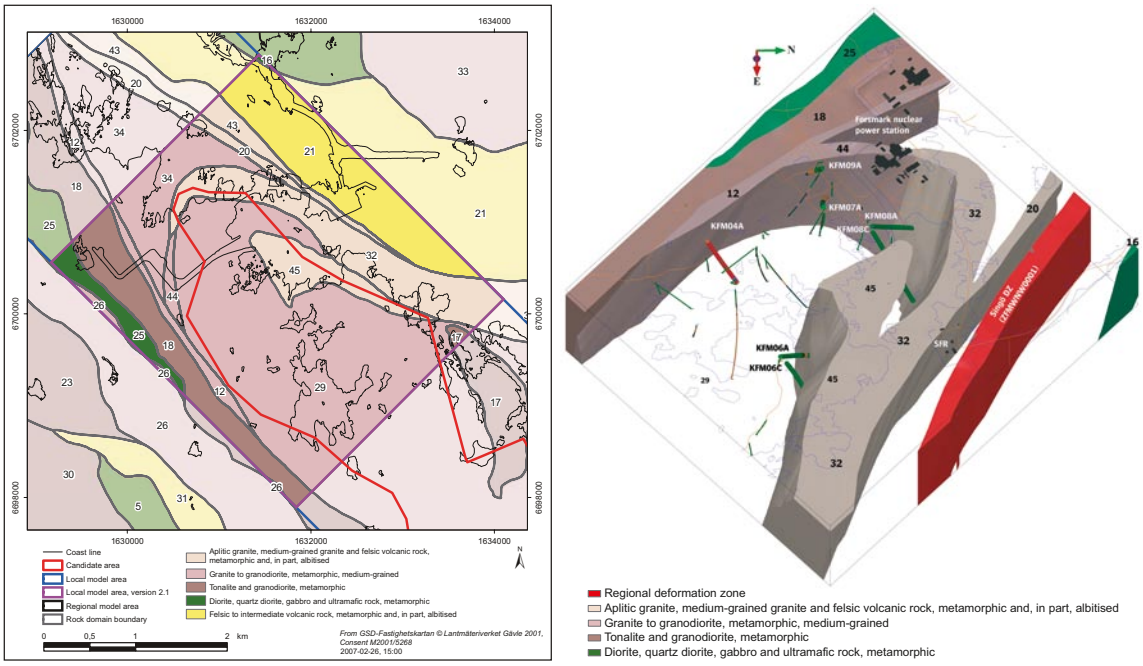

Figure 3-3. *Left: Rock domains within and close to the local model area. Right: The local model domain viewed to the west towards the SFR repository and the nuclear power station. RFM029 in the volume where most boreholes are present is transparent. (Figure 4-1 in /Olofsson et al. 2007/ and Figure 4-6 in /Stephens et al. 2007/.)*

Table 3-2. Terminology and general description (length and width are approximate) of brittle structures. (Modified after Table 4-1 in /Andersson et al. 2000/.)

Terminology	Length	Width	Geometrical description
Regional deformation zone	> 10 km	> 100 m	Deterministic
Local major deformation zone	1 km–10 km	5 m–100 m	Deterministic (with scale-dependent description of uncertainty
Local minor deformation zone	10 m–1 km	0.1–5 m	Statistical (if possible, deterministic)
Fracture	< 10 m	< 0.1 m	Statistical

The borderlines between the different structures are approximate. The three-dimensional block model described in /Stephens et al. 2007/ contains 103 deterministically modelled deformation zones. These are referred to as ZFMxxxx, where xxxx is an identification label. All but 11 of the 103 deformation zones have trace lengths longer than one kilometre, which implies that the block model, in principle, consists of regional and local major deformation zones, cf Table 3-2. The eleven deformation zones with trace lengths shorter than one kilometre are either a part (splay) of a nearby deformation zone longer than one kilometre, or gently dipping.

In addition to the 103 deterministically modelled deformation zones, /Stephens et al. 2007/ describe 28 minor deformation zones deterministically, i.e. deformation zones with trace lengths shorter than one kilometre. These are also referred to as ZFM, but *not* part of the 3D deformation zone block model. Finally, /Stephens et al. 2007/ discuss 43 so-called "possible deformation zones", i.e. borehole intervals with "deformation zone type properties". These are probably shorter than one kilometre, hence judged to be minor deformation zones, and not modelled deterministically.

Conceptually, the 28 minor deformation zones are no different than the possible deformation zones not modelled deterministically. Despite the conceptual inconsistency created, it was decided by the hydrogeological modelling group to incorporate the 28 deterministically modelled minor deformation zones in the deformation zone model used in the hydrogeological SDM. The motive for this decision is purely pragmatic; that is, it is better to use the geometrical data available than having them modelled as stochastic features. In effect, the deformation zone model for the hydrogeological SDM contains 131 deterministically modelled deformation zones.

Figure 3-4 shows a 3D visualisation of the 131 deformation zones modelled deterministically in the hydrogeological SDM for Forsmark stage 2.2. The steeply dipping deformation zones (107) are shaded in different colours and labelled with regard to their principle direction of strike. The gently dipping zones (24) are shaded in pale grey and denoted by a G. The inset shows the direction of the main principal stress, cf /Stephens et al. 2007/. All of the 28 minor deformation zones modelled deterministically by /Stephens et al. 2007/, but not included in the 3D DZ block model, occur inside the local model domain, see Figure 3-5. The local model domain encompasses the target volume defined in stage 2.1 /SKB 2006a/ hence investigated to a greater extent than the regional model domain. The bottom of the local model ends at the elevation –1,200 m, which means that it matches fairly well the maximum penetration depths of the deepest cored boreholes.

Table 3-3 shows a summary of the information presented above. We note in particular:

- 39 (28+11) deformation zones have trace lengths shorter than one kilometre and 45 deformation zones have trace lengths longer than three kilometres.
- 31 of the 103 deformation zones contained by the 3D deformation zone model occur inside the local model domain solely, 43 major deformation zones occur outside the local model domain solely and 29 major deformation zones occur both inside and outside. All of the 28 minor deformation zones modelled deterministically in the hydrogeological SDM are steeply dipping and occur inside the local model domain.
- There are 43 possible deformation zones identified in the geological single-hole interpretation but not modelled deterministically for Forsmark in stage 2.2; 34 of these intersect cored boreholes and nine the percussion-drilled holes.

The orientations of the 43 possible deformation zones not modelled deterministically may be tentatively estimated from the fracture poles. However, the lack of other strands of evidence to support a more deterministic interpretation implies that they, in theory at least, should be treated stochastically, i.e. as discrete fracture network (DFN) features.

Figure 3-6 shows three profile planes (cross-sections); one WNW-ESE cross-section along the central part of the candidate volume (cf. Figure 3-5), and two parallel WSW-ENE cross-sections in the eastern and central parts of the local model volume, respectively. Profile plane (c) in Figure 3-6 is shown in Figure 3-7. It is located 1,255 m north-west of cross-section (b) in Figure 3-6 and parallel.

The WNW-ESE cross-section demonstrates the significant structural difference in the deformation zone pattern on both sides of the gently dipping and sub-horizontal deformation zones A2 and F1, respectively. The bedrock above these zones is here referred to as the *hanging wall* and the bedrock below as the *footwall*. The hanging wall bedrock contains a number of gently dipping deformation zones, many of which extend down to one kilometre depth, or more. In contrast, there are less gently dipping zones in the footwall bedrock. The difference in the deformation pattern between the hanging wall and the footwall is steered by, among other things, the older anisotropy at the site, with gently dipping ductile structures and rock contacts in the south-eastern part of the candidate volume and more steeply dipping structures and contacts in the north-western part, in different parts of a major, sheath fold structure /Stephens et al. 2007/. It should be noted that the bedrock to the north-west of the steeply dipping deformation zone referred to as NE0065, both above and below zones A2 and F1, is intersected by a number of steeply dipping brittle deformation zones (fracture zones), many of which strike NNE and ENE. For purposes of simplicity, however, only the two zones that are included in the regional model are shown in Figure 3-6, i.e. ENE0060A and ENE0062A.

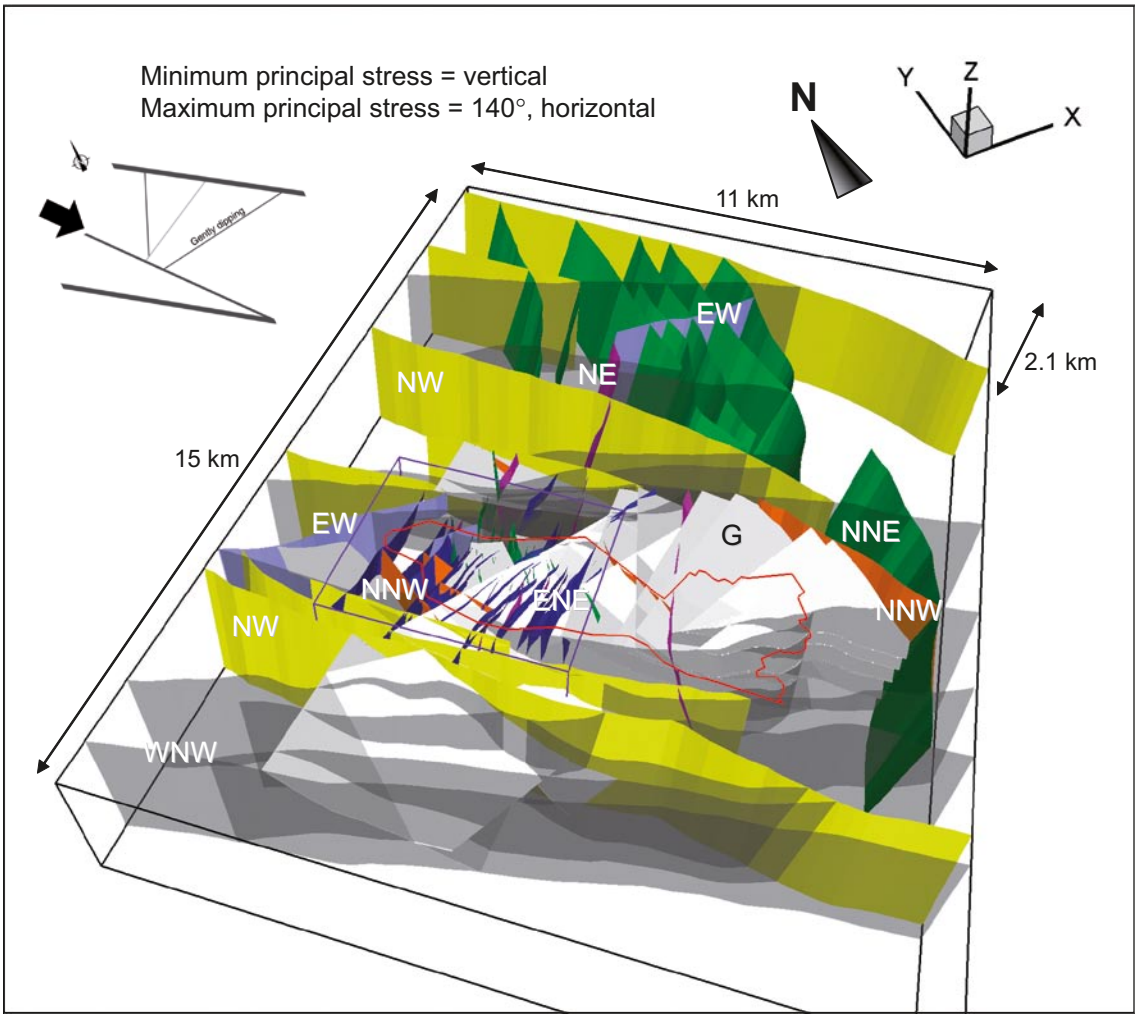

Figure 3-4. *3D visualisation of the regional model domain and the 131 deformation zones modelled deterministically for Forsmark stage 2.2 /Stephens et al. 2007/. The steeply dipping deformation zones (107) are shaded in different colours and labelled with regard to their principle direction of strike. The gently dipping zones (24) are shaded in pale grey and denoted by a G. The border of the candidate area is shown in red and regional and local model domains in black and purple, respectively. The inset in the upper left corner of the figure shows the direction of the main horizontal principal stress, σ_{1H}. (Modified after Figure 3-3 in /Follin et al. 2007b/).*

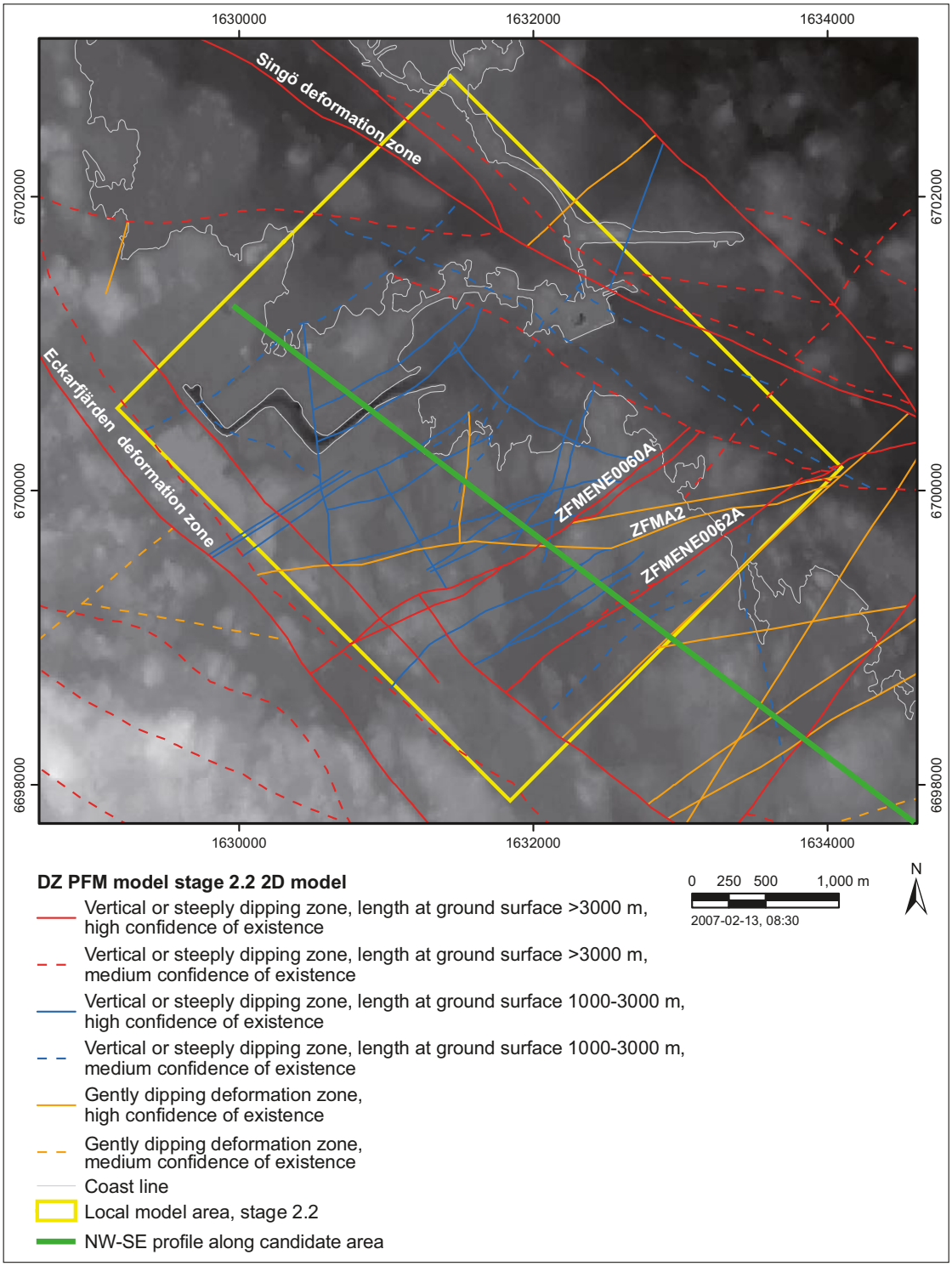

Figure 3-5. *Surface intersection of deterministic deformation zones in the local model. The background corresponds to the digital elevation model of the site. The 28 minor deformation zones modelled deterministically and included in the hydrogeological SDM have a green colour. The green line shows the position of the vertical profile shown in Figure 3-6. (Modified after Figure 5-10 in /Stephens et al. 2007/.)*

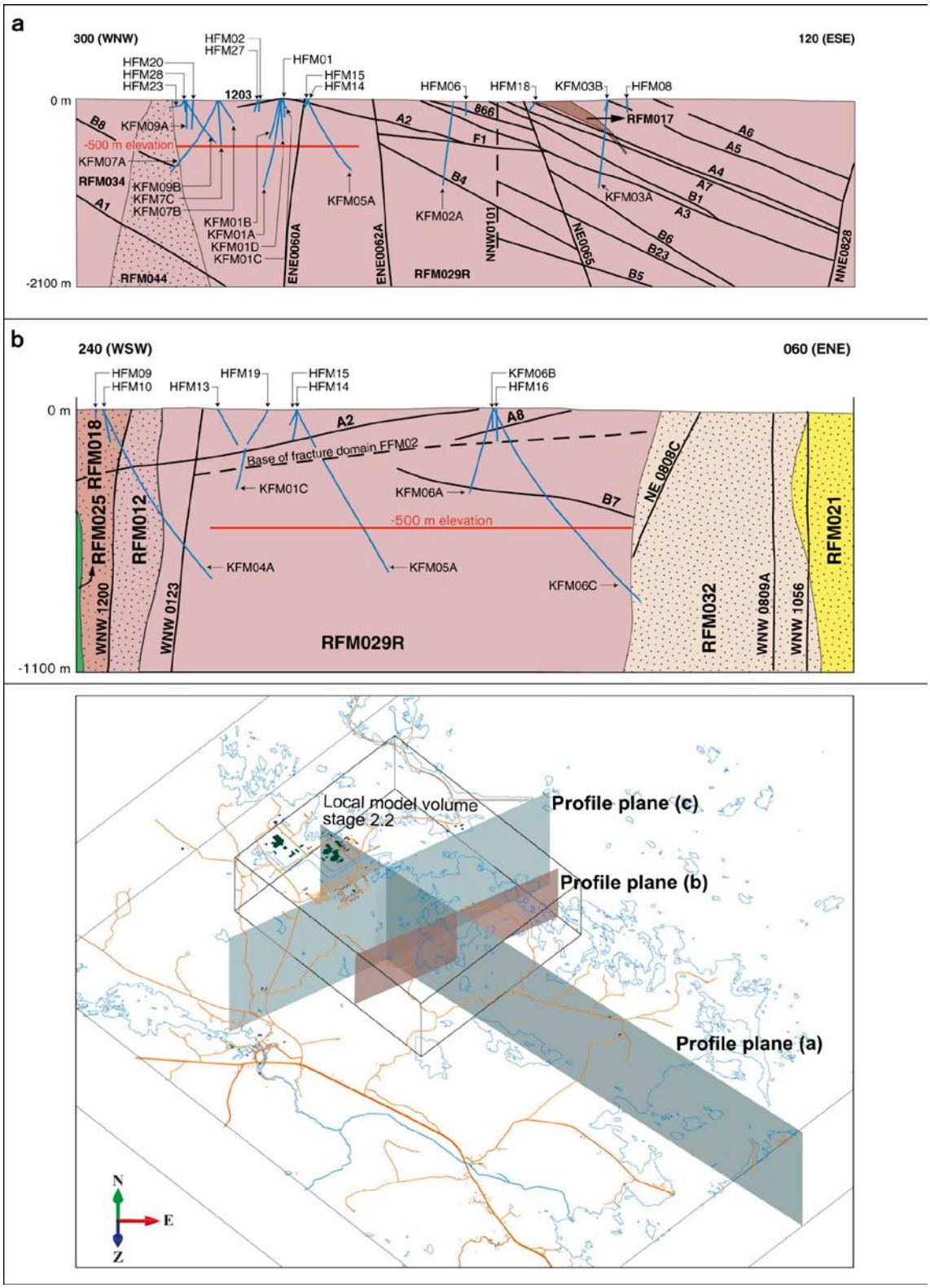

Figure 3-6. *Profile plane (a): A c 7 km long WNW-ESE cross-section along the central part of the candidate volume. Profile plane (b) A c 3 km long WSW-ENE cross-section along the south-eastern part of the local model volume. The important gently dipping deformation zones identified with reflection seismics are highlighted in these cross-sections. The bedrock above and below deformation zones A2 and F1 are referred to here as the hanging wall and the footwall, respectively. RFM029R is a regional rock domain. On a local scale RFM029R is split into the local rock domains RFM029 and RFM045 (cf. Figure 3-3). (Modified after Figure 5-21in /Stephens et al. 2007/.)*

Table 3-3. Summary of trace length data (L) for the deterministically modelled deformation zones tabulated with regard to orientation. Note that ten of the 24 gently dipping deformation zones do not outcrop. The two numbers separated by a slash in the second and fifth columns show the number of major and minor deformations zones, respectively. All minor deformation zones are steeply dipping and shorter than 1 km. The colours shown in the table correspond to the colours used in Figure 3-4. (Table 3-2 in /Follin et al. 2007b/.)

Orientation category	No. of DZ major/minor	No. of DZ L ≥ 3 km	No. of DZ 3 km > L ≥ 1 km	No. of DZ L < 1 km major/minor	No. of DZ Possible
G	24 / –	6	6	2 / –	17
WNW	23 / 1	15	7	1 / 1	3
NW	9 / –	9	0	0 / –	0
NNW	4 / 3	1	2	1 / 3	7
NNE	13 / 10	8	4	1 / 10	6
NE	4 / 6	2	1	1 / 6	0
ENE	24 / 7	2	17	5 / 7	9
EW	2 / 1	2	0	0 / 1	0
Total	103 / 28	45	37	11 / 28	42[1]

[1] One of the 43 possible deformation zones interpreted has no orientation data.

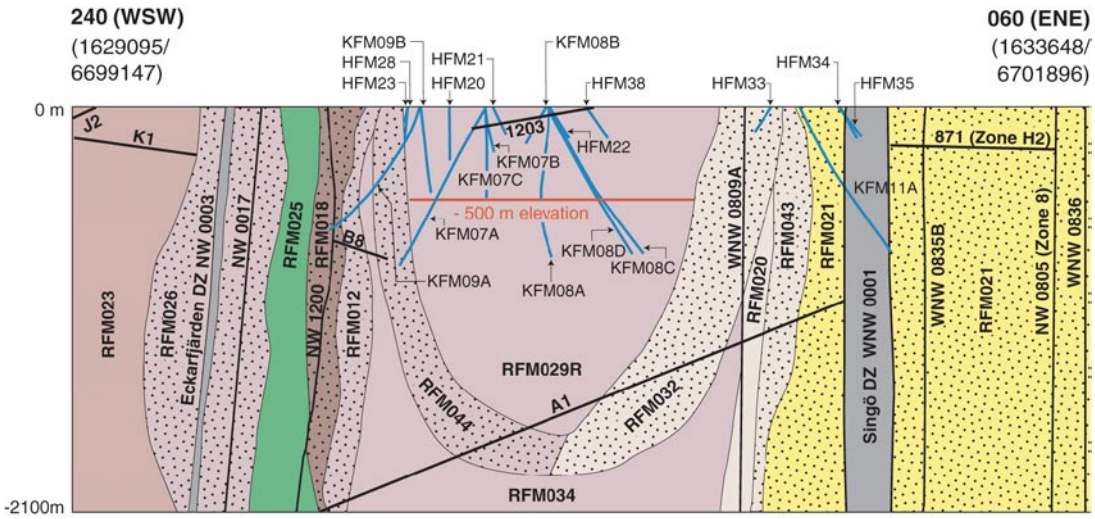

Figure 3-7. *Profile plane (c): A c 5 km long long WSW-ENE cross-section along the north-western part of the local model domain, see Figure 3-7. (Modified after Figure 5-41 in /SKB 2008b/.)*

The cross-section in Figure 3-7 is closer to the north-west boundary of the tectonic lens and visualises how the thickness and width of rock domain RFM029R narrow as the sheath fold structure gets steeper and the major Eckarfjärden and Singö deformation zones come closer to each other. The only major gently dipping deformation zone detected with reflection seismics in this part of the candidate volume is A1 (cf. profile plane (a) in Figure 3-6).

3.2.3 Fracture domain model

The fractured bedrock between the deterministically modelled deformation zones was divided into six fracture domains, FFM01–FFM06 based on the fracture frequency of *all* fractures, $P_{10,all}$. The geological modelling /Fox et al. 2007/ analysed several variants of discrete fracture network (DFN) models. The relationship between the geological DFN modelling and the hydrogeological DFN modelling are discussed in section 2.3.1 and in Appendix C.

Four of the six fracture domains outcrop, FFM02–FFM05, see Figure 3-8. The key fracture domains in the target area, FFM01 and FFM06 occur below fracture domain FFM02, see Figure 3-9. Figure 3-10 and Figure 3-11 visualise the geometry of fracture domains FFM01–FFM03 and FFM06. Fracture domain FFM01 dominates in the lowermost part of the target volume. The darker grey volume shows the position of fracture domain FFM06. The uppermost part of the bedrock, in the north-western part of the model, is fracture domain FFM02. This domain dips gently towards the south. Fracture domain FFM03 is situated directly above the gently dipping and sub-horizontal zones A2 and F1 at depth, and above domain FFM02 close to the surface. Fracture domains FFM04-FFM05 are not visualised in Figure 3-10 and Figure 3-11. FFM04–FFM05 occur in the bedrock bordering the target volume.

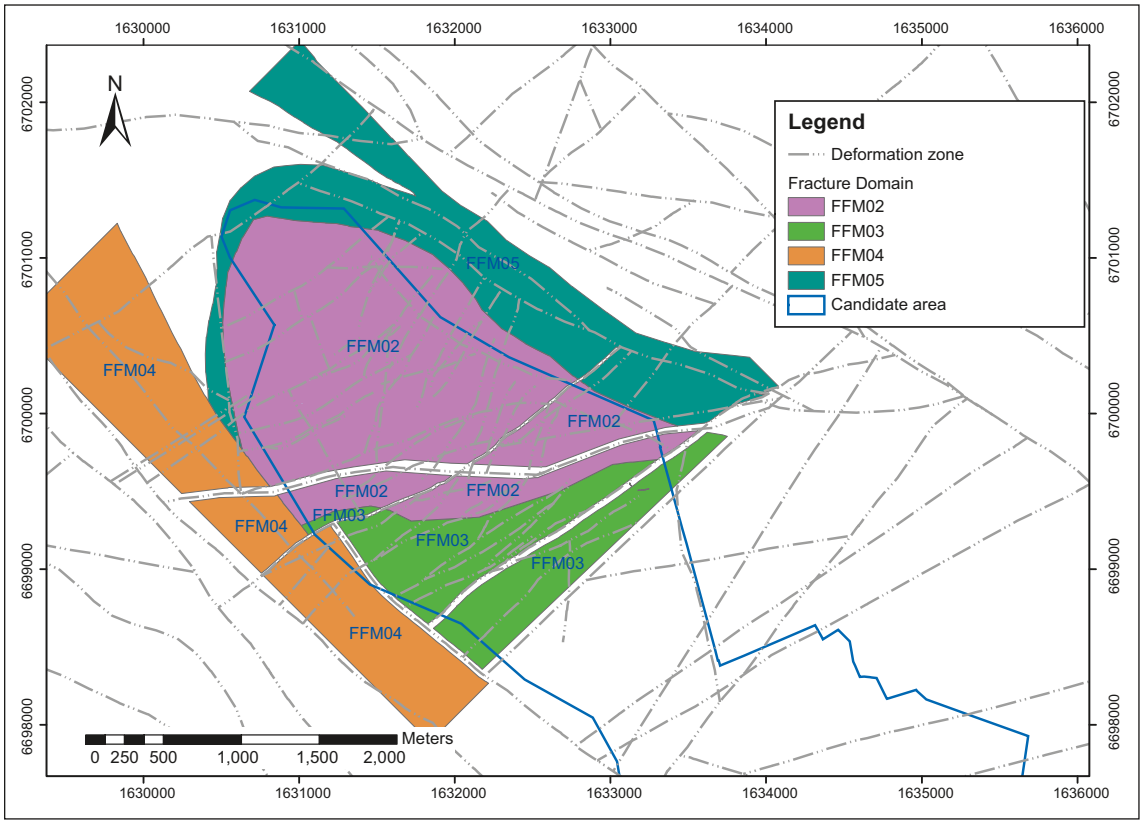

Figure 3-8. *Simplified horizontal slice at z = 0 showing outcropping fracture domains within the local model area for Forsmark stage 2.2. (Modified after Figure 1-2 in /Fox et al. 2007/.)*

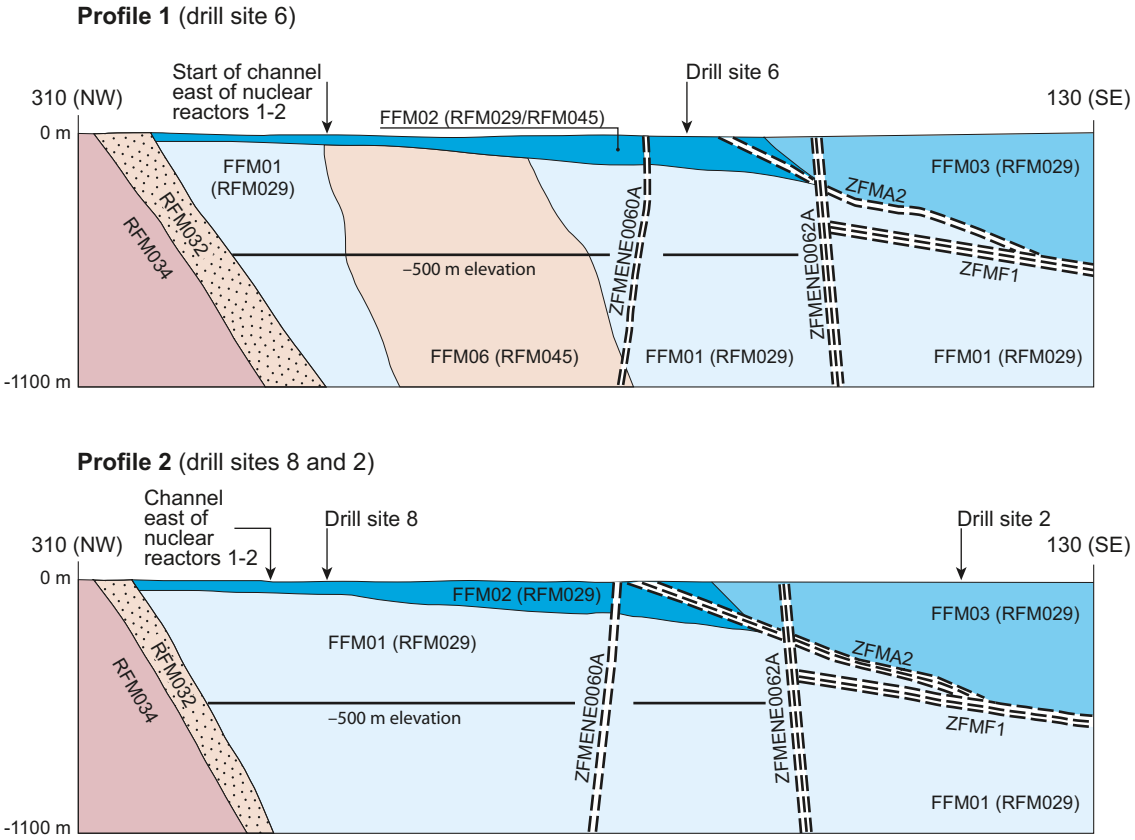

Figure 3-9. *Simplified profiles in a NW-SE direction that pass through drill sites 2 and 8 (lower profile) and drill site 6 (upper profile). (The profiles are shown in Figure 3-11.) The key fracture domains FFM01,-02 and -06 occur in the footwall of zones A2 (gently dipping) and F1 (sub-horizontal). The major steeply dipping zones ENE0060A and ENE0062A are also included in the profiles. (Figure 5-4 in /Olofsson et al. 2007/.)*

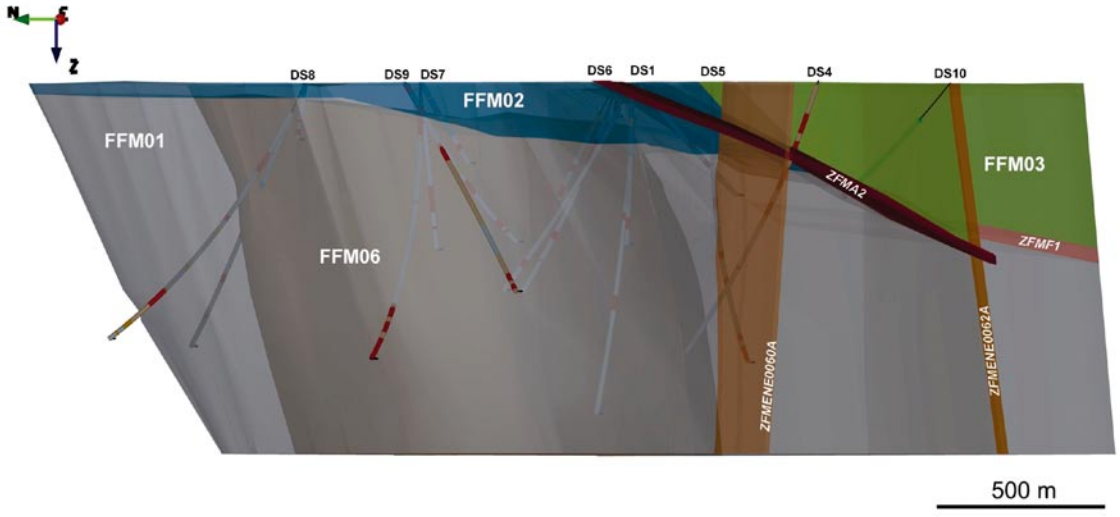

Figure 3-10. *Three-dimensional view of the fraction domain model, viewed towards the east-north-east. Fracture domains FFM01, FFM02, FFM03 and FFM06 are coloured grey, dark grey, blue and green, respectively. The gently dipping and sub-horizontal zones A2 and F1 as well as the steeply dipping deformation zones ENE0060A and ENE0062A are also shown. (Figure 5-7 in /Olofsson et al. 2007/.)*

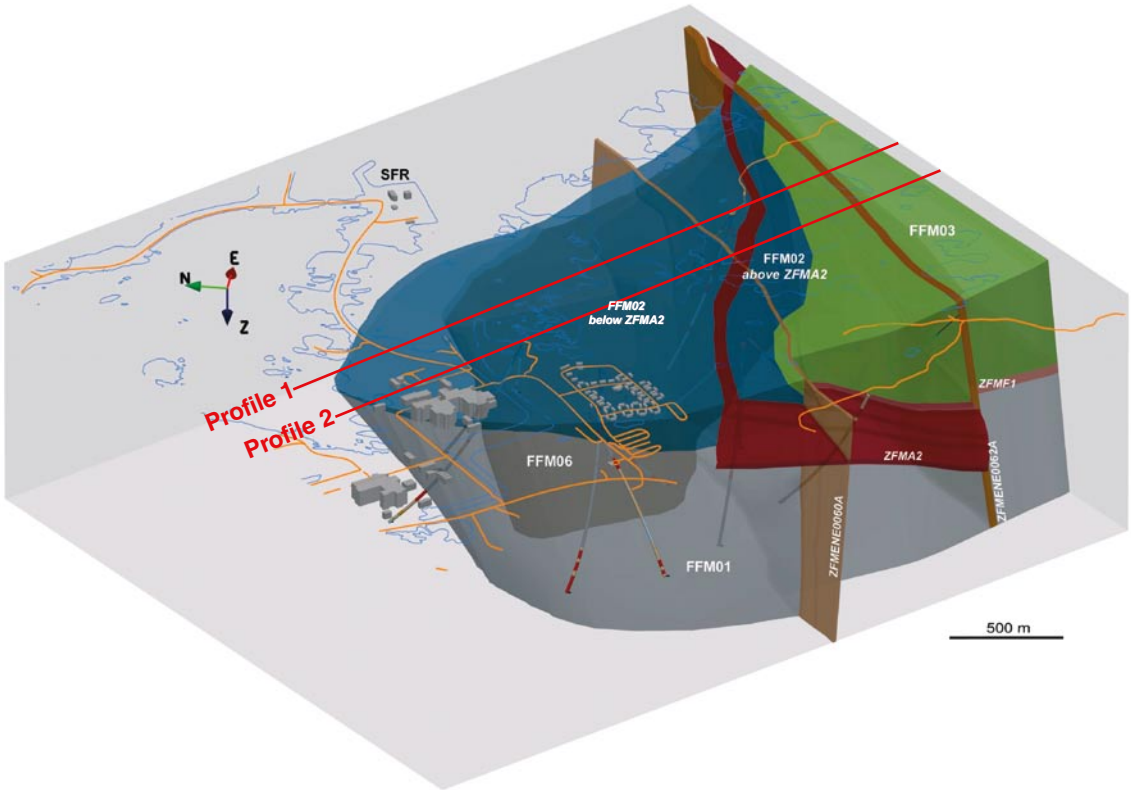

Figure 3-11. *Three-dimensional view to the east-north-east showing the relationship between deformation zone A2 (red) and fracture domain FFM02 (blue). Profile 1 and 2 are shown as cross-sections in Figure 3-9. (Modified after Figure 11-14 in /SKB 2008b/.)*

4 Evaluation of primary data

Appendix A provides an overview of the hydrogeological investigations performed at Forsmark and the data reports supporting the hydrogeological model development are listed in Appendix B.

A cornerstone of the bedrock hydrogeological description concerns the hydraulic characterisation of the more intensely fractured deformation zones and the less fractured bedrock in between. The adopted modelling approach combines a deterministic representation of the major deformation zones with a stochastic representation of the less fractured bedrock outside these zones using the discrete fracture network concept, see Figure 2-3.

4.1 Evaluation of single-hole tests

Figure 4-1 shows an example of the structural interpretation of a PFL-f transmissivity using the geometrical information visible in a so-called BIPS image. The PFL-f transmissivity where the open fracture intersects is $1.83 \cdot 10^{-7}$ m^2/s and the inferred strike, dip and aperture of the fracture are 101°, 12° and 3 mm, respectively. The assumption and uncertainties involved in the structural interpretations of PFL-f transmissivity data are explained in section 11.2.2 in /Follin et al. 2007b/ and the uncertainty regarding the meaning of the interpreted transmissivity value are addressed previously in section 2.3.4. In short, the structural interpretation of the PFL-f data is made in two steps:

1. To begin with, each PFL-f transmissivity value is associated with the nearest open fracture. How this interpretation work is carried out is described in /Forsman et al. 2004, Forssman et al. 2007, Teurneau et al. 2007/. In essence, the orientations of the PFL-f data are determined by comparing their positions in the boreholes with the positions of the open fractures identified during the core mapping (Boremap) and the viewer logging (BIPS).
2. Secondly, the orientated PFL-f transmissivities are categorised into fracture sets using the definitions derived in the geological DFN modelling in version 1.2. On a whole, the fractures sets reported in stage 2.2 in /Fox et al. 2007/ are very similar to the sets reported in version 1.2 in /La Pointe et al. 2005/, see Appendix C in /Follin et at. 2007c/. In summary, five fracture sets were used in the hydrogeological DFN modelling: NS, NE, NW, EW and HZ.

Figure 4-2 and Figure 4-3 show four examples of PFL-f transmissivity data and interpreted orientations from the core-drilled boreholes KFM01A–04A at drill sites 1–4 available for hydraulic parameterisation of deformation zones and fracture domains in version 1.2. Table 4-1 shows a summary of the PFL-f data available for hydraulic parameterisation of deformation zones and fracture domains in stage 2.2. Figure 4-4 shows an example of PSS hydraulic conductivity data from the core-drilled boreholes KFM03A and KFM03B at drill site 3, used for comparisons and consistency checks. The PSS tests are carried out with three different packer spacings, 5 m, 20 m and 100 m. The spatial resolution of the PFL-f method is 0.1 m.

4.2 Evaluation of cross-hole (interference) tests

The premises for disciplinary evaluation of hydraulic cross-hole (interference) tests in fractured crystalline rock are highly dependent on the structural geology, the hydraulic properties of the fracture system and the configuration of the data acquisition system. The structural-hydraulic conditions in the Forsmark area are exceptional in this regard, which has affected the bedrock hydrogeological modelling.

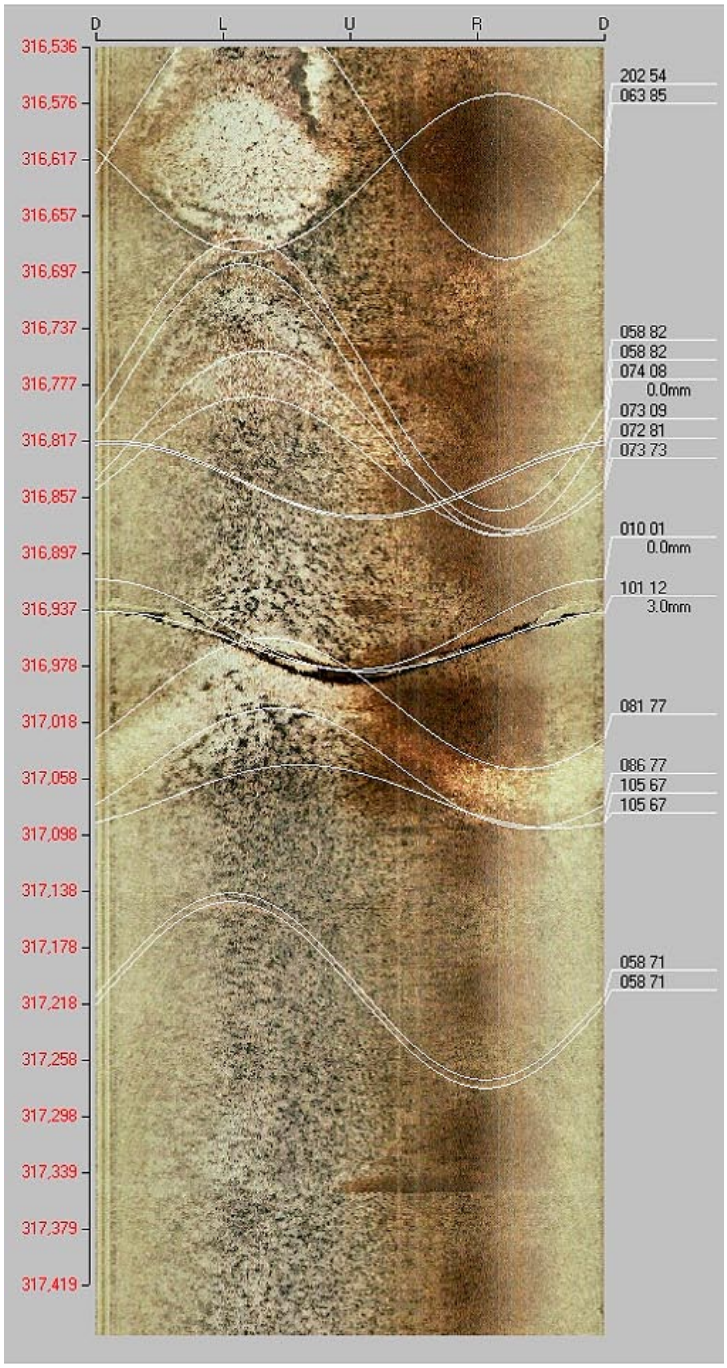

Figure 4-1. *Structural interpretation of PFL-f transmissivity no. 27 observed in borehole KFM01D at about 317 m borehole length. The transmissivity of the open fracture is $1.83 \cdot 10^{-7}$ m^2/s and the inferred strike, dip and aperture are 101°, 12° and 3 mm, respectively. (Modified after Figure 5-22 in /Follin et al. 2007b/.)*

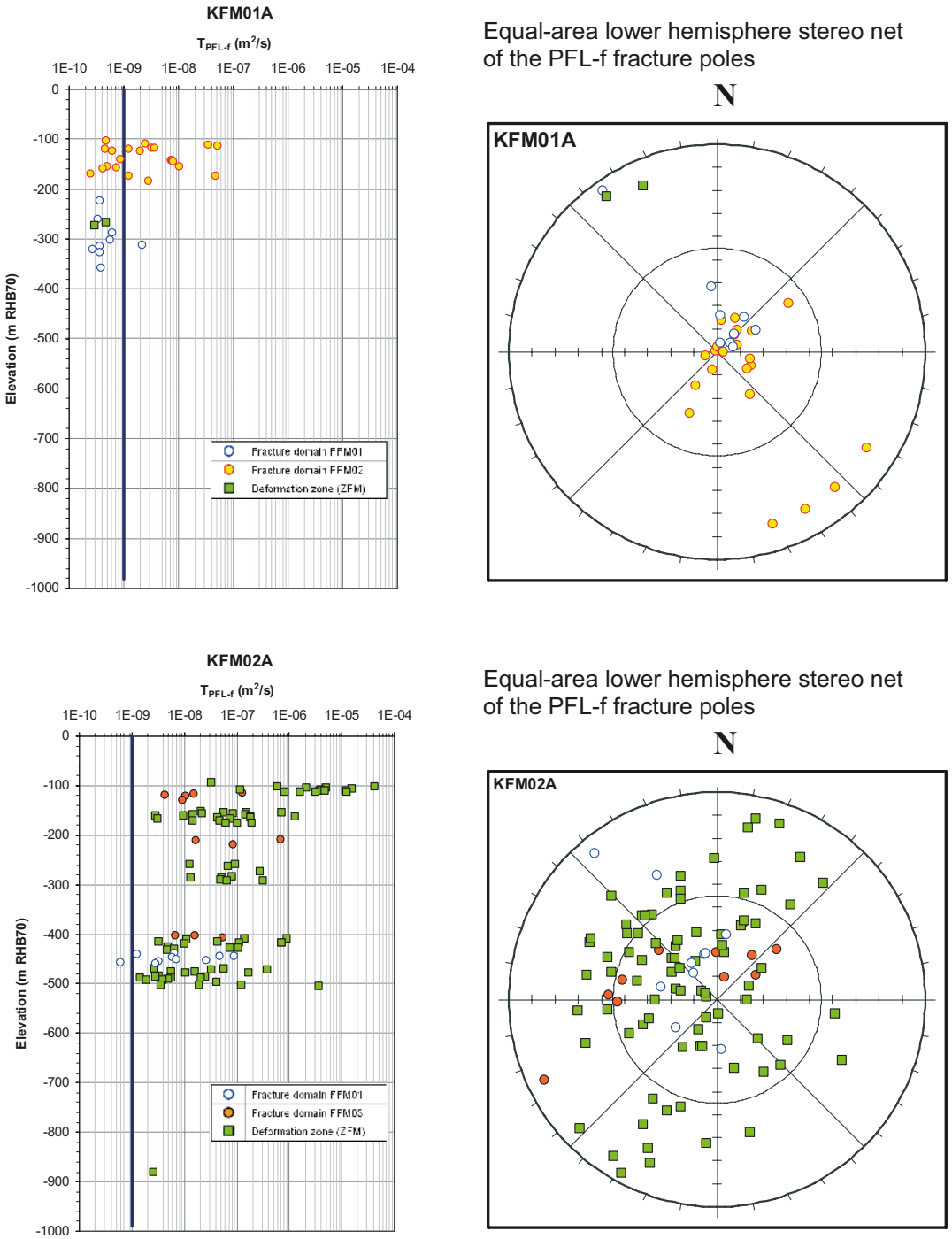

Figure 4-2. *Hydrogeological data in boreholes KFM01A and -02A. There are 32 PFL-f transmissivities associated with single fractures and two associated with one deterministically modelled deformation zone (2/1) in KFM01A. The corresponding figures for KFM02A are 22 and 82/6, respectively. The blue lines indicate the typical threshold value reported from the investigations in the Forsmark area, $1 \cdot 10^{-9}$ m^2/s. The lengths of the blue lines correspond to the depths investigated with the PFL-f method. (Modified after Figure 5-1 and Figure 5-3 in /Follin et al. 2007b/.)*

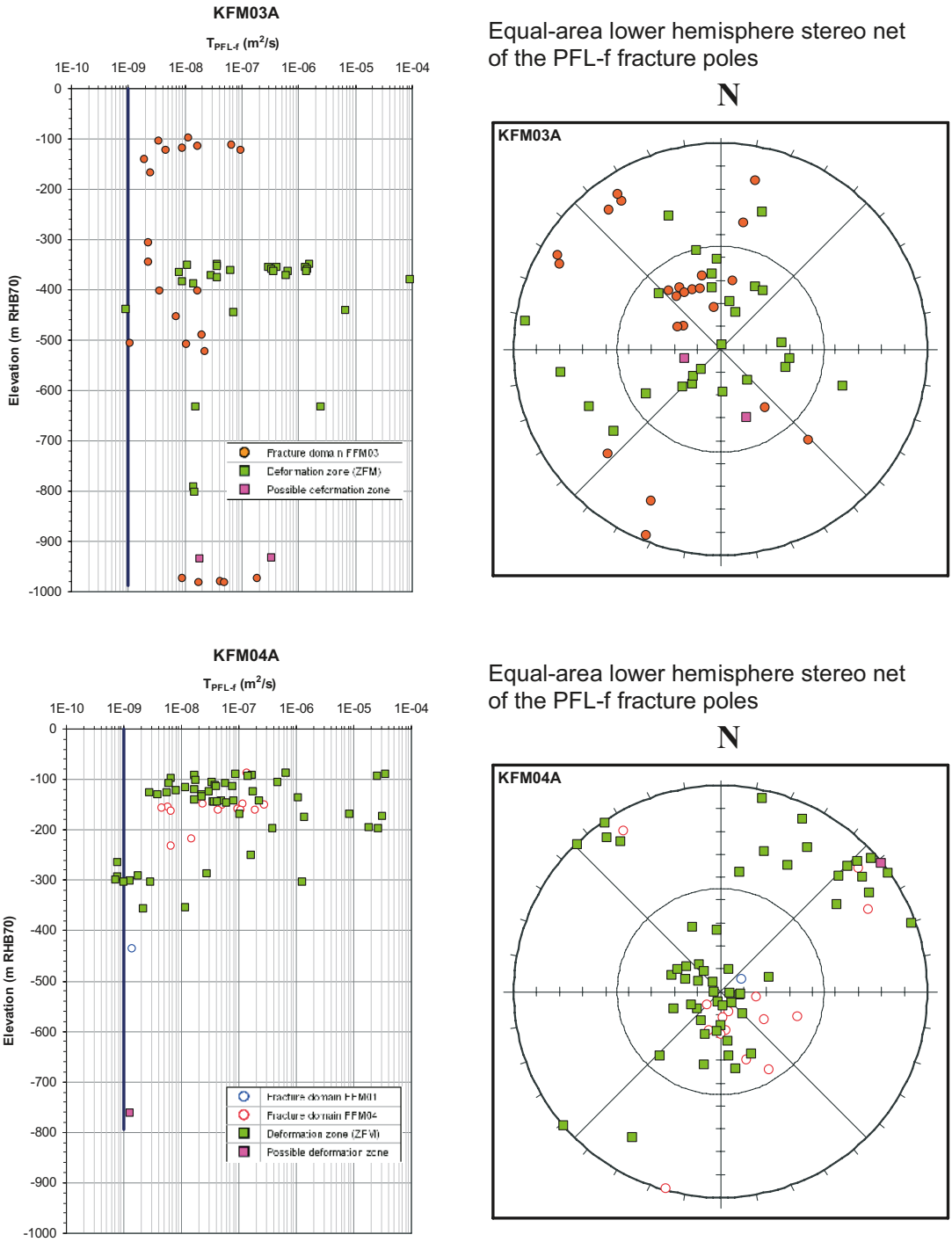

Figure 4-3. *Hydrogeological data in boreholes KFM03A and -04A. There are 23 PFL-f transmissivities associated with single fractures, 27 associated with four deterministically modelled deformation zones (27/4), and two associated with one possible deformation zone (2/1) in KFM03A. The corresponding figures for KFM04A are 16, 54/2, and 1/1, respectively. The blue lines indicate the typical threshold value reported from the investigations in the Forsmark area, $1{\cdot}10^{-9}$ m^2/s. The lengths of the blue lines correspond to the depths investigated with the PFL-f method. (Modified after Figure 5-4 and Figure 5-5 in /Follin et al. 2007b/.)*

Table 4-1. Summary of sample lengths and numbers of fractures according to different categories in each of the boreholes measured with the PFL-f method at the time of stage 2.2. Fractures that are judged to be open are assigned a confidence: certain, probable or possible. The number of PFL-f transmissivities in each borehole is also given. (Table 10-2 in /Follin et al. 2007b/.)

BH	Top [m]	Bottom [m]	Length [m]	Total number	Number of open (+partly)	Open & certain	Open & prob.	Open & poss.	Number of PFL-f transm.
KFM01A	102.67	993.49	890.82	1,517	752	174	143	435	34
KFM01D	91.67	799.62	707.95	1,636	468	99	178	191	34
KFM02A	101.54	1,000.36	898.82	2,199	443	152	267	24	104
KFM03A	102.45	999.67	897.22	1,825	375	146	137	92	52
KFM04A	109.1	985.07	875.97	4,327	1,357	257	630	470	71
KFM05A	102.27	999.62	897.35	2,838	633	91	180	362	27
KFM06A	102.21	997.37	895.16	3,680	816	172	235	409	99
KFM07A	102.04	993.77	891.73	3,183	617	103	162	352	26
KFM07C	98.62	498.67	400.05	1,765	285	78	116	91	14
KFM08A	103.36	949.67	846.31	4,268	713	149	210	354	41
KFM08C	102.29	948.99	846.70	4,198	676	56	199	421	21
KFM10A	62.86	499.98	437.12	2,755	999	264	299	436	54
All BH			**9,485.20**	**34,191**	**8,134**	**1,741**	**2,756**	**3,637**	**577**

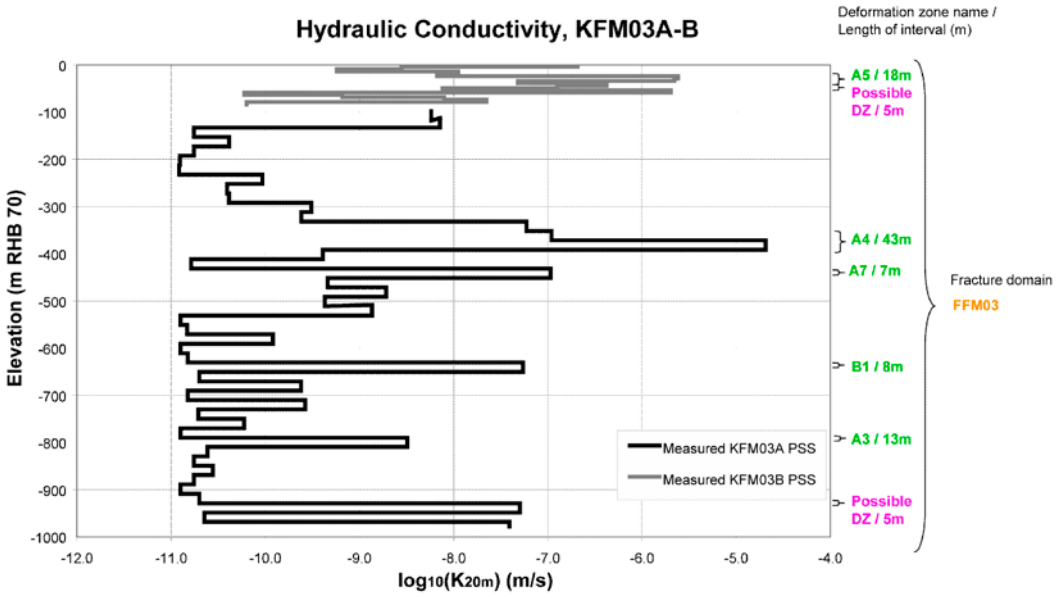

Figure 4-4. *Hydraulic conductivity data in KFM03A and KFM03B evaluated from PSS transmissivity measurements using a 20 m long test section. The typical transmissivity threshold of the PSS method is about $7 \cdot 10^{-10}$ m²/s, which corresponds to a threshold of about $3 \cdot 10^{-11}$ m/s in terms of a 3D hydraulic conductivity on a 20 m support scale. (Modified after Figure 4-1 in /Follin et al. 2007c/.)*

A summary of the test configuration used and the analyses undertaken for one of the most important large-scale interference test conducted within the target area during the CSI phase, the year 2006 interference test in borehole HFM14 at drill site 5, is provided in /Follin et al. 2007c/. The interference test was performed by pumping with a flow rate of about 350 L/min. The groundwater levels were monitored at 105 observation sections in 36 observation boreholes. Twelve of the 36 boreholes were core-drilled with a total of 55 monitoring sections. 24 boreholes were percussion-drilled with a total of 50 monitoring sections. For each observation section, the estimated drawdown was supplied as a time-series over the 21 days of pumping. The hydraulic analyses comprised hydraulic diffusivity estimations, boundary condition interpretations, comparisons with a simplified 2D analytical solution and detailed 3D numerical flow simulations. Figure 4-5 shows a simplified 2D view of the monitoring network used during the year 2006 interference test in HFM14 together with response times corresponding to a drawdown of 0.01 m. Figure 4-6 shows the final drawdowns after 21 days of pumping.

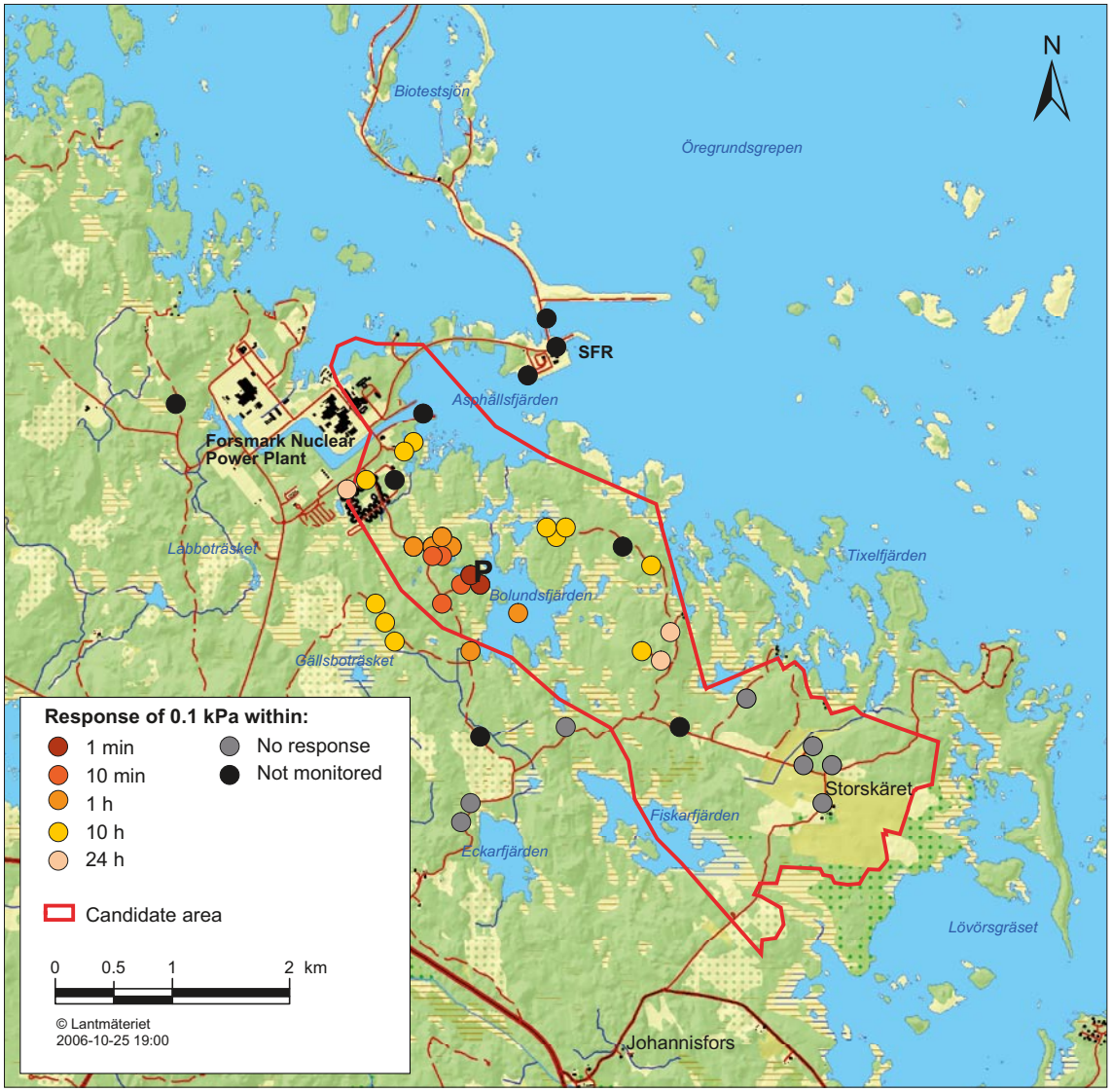

Figure 4-5. *Map showing response times in the bedrock to the three-weeks long interference test conducted in HFM14 (P) at drill site 5 during the dry summer of 2006. Clear test responses were observed in 71 out of a total of 110 monitoring sections. The maximum radius of influence was about 1.8 km. (Figure 3-28 in /Follin et al. 2007c/.)*

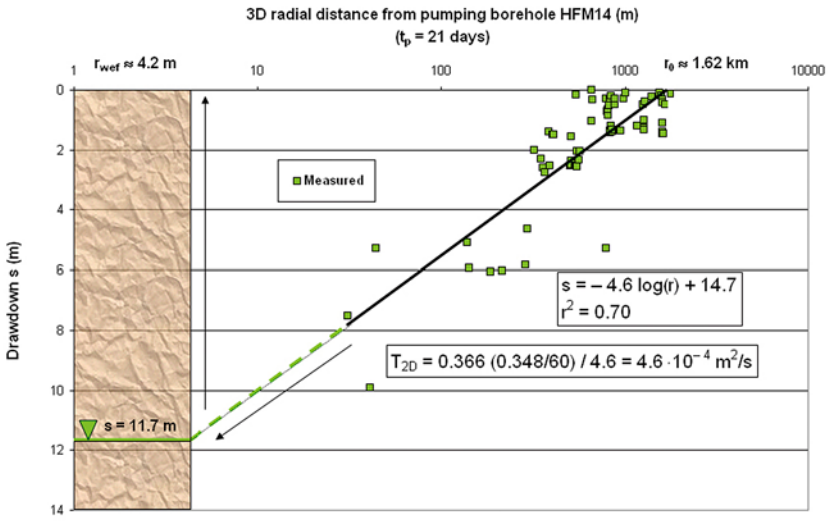

Figure 4-6. *Plot of measured drawdowns vs. log(3D radial distance) at the end of the 21-day long interference test in HFM14. The drawdown in HFM14 was 11.7 m and the flow rate was 348 L/min implying a specific capacity of approximately $5 \cdot 10^{-4}$ m^2/s. The black line shows a least-square fit to the measurements. The value of the correlation coefficient (r^2 = 0.70) indicates a heterogeneous system. A steady state, radial flow approximation using the slope of the least-squares fit for an estimate of Δs (difference in drawdown per log cycle of distance) renders a large-scale effective transmissivity of $5 \cdot 10^{-4}$ m^2/s. An extrapolation of the regression model to 11.7 m suggests an effective radius of HFM14 of about 4 m, which corresponds to a negative skin of about –4.1. (Figure 3-30 in /Follin et al. 2007c/.)*

Although the spatial distribution of the abstraction flow rate is governed by the structural-hydraulic properties of the fracture system and its hydraulic contact with the near-surface hydrogeological and hydrogeological system (the groundwater in the Quaternary deposits and the surface waters), it is feasible to estimate the hydraulic diffusivity, $\alpha = r_s^2 / dt_s$ where r_s is the 3-D radial distance in metres between the pumped borehole section and the monitoring interval and dt_s is the effective hydraulic response time in seconds. According to /Streltsova 1988/, dt_s may be written as:

$$dt_s = [4\, dt_L\, (1 + dt_L / t_p) \ln (1 + t_p / dt_L)] \quad (4\text{-}1)$$

dt_L = measured response time (s)

t_p = duration of the pumping (s)

For a confined and homogeneous radial flow system, the hydraulic diffusivity is defined as the ratio of the transmissivity to the storativity, $\alpha = T / S$. The hydraulic diffusivity in porous media is typically in the range 0.1–10 m^2/s. Values for fractured rocks are rare in the literature. /Rhén et al. 2008/ suggest that the hydraulic tests conducted at Laxemar indicate that $S = 1.1 \cdot 10^{-2}\, T^{0.71}$, which implies a similar range of the α value as above. The hydraulic diffusivities inferred at Forsmark are discussed in section 5.5.

4.3 Evaluation of hydrochemistry

It has been suggested that an understanding of the evolution throughout geological time is a powerful tool to predict the future development of groundwater flow and its chemical composition, see e.g. /NEA/OECD 1993, Bath and Lalieux 1999/. Testing and developing tools for coupled hydrogeological-hydrochemical modelling over time was also the focus of an international project referred to as *Task 5*, which was based on multidisciplinary data from the Äspö Hard Rock Laboratory in Sweden /Laaksoharju and Wallin (eds) 1997, Wikberg 1998, Rhén and Smellie 2003/.

Conceptually, the different reference water types discussed in section 2.3.7 together reflect important aspects of the geological evolution, the changes in the palaeoclimate and the historic development of the hydrological conditions. However, it is emphasised that the focus on mixing rather than on chemical reactions as a dominant process for the present-day hydrochemical conditions in low-temperature, fractured crystalline bedrock is a working hypothesis of the hydrogeological modelling work mainly. The hydrochemical modelling work /Laaksoharju et al. 2008/ is more diversified.

Reactions involving ion exchange and microbiologically mediated processes clearly affect the composition of the listed non-conservative constituents and may mislead the interpretation of the physical system studied, if mixing alone is assumed for model calibration /Laaksoharju et al. 2008/. Nevertheless, magnesium, for instance, which is a reactive cation, has been an excellent qualitative indicator in distinguishing between marine versus non-marine saline water conditions /SKB 2005a, 2006b/.

The strong correlation between geological-hydrogeological-hydrochemical data evident from the multidisciplinary modelling undertaken in previous model stages /SKB 2005a, 2006a/ is key to the hydrogeological conceptual modelling in general and to the long-term groundwater flow and solute transport modelling in particular /Follin et al. 2008b/. Table 4-2 shows a summary of the constituents and boreholes considered in the model calibration reported here. Figure A-1 and Figure A-2 in Appendix A show the location of the boreholes of interest.

The key chemical constituents considered in the hydrogeological modelling work are Cl, Br, $\delta^{18}O$ and $\delta^{2}D$, which may perhaps be considered to be transported more conservatively than many other constituents, for instance Mg, HCO_3 and SO_4. The Br/Cl ratio was used to indicate the transition zone from *Littorina Sea Water* to *Deep Saline Water*. The environmental isotopes δD and $\delta^{18}O$ help to differentiate between *Holocene Glacial melt Water* and meteoric reference waters such as *Old Meteoric-Glacial Waters* and *Present-day Meteoric Water*.

In general, the size of the hydrochemical database has increased significantly since the preliminary site description. In particular, this concerns matrix porewater data, see Table 4-3, which were not available in the preliminary site description. However, in terms of reliable fracture water data at depth, the amount of high quality hydrochemical data available for palaeohydrogeological modelling is still very limited (30 fracture water samples).

Table 4-2. Coverage of hydrochemistry data in the boreholes used as calibration targets in the hydrogeological modelling work. (Modified after Table 4-1 in /Follin et al. 2007c/.)

Name	Salinity	Major ions	Isotopes	Water types	Porewater	Highest / lowest elevation (m RHB 70)
KFM01A	Yes	Yes	Yes	Yes	–	–47 / –176
KFM01B	Yes	Yes	Yes	Yes	–	–37 / –37
KFM01D	Yes	Yes	Yes	Yes	Yes	–156 / –445
KFM02A	Yes	Yes	Yes	Yes	–	–52 / –962
KFM03A	Yes	Yes	Yes	Yes	–	–137 / –978
KFM04A	Yes	Yes	Yes	Yes	–	–11 / –197
KFM05A	Yes	Yes	Yes	Yes	–	–90 / –90
KFM06A	Yes	Yes	Yes	Yes	Yes	–15 / –645
KFM07A	Yes	Yes	Yes	Yes	–	–316 / –760
KFM08A	Yes	Yes	Yes	Yes	–	–564 / –648
KFM08C	–	–	–	–	Yes	–
KFM09A	Yes	Yes	Yes	Yes	–	–56 / –614
KFM09B	Yes	Yes	Yes	Yes	Yes	–65

Table 4-3. Coverage of the matrix porewater data as used in the hydrogeological flow modelling. (Table 4-4 in /Follin et al. 2007c/.)

Borehole ID	Number of samples for each component			Depth interval (m RHB 70)
	Cl	δD	$\delta^{18}O$	
KFM01D	14	13	13	–112 to –603
KFM06A	20	–	–	–126 to –865
KFM08C	10	8	8	–131 to –771
KFM09B	8	3	3	–436 to –445

4.4 Evaluation of groundwater levels

Seasonal changes in surface water levels and groundwater levels are of interest for the conceptual modelling of hydraulic gradients, the identification of recharge and discharge areas and the calibration of hydrogeological models. Transient changes in the surface water and groundwater levels during drilling and interference tests are of interest for the interpretation of the hydraulic properties of geological structures and for model calibration.

The surface water and groundwater levels at Forsmark are monitored by means of calibrated pressure transducers. The levels are corrected for barometric changes and expressed in length units (m) in relation to RHB 70 for the prevailing salinity and temperature conditions. The data recorded are best envisaged as point water heads /Lusczynski 1961/, see Figure 4-7. Figure 4-8 shows the principle of point water head measurements with a multipacker system. At Forsmark, the monitored intervals along the deep, cored boreholes generally have different fluid salinities and temperatures. Hence, the fluid density and viscosity varies in space. Vertical gradients of flow in the bedrock in close proximity to the borehole can be discussed provided that the point water heads are transformed to environmental water heads.

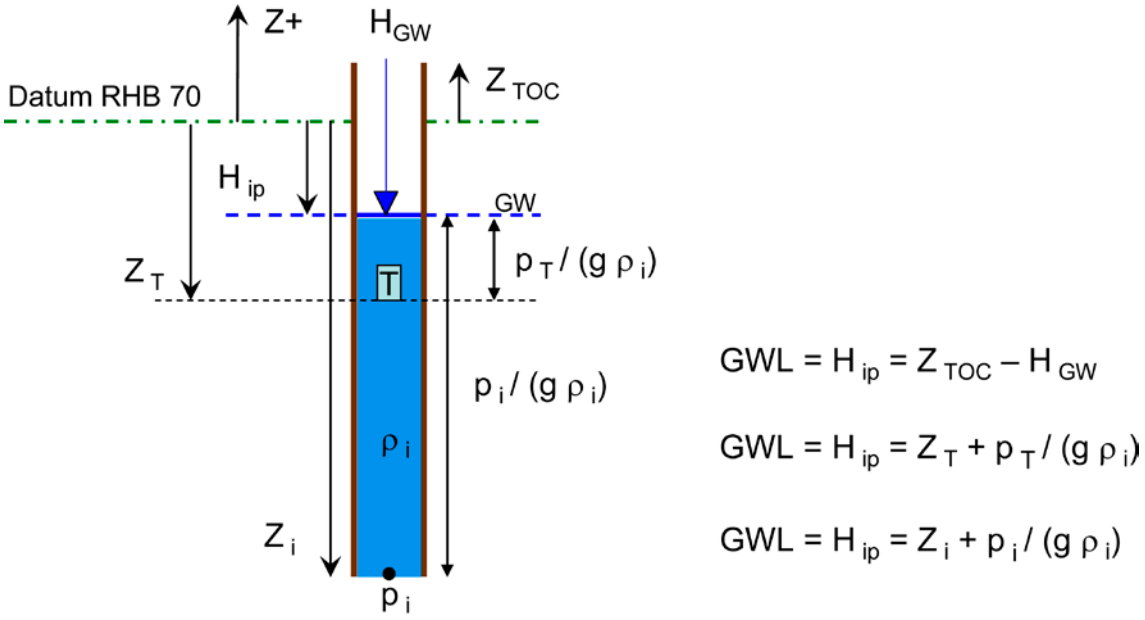

Figure 4-7. *The definition of groundwater level (GWL) in a borehole filled with a fluid of constant density ρi. The weight of the column balances the fluid pressure pi at the point i in the borehole were the water enters. TOC = top of casing. (Figure K-1 in /Follin et al. 2007c/.)*

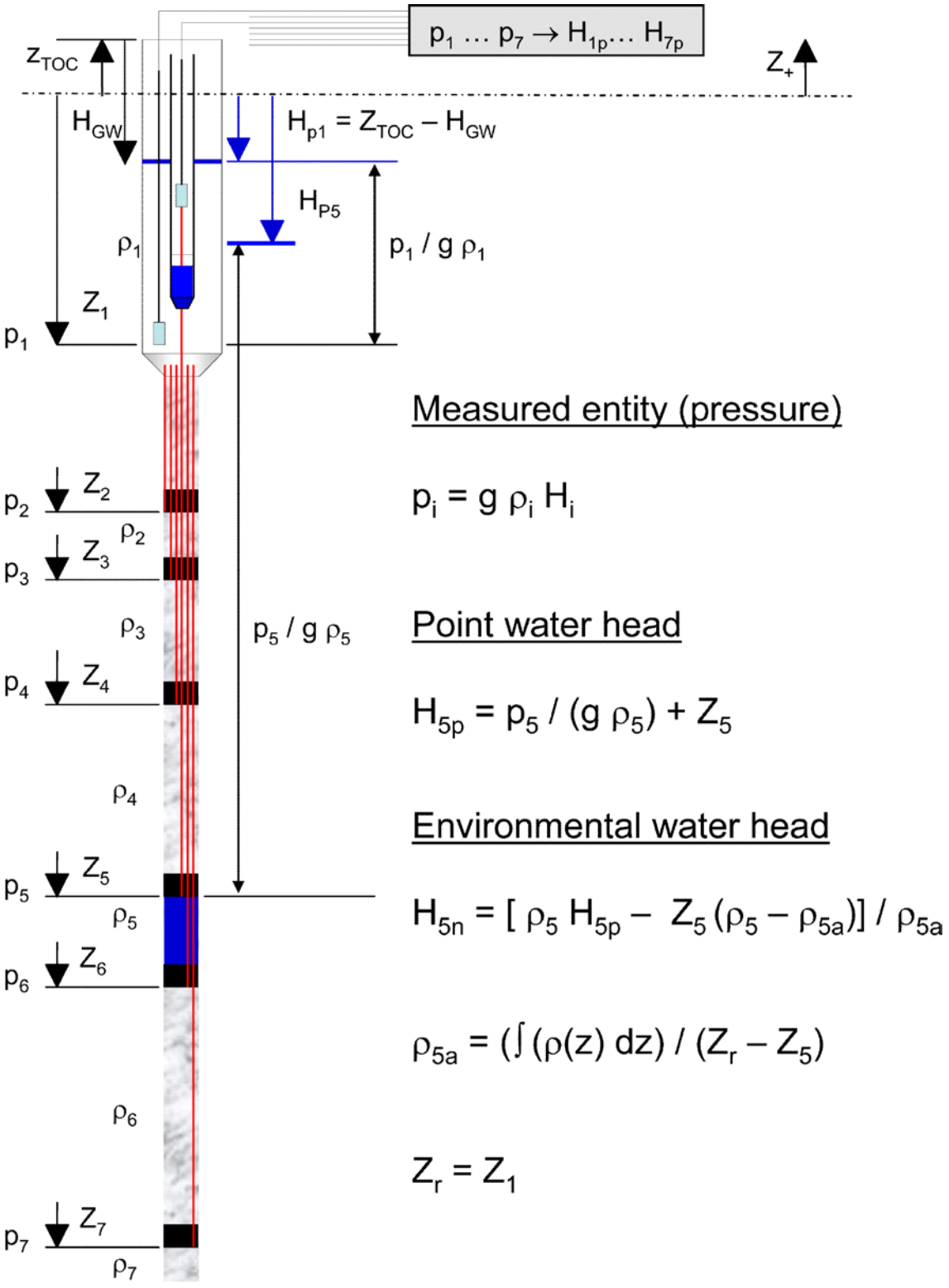

Figure 4-8. *Principle for point water head measurements in a borehole equipped with a multipacker system. /Lusczynski 1961/ is the key reference used in the SDM for transferring point water heads H_{ip} to environmental water heads H_{in}. (Figure K-2 in /Follin et al. 2007c/.)*

Since groundwater flow at Forsmark is subject to buoyancy forces that arise due to variations in fluid density according to salinity, temperature and total pressure, the point water heads are not hydraulic heads ("potential") *sensu stricto* and comparisons between calculated point water heads and measured groundwater levels must be made with caution. However, at Forsmark the groundwater salinity in the uppermost 150 m of bedrock is quite brackish (< 10 g/L Total Dissolved Solids) and the groundwater temperature variations are fairly moderate (6.5–8°C), see Figure 4-9. These conditions render small relative errors in the head calculations over the considered depth range, 150 m (a few centimetres at the most), thus suggesting that comparisons between measured and modelled point water heads in the Quaternary deposits and in the shallow bedrock aquifer is a meaningful calibration target at Forsmark. That is, transformations to environmental water heads are not required. These circumstances in the field conditions also facilitate the comparisons of the ConnectFlow and MIKE SHE modelling results. For the sake of clarity, it is stressed that the modelling with ConnectFlow considered variations in fluid density according to salinity, temperature and total pressure. Variations in fluid viscosity with temperature, salinity and total pressure were also considered. A fixed geothermal gradient of 10°C/km was assumed in ConnectFlow with a temperature of 6°C at the surface.

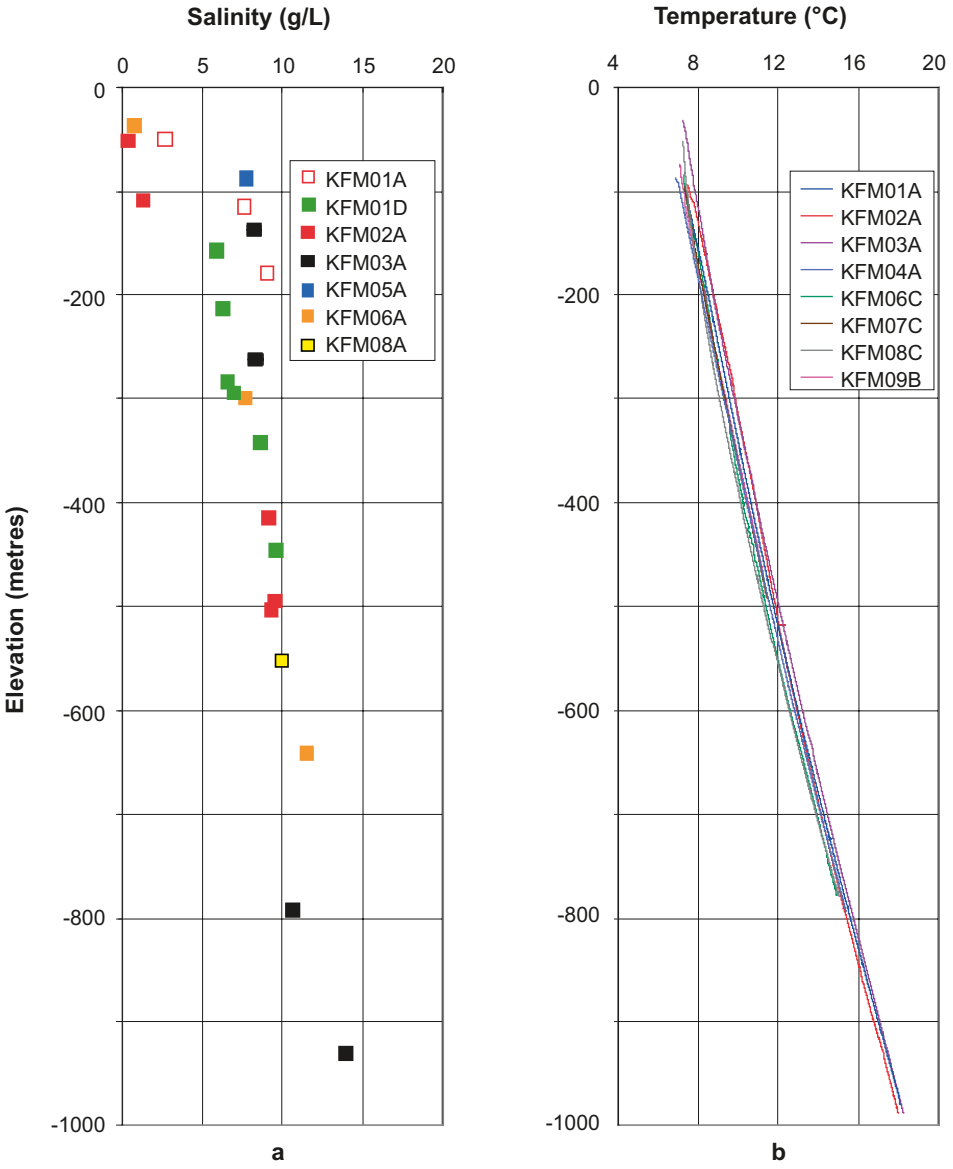

Figure 4-9. *Summary of fluid salinity (a) and temperature (b) for seven (a) and eight (b) boreholes at Forsmark. (Modified after Figure 5-15 in /Follin et al. 2008a/ and Figure 6-5 in /SKB 2008b/, respectively.)*

5 Conceptual hydrogeological modelling

The bedrock hydrogeological model consists of three hydraulic domains: HSD, HCD, and HRD, cf Figure 2-1. This chapter summarises the conceptual modelling of the HCD and HRD presented in /Follin et al. 2007bc/. The conceptual modelling of the HSD is presented in /Hedenström et al. 2008/ and /Johansson 2008/. With regard to the hydraulic data acquisition in the bedrock (Appendix A), the description of the conceptual modelling of the HCD and HRD may be divided into four segments:

1. The deformation zones within the candidate area.
2. The fracture domains within the candidate area.
3. The fracture domains bordering the target area.
4. The superficial bedrock within the target area.

5.1 Deformation zones within the candidate area

The deformation zone model developed during the ISI stage was elaborated and consolidated during the CSI stage, a work that was essentially concluded in stage 2.2. The deformation zone model is shown in Figure 3-4. The division into sets (WNW, NW, …) follows the naming and colours used in Table 3-3. Here, G represents the gently dipping deformation zones.

In the preliminary SDM /SKB 2005a/, 44 deformation zone intercepts representing 28 different deformation zones were investigated hydraulically. In SDM-Site, these numbers are 116 and 57, respectively, which imply a more or less doubled information density. The transmissivity data acquired from the single-hole tests constitute the basis for the assignment of hydraulic properties to the deformation zones in the SDM; see Figure 4-2 through Figure 4-4 for examples.

The assignment of hydraulic properties to the different deformation zones modelled in the preliminary SDM was based on depth trend regression analyses of single-hole transmissivity data acquired at a reasonable number of deformation zone intercepts (28 deformation zones had more than one measurement). The difference in the inferred transmissivity trends between steeply dipping and gently dipping deformation zones was found to be considerable at repository depth (c. two orders of magnitude) /SKB 2005a/. However, the palaeohydrogeological simulations carried out showed that the matching against hydrochemical data was sensitive to how the deformation zone transmissivity depth trend was implemented. That is, poor matches were obtained unless the regression model honoured the measured data at the measurement points (conditional simulation).

Figure 5-1 shows a plot of the transmissivity data available for flow and solute transport modelling in the SDM. The transmissivity data are plotted versus depth and are marked up by different colours in relation to the division of the deformation zones into sets, see section 5.5. Figure 5-1 shows that the gently dipping deformation zones (G), which predominantly occur in the hanging wall bedrock, are the most transmissive at all depths. The steeply dipping, local major, deformation zones that strike WNW and NW and border the candidate area form structures with a second order of importance as far as transmissivity is concerned. The steeply dipping deformation zones that strike ENE and NNE occur mainly in the footwall bedrock. These are significantly heterogeneous from a hydraulic point of view. In summary, these observations suggest a pronounced hydraulic anisotropy on a regional scale, where the largest transmissivities observed are associated with deformation zones with a high angle to the minimum principal stress reported by /Glamheden et al. 2007/. Furthermore, Figure 5-1 suggests that the transmissivities are affected by a substantial depth trend (vertical heterogeneity). The depth trend in

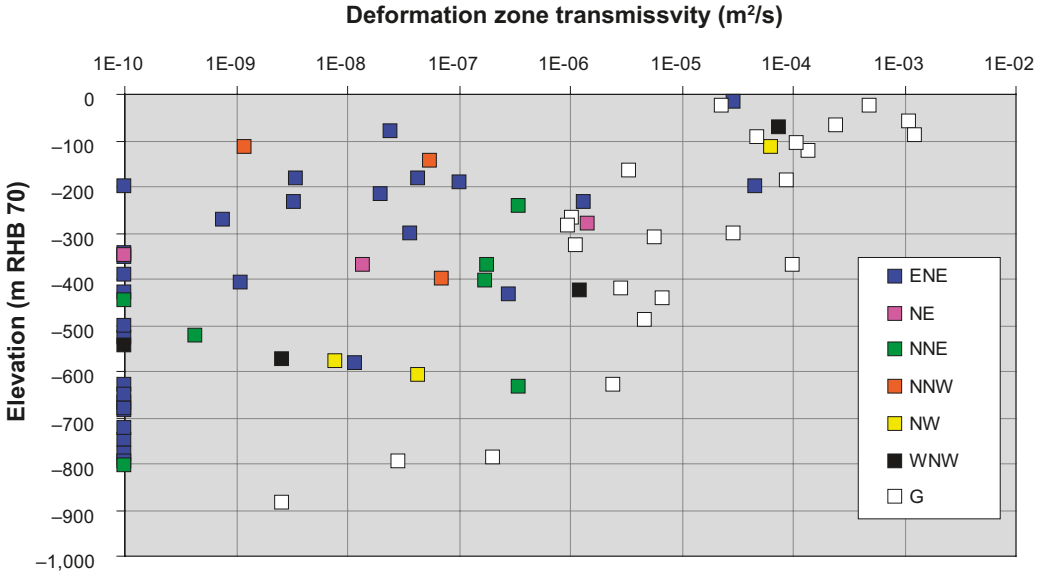

Figure 5-1. *Transmissivity data versus depth for the deterministically modelled deformation zones in stage 2.2. The transmissivities are coloured with regard to the orientations of the deformation zones, where G means gently dipping. The deformation zones with no measurable flow are assigned an arbitrary low transmissivity value of $1 \cdot 10^{-10}$ m^2/s in order to make them visible on the log scale. (Figure 9-1 in /Follin et al. 2007b/.)*

transmissivity spans four to six orders of magnitude, from 10^{-4}–10^{-3} m^2/s near the surface to 10^{-9}–10^{-8} m^2/s at c 1,000 m depth. Figure 5-1 also shows that the lateral heterogeneity in the in-plane transmissivity is also considerable; take the ENE data set at c 200 m depth for an example. A closer analysis of the data for this set reveals that the transmissivities vary laterally by several orders of magnitude between zones of similar orientation, as well as between different parts of a specific zone (Figure 5-2). The conclusion drawn from these findings is that the previously described anisotropy in the structural geology (see section 3.2.2) is accompanied by significant vertical and lateral hydraulic heterogeneity. This observation suggests a strongly channelised flow field within the planes of the deformation zones.

The transmissivity data acquired during stage 2.3 (the verification stage, cf Table 1-2) provide transmissivity data from the regional Singö and Forsmark deformation zones outside the candidate area, and from the local major deformation zones modelled to intersect borehole KFM08D within the target volume, see section 5.8. The variability of the verification data agree with the variability of data used in the SDM, see Figure 5-3.

5.2 Fracture domains within the candidate area

Transmissivity data from four of the five cored boreholes available for modelling in the preliminary SDM are displayed in Figure 4-2 and Figure 4-3. Besides discrete differences in fracture transmissivity, the figures also reveal significant differences in conductive fracture frequencies. KFM01A and the lower halves of KFM02A and KFM04A show data in the footwall bedrock of zone A2. KFM03A and the upper half of KFM02A show data gathered in the hanging wall bedrock with its gently dipping zones. (The upper half of KFM04A shows data gathered in the bedrock bordering the tectonic lens within the candidate area, see section 5.3.) The intensely fractured interval between c 400 and 500 m depth in KFM02A corresponds to the gently dipping deformation zones referred to as A2 and F1 in stage 2.2. In the preliminary SDM, this interval was modelled as a single zone (A2).

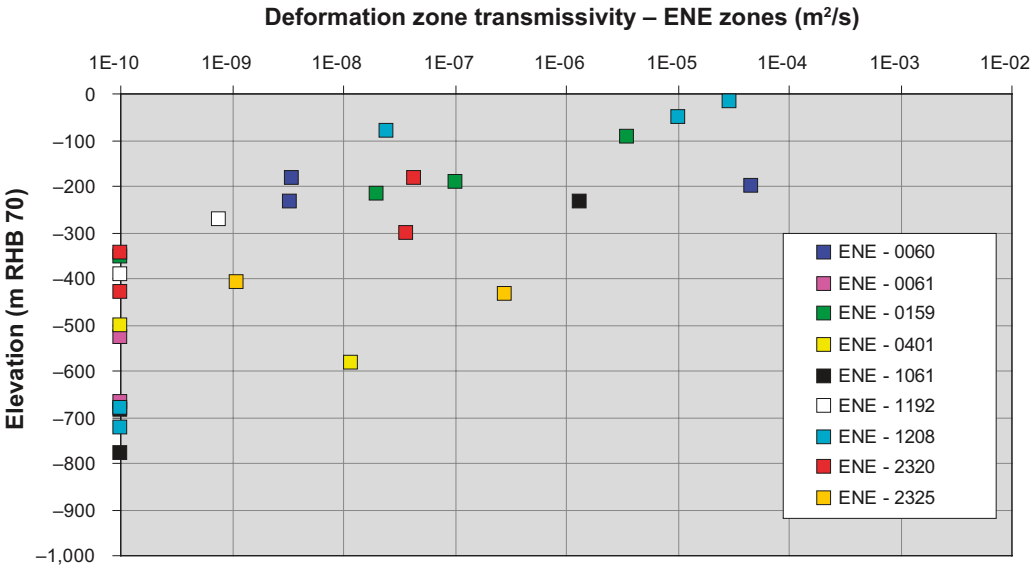

Figure 5-2. *Transmissivity data versus depth for the ENE category of the steeply dipping deformation zones in stage 2.2. Tests with no measurable flow are assigned an arbitrary low transmissivity value of $1 \cdot 10^{-10}$ m²/s in order to make them visible on the log scale. (Figure 9-4 in /Follin et al. 2007b/.)*

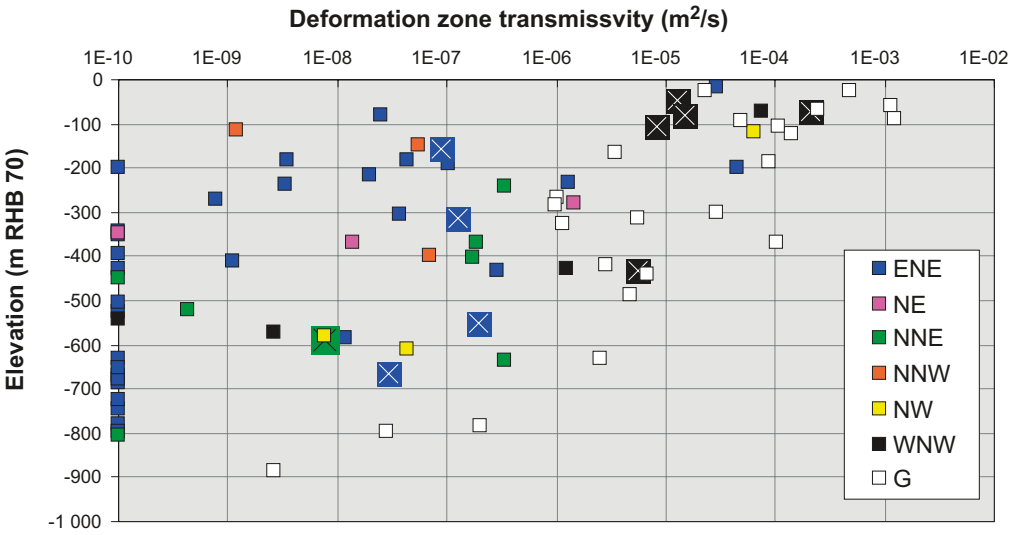

Figure 5-3. *The transmissivity data acquired from the hydraulic testing carried out in stage 2.3 in boreholes KFM08D, KFM11A, KFM12A, HFM34, HFM36 and HFM37 are here added to the transmissivity plot shown in Figure 5-1 and indicated with ☒. (Figure 4-2 in /Follin et al. 2008a/.)*

Based on the structural-hydraulic information available for modelling in the preliminary SDM, it was suggested that the bedrock in between the deformation zones within the candidate area should be divided into four hydrogeological sub volumes, A–D, depending on the fracture intensity of flowing fractures, see Figure 5-4. Moreover, it was noted that the flowing fractures identified in the footwall bedrock of zone A2 are predominantly gently dipping and that steeply dipping fractures with a NS-NE strike are the second most dominant orientation from a hydraulic viewpoint. The transmissivity data acquired from boreholes KFM06A and KFM07A in stage 2.1 confirmed the notion of hydrogeological sub volumes, see Figure 5-5. As a consequence, it was decided that an interdisciplinary assessment of the bedrock properties in between deformation zones should be attempted starting with a geological definition, i.e. without use of hydraulic or other data sets. The final description of the bedrock in between the deformation zones

consists of six fracture domains referred to as FFM01–06, see chapter 3.2.3. The hydrogeological data acquired in four of the twelve cored boreholes drilled during stage 2.2, KFM07C, KFM01D, KFM08A, and KFM08C, are shown in Figure 5-6 and Figure 5-7. There is a clear transition in the frequency of the PFL-f data with depth.

The four plots shown in Figure 5-8 and Figure 5-9 suggest that about 60% of the Terzaghi corrected PFL-f data in the footwall has a dip angle of less than 25° regardless of fracture domain and elevation. Table 5-1 and Table 5-2 summarise the change in Terzaghi corrected linear fracture intensities, $P_{10,corr}$ of open fractures vis-à-vis flowing (PFL-f) fractures in fracture domain FFM01 with regard to depth and fracture set.

For the top 400 m of FFM01 (Table 5-1), the HZ and NE sets dominate the open fractures, followed by the NW and NS sets, and finally the EW set. However, among the flowing fractures, there are only three sets: HZ, NE and NS with HZ very dominant. Below 400 m depth in FFM01 (Table 5-2), the few flowing fractures observed occur in the HZ and NE sets with an average "true" spacing of about 200 m. In conclusion, below 400 m depth, the flowing fractures in FFM01 are almost exclusively restricted to deformation zones, symptomatic of a very sparse and poorly connected network of fractures that does not reach a threshold for percolation of water into the deep rock. Indeed, the meaning of an average spacing of flowing fractures under these conditions is highly questionable.

Table 5-3 summarises the statistics of open fractures and flowing fractures deduced in stage 2.2 for FFM01–FFM03. The decreasing frequency of flowing fractures with depth is based on the measurements carried out with the PFL-f method. In summary, the depth interval 100–200 m in FFM02 and FFM01 coincides more or less with sub volume A in Figure 5-4, the depth interval 200–400 m in FFM01 coincides approximately with sub volume B, the depth interval 400–1,200 m in FFM01 coincides essentially with sub volume C, and the two depth intervals 100–400 m and 400–1,200 m in FFM03 coincides more or less with sub volume D. Hence, the hydrogeological division into sub volumes based on flowing fractures suggested in version 1.2 (and formed the basis for SR-Can /Hartley et al. 2006//) was found to be highly consistent with the definition of fracture domains based independently on geological data in stage 2.2.

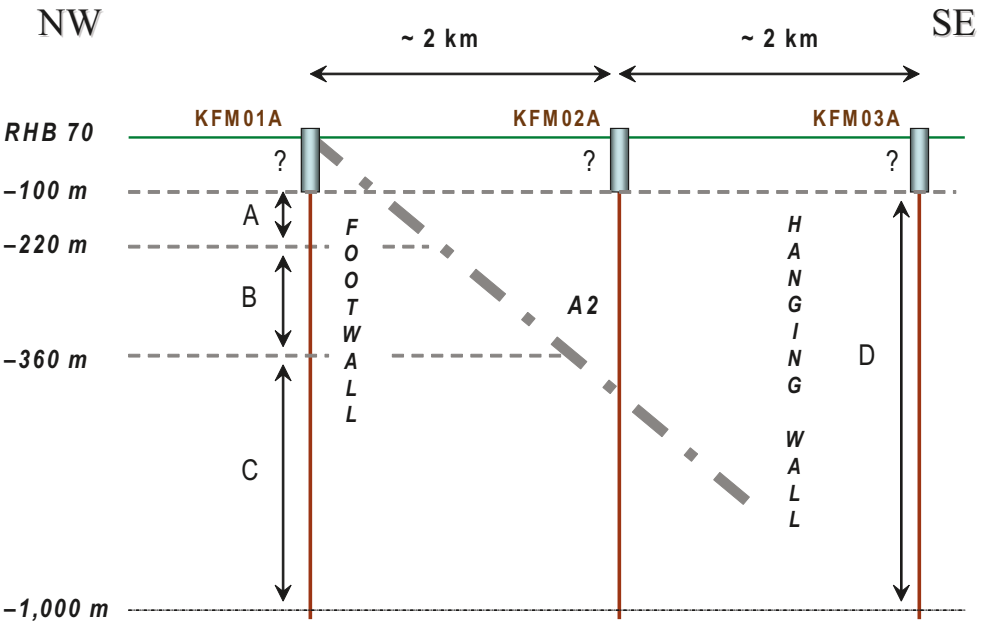

Figure 5-4. *Suggested division of the bedrock in between the deformation zones along a NW-SE cross-section within the candidate area into four hydrogeological sub volumes, A–D in version 1.2. (Modified after Figure 7-1 in /Follin et al. 2005/.)*

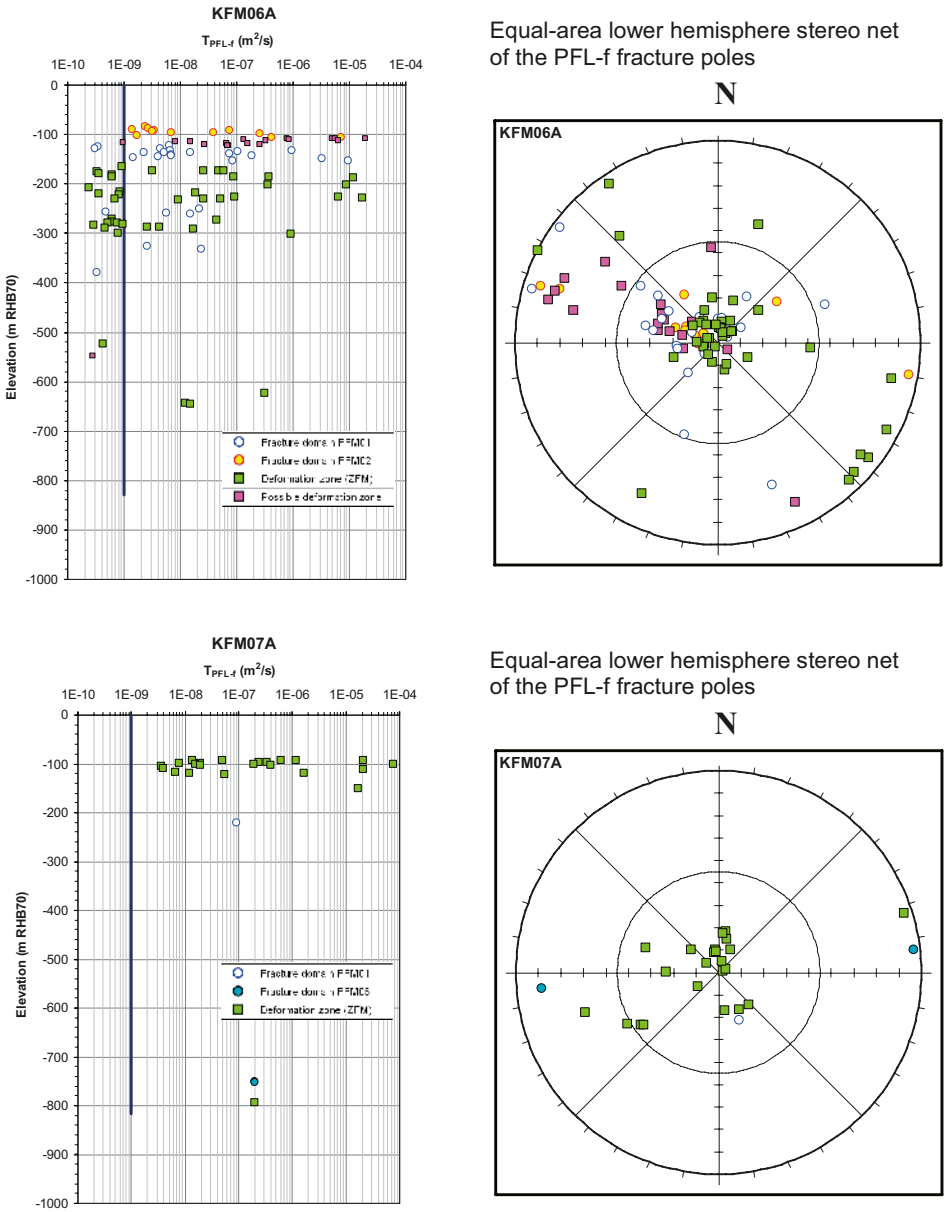

Figure 5-5. *Hydrogeological data in boreholes KFM06A and KFM07A. There are 38 PFL-f transmissivities associated with single fractures, 43 associated with three deterministically modelled deformation zones (43/3), and 18 associated with two possible deformation zones (18/2) in KFM06A. The corresponding figures for KFM07A are 3, 23/2, and 0/0, respectively. The blue lines indicate the typical threshold value reported from the investigations in the Forsmark area, $1 \cdot 10^{-9}$ m²/s. The lengths of the blue lines correspond to the depths investigated with the PFL-f method. (Modified after Figure 5-7 and Figure 5-8 in /Follin et al. 2007b.)*

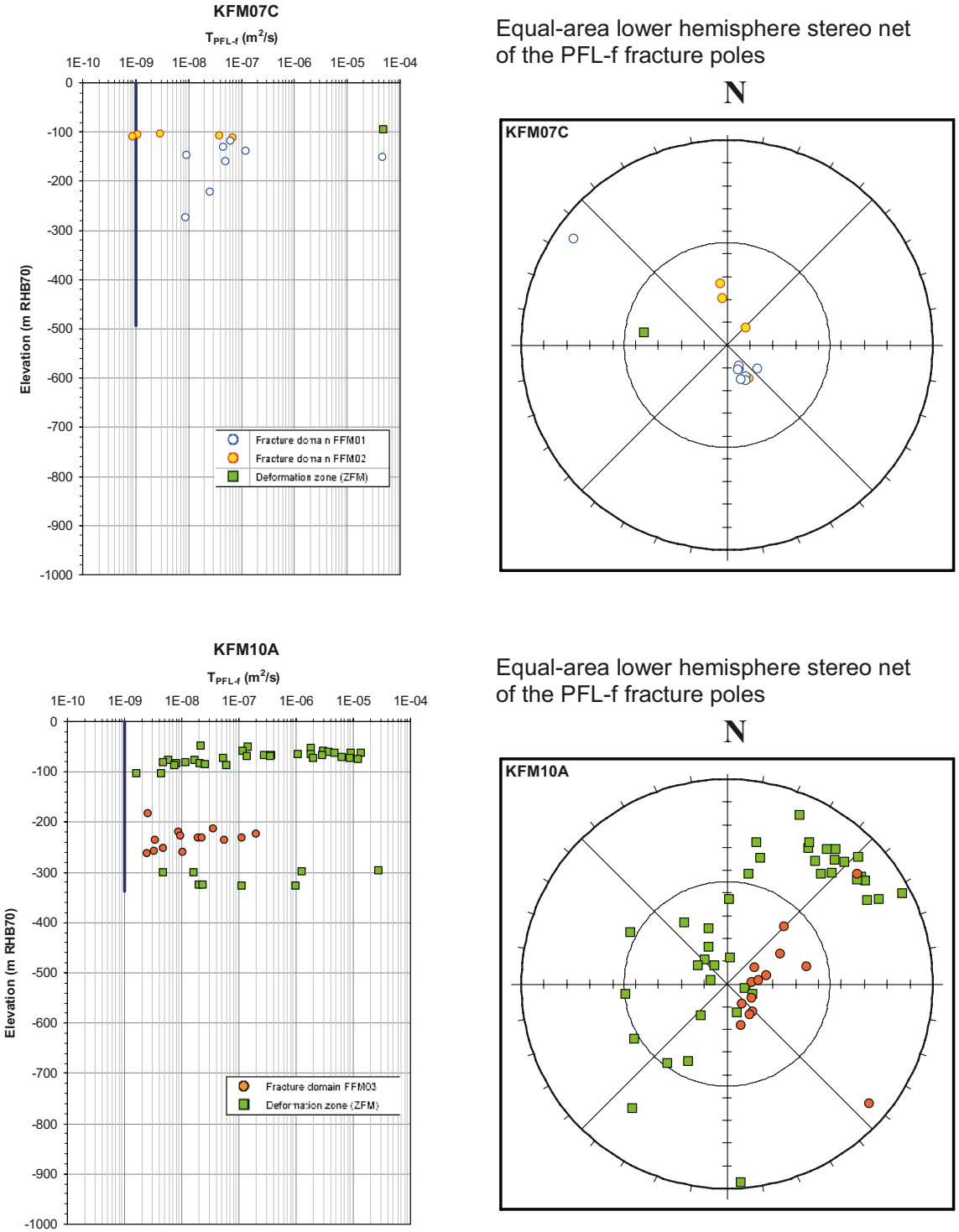

Figure 5-6. *Hydrogeological data in boreholes KFM07C and KFM10A. There are 13 PFL-f transmissivities associated with single fractures and one associated with one deterministically modelled deformation zone (1/1) in KFM07C. The corresponding figures for KFM010A are 34 and 34/0, respectively. The blue lines indicate the typical threshold value reported from the investigations in the Forsmark area, $1{\cdot}10^{-9}$ m^2/s. The lengths of the blue lines correspond to the depths investigated with the PFL-f method. (Modified after Figure 5-9 and Figure 5-2 in /Follin et al. 2007b/.)*

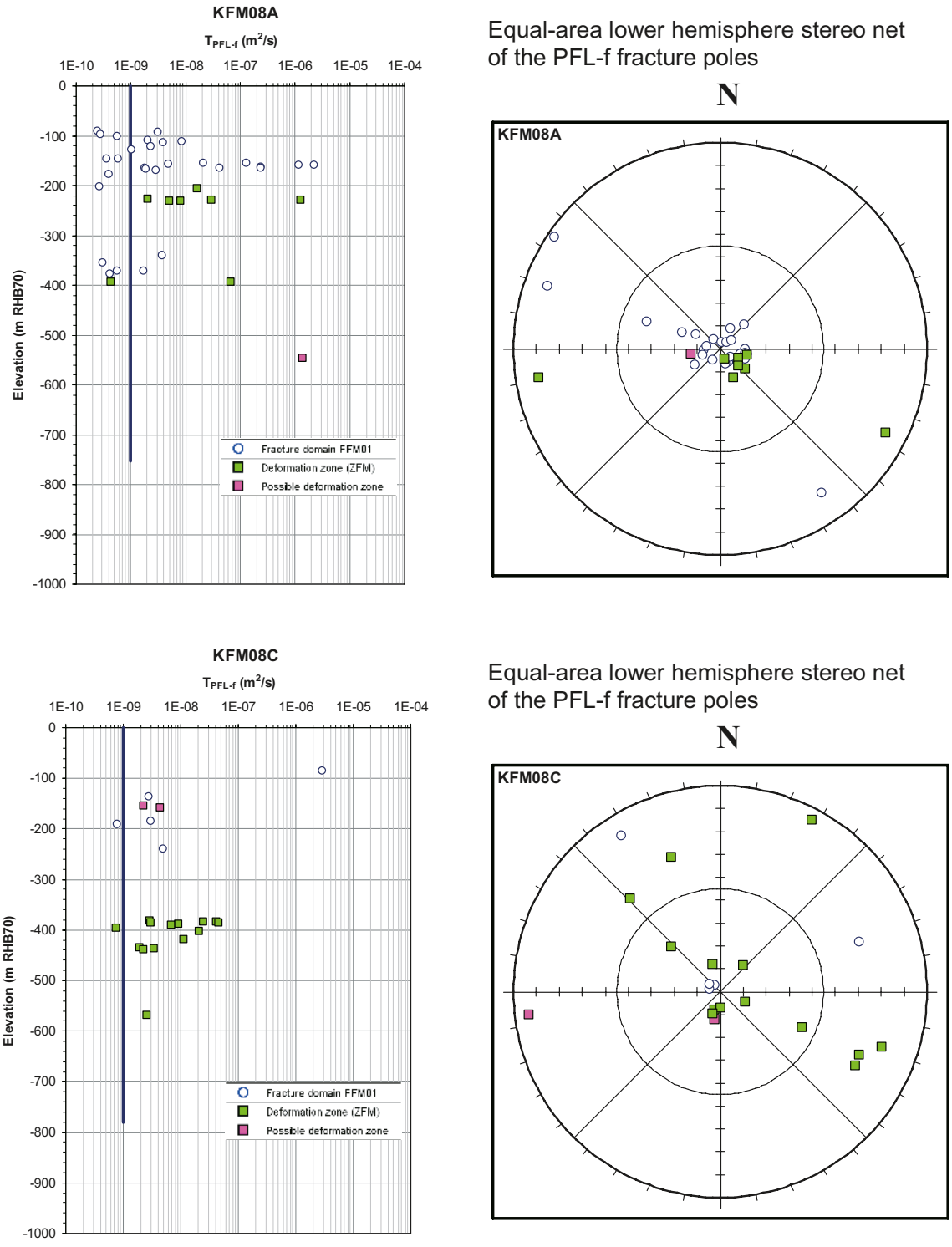

Figure 5-7. *Hydrogeological data in boreholes KFM08A and KFM08C. There are 32 PFL-f transmissivities associated with single fractures, eight associated with two deterministically modelled deformation zones (8/2), and one associated with one possible deformation zone (1/1) in KFM08A. The corresponding figures for KFM08C are 5, 14/2, and 1/1, respectively. The blue lines indicate the typical threshold value reported from the investigations in the Forsmark area, $1{\cdot}10^{-9}$ m^2/s. The lengths of the blue lines correspond to the depths investigated with the PFL-f method. (Modified after Figure 5-10 and Figure 5-11 in /Follin et al. 2007b/.)*

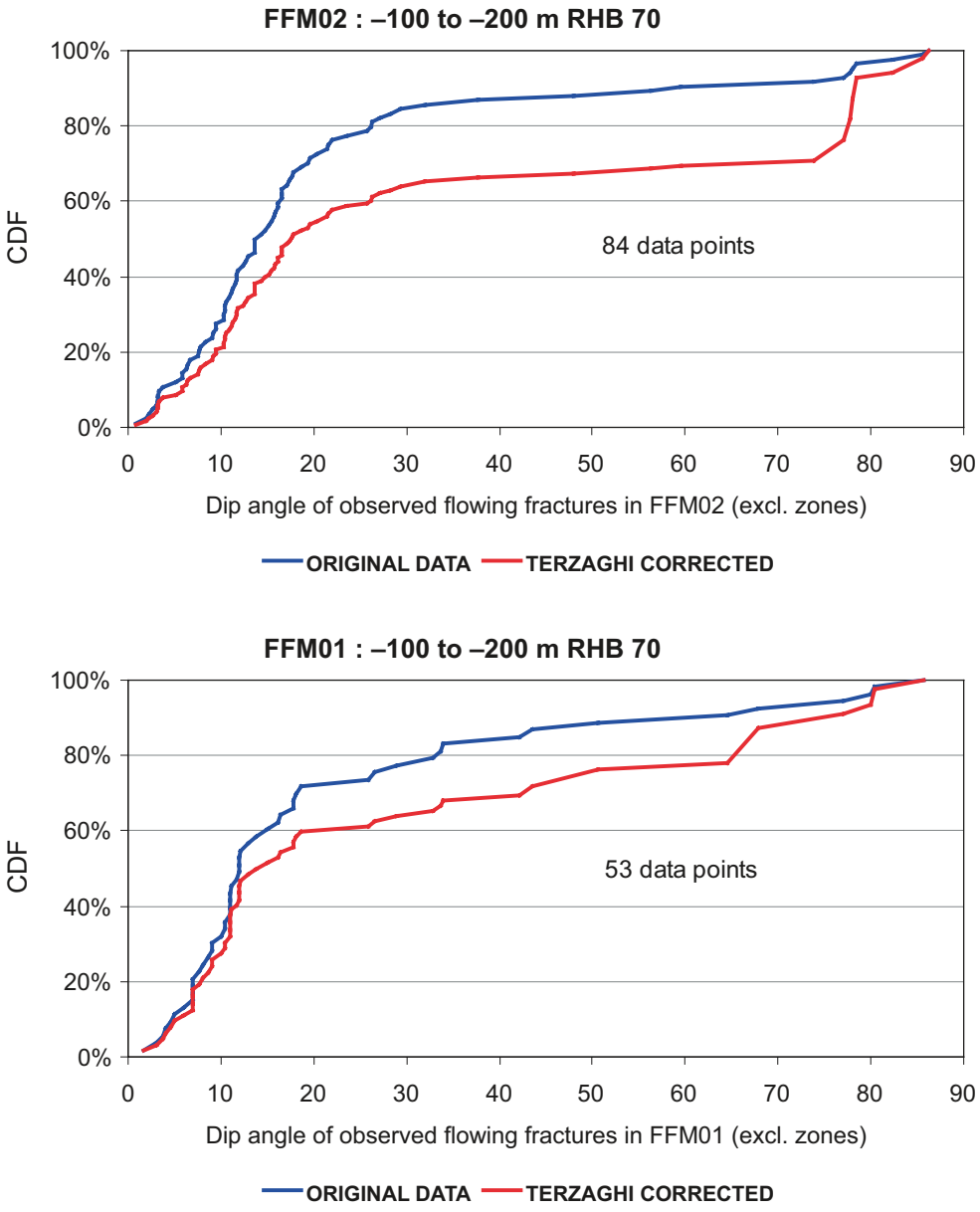

Figure 5-8. *Terzaghi corrected dip distributions between 100 and 200 m depth in FFM02 and FFM01. (Modified after figures in Appendix E in /Follin et al. 2007c/.)*

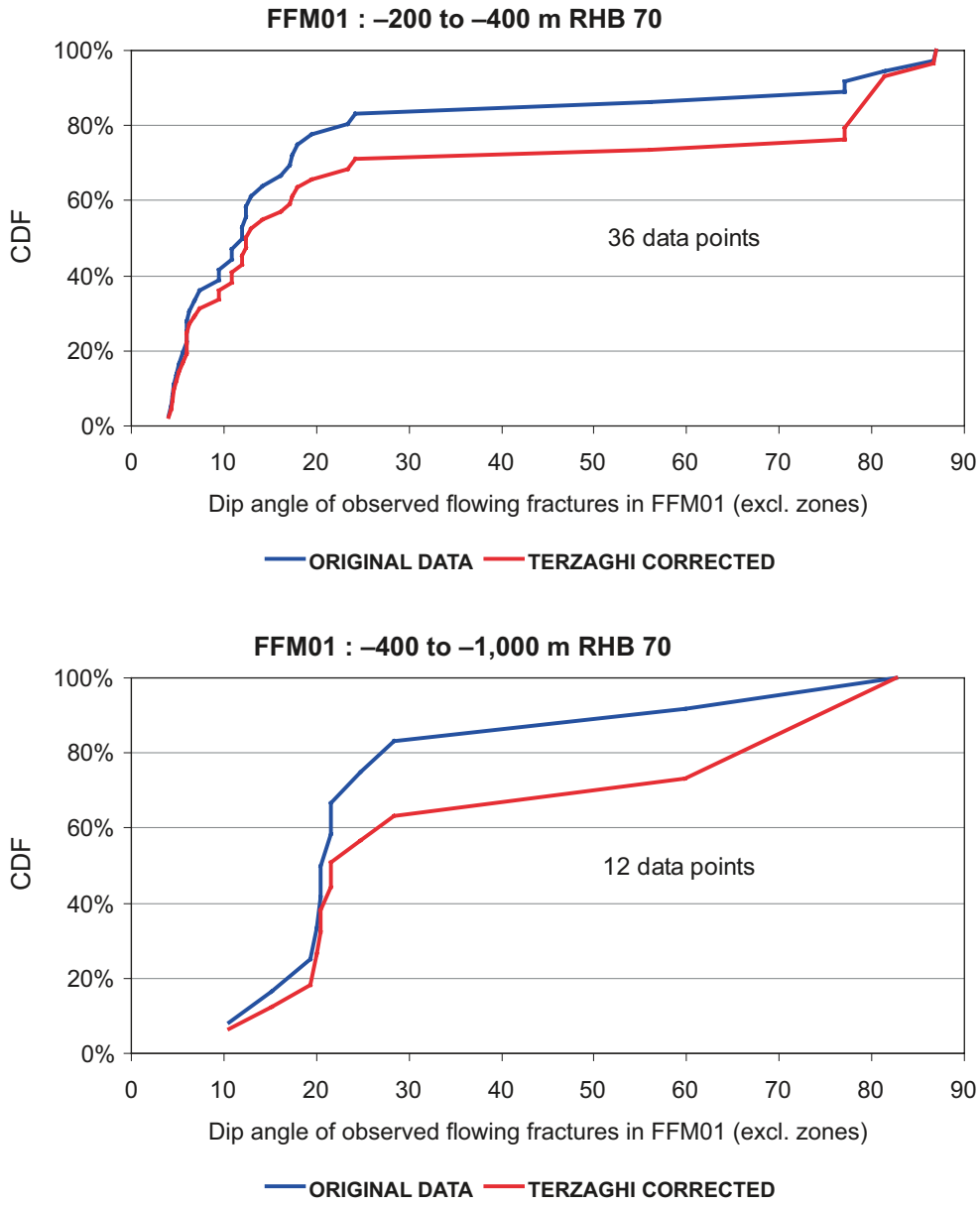

Figure 5-9. *Terzaghi corrected dip distributions between 200 and 400 m and between 400 and 1,000 m depth in FFM01. Ten of the twelve data points in the lower plot were observed in KFM02A between zones A2 and F1, see Figure 3-9. (Modified after Appendix E in /Follin et al. 2007c/.)*

Table 5-1. Summary of Terzaghi corrected linear fracture intensities by set of open fractures and PFL-f fractures within fracture domain FFM01 above 400 m depth and excluding deformation zones. (Table 10-13 in /Follin et al. 2007b/.)

BH	$P_{10,o,corr}$ [1/m]					$P_{10,PFL,corr}$ [1/m]				
	NS	NE	NW	EW	HZ	NS	NE	NW	EW	HZ
KFM01A	0.195	0.790	0.119	0.066	0.824	0.000	0.033	0.000	0.000	0.053
KFM01D	0.116	0.004	0.185	0.010	0.404	0.000	0.000	0.000	0.000	0.040
KFM02A	-	-	-	-	-	-	-	-	-	-
KFM03A	-	-	-	-	-	-	-	-	-	-
KFM04A	-	-	-	-	-	-	-	-	-	-
KFM05A	0.097	0.177	0.154	0.055	0.120	0.000	0.000	0.000	0.000	0.006
KFM06A	0.071	0.291	0.085	0.053	0.508	0.025	0.042	0.000	0.000	0.123
KFM07A	0.107	0.409	0.051	0.086	0.148	0.000	0.000	0.000	0.000	0.005
KFM07C	0.020	0.443	0.067	0.037	0.238	0.000	0.035	0.000	0.000	0.035
KFM08A	0.208	0.473	0.188	0.166	0.466	0.014	0.021	0.000	0.000	0.107
KFM08C	0.135	0.281	0.106	0.151	0.277	0.006	0.000	0.000	0.000	0.017
KFM10A	0.707	0.580	0.526	0.600	2.841	0.000	0.000	0.000	0.000	0.000
All BH	**0.125**	**0.339**	**0.126**	**0.083**	**0.374**	**0.006**	**0.015**	**0.000**	**0.000**	**0.049**

Table 5-2. Summary of Terzaghi corrected linear fracture intensities by set of open fractures and PFL-f fractures within fracture domain FFM01 below 400 m depth and excluding deformation zones. (Table 10-14 in /Follin et al. 2007b/.)

BH	$P_{10,o,corr}$ [1/m]					$P_{10,PFL,corr}$ [1/m]				
	NS	NE	NW	EW	HZ	NS	NE	NW	EW	HZ
KFM01A	0.089	0.072	0.026	0.000	0.150	0.000	0.000	0.000	0.000	0.000
KFM01D	0.087	0.034	0.178	0.026	0.080	0.000	0.000	0.000	0.000	0.006
KFM02A	0.099	0.094	0.104	0.005	0.040	0.000	0.016	0.000	0.000	0.021
KFM03A	-	-	-	-	-	-	-	-	-	-
KFM04A	0.109	0.094	0.198	0.022	0.273	0.000	0.000	0.000	0.000	0.002
KFM05A	0.127	0.270	0.127	0.013	0.174	0.000	0.000	0.000	0.000	0.000
KFM06A	0.110	0.426	0.062	0.112	0.134	0.000	0.000	0.000	0.000	0.000
KFM07A	0.030	0.133	0.057	0.016	0.024	0.000	0.000	0.000	0.000	0.000
KFM07C	0.168	0.953	0.000	0.128	0.222	0.000	0.000	0.000	0.000	0.000
KFM08A	0.077	0.078	0.108	0.055	0.142	0.000	0.000	0.000	0.000	0.000
KFM08C	0.088	0.180	0.056	0.138	0.163	0.000	0.000	0.000	0.000	0.000
KFM10A	-	-	-	-	-	-	-	-	-	-
All BH	**0.094**	**0.163**	**0.098**	**0.039**	**0.141**	**0.000**	**0.002**	**0.000**	**0.000**	**0.003**

Table 5-3. Terzaghi corrected values of the intensity of open and flowing fractures. There are significant differences between the three fracture domains FFM01-03 and a substantial decrease with depth of both open and flowing fractures in both FFM01 and FFM03. (Based on Table 3-4 and Table 3-5 in /Follin et al. 2007b/.)

Fracture domain	FFM01			FFM02	FFM03	
Depth interval, m	100–200	200–400	400–1,200	100–200	100–400	400–1,200
Intensity of observed open fractures, m^{-1}	1.13	1.02	0.54	3.17	1.10	0.77
Intensity of observed flowing fractures, m^{-1}	0.15	0.04	< 0.01	0.33	0.09	0.05
PFL–f T_{min}, m^2/s	$2.5 \cdot 10^{-10}$	$2.7 \cdot 10^{-10}$	$6.2 \cdot 10^{-10}$	$2.5 \cdot 10^{-10}$	$1.9 \cdot 10^{-9}$	$1.1 \cdot 10^{-9}$
PFL–f T_{max}, m^2/s	$4.7 \cdot 10^{-5}$	$1.8 \cdot 10^{-7}$	$8.9 \cdot 10^{-8}$	$7.3 \cdot 10^{-6}$	$6.8 \cdot 10^{-7}$	$1.9 \cdot 10^{-7}$

The depth interval 0–100 m has not been investigated with the PFL-f method due to the telescopic drilling technique used (cf. Figure 5-4) and the PSS data available from this interval are too scarce for a good hydraulic description. However, based on the available geological data it was suggested in stage 2.2 that this interval of the bedrock should be modelled as FFM02 in the footwall of zone A2 (more or less) and as FFM03 in the hanging wall of this zone, see Figure 3-9 and Figure 3-10. Indeed, this suggestion was adopted in the groundwater flow and solute transport modelling in stage 2.2. However, the exceptional hydraulic data acquired from the single-hole and cross-hole hydraulic testing of the 32 percussion-drilled boreholes available for hydrogeological modelling in stage 2.2 suggested that the uppermost 100–150 m does not just consist of a stochastic network of discrete fractures but also of horizontal sheet joints that need to be treated in a more deterministic fashion than the rest of FFM02, see section 5.4.

The left image in Figure 5-10 shows a view from above of the fracture domains in the target volume below FFM02, i.e. FFM01 and FFM06, and the nearby, cored boreholes at drill sites 1–2, 4–8 and 10 available for hydrogeological DFN modelling in stage 2.2. FFM06 is located in the northern part of the target volume in the footwall bedrock, but no hydraulic information about the bedrock in between the deformation zones in this fracture domain was available in stage 2.2. Based on the geological description of the fracture domains and the available statistics of open fractures in the nearby cored boreholes, it was assumed in stage 2.2 that fracture domain FFM06 has the same hydrogeological properties as inferred for FFM01, see Table 5-3. The right image in Figure 5-10 shows a view from above of the cored borehole KFM08D that was drilled and investigated in stage 2.3. A prediction of the structural-hydraulic properties along KFM08D is found in /Follin et al. 2007c/. Figure 5-11 shows the measured hydrogeological data in KFM08D. The acquired data agree with the prediction and do not contradict the hypothesis that the hydrogeological properties of FFM06 resemble those deduced for FFM01. In conclusion, what is quantified for FFM01 in Table 5-1, Table 5-2 and Table 5-3 is also concluded to be applicable for FFM06.

Figure 5-12 summarises the findings of the investigations with PFL-f method in fracture domains FFM01-03 and -06 as shown in Figure 4-2, Figure 4-3, Figure 5-5, Figure 5-6, Figure 5-7 and Figure 5-11. It is recalled that the investigated boreholes are cased in the uppermost 100 m, which effectively prohibits any data acquisition in this part of the bedrock. Noteworthy, the amount of PFL-f data below 400 m depth in FFM01 is very scarce despite the many boreholes drilled in the footwall of zone A2. Further, ten of the twelve data points below the elevation –400 in FFM01 come from borehole KFM02A at drill site 2 (Figure 5-10). The values occur between the zones A2 and F1 (Figure 3-9).

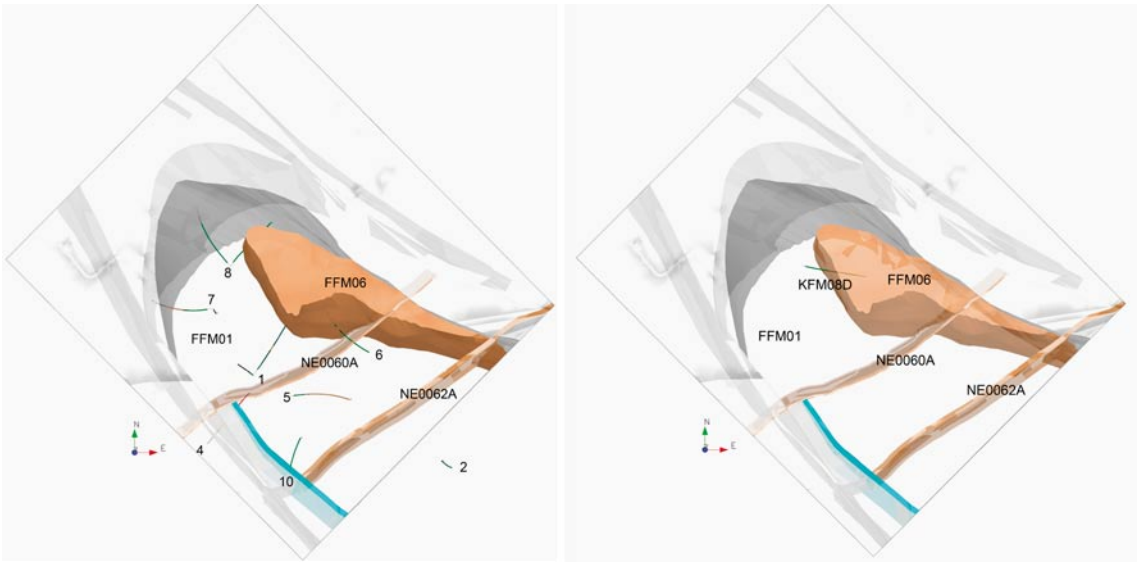

Figure 5-10. *Left: The core-drilled boreholes available for hydrogeological DFN modelling of the target volume in stage 2.2. Right: The cored borehole KFM08D was drilled and investigated during the verification stage. KFM08D penetrates FFM06 at about 292 m depth. (Figure 8-1 in /Follin et al. 2007c/.)*

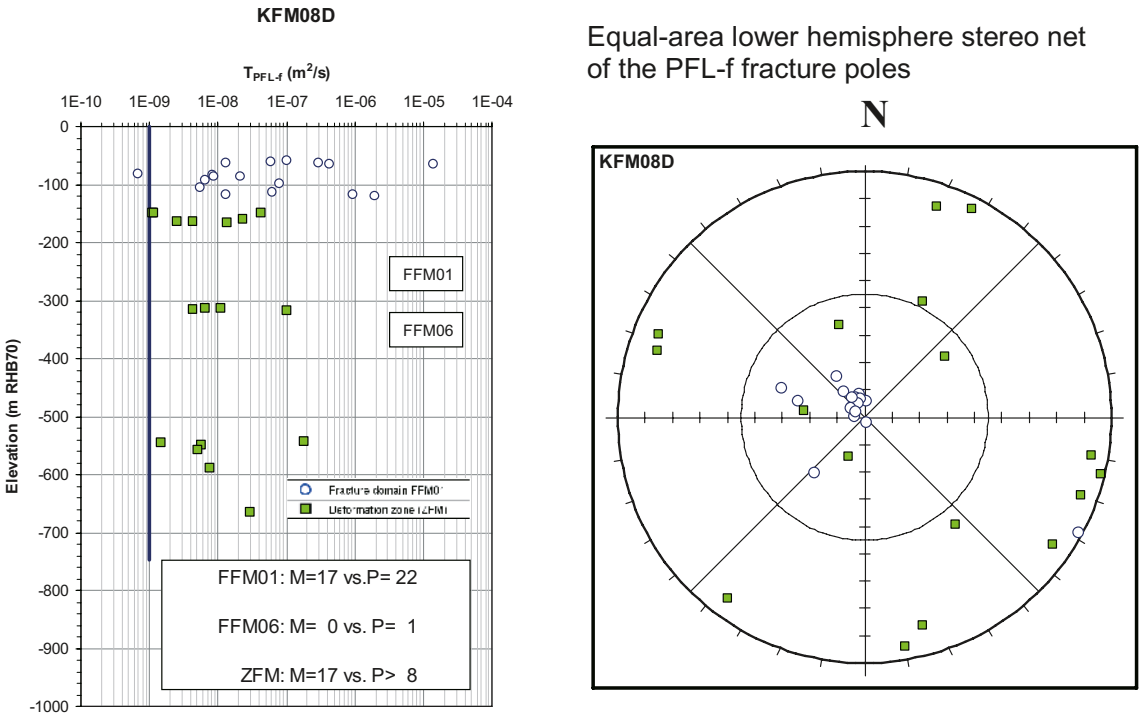

Figure 5-11. *There are 17 PFL-f transmissivities associated with single fractures and 17 associated with five deterministically modelled deformation zones in borehole KFM08D. The blue line indicates the typical threshold value reported from the investigations in the Forsmark area, $1 \cdot 10^{-9}$ m^2/s. The length of the blue line corresponds to the depth investigated with the PFL-f method. Fracture domain FFM06 begins at about 292 m depth. M = measured number of flowing fractures, P = predicted number of flowing fractures, ZFM = deformation zone. (Figure 4-4 in Follin et al. 2008a/.)*

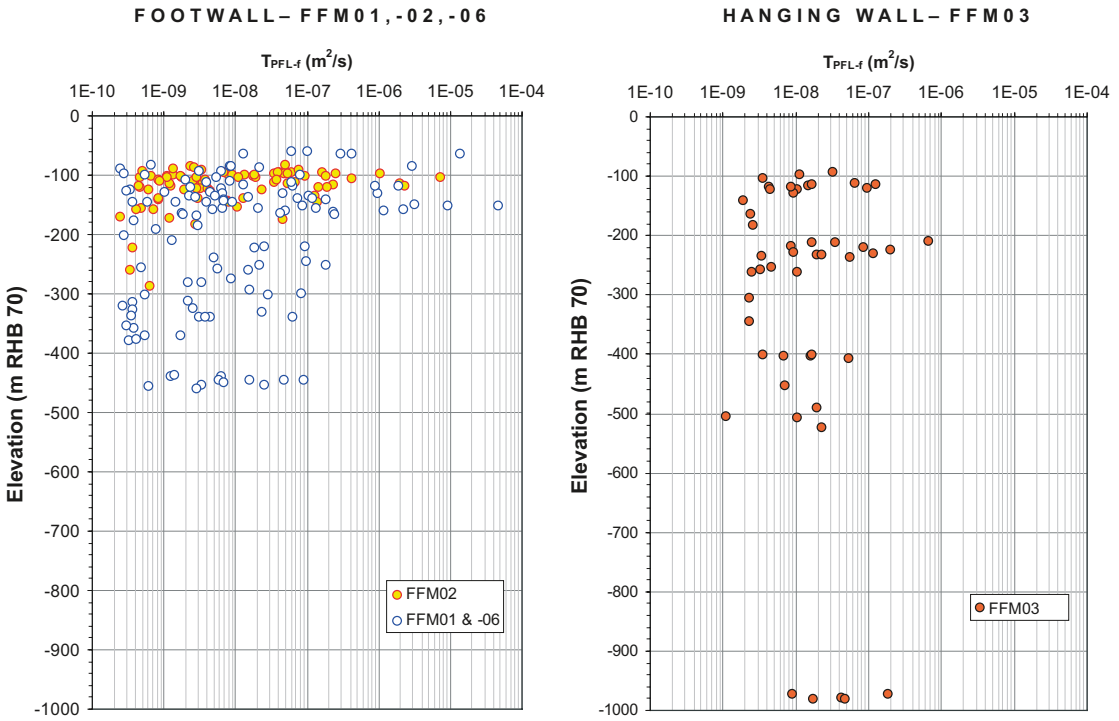

Figure 5-12. *Inferred transmissivities of connected open fractures detected with the PFL-f method in fracture domains FFM01-02 and -06 (left) and in FFM03 (right).*

5.3 The fracture domains bordering the target volume

Strong bedrock anisotropy with high ductile strain and ductile structures that dip steeply to the south-west are prominent in the bedrock bordering the tectonic lens to the south-west of the target volume, see section 5.2.4. A folded, ductile, high-strain rock unit is also present inside the tectonic lens (section 3.2). Hydrogeological observations in the bedrock bordering the target volume are made in boreholes KFM04A, KFM06C, KFM07A, KFM08A and KFM09A. For an illustration, the findings in boreholes KFM04A, KFM09A and KFM07A (cf. Appendix A) are commented upon here. The hydraulic data acquired with the PSS method in these three boreholes are shown in Figure 5-13. The hydraulic differences between the bedrock inside the target volume and the bordering bedrock are fairly obvious. The hydraulic differences with depth within the target volume are also clear for this type of hydraulic data.

KFM04A is located in the intensely fractured bedrock bordering the lens (FFM04). It is inclined 60° towards the lens and enters the sparsely fractured bedrock in the target volume (FFM01) as it reaches 400 m depth (borehole length 500 m).

KFM09A is located on the border of the lens and is inclined 60° away from the lens. It investigates at first the intensely fractured superficial bedrock in the lens (FFM02 and FFM01) and secondly the intensely fractured bedrock bordering it (FFM05 and FFM04) beginning at 230m depth (borehole length 280 m).

KFM07A is located in the lens. It investigates the intensely fractured superficial bedrock in the lens (FFM02) and the very sparsely fractured bedrock in the target volume below (FFM01). KFM07A enters the folded, ductile, high-strain and strongly fractured rock unit inside the lens (FFM05) at 665m depth (borehole length 793 m).

FFM04 and FFM05 lie in the periphery of the candidate area and the statistical significance of the data gathered in these fracture domains is very limited, being based on about 120–150 m of borehole data. However, based on the statistics available, it was proposed that FFM04 and FFM05 have the same fracture properties as inferred for FFM03 with depth, see Table 5-3, with FFM04 having slightly more transmissive fractures.

No cored boreholes were drilled in between deformation zones outside FFM04 and FFM05. Therefore, a simplified conceptual model was used to specify homogeneous continuous porous medium (CPM) properties for this part of the domain. The property assignment was assigned a depth trend in the hydraulic conductivity based on the hydraulic data deduced from the PSS measurements carried out at the Finnsjön study site, see Table 3-6 in /Follin et al. 2007c/.

5.4 The superficial bedrock within the target area

The uppermost part of the bedrock in the Forsmark area is recognised for its large horizontal fractures/sheet joints; see Figure 5-14 for an example. Besides this structural evidence, there are three pieces of hydrogeological evidence that support the hydraulic importance of these structures:

1. Exceptionally high water yields. The median yield of the first 22 percussion-drilled boreholes is c 12,000 L/h. This is c 20 times higher than the median yield of the domestic water wells drilled outside the candidate area /Gentzschein et al. 2006/, which is no different from the median yield of all bedrock wells (c 200,000) registered at the Geological Survey of Sweden /Berggren 1998/.
2. The near uniform groundwater level in the uppermost c 150 m of bedrock observed among the percussion-drilled boreholes within the target area. The near uniform level is c + 0.5 m above the datum plane. In contrast, the average groundwater level among the percussion-drilled boreholes drilled outside the target area is c + 2.8 m above the datum plane, see Figure 5-15. The hydraulic gradient between the Quaternary deposits and the superficial bedrock appears to be downwards both inside and outside the target area. However, the statistical significance of this observation can only be advocated inside thee target area.
3. The extensive and rapid transmission of fluid pressure changes (drawdown) during the large-scale interference test that was run over three weeks during the summer of year 2006 in borehole HFM14 located in the centre of the target area, see Figure 4-5 and Figure 4-6.

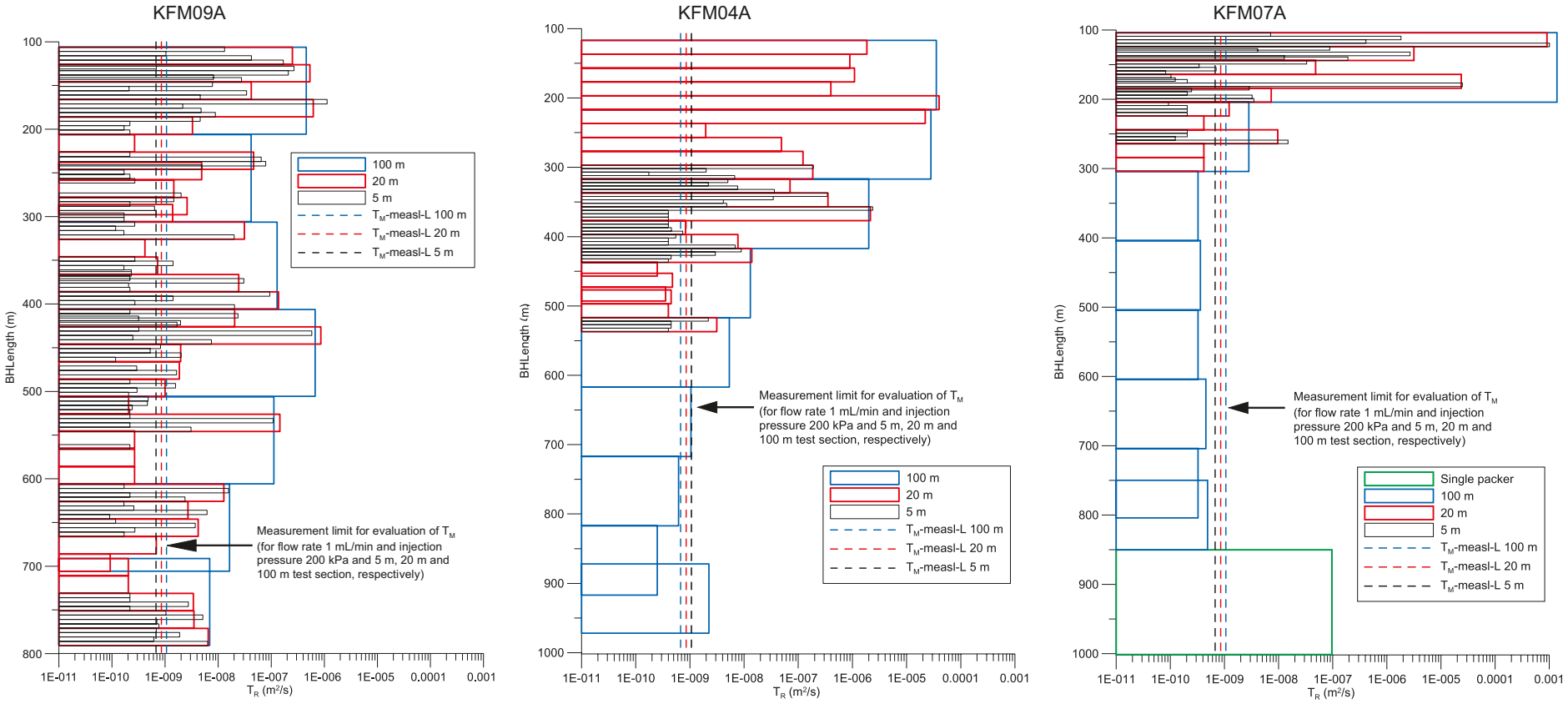

Figure 5-13. *Comparison of PSS transmissivity data gathered in the bedrock with relatively low ductile strain inside the tectonic lens, and in the bedrock with high, ductile strain both on the south-western margin of the tectonic lens and in the folded unit inside the lens. Left: KFM09A; Middle: KFM04A; Right: KFM07A. The PSS measurements are carried out with three different packer spacings, 100 m, 20 m and 5 m, depending on the results. Note that the nominal lower measurement limit of the PSS method varies slightly with the packer spacing. (Figure 3-32 in /Follin et al. 2007b/.)*

Figure 5-14. *Picture from the construction of the 13 m deep and more than one kilometre long canal between the Baltic Sea and the nuclear power reactors in Forsmark. Horizontal fractures/sheet joints are encountered along the entire excavation. The sheet joints follow the undulations of the bedrock surface implying that many of them do not outcrop, but stay below the bedrock surface as this dips under the Baltic Sea. There are several "horizons" of extensive sheet joints on top of each other according to the hydraulic interference tests. The picture is taken from the southern side of the canal where the bridge crosses the canal between drill sites 7 and 8. Photograph by G Hansson.*

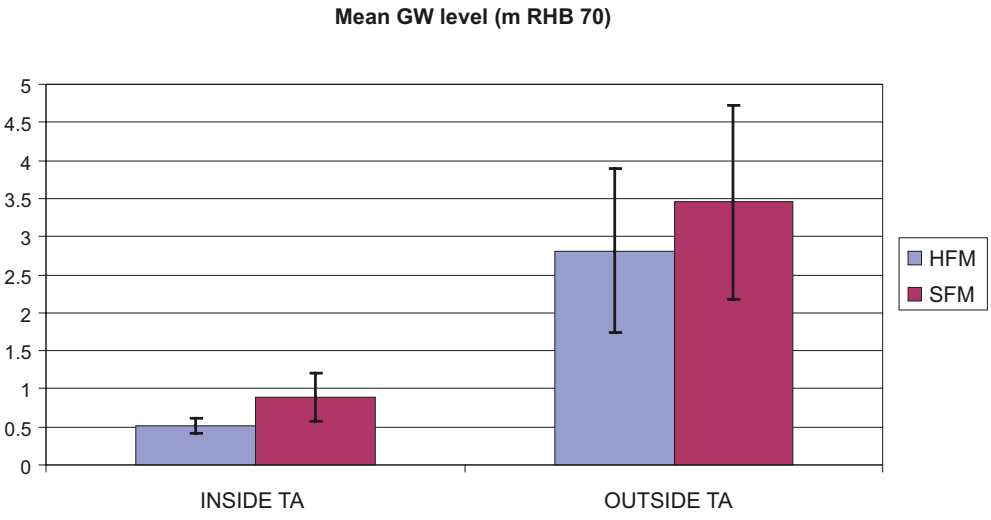

Figure 5-15. *Diagram showing average (arithmetic mean) groundwater levels in space and time of all time series data recorded in 28 percussion boreholes (HFM) drilled in the uppermost c 150 m of the bedrock, and in 28 monitoring wells (SFM) drilled in the Quaternary deposits. The average values shown for the HFM boreholes (+0.52 and +2.81 m RHB 70) were calculated from the arithmetic means of 37 time series inside the target area and 16 outside the target area, respectively. (Several boreholes have multi-packers.) The average values shown for the SFM boreholes (+0.89 and +3.45 m RHB 70) were calculated from the arithmetic means of 9 time series inside the target area and 19 outside the target area, respectively. The error bars show the 95% confidence intervals for the four averages. The mean sea water level during the monitoring period was –0.04 m RHB 70. The HFM and SFM boreholes are not drilled at the same locations. (Figure 3-13 in /Follin et al. 2008a/.)*

In conclusion, geological and hydrogeological observations indicate a well-connected network of structures of high transmissivity in the uppermost c 100–150 m of the bedrock in the target area. The network is thought to consist of extensive horizontal fractures/sheet joints, outcropping deformation zones and increased fracture intensity in the bedrock in between. The strong contrasts in the structural-hydraulic properties with depth encountered inside the target volume suggest a hydraulic phenomenon that causes a short circuit in the near-surface groundwater flow system. The cartoon shown in Figure 5-16 illustrates the shallow bedrock aquifer concept suggested in /Follin et al. 2007c/. The strong contrasts in the structural-hydraulic properties probably contribute to the observed slow transient evolution of fracture water and porewater hydrochemistry at repository depth within the target volume.

Based on the results obtained from the interference test that was run in HFM14 for three weeks during the summer of 2006 (Figure 4-5), the envisaged lateral extent of the horizontal fractures/sheet joints was hypothesised to correspond approximately to fracture domain FFM02, but stretching north all the way to the Singö deformation zone (WNW001) as shown in Figure 5-17. The other hypothesised physical boundaries are deformation zone ENE0062A to the south-east and the border of fracture domain FFM02 to the south-west and west, with the modification that the boundary passes between boreholes HFM20 and HFM28. The crosses in Figure 5-17 mark the positions of the percussion-drilled and core-drilled boreholes for which transmissivity measurements were available for parameterisation of the three deterministic discrete features implemented in the ConnectFlow code to model the sheet joints component of the shallow bedrock aquifer, see Figure 5-18 and Figure 5-19.

In 2007, two vital, confirmatory, large-scale, interference tests were conducted, one during the summer over three months in HFM14 and the other during the fall over two weeks in HFM33. Neither of the two tests falsified the hypothesised lateral extent of the shallow bedrock aquifer. On the contrary, they reinforced the hypothesis. Figure 5-20 shows the location of the observed pressure responses while pumping in HFM33.

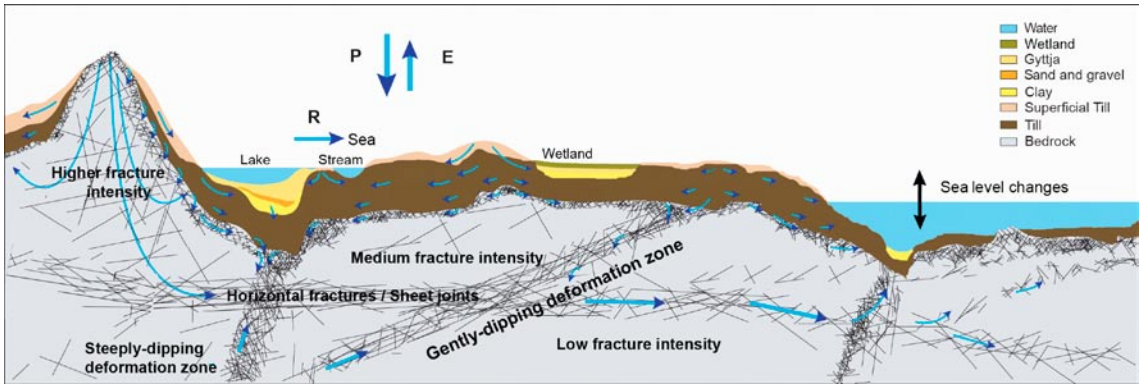

Figure 5-16. *Cross-section cartoon visualising the notion of a shallow bedrock aquifer and its envisaged impact on the groundwater flow system in the uppermost part of the bedrock within the target area. The shallow bedrock aquifer is probably hydraulically heterogeneous but at many places it is found be very anisotropic causing a short circuit of the recharge from above. The shallow bedrock aquifer is conceived to constitute an important discharge horizon for the groundwater flow in outcropping deformation zones. P = precipitation, E = evapotranspiration, R = runoff. (Figure 3-21 in /Follin et al. 2007c/.)*

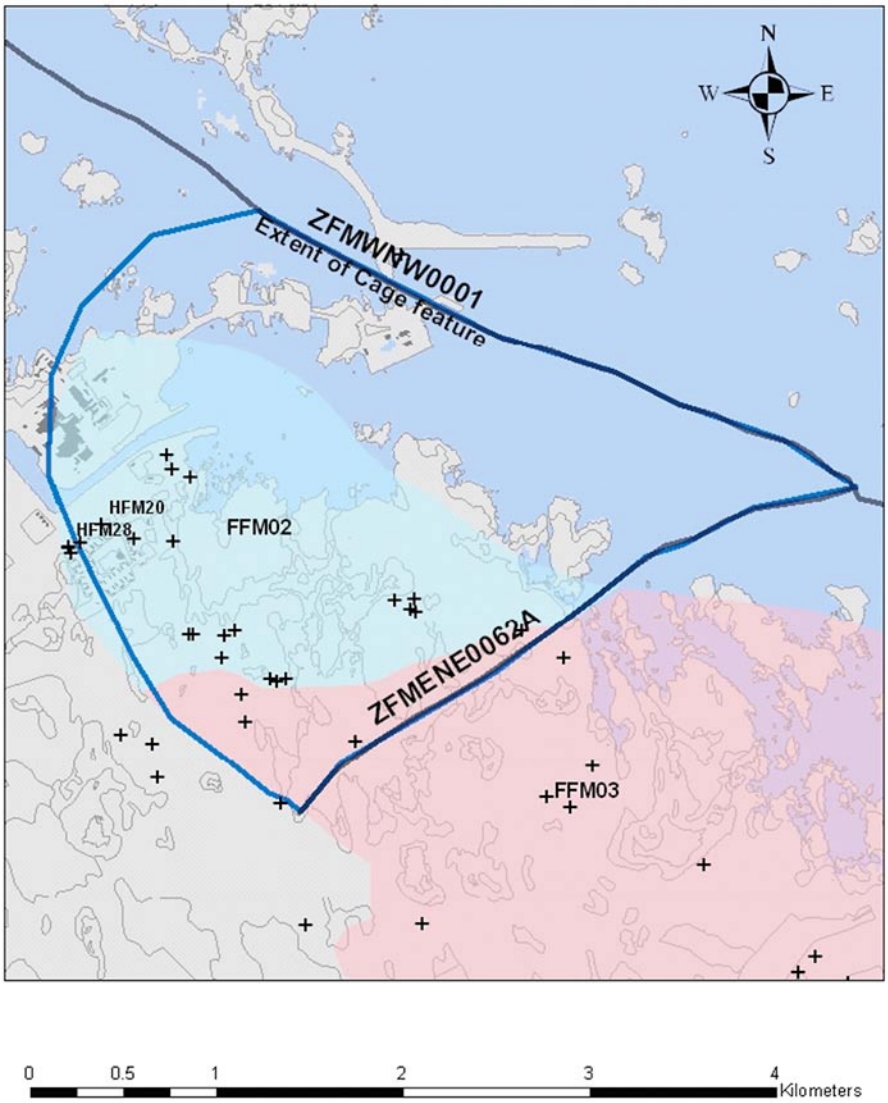

Figure 5-17. *The hypothesised lateral extent of the discrete features implemented in the ConnectFlow code to model the sheet joints in the shallow bedrock aquifer. The crosses mark the positions of percussion- and core-drilled boreholes for which transmissivity measurements were available. The bluish area represents fracture domain FFM02 and the pinkish area represents fracture domain FFM03. (Figure 3-31 in /Follin et al. 2007c/.)*

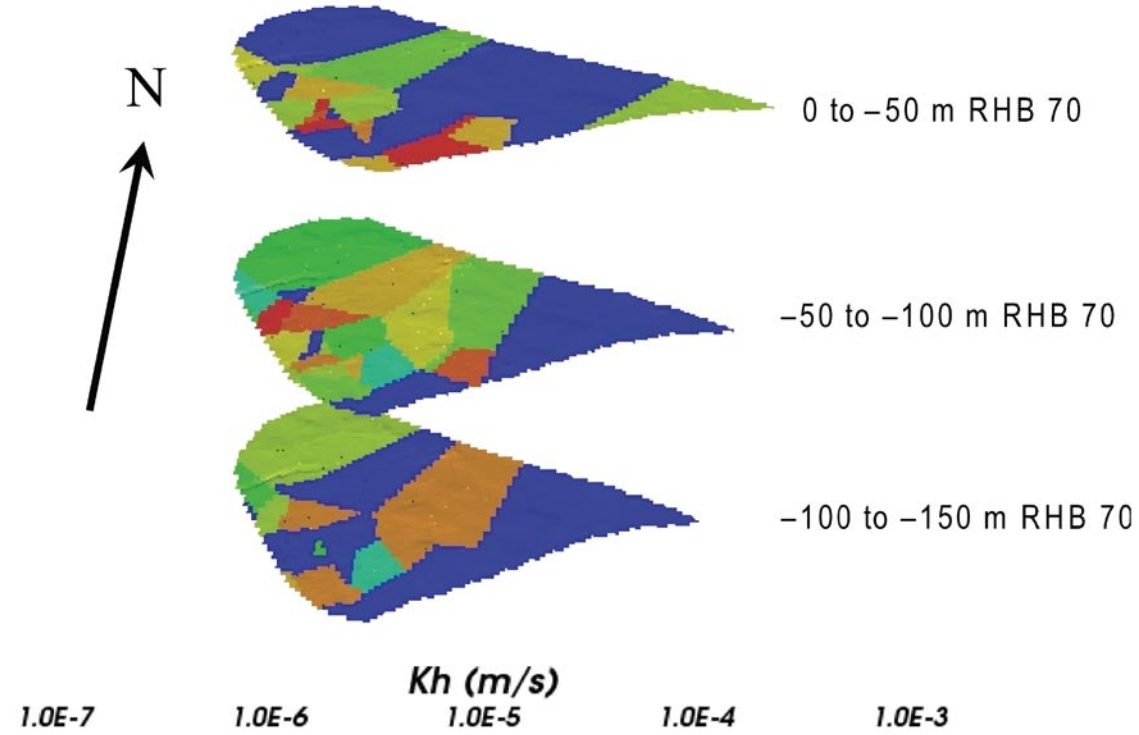

Figure 5-18. *Visualisation of the three layers implemented in ConnectFlow to model the sheet joints component of the shallow bedrock aquifer. (Figure 3-37 in /Follin et al. 2007c/.)*

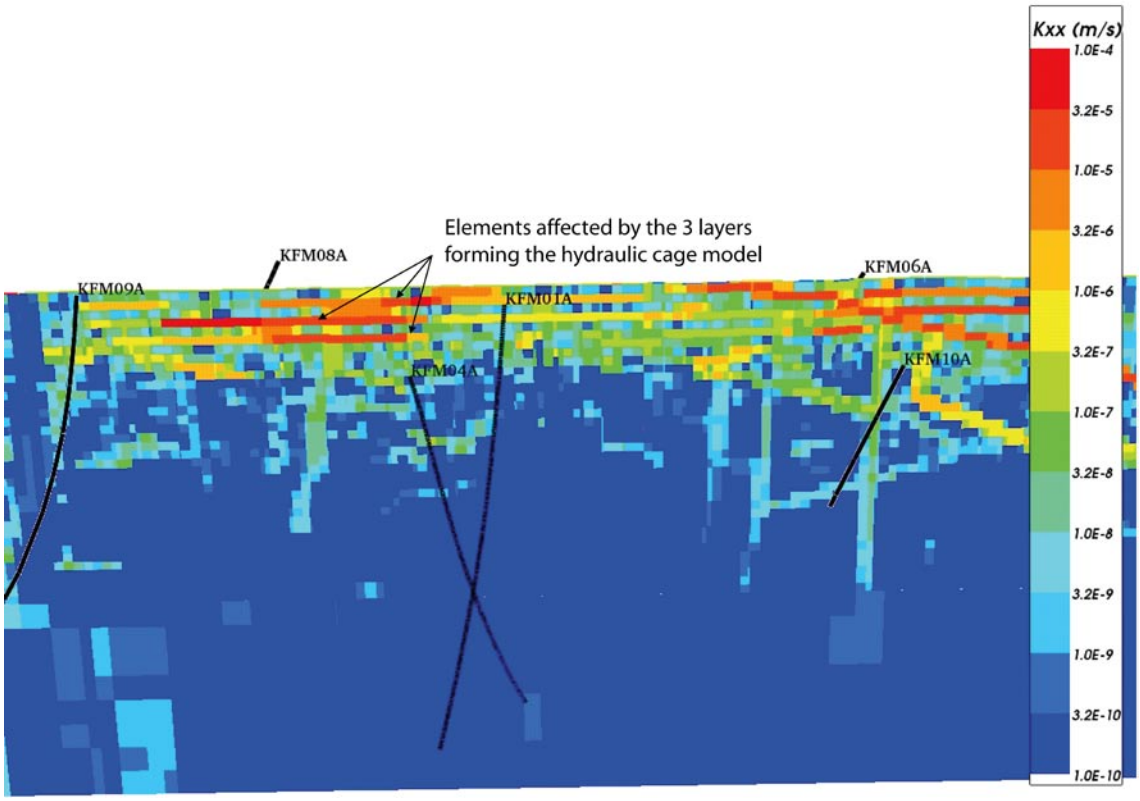

Figure 5-19. *Visualisation of the horizontal hydraulic conductivity in ConnectFlow on a WNW-ESE vertical slice through the target area. Note the effect of the three layers shown in Figure 5-18 that were implemented to model the sheet joints component of the shallow bedrock aquifer. (Modified after Figure 3-38 in /Follin et al. 2007c/.)*

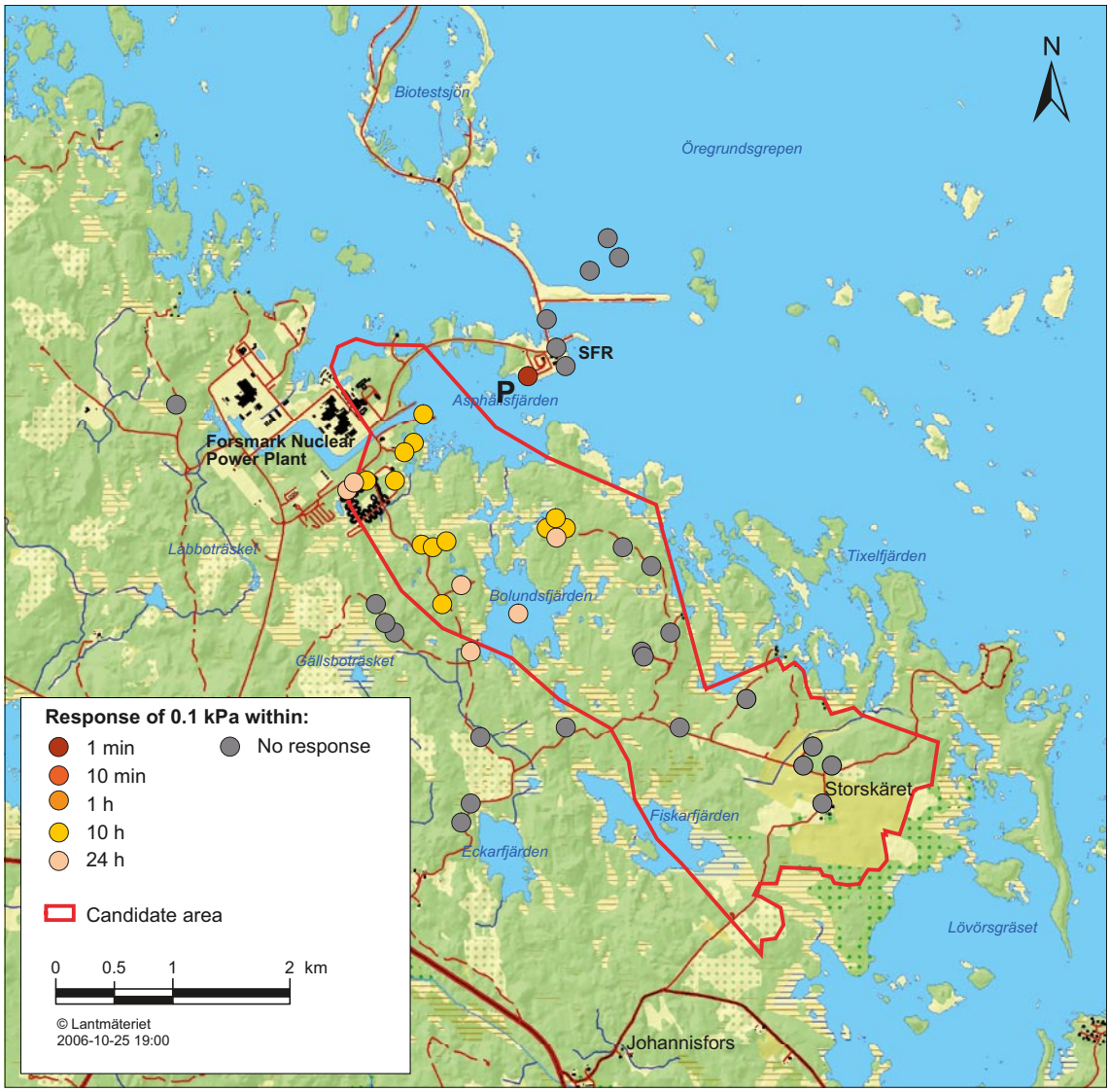

Figure 5-20. *Map showing the response times in the bedrock to the two-week long interference test conducted during the fall of 2007 in HFM33 (P) north of the candidate area. The created pressure changes propagated rapidly under the Baltic Sea, and clear hydraulic responses were observed in many boreholes in the uppermost c 100–150 m of the bedrock within the target area including HFM14. The maximum radius of influence was about 2.2 km. (Figure 4-5 in /Follin et al. 2008a/.)*

Besides confirming the hypothesis of a shallow bedrock aquifer, the two confirmatory, large-scale interference tests provided three additional important results:

1. The interference test that was run over three months in HFM14 resulted in almost identical final drawdowns at many observation points compared with the previous interference test that was run in this borehole over three weeks in the summer of 2006, in spite of the significant difference in test time. This observation indicates a positive hydraulic boundary nearby and/or leakage from groundwater storage in the Quaternary deposits above. (In the context of interference tests, a positive hydraulic boundary means an infinite source of water, e.g. the Baltic Sea).
2. The interference test that was run over two weeks in HFM33 was conducted in a horizontal fracture located at about 100 m depth. The transmissivity of the horizontal fracture was determined to be about $3 \cdot 10^{-4}$ m^2/s. The pressure changes during the pumping propagated rapidly under the Baltic Sea, and clear hydraulic responses were observed in many boreholes within the target area including HFM14 (Figure 5-20). Interestingly, no visible responses

were observed in the nearby boreholes HFM34 and HFM35, which are located on the other side of the Singö deformation zone, see Figure 5-21. Also, no visible responses were observed in borehole KFM11A or in the monitoring network in the proximity of the SFR repository.

In contrast, the abstraction of drainage water in the SFR repository (c. 5–6 L/s) has a strong impact (metres to tens of metres) on the groundwater levels in the monitoring network in the bedrock in the proximity of the repository, including HFM34 (c. 3 m) and HFM35 (c. 5.5 m), which are located at a distance of c 500 m from the SFR repository, see Figure 5-22. Furthermore, the monitoring of groundwater levels in KFM11A that began at the end of 2007 indicates that all monitoring intervals on both sides of the Singö deformation zone respond to the abstraction of drainage water in the SFR repository. For instance, the uppermost monitoring section in KFM11A (0–130 m borehole length) has a groundwater level of c two metres below the datum and the bottom most monitoring section in KFM11A (711–850 m borehole length) has a groundwater level of c seven metres below the datum. The estimated transmissivities of these two bedrock intervals are $8 \cdot 10^{-6}$ m^2/s and $1 \cdot 10^{-6}$ m^2/s, respectively.

3. Figure 5-23 shows an overview of the responses observed at repository depth within the target area during the two large-scale interference tests conducted in HFM14 and HFM33 in the summer and autumn of 2007, respectively. The two pictures suggest that most of the monitoring sections did not respond to these tests. However, the monitoring sections installed in zone ENE0060A were in hydraulic contact with the shallow bedrock aquifer on top during both tests. The hydraulic contact with zone A2 in borehole KFM02A is as expected.

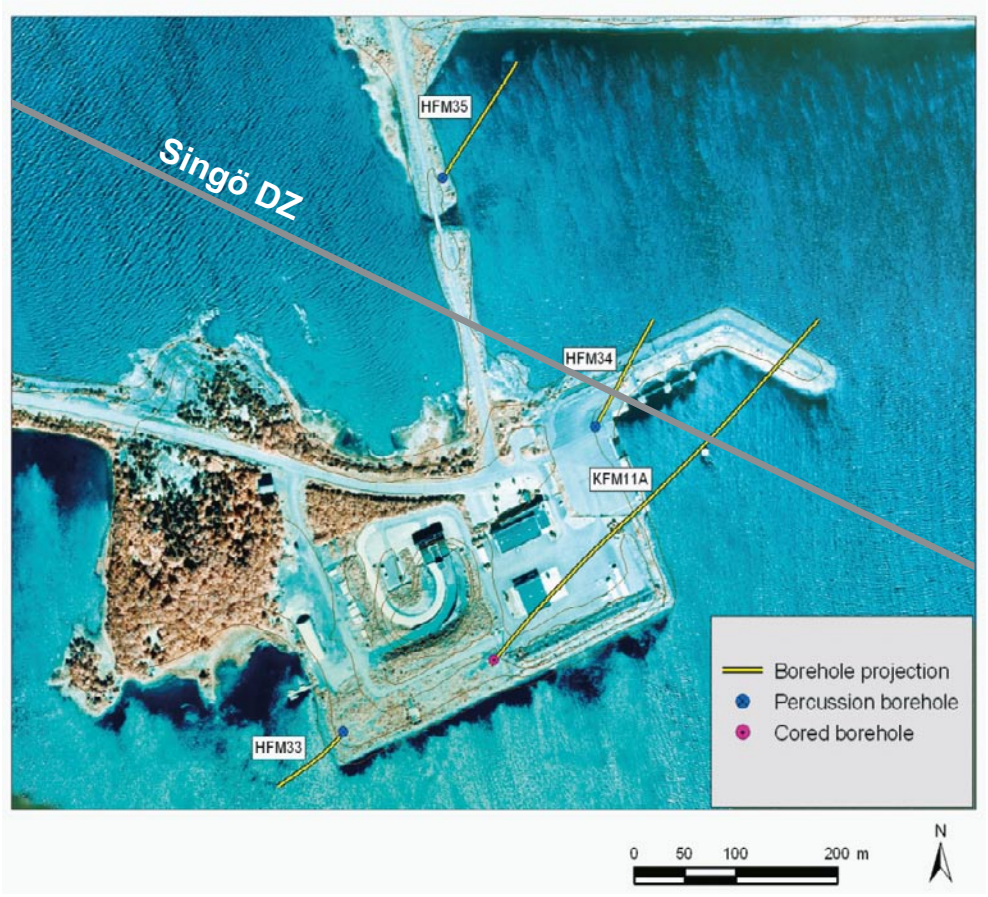

Figure 5-21. *Map showing the SFR office buildings, the Singö deformation zones and borehole locations of HFM33, HFM34, HFM35 and KFM11.*

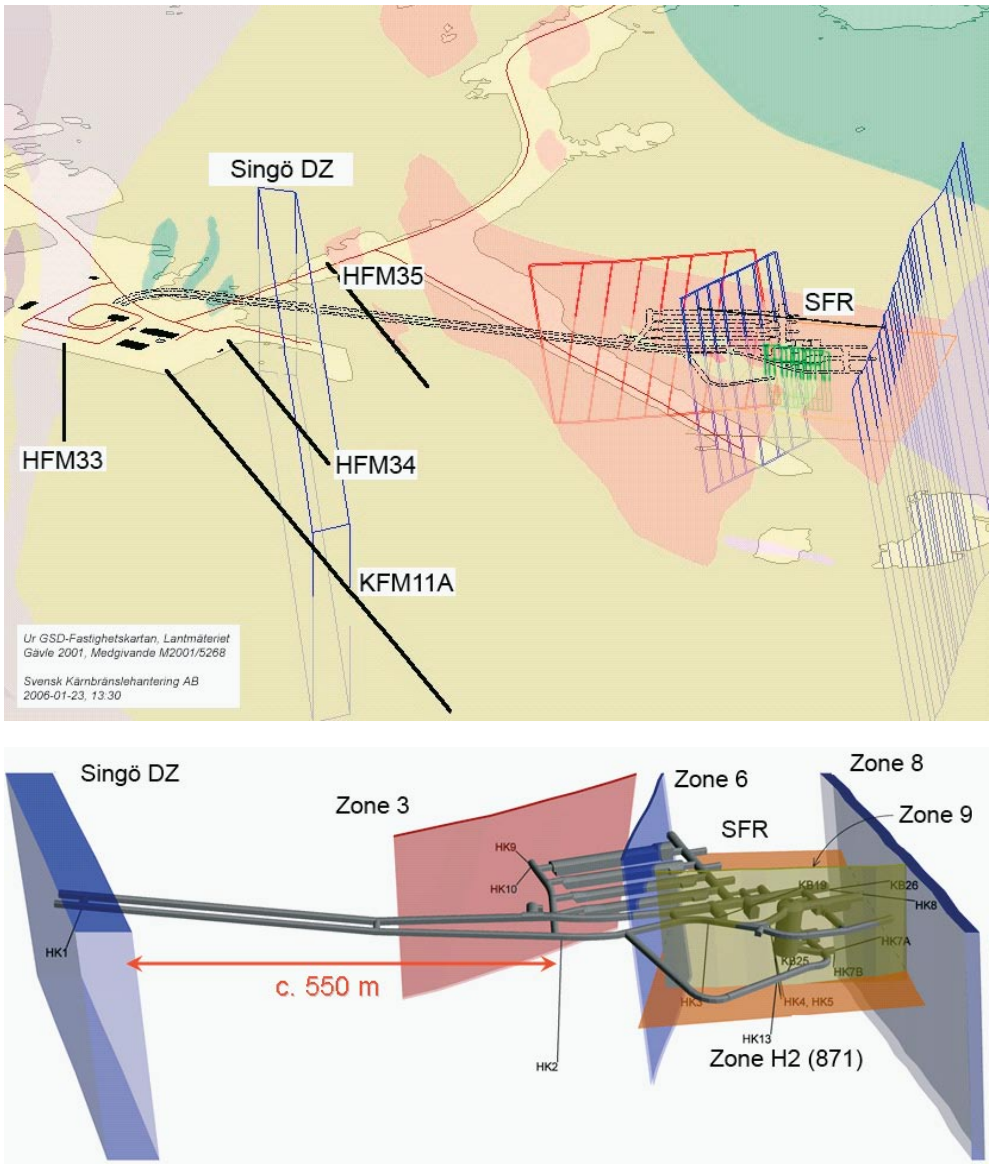

Figure 5-22. *Two views towards WNW showing the SFR area. Top: The Singö deformation zone (Singö DZ), the SFR repository and the boreholes closest to the Singö deformation zone. Bottom: The boreholes closest to the repository. (Figure 4-8 in /Follin et al. 2008a/.)*

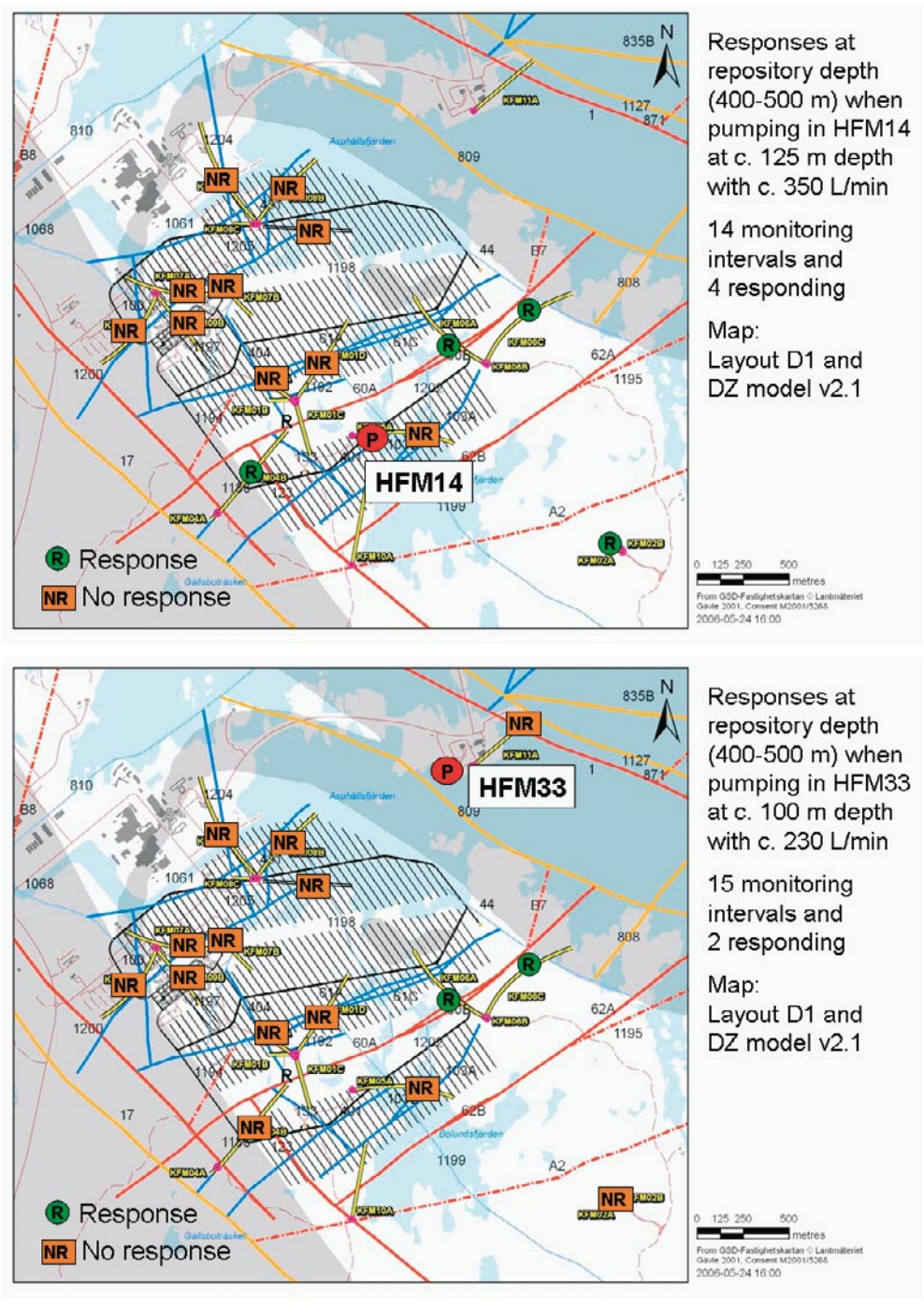

Figure 5-23. *Overview of hydraulic responses observed between 400 and 500 m depth during the twelve-week long pumping in HFM14 during the summer of 2007 (top) and during the two-week long pumping in HFM33 during November 2007 (bottom). (Figure 4-9 in /Follin et al. 2008a/.)*

5.5 Hydraulic diffusitvity of the shallow bedrock aquifer

The extensive and rapid transmission of fluid pressure changes (drawdown) during the large-scale interference test that was run over three weeks during the summer of year 2006 in borehole HFM14, see Figure 4-5 and Figure 4-6, suggests that the sheet joint features together with the sub-horizontal fracture set and outcropping deformation zones create a well connected network of structures in the uppermost 150 m of the bedrock. In effect, the shallow bedrock aquifer illustrated in Figure 5-16 is highly anisotropic and has little or no storativity. That is, the fracture system is simply very transmissive in the horizontal direction with a good hydraulic contact with outcropping zones. This interpretation is supported by other observations at the site including the two interference tests discussed in the previous section and the natural transients discussed in Appendix G in /Follin et al. 2007c/.

Figure 5-24 shows a plot of the hydraulic diffusivities and the maximum drawdowns at the 71 observation points that responded to the 2006 interference test in HFM014. The hydraulic diffusivities shown in Figure 5-24 were evaluated based on the work by /Streltsova 1988/, cf Eq. (4-1).

One reason for the high hydraulic diffusivities (cf. section 4.2) is illustrated in Figure 5-25, which shows a sheet joint encountered at c 40 m depth at drill site 1. The BIPS images reveal a very wide aperture (decimetres). The boreholes shown are HFM01 and HFM02, which lie c 220 m apart. The sheet joint shown in Figure 5-25 is in excellent hydraulic contact with zone A2, which outcrops close to drill site 1. Zone A2 intersects borehole KFM02A at c 400 m depth at drill site 2 at about 2 km to the southeast of drill site 1 and a hydraulic interference between drill sites 1 and 2 has been demonstrated by several interference tests. Hydraulic interference exists also between the gently dipping zones encountered at drill sites 2 and 3, which are also about 2 km apart, but in the opposite direction to drill site 1, see Figure 5-4.

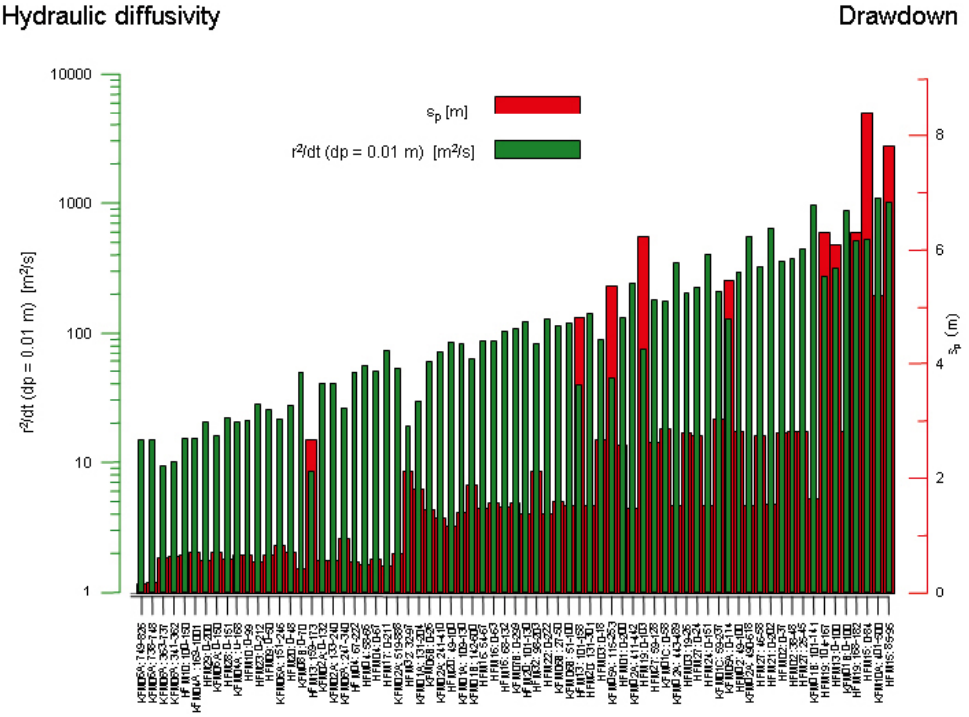

Figure 5-24. *Hydraulic diffusivities evaluated according to /Streltsova 1988/, and maximum drawdowns at the 71 observation points that responded to the 2006 interference test in HFM014, cf Figure 4-5. The interpreted diffusivities range between 10–1,000 m²/s, which implies a quite transmissive network of flowpaths of little or no storativity. (Figure3-29 in /Follin et al. 2007c/.)*

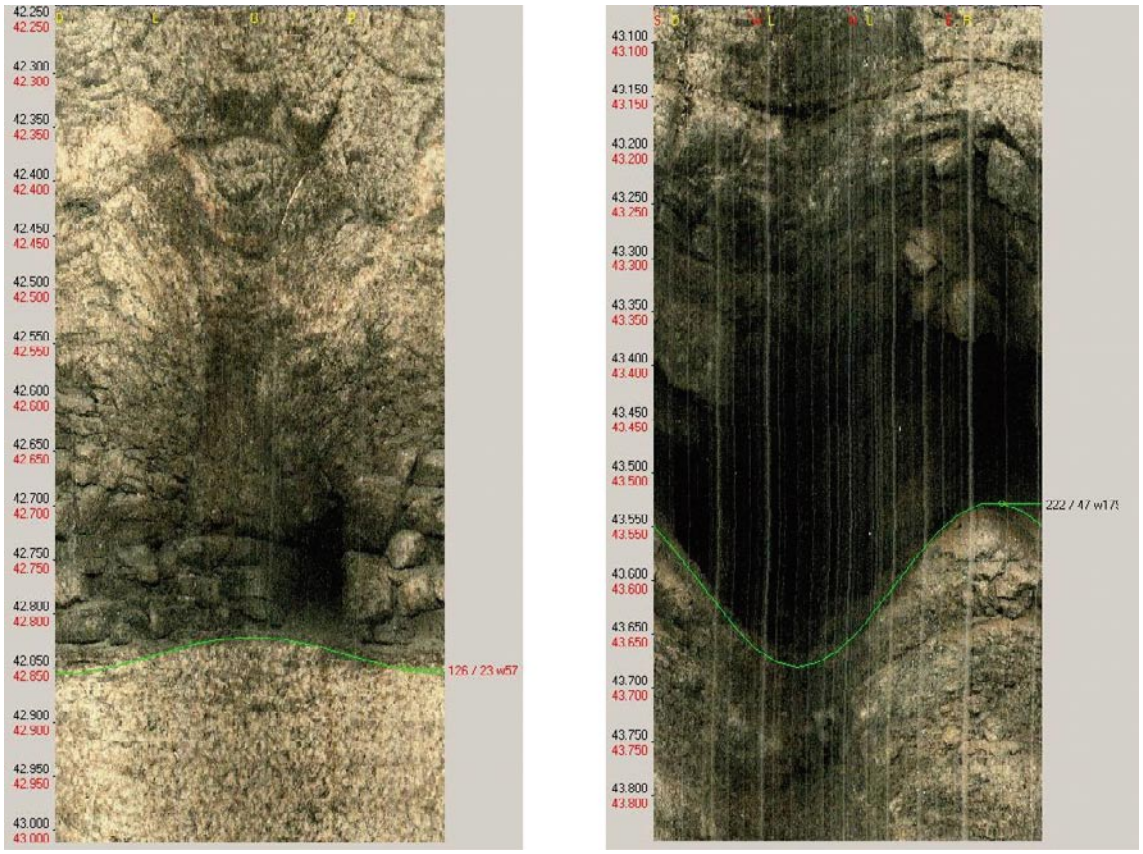

Figure 5-25. *Two BIPS pictures showing the intersections with the horizontal fracture/sheet joint encountered at c 40 m depth at drill site 1. Left: HFM01; T = $4.5 \cdot 10^{-5}$ m^2/s. Right: HFM02, T = $5.9 \cdot 10^{-4}$ m^2/s. The apertures in the pictures are 1–3 dm wide and show evidence of being channelised due to infill. The two boreholes are c 220 m apart. The hydraulic diffusivities associated with these boreholes while pumping in HFM14 are in the range 100–300 m^2/s, see Figure 5-24. (Figure G-1 in /Follin et al. 2007c/.)*

6 Parameterisation of hydraulic domains

6.1 Hydraulic conductor domain (HCD) model

An exponential model for the depth dependency of the in-plane deformation zone transmissivity was suggested for use in stage 2.2 based on the data shown in Figure 5-1. The depth trend model may be written as:

$$T(z) = T(0)\ 10^{z/k} \tag{6-1}$$

where T(z) is the in-plane deformation zone transmissivity, z is the elevation (RHB 70), $T(0)$ is the expected value of the transmissivity of the deformation zone at zero elevation and k is the depth interval that gives an order of magnitude decrease of the transmissivity. The value of k was determined to 232.5 m from the data shown in Figure 5-1 (see section 9.4.2 in /Follin et al. 2007b/). The value of $T(0)$ was estimated by inserting a measured value [z', $T(z')$] in Eq. (6-1), i.e.:

$$T(0) = \mathrm{T}(z')10^{-z'/k} \tag{6-2}$$

In the case of several measurements at different locations in the same zone, the geometric mean of the calculated values of $T(0)$ was used as an effective value, $T_{eff}(0)$ in Eq. (6-1). With this approach, the effect of conditioning to a measurement was to extrapolate the conditioned value over the entire length of the deformation zone laterally, but not more than 100 m vertically, see Figure 6-1. Lateral heterogeneity was simulated in stage 2.3 by adding a log-normal random deviate to the exponent in Eq. (6-1), i.e.:

$$T(x,y,z) = T(0)10^{\,z/k+\mathbf{N}(0,\sigma_{\log(T)})} \tag{6-3}$$

where $\sigma_{\log(T)} = 0.632$. The applied value of $\sigma_{\log(T)}$ implies that 95% of the lateral spread in $\log(T)$ is assumed to be within 2.5 orders of magnitude (see section 9.4.2 in /Follin et al. 2007b/). Furthermore, the transmissivity model assumed a nugget covariance model for the lateral spatial variability, which was conditioned on transmissivity data measured. Since the heterogeneity away from the measurement boreholes is undetermined, this required a stochastic approach using several model realisations, see Figure 6-2 for an example. The calibrated *deterministic base model realisation* derived in stage 2.2 corresponds to the case where $\sigma_{\log(T)}$ was set to zero.

6.2 Hydraulic rock domain (HRD) model

The methodology for a combined analysis of fracture geological and hydrogeological information (hydrogeological DFN modelling) was first derived and applied in the preliminary SDM /SKB 2005a/. For the CSI stage, a much greater quantity of data was available, and in particular data were available for core-drilled boreholes in a variety of orientations. The methodology used to parameterise the fracture domains starts with a connectivity-sensitivity analysis of different DFN models and ends with flow simulations using the most reliable DFN model deduced in the connectivity analysis. Flow simulations were carried out using three different kinds of correlations between fracture transmissivity and fracture size, see Table 2-2.

The hydrogeological DFN modelling is based on the assumption that:

$$P_{10,all} \geq P_{10,open} \geq P_{10,cof} \geq P_{10,PFL} \tag{6-4}$$

where $P_{10,cof}$ denotes the frequency of *connected open fractures*, a key property of any hydrogeological DFN model. The meaning of the different suffixes (*all*, *open*, *cof* and *PFL*) in Eq. (6-4) is explained in Figure 6-3.

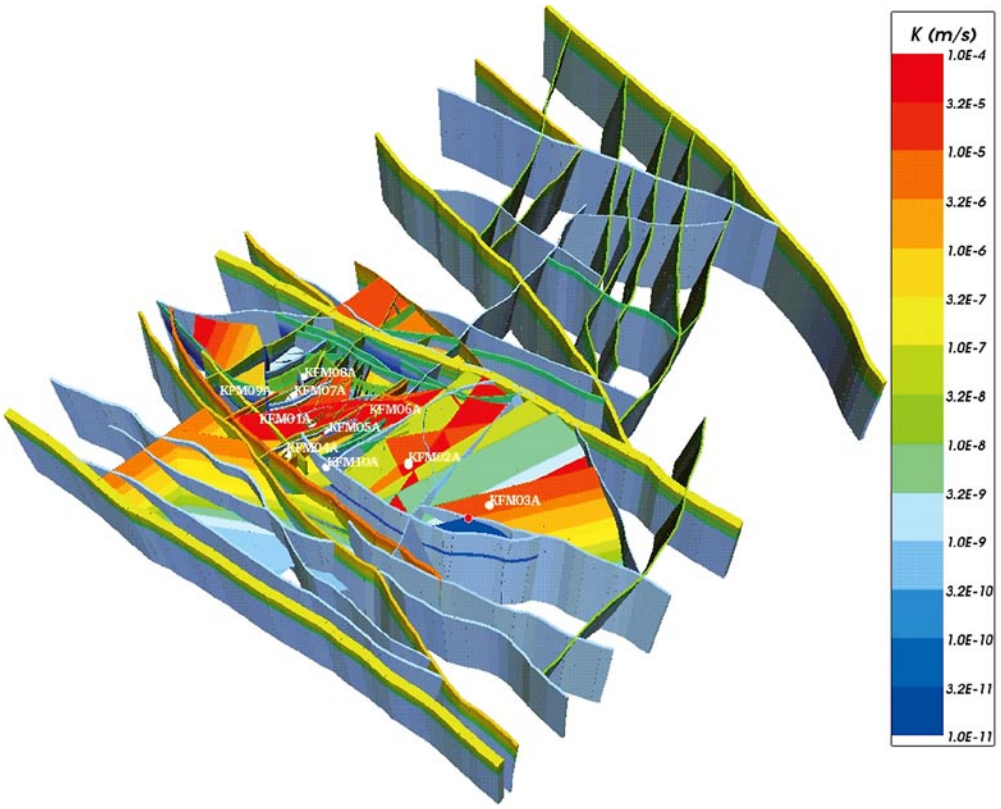

Figure 6-1. *The resulting property model using Eq. (6-1). Here, the regional scale deformation zones are coloured by the hydraulic conductivity within the zones and drawn as volumes to show their assigned hydraulic width. The depth dependency is clearly apparent. The effect of conditioning to a measurement was to extrapolate the conditioned value over the entire length of the deformation zone laterally, but not more than 100 m vertically. (Figure 3-35 in /Follin et al. 2007c/.)*

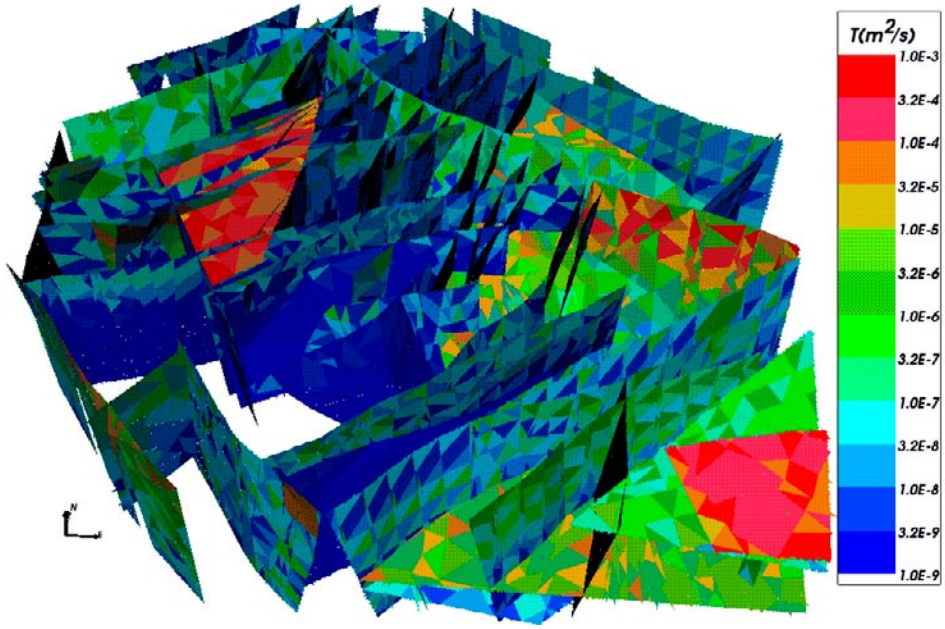

Figure 6-2. *Visualisation of an example realisation of the deformation zones occurring inside the local model domain using Eq. (6-3); the deformation zone transmissivity model assumed a nugget covariance model for the lateral spatial variability in log(T), which was conditioned on transmissivity data measured. The optimal size of the finite element mesh used to model the nugget covariance was c 100 m.*

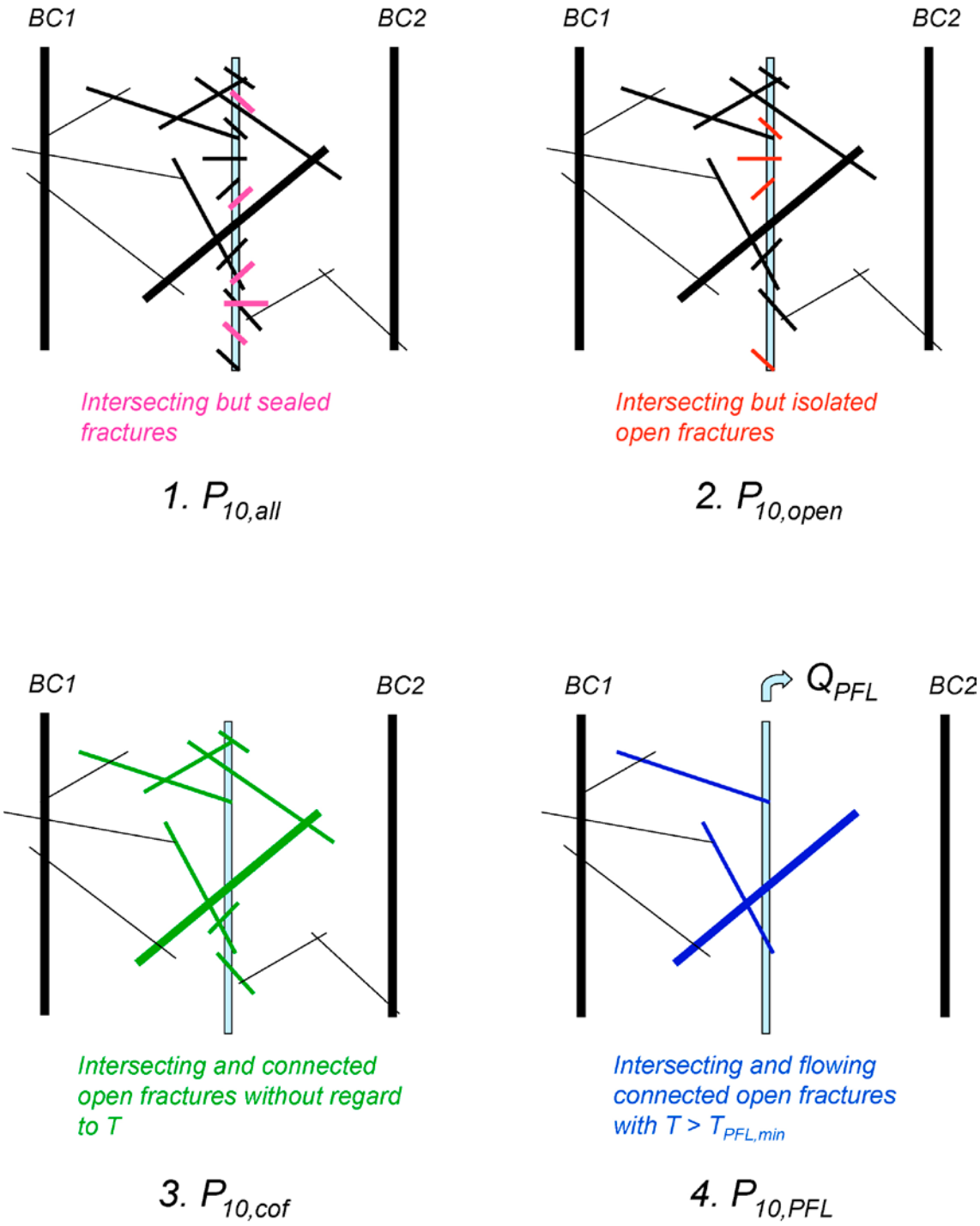

Figure 6-3. *$P_{10,all}$ is the frequency of all fractures intersecting the borehole, $P_{10,open}$ is the frequency of open fractures, $P_{10,cof}$ is the frequency of connected open fractures and $P_{10,PFL}$ is the frequency of flowing connected open fractures identified with the PFL-f method. BC1 and BC2 represent hydraulic boundary conditions, e.g. the surface and/or nearby deformation zone which is connected to the surface. $P_{10,cof}$ cannot be measured, but simulated values can be compared with the measured value of $P_{10,PFL}$. (Figure 11-1 in /Follin et al. 2007b/.)*

The Terzaghi corrected linear intensities $P_{10,open,corr}$ and $P_{10,PFL,corr}$ shown in Table 5-1 and Table 5-2 reveal that there are essentially three flowing fracture sets in fracture domain FFM01 above 400 m depth (NS, NE and HZ) and two flowing fractures sets below this depth (NE and HZ). Corresponding data for the other fracture domains are reported in /Follin et al. 2007b/. The computed values of $P_{10,open,corr}$ and $P_{10,PFL,corr}$ were used to constrain the derivation of optimal parameter values for the tectonic continuum DFN model envisaged in Figure 2-3. In short, five different combinations of values of two parameters referred to as k_r and r_0 were tested based on the results reported in the preliminary SDM. k_r and r_0 are characteristic parameters of a power-law feature size probability density function, see Appendix C. For each combination of parameter values, the value of the 3D fracture intensity parameter referred to as $P_{32,open}[r \geq r_0]$ (the total fracture surface area per unit volume of rock of all open fractures with radii greater that r_0) was altered until a fair match between simulated and computed values of $P_{10,open,corr}$ was achieved, i.e.:

$$P_{32,open} \approx P_{10,open,corr} \tag{6-5}$$

The hydrogeological DFN simulations were repeated ten times (ten realisations) using the Monte Carlo method. Secondly, a connectivity analysis was carried out for each combination of parameter values and realisation, and the obtained values of $P_{10,cof,corr}$ were recorded. The results indicated which of the five combinations of parameter values gave the closest match between $P_{10,cof,corr}$ and $P_{10,PFL,corr}$, i.e.:

$$P_{10,cof,corr} \geq P_{10,PFL,corr} \tag{6-6}$$

Finally, a 'fine-tuning' of the power-law size parameters for each fracture set i was carried out to produce an optimised match between $P_{10,cof,corr}$ and $P_{10,PFL,corr}$, i.e.:

$$P^i_{10,cof,corr} \approx P^i_{10,PFL,corr} \qquad i \in (NS, NE, NW, EW, HZ) \tag{6-7}$$

Figure 6-4 illustrates the match for the optimised case above and below 400 m depth for each set. The same power-law size distribution parameters were used for both depth intervals, but are different between the sets. Hence, it was assumed that the large change in flow-anomaly frequency is due to the reduction in fracture intensity with depth. However, the optimisation of size parameters was based on data above 400 m depth, since the intensity values are non-zero in this depth interval.

Below 400 m depth, the model predicts very low mean connected open fracture intensities using the optimised model, but it does not reproduce the zero intensities observed in the data for the NW and EW orientation sets. Partly, this is to be expected since a stochastic approach is being used, and some realisations happen to have a small number of connected fractures intersecting the borehole. One way of reconciling the hydrogeological DFN modelling is to also consider a depth variation in the hydraulic properties such that fractures below 400 m depth have a lower fracture transmissivity as well as intensity chosen so that a number of the fractures simulated below 400 m depth have transmissivities below the detection limit for the PFL-f method.

To complete the hydrogeological DFN parameterisation, flow simulations were performed to calibrate a set of alternative relationships between fracture transmissivity and size that reproduced the numbers of inflows and the distribution of their magnitude as measured with the PFL-f tests. The four calibration targets used in this process are listed in section 2.3.4.

Figure 6-5 shows an example of a flow simulation carried out. Here, the fractures are coloured by head, or coloured grey where they are not connected to the network. The only combinations of parameter values considered in the flow modelling were those based on the optimised power-law size distributions.

The relatively high flow rates above 400 m depth are actually concentrated at shallow depths, and hence the initial assumption of a two-layer model was refined to introduce a further depth zone in the top 200 m to give a three-layer model: above 200 m depth, between 200 m and 400 m depth, and below 400 m depth. The measured open fracture intensities in each of these sections were

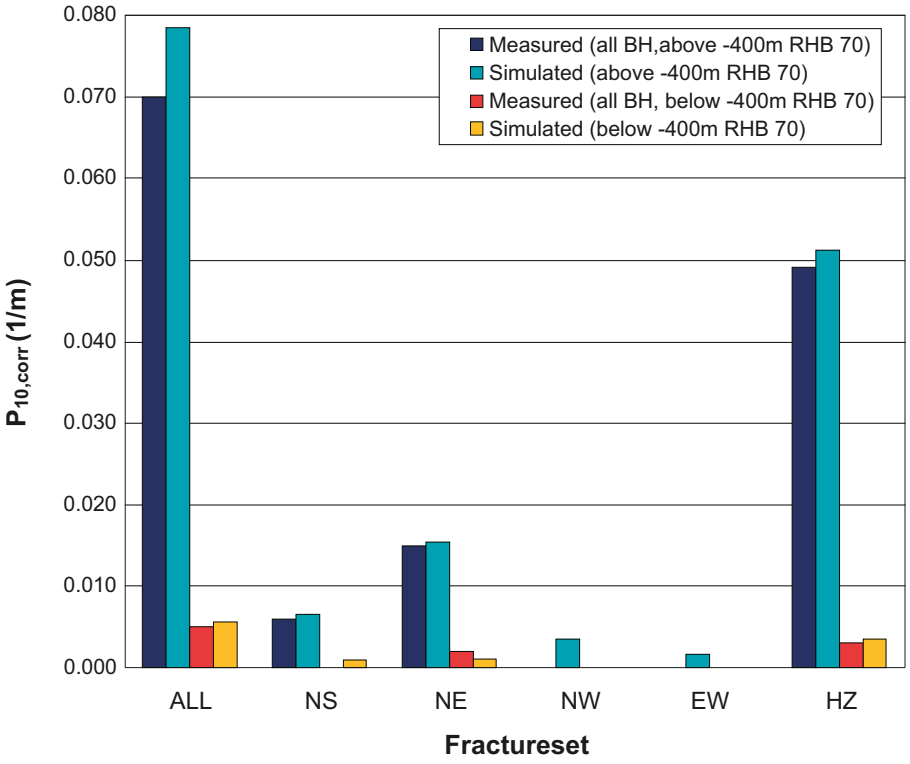

Figure 6-4. *Comparison between the Terzaghi corrected linear intensities of PFL-f data, $P_{10,PFL,corr}$, and the mean intensities of connected open fractures, $P_{10,cof,corr}$, over ten realisations of a vertical borehole above and below 400 m depth for fracture domain FFM01, respectively. The simulation results represent the optimised power-law size model of each fracture set. (Modified after Figure 11-10 in /Follin et al. 2007b/.)*

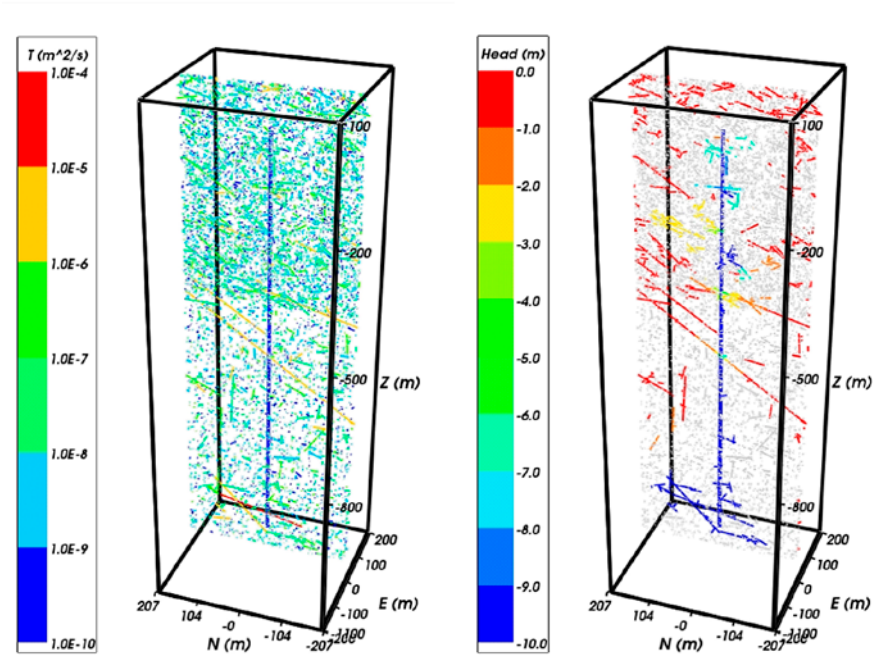

Figure 6-5. *Vertical cross-section through one realisation of the hydrogeological DFN model of fracture domain FFM01 with different fracture intensity above and below 400 m depth. Left: All open fractures coloured by transmissivity. The 1 km generic vertical borehole is coloured blue in the middle of the figure. Right: The connected open fractures coloured by drawdown with unconnected fractures coloured grey. (Modified after Figure 11-9 in /Follin et al. 2007b/.)*

used as input data for the hydrogeological DFN model and the transmissivity parameters were adjusted within each depth zone until a reasonable match to the inflow distribution and total flow was achieved. The resulting hydrogeological DFN parameterisation for a three-layer model of FFM01 is given in Appendix C. The coefficients, exponents or standard deviations as appropriate to each transmissivity model reflect the rapid reduction in inflow magnitudes with depth. This trend is quantified in the comparison of measured and simulated total flow rates for each of the three transmissivity models tabulated in Table 6-1. The flow rates decrease by about two orders of magnitude below 200 m depth, then by about another order of magnitude below 400 m depth. Table 6-1 indicates that the semi-correlated transmissivity-size model gave the lowest overall ratios of the geometric mean of the modelled inflows over ten hydrogeological DFN realisations to the measured inflows for the three depth intervals in FFM01.

An example of the comparison of inflows between model and data is given for the deduced three-layer model using a semi-correlation between fracture size and transmissivity. Figure 6-6 shows a histogram plot of Q/s for each layer. The match to the observed flow is poorest for the deepest layer (below 400 m depth). However, it should be noted that there are very few features carrying flow at this depth, so the distributions of PFL-f data or flows are not very well defined. Figure 6-7 shows bar and whisker plots that compare the measured and simulated inflows for the different fracture sets, normalised to appropriate borehole length sections. The numbers alongside the bars represent the numbers of inflows above the detection limit per 200 m or 600 m borehole section. The detection limit of the PFL-f method is assumed to be the minimum transmissivity measured in the modelled volume ($2.5 \cdot 10^{-10}$ m^2/s for FFM01)

Figure 6-7 shows that the inflows are dominated by the HZ fracture set with a small contribution from the NS and NE sets; the NW and EW fractures sets make no contribution. The frequency of inflows decreases to about a quarter below 200 m depth, and by almost a further order of magnitude below 400 m depth. A complete set of comparisons for the three-layer model is given in /Follin et al. 2007b/.

The matches for all three transmissivity models are reasonable. To illustrate how the different transmissivity-size relationships compare, they are plotted as log-log plots in Figure 6-8 for each of the three layers based on the parameters given in Table C-1 in Appendix C. The semi-correlated and correlated models follow similar trends and also intercept the uncorrelated model for fractures of about 10 m radius. This is to be expected, since fractures of around 10–100 m are the ones that form the body of the connected network giving the inflows in the simulations. There is less consistency between the transmissivity models below 400 m depth as the distribution of inflows is poorly determined at these depths, there being so few data points to guide the fit.

Table 6-1. Comparison of measured total inflows to boreholes in FFM01 (PFL-f data) and the geometric means of ten hydrogeological DFN realisations for a three-layer model with depth dependency in transmissivity as detailed in Table C-1 in Appendix C. The flow rates are normalised to a 200 m section above 200 m depth and between 200 m and 400 m depth, and to a 600 m section below 400 m depth. The ratio of the geometric means to the PFL-f data are shown in *italics*. (Modified after Table 11-21 in /Follin et al. 2007b/.)

	Total flow rate divided by drawdown Q/s [m²/s]					
	Above 200 m depth per 200 m of borehole		Between 200 m and 400 m depth per 200 m of borehole		Below 400 m depth per 600 m of borehole	
Measurements (PFL-f)	$2.9 \cdot 10^{-5}$	*1*	$1.0 \cdot 10^{-7}$	*1*	$3.8 \cdot 10^{-8}$	*1*
Semi-correlated model	$3.1 \cdot 10^{-5}$	*1.07*	$1.1 \cdot 10^{-7}$	*1.10*	$5.4 \cdot 10^{-8}$	*1.42*
Correlated model	$3.0 \cdot 10^{-5}$	*1.03*	$2.0 \cdot 10^{-7}$	*2.00*	$5.4 \cdot 10^{-8}$	*1.42*
Uncorrelated model	$1.4 \cdot 10^{-5}$	*0.48*	$2.1 \cdot 10^{-7}$	*2.10*	$8.1 \cdot 10^{-9}$	*0.23*

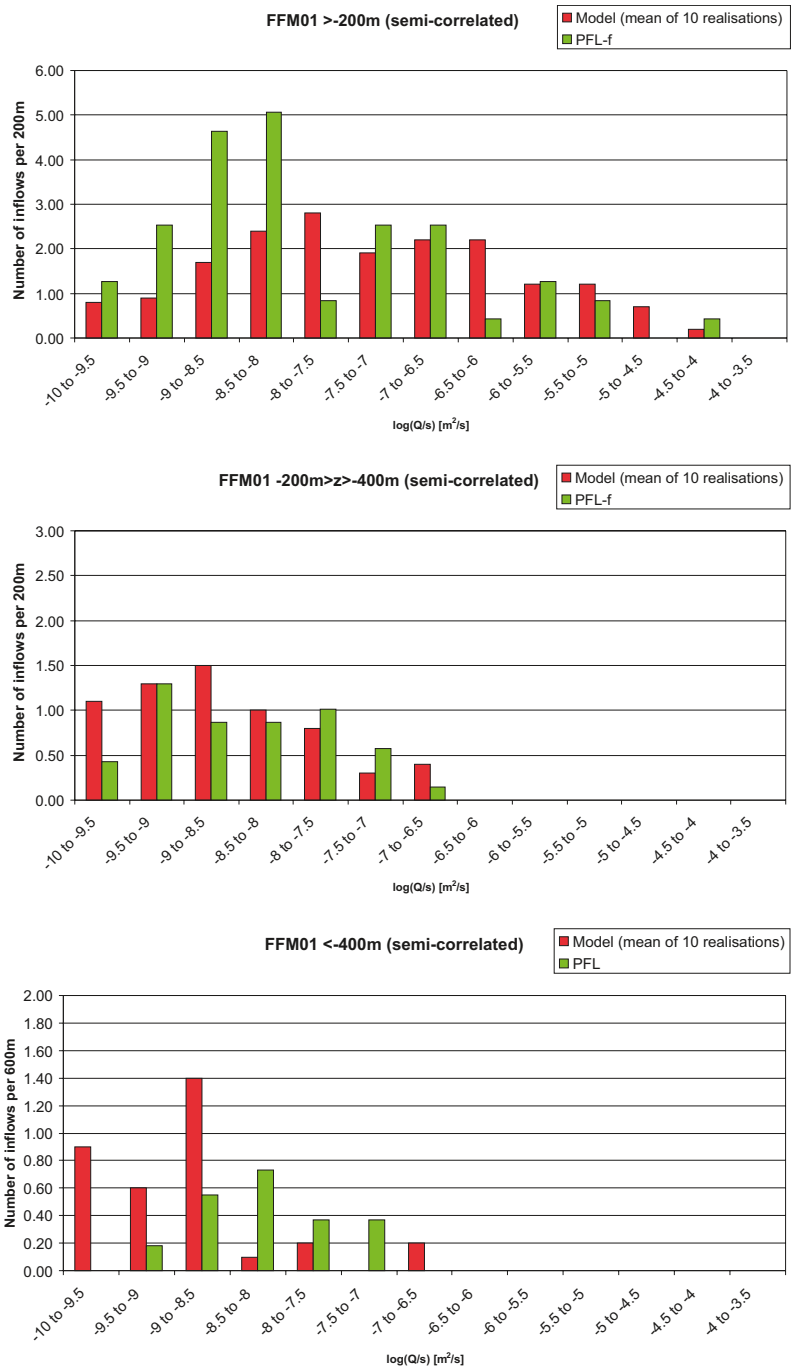

Figure 6-6. *Histogram comparing the distribution of the magnitude of inflows divided by drawdown, Q/s, at abstraction boreholes in fracture domain FFM01 with a semi-correlated transmissivity model (see Table C-1 in Appendix C for parameter values). Top: above 200 m depth; Middle: between 200 m and 400 m depth; Bottom: below 400 m depth. The PFL-f measurements are treated as ensemble over all borehole sections within FFM01. Above 200 m depth and between 200 m and 400 m depth, the number of inflows is normalised with respect to a borehole section of 200 m length, and below 400 m depth relative to a 600 m section. The simulations represent statistics taken from an ensemble over ten realisations of the hydrogeological DFN model. (Figure 11-15 in /Follin et al. 2007b/.)*

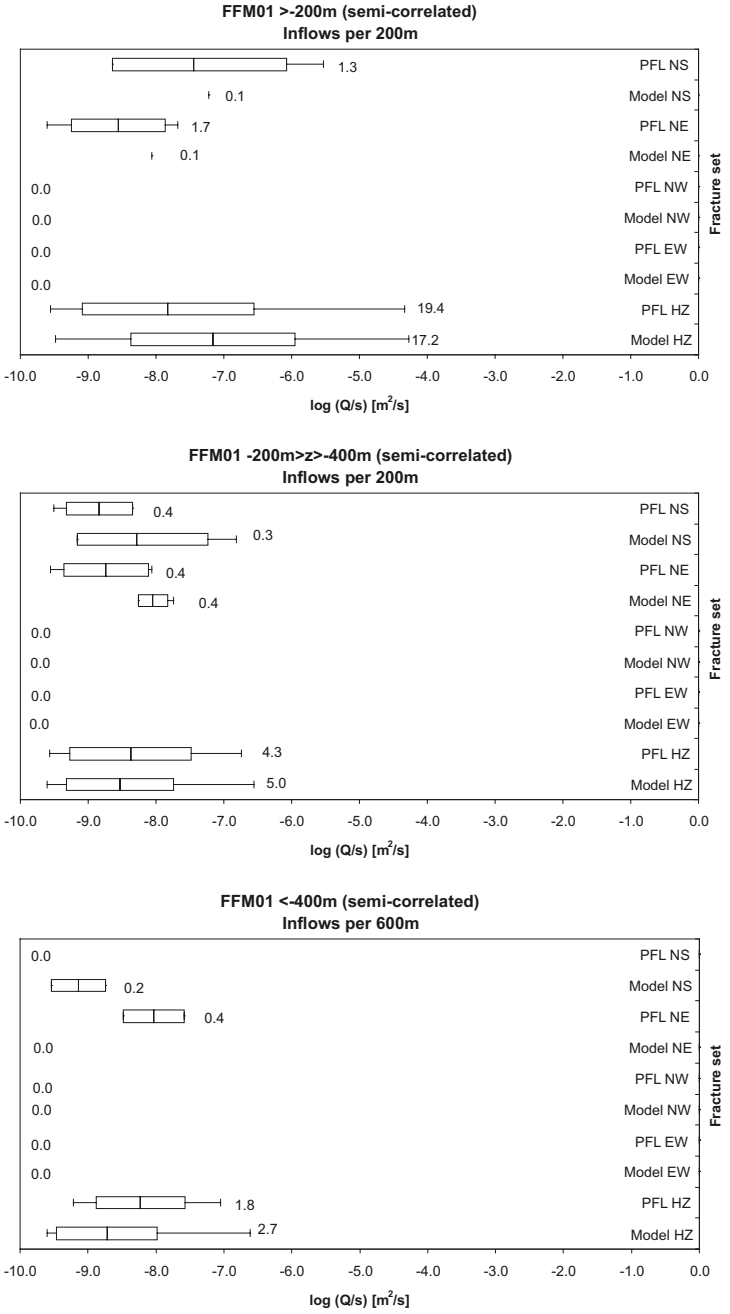

Figure 6-7. *Bar and whisker plots comparing statistics for the individual inflows, Q/s, for each fracture set derived from the PFL-f data in borehole sections within FFM01 against statistics taken from an ensemble over 10 realisations of the hydrogeological DFN model with a semi-correlated transmissivity. Top: above 200 m depth; Middle: between 200 m and 400 m depth; Bottom: below 400 m depth. The centre of the bar indicates the mean value, the ends of the bar indicate ±1 standard deviation, and the error bars indicate the minimum and maximum values. Above 200 m depth and between 200 m and 400 m depth, the total number of fractures with inflows above the detection limit is given per 200 m borehole section. Below 400 m depth, the numbers of inflows per 600 m borehole section is given. For the data, statistics are taken over the identified flowing fractures within each set, and for the model, statistics are taken over the fractures generated within each set and over ten realisations. (Figure 11-16 in /Follin et al. 2007b/.)*

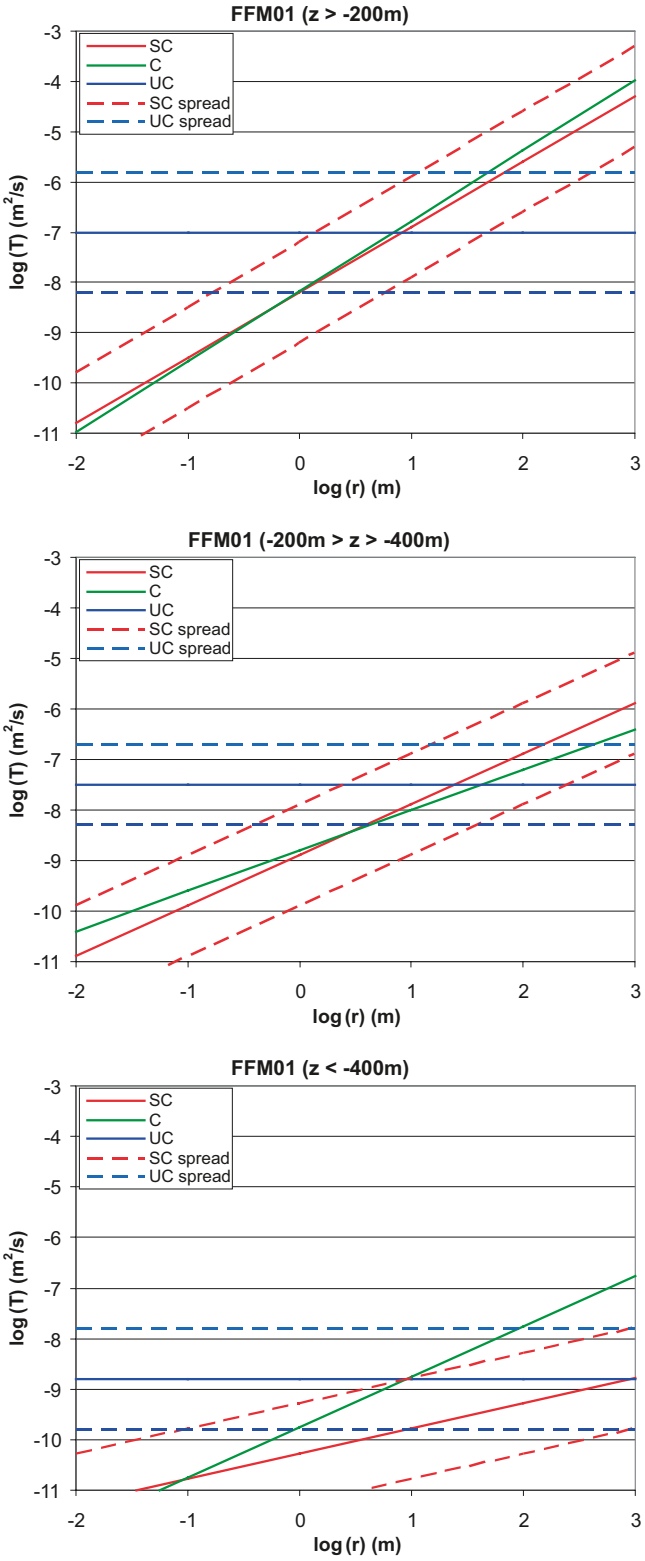

Figure 6-8. *Plots of the profile of transmissivity as a function of fracture radius for the three-layer model of fracture domain FFM01 for each of the three transmissivity versus size relationships (SC = semi-correlated, C = correlated, UC = uncorrelated) based on the parameterisation given in Table C-1 in Appendix C. (Figure 11-17 in /Follin et al. 2007b/.)*

Bearing in mind the strong variations with depth, /Follin et al. 2007b/ suggested that a three-layer model should be adopted as the basis for further hydrogeological modelling of fracture domain FFM01. Furthermore, /Follin et al. 2007b/ concluded that the fractures in those minor parts of fracture domain FFM01 that lie above 200 m depth show similar hydrogeological characteristics to the fractures in fracture domain FFM02, and that the variation in fracture intensity and flow in fracture domain FFM03 is much less dramatic than in FFM01. The results of the hydrogeological DFN modelling of all fracture domains FFM01–FFM06 modelled in /Olofsson et al. 2007/ are given in Appendix C. The *deterministic base model realisation* that is discussed below consists of a single realisation based on these properties.

Figure 6-9 shows an example of a hydrogeological DFN realisation using the network properties listed in Appendix C. The realisation is shown as a NW-SE cross-section and two horizontal trace planes at 30 m depth and 500 m depth, respectively. The images in the left column show the traces of *open fractures*. The images in the right column show the traces of the *connected open fractures*. The low connectivity below 400 m depth is clearly visible.

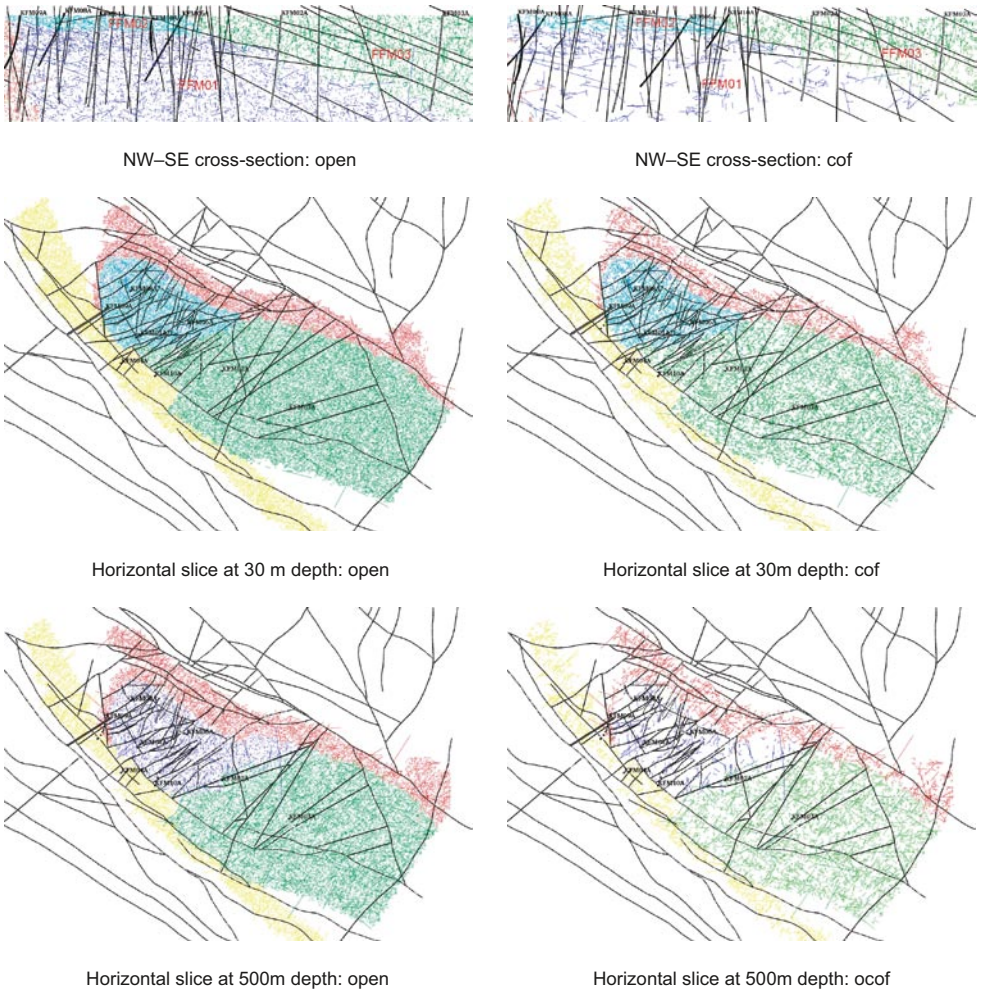

Figure 6-9. *An example of a hydrogeological DFN realisation using the network properties listed in Appendix C. The realisation is shown as a NW-SE cross-section and two horizontal trace planes at 30 m depth and 500 m depth, respectively. The depth extension of the cross-section is c 1.2 km and the length is c 5 km. The images in the left column show the traces of open fractures. The images in the right column show the traces of the connected open fractures (cof). The DFN fracture traces are coloured by fracture domain: FFM01 and FFM06 are dark blue, FFM02 is light blue, FFM03 is green, FFM04 is yellow, and FFM05 is red. Slices through the deformation zones (local and regional models) at the same depths are superimposed in black. The stochastic fractures are generated with radii between 5.64–564 m. (Figure 3-16 in /Follin et al. 2007c/.)*

6.3 Hydraulic soil domain (HSD) model

Table 6-2 and Table 6-3 show the parameter values provided for groundwater flow modelling by the surface system group /Bosson et al. 2008/. Most of the values represent so-called 'best estimates' based on site specific data supported by generic data when site specific data are scarce, cf Table 3-13 in /Johansson 2008/.

The thickness of the Quaternary deposits within the model area varies from less than a decimetre to over 25 m, not all layers exist everywhere, and the thickness of individual layers varies significantly. The modelling approach used in ConnectFlow implies a considerable simplification of the detailed geometrical description of the near-surface system, see section 2.3.5. The resulting equivalent hydraulic conductivity distribution is illustrated in Figure 6-10.

Table 6-2. Values of the total porosity and the specific yield of the Quaternary deposits suggested for groundwater flow modelling in stage 2.2. (Modified after Table 2-4 in /Bosson et al. 2008/.)

Layer	Total porosity [–] and specific yield [–] of layers with several types of Quaternary deposits					
	Fine till	Coarse till	Gyttja	Clay	Sand	Peat
L1	–	-	0.50 / 0.03	-	-	0.60 / 0.20
Z1	0.35 / 0.15	0.35 / 0.15	-	0.55 / 0.05	0.35 / 0.20	0.40 / 0.05
Z5	0.25 / 0.03	0.25 / 0.05	-	-	-	-
	Total porosity [–] and specific yield [–] of layers with one type of Quaternary deposits					
L2	0.35 / 0.20					
L3	0.55 / 0.05					
Z2	0.40 / 0.05					
Z3	0.35 / 0.20					
Z4	0.45 / 0.03					

Table 6-3. Values of the saturated hydraulic conductivity of the Quaternary deposits suggested for groundwater flow modelling in stage 2.2. (Modified after Table 2-4 in /Bosson et al. 2008/.)

Layer	*K* [m/s] of layers with several types of Quaternary deposits					
	Fine till	Coarse till	Gyttja	Clay	Sand	Peat
L1	–	-	$3 \cdot 10^{-7}$	-	-	< 0.6m: $1 \cdot 10^{-6}$
Z1	$3 \cdot 10^{-5}$	$3 \cdot 10^{-5}$	-	$1 \cdot 10^{-6}$	$1.5 \cdot 10^{-4}$	> 0.6m: $3 \cdot 10^{-7}$
Z5	$1 \cdot 10^{-7}$	$1.5 \cdot 10^{-6}$	-	-	-	-
	***K* [m/s] of layers with one type of Quaternary deposits**					
L2	$1.5 \cdot 10^{-4}$					
L3	$1.5 \cdot 10^{-8}$					
Z2	$3 \cdot 10^{-7}$					
Z3	$1.5 \cdot 10^{-4}$					
Z4	$1.5 \cdot 10^{-8}$					

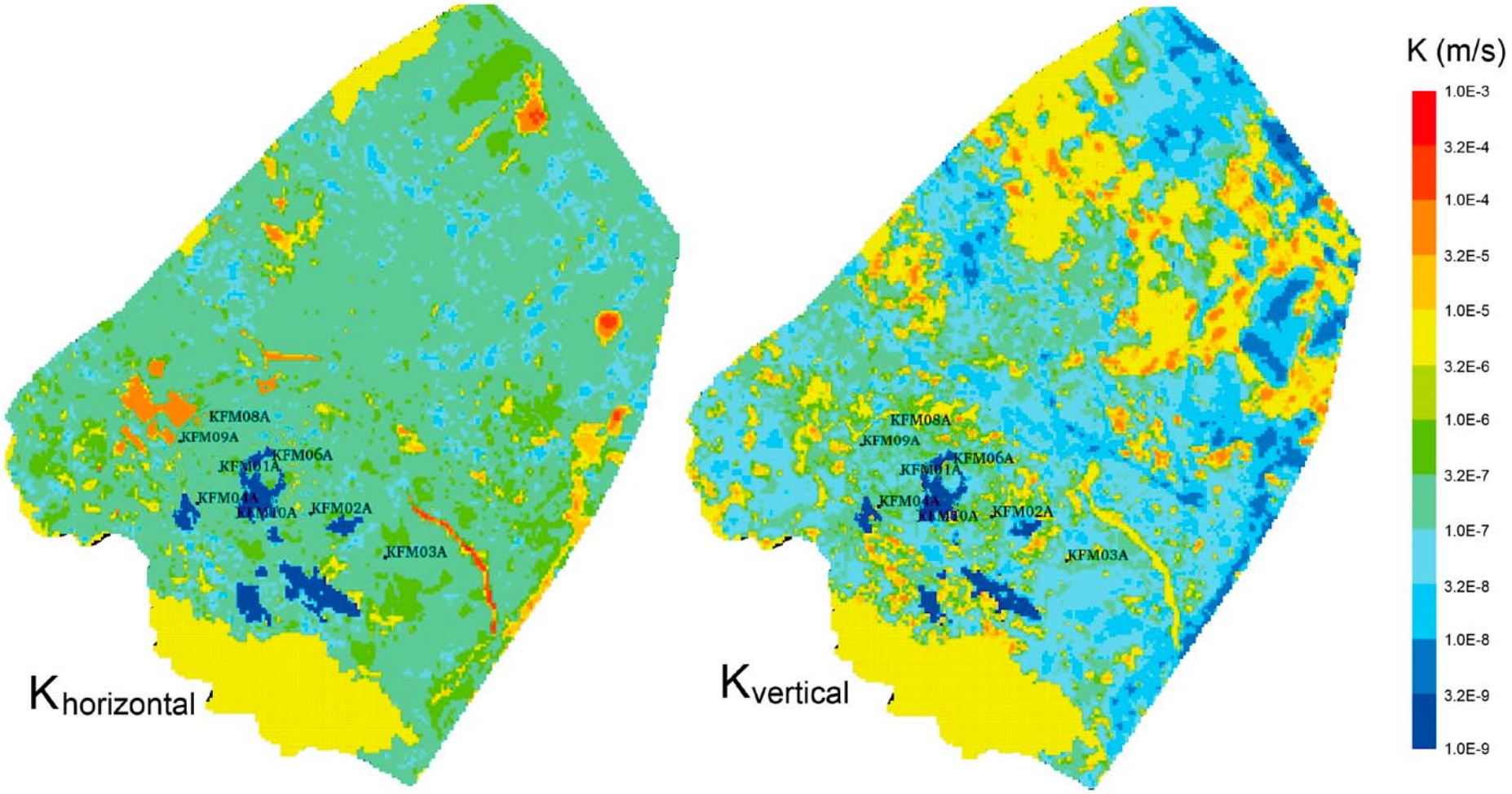

Figure 6-10. *Resulting effective hydraulic conductivity for HSD top layer based on QD layer thicknesses and hydraulic properties. Top: E-W horizontal component. Bottom: vertical component. (Modified after Figure 3-53 in /Follin et al. 2007c/.)*

7 Flow model calibration

7.1 General

Forward model calibration consists of changing values of model input parameters in an attempt to match field observations within some acceptable criteria. By comparing the model predictions with different types of field data/measurements, the overall model development can be partially calibrated to improve the parameterisation, improve understanding of the hydrogeological system, and help build confidence in the hydrogeological conceptual model of the Forsmark area. The general approach applied in the CSI stage was to use essentially the same groundwater flow and solute transport model in terms of grid discretisation and parameter settings for matching the three types of field data referred to as data sets B, C and D in section 2.2.

The ConnectFlow code was used to first generate a 3D DFN model of the site, upscale that to an equivalent continuous porous medium (ECPM) model, and use this as the basis for the 3D groundwater flow and solute transport modelling carried out in stages 2.2 and 2.3. The upscaling of a discrete system of transmissive features to an equivalent porous medium is a vital step using ECPM models. Upscaling in ConnectFlow generally employs a guard zone approach /Jackson et al. 2000/. The approach accounts for cross fluxes at the element boundaries, which typically occur when the fracture intensity in different directions is fairly high. The fracture intensity at Forsmark is fairly low and also uneven in different directions (anisotropic). It was concluded by means of numerical calculations that sufficiently good upscaling results were obtained for a simplistic upscaling approach that did not involve the more complex guard zone approach.

To become a meaningful activity in a highly heterogeneous and anisotropic medium such as the crystalline bedrock in the Forsmark area, forward model calibration requires that the structural-hydraulic properties of the deformation zones and fracture domains are properly characterised and implemented in an ECPM code. The parameterisation in ConnectFlow is a two stage process. Firstly, transmissivities inferred from the hydraulic tests are used to parameterise the deformation zone and fracture domain models as described in sections 6.1 and 6.2. Secondly, the geometrical and hydraulic properties of these two discrete models are transformed into ECPM hydraulic conductivities using a specified grid resolution (20 m within the target volume and 100 m outside). It should be noted that the ECPM properties are not needed in the migration simulations run in the safety assessment, since these are carried out on a much smaller scale than the simulations treated in the SDM. That is, the safety assessment is based on the hydrogeological DFN model directly.

The calibrated groundwater flow and solute transport model derived in stage 2.2 is also referred to as the *deterministic base model simulation*. It consists of a *single realisation* of the stochastic HRD model shown in Table C-1 through Table C-3 in Appendix C, the deterministic HSD model shown in Table 6-2 and Table 6-3 and a deterministic realisation of the HCD model shown in Eq. (6-3), i.e. with $\sigma_{\log(T)}$ set to zero. The HRD model realisation was based on the semi-correlated transmissivity-size model.

7.2 Matching the 2006 interference test in HFM14

The interference test in borehole HFM14 conducted during the dry summer of 2006 was expected to test model predictions of hydraulic communications on the scale of a kilometre or so, see Figure 4-5 and Figure 4-6. Structures of high transmissivity were expected to dominate the hydraulic responses, and so the interference test should provide a good test of the structural model and hydraulic property assignment, such as the transmissivity of zone A2 and its connections to sub-vertical zones and the sheet joint features. A large number of boreholes were monitored at dif-

ferent depth intervals, and where there are differences in the responses at different depths, the data provide a way of understanding distinctions in the hydraulic properties of the deformation zones, the fracture domains and the Quaternary deposits. HFM14 is c 125 m deep and is interpreted to intersect zone A2 between c 60–80 m depth. It is located very close to Lake Bolundsfjärden, which provides a possible source of recharge to the abstraction. Calibrating the model against hydraulic responses in monitoring holes surrounding the lake provides a means of understanding the vertical hydraulic contact between the lake, the underlying regolith and the superficial bedrock.

As an overall representation of the match against the measurements in the monitored intervals, the simulated drawdowns after 21 days are plotted as a distance-drawdown diagram in Figure 7-1. The drawdown for the nearest monitoring intervals on the left side of the graph is controlled by the hydraulic properties close to HFM14. This mainly relates to the transmissivity of the extensive sub-horizontal deformation zone A2 and the features implemented in the ConnectFlow code to model the sheet joints in the shallow bedrock aquifer. These are the key controls for most intervals up to about 500–600 m distance from HFM14. Beyond this, the responses are controlled by a more complex balance of parameters representing the hydraulics of the more distant deformation zones, the "sheet joint features", the Quaternary deposits and, presumably, the Baltic Sea.

The abstraction in borehole HFM14 during the three-week long interference test equates to an effective sink of about 183,000 m^3/year. For the infiltration rate of 20 mm/year used in the simulations, this is equal to the total annual recharge from an area of about 1,700 m radius. However, this radius of influence is reached already within three weeks of testing, see Figure 7-1. This suggests laterally extensive sheet joints with a high hydraulic diffusivity, and a low leakage from the Quaternary deposits and the surrounding fracture domains. Moreover, 1,700 m is beyond the shortest distance to the Baltic Sea, see Figure 4-5, which implies that the Baltic Sea may act as a positive hydraulic boundary.

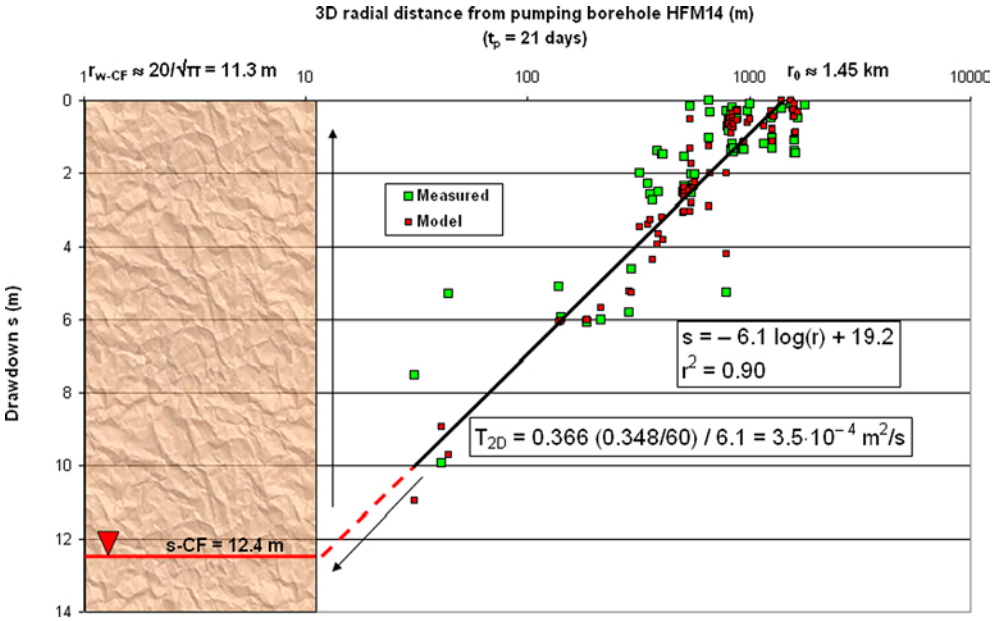

Figure 7-1. *Plot of measured drawdowns (green) and simulated (red) vs. log(3D radial distance) at the end of the 21-day log interference test in HFM14. The measured drawdown in HFM14 was 11.7 m and the simulated 12.4 m using the deterministic base case simulation. The black line shows a least-square fit to the simulated drawdowns. The value of the correlation coefficient (r^2 = 0.90) indicates a less heterogeneous model than does the regression of the measured data in the real system, cf Figure 4-6. A 2D steady state, radial flow approximation using the slope of the least-squares fit for an estimate of* Δs *(difference in drawdown per log cycle of distance) renders a large-scale effective transmissivity of* $3.5 \cdot 10^{-4}$ m^2/s. *This value is essentially a composite of the transmissivities assigned to A2, the near-surface sheet joints, and a bit of ENE0060. An extrapolation of the regression model to the edge of the pumped 20 m element matches the simulated drawdown in this cell in ConnectFlow* ($r_{w,CF} = 20/\sqrt{\pi} \approx 11.3$ *m). (Figure 5-35 in /Follin et al. 2007c/.)*

7.3 Matching natural groundwater levels

Calibration against the natural groundwater levels observed in the Quaternary deposits and in the uppermost part of the bedrock is expected to provide information on the interaction between the groundwater in these two domains, HSD and HRD. For this reason, this calibration is likely to be focused on the hydraulic properties of the Quaternary deposits and the shallow bedrock aquifer as well as providing confirmatory testing of the hydraulic boundary conditions.

The boreholes shown in Figure 7-2 and Figure 7-3 are ordered by bedrock elevation. The simulated groundwater levels are in both plots a bit higher than the measured levels; c +0.7 m of mean difference for both the HFM holes and the SFM holes within the target volume. This magnitude of discrepancy is fairly large considering the low magnitudes of the mean groundwater levels inside the target area shown in Figure 5-15. However, it was considered acceptable for comparing steady state model predictions with seasonally averaged head data that fluctuate by about 1.3–1.6 m over recordings made at different dates. It is noted that the calibrated *deterministic base model simulation* is in accordance with the observed downward gradient in the monitoring data within the target area, see Figure 5-15, with about 0.5–1 m higher groundwater levels in the Quaternary deposits than in the shallow bedrock aquifer.

7.4 Matching hydrochemical profiles in cored boreholes

Modelling the evolution of the hydrological and hydrochemical conditions during Holocene time is an essential part of the site descriptive model. In this context, the calibration against measured hydrochemical profiles in cored boreholes is fundamental to the understanding of the hydrogeological processes in the fractured rock, since it addresses the impact of variable-density flow, and the solute transport interaction between the fracture system and matrix as this can have a considerable impact on how the flow rates and trajectories evolve over time.

Figure 7-4 through Figure 7-8 show an excerpt of the palaeohydrogeological comparisons made for the *deterministic base model simulation*. Four main hydrochemical indicators were used in the calibration: Cl, Br/Cl, $\delta^{18}O$ and HCO_3 (see section 2.3.7 and section 4.3 in the present report and section 6.1.3 in /Follin et al. 2007c/ for a description of the conceptual model behind these indicators).

The performance of the *deterministic base model simulation* in the SDM in predicting salinity is generally improved compared with the preliminary SDM (version 1.2). For example, the model predicts the high salinity encountered at shallow depth in the footwall bedrock of zone A2 at drill site 1, see Figure 7-4, which was a major problem in the preliminary SDM. The predictions of salinity in the hanging wall of zone A2 have also improved.

Figure 7-5 shows the results for the boreholes located in the hanging wall. Figure 7-5 indicates that the predictions of transitions from *Littorina Sea Water* to *Deep Saline Water* shown by Br/Cl, and from *Present-day Meteoric Water* to *Littorina Sea Water* shown by HCO_3 are both at the correct depths. Similarly good results are obtained for the series of boreholes in the border of the tectonic lens and in the footwall of A2 (target volume); see Figure 7-6 for an example. However, it is noted that the high values of Br/Cl observed at Forsmark do not match the defined composition of the *Deep Saline Water*, hence they cannot be matched in the flow modelling. Reasons for this discrepancy are discussed in section 5.2 in /Laaksoharju et al. 2008/.

For completeness, predicted profiles of other major ions, Na, Ca, Mg and SO_4, are shown in Figure 7-7 for some of the boreholes in the footwall of zone A2. These results are also in reasonable agreement, despite that the model only includes mixing and does not address reactions such as cation exchange.

Considering the depths at which Mg was detected rather than the absolute magnitudes of concentration measured, the model is in good agreement with the measurements. *Littorina Sea Water* apparently penetrated only the top 300–400 m of the bedrock in the footwall of zone A2, whereas it seems to have penetrated the top 500–600 m of the bedrock in the hanging wall of this zone.

Examples of the predictions of Cl in the porewater compared with the fracture system are shown for KFM01D and KFM06A in Figure 7-8. The matches are not perfect for the *deterministic base model simulation*, but the model predicts the observed higher salinity in the fracture system relative to the matrix porewater.

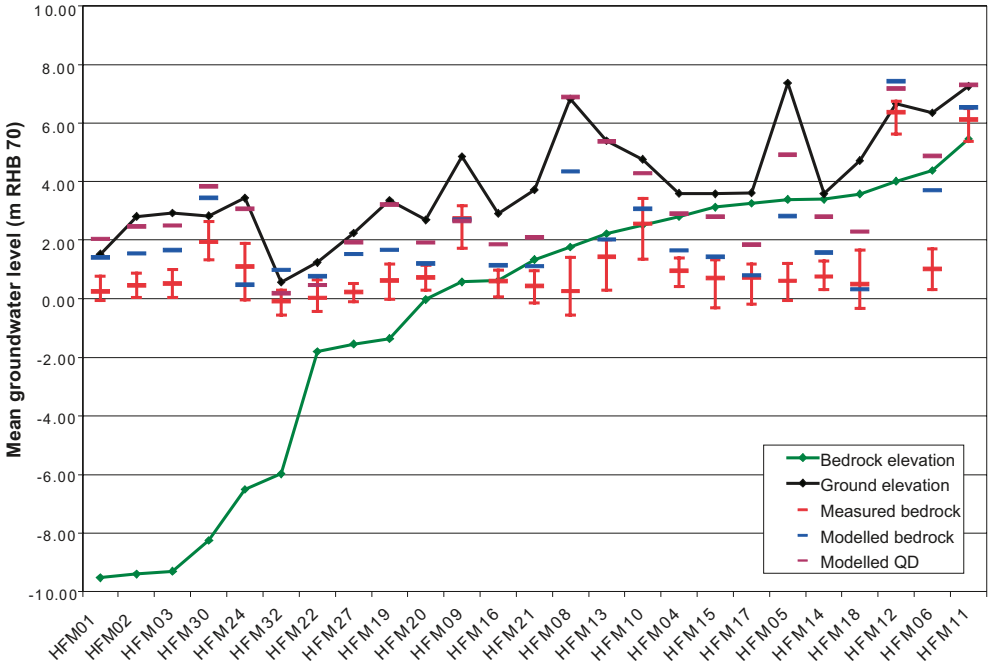

Figure 7-2. *Comparison between the deterministic base model simulation (blue) and the measured groundwater levels in the percussion-drilled boreholes (red). The boreholes are ordered by increasing bedrock elevation. The measured groundwater levels are plotted as mean levels with error bars to show the range of the diurnal variations over time. The simulated groundwater levels within the target volume are on the average c 0.7 m higher than the corresponding measured levels. For the model, values are also given for the Quaternary deposits, QD, (purple) at the same locations as the boreholes. (Figure 5-13 in /Follin et al. 2008a/.)*

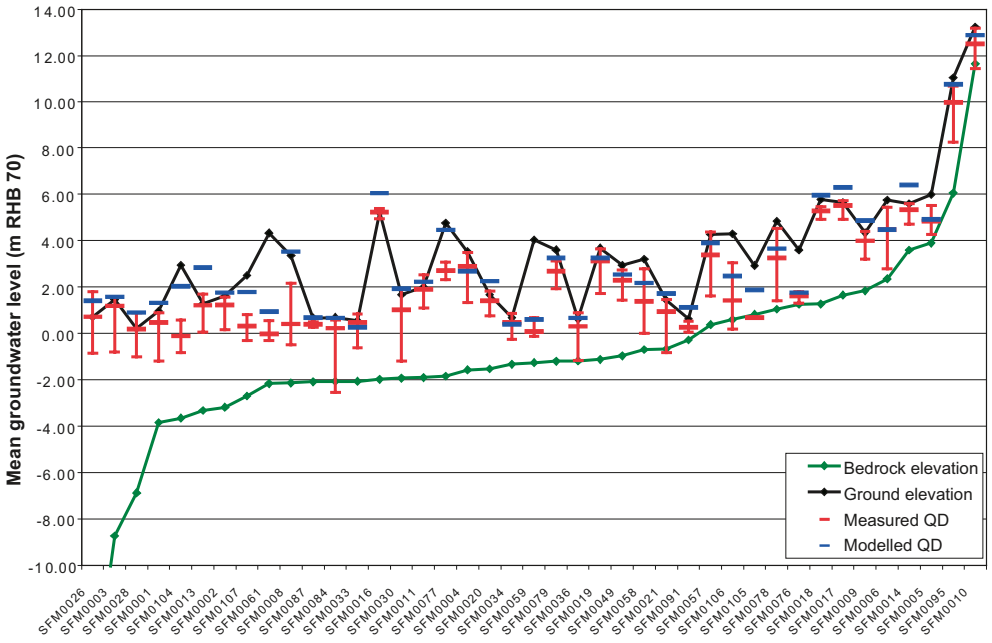

Figure 7-3. *Comparison between the deterministic base model simulation (blue) and the measured groundwater levels in the monitoring wells in the Quaternary deposits (red). The monitoring wells are ordered by bedrock elevation. The measured data are plotted as mean groundwater levels with error bars to show the range of the diurnal recordings over time. The simulated groundwater levels in the SFM boreholes within the target volume are on the average c 0.7 m higher than the corresponding measured levels. (Figure 5-14 in /Follin et al. 2008a/.)*

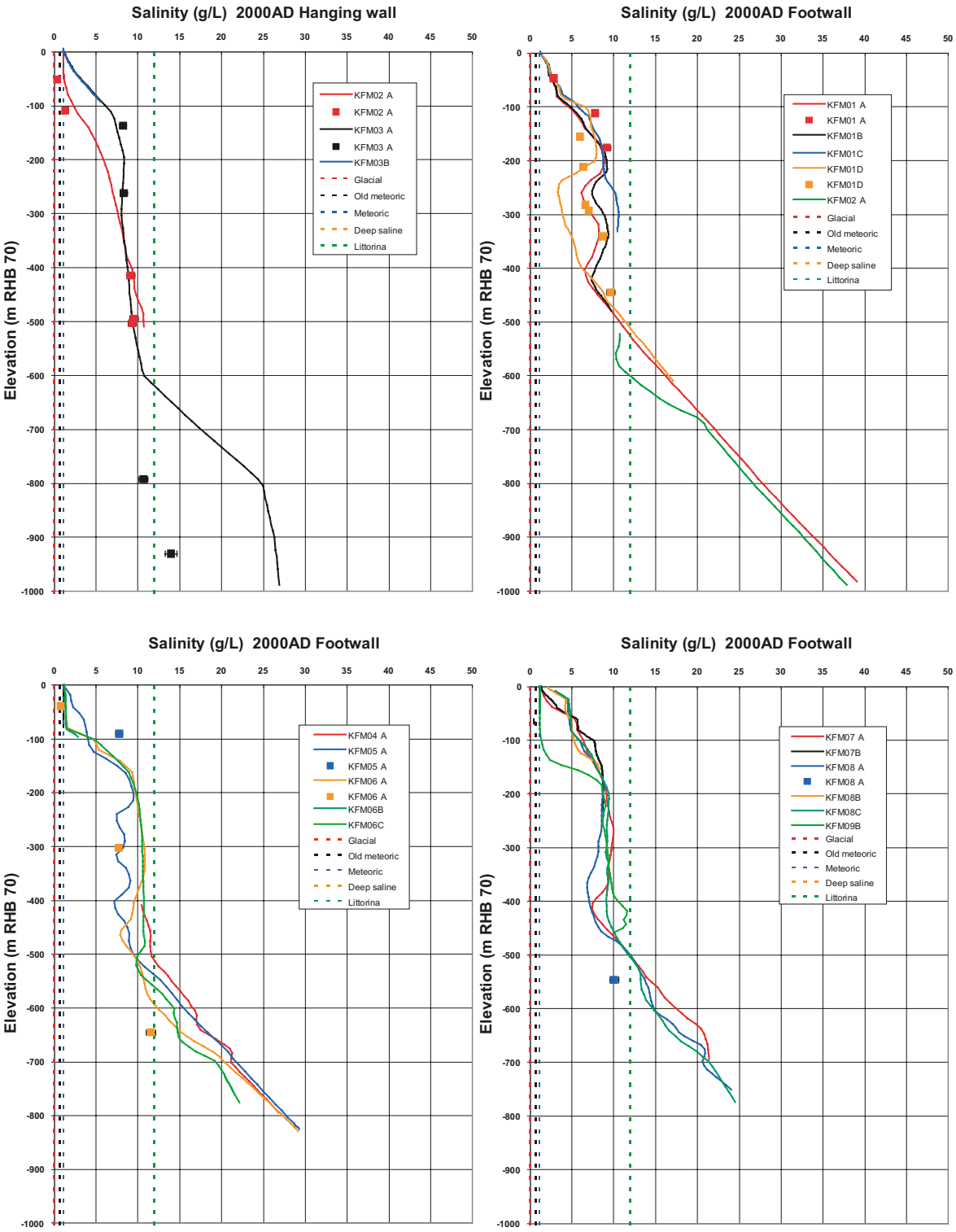

Figure 7-4. *Comparison between the deterministic base model simulation (solid lines) and measured salinity concentrations (TDS) in the fracture system (filled squares) for different groups of calibration boreholes. The error bars on the measured data indicate the laboratory analytical error. The dashed lines show the specified concentration of TDS in the reference waters. (Figure 5-15 in /Follin et al. 2008a/.)*

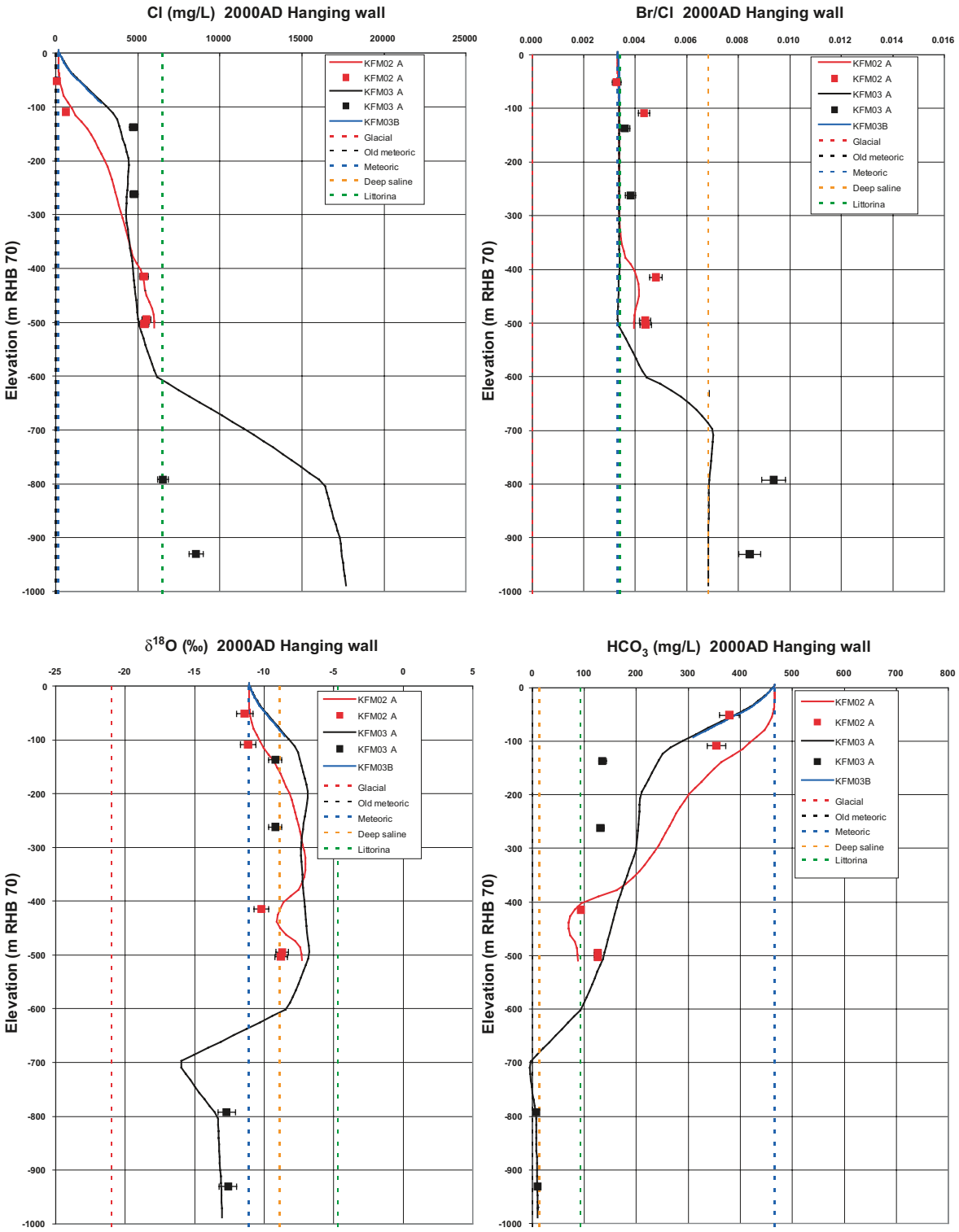

Figure 7-5. *Comparison between the deterministic base model simulation (solid lines) and measured concentrations of Cl, Br/Cl, $\delta^{18}O$ and HCO_3 in the fracture system (filled squares) for boreholes in the hanging wall of A2. The error bars on the measured data indicate the laboratory analytical error. The dashed lines show the specified concentration of Cl, Br/Cl, $\delta^{18}O$ and HCO_3 in the reference waters. (Figure 5-16 in /Follin et al. 2008a/.)*

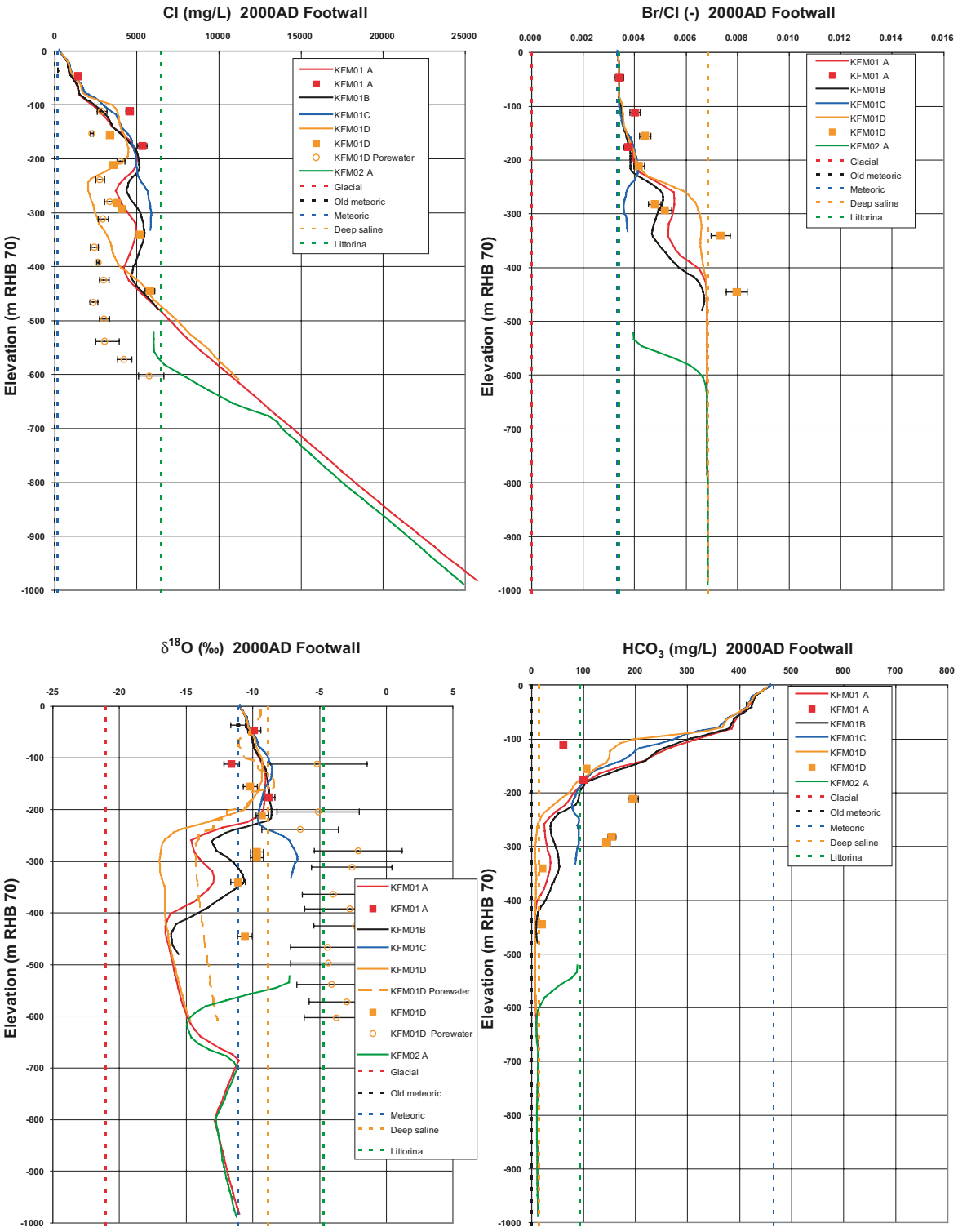

Figure 7-6. *Comparison between the deterministic base model simulation (solid lines) and measured concentrations of Cl, Br/Cl, $\delta^{18}O$ and HCO_3 in the fracture system (filled squares) for the first set of boreholes in the footwall of A2. The error bars on the measured data indicate the laboratory analytical error. The dashed lines show the specified concentration of Cl, Br/Cl, $\delta^{18}O$ and HCO_3 in the reference waters. (Figure 5-17 in /Follin et al. 2008a/.)*

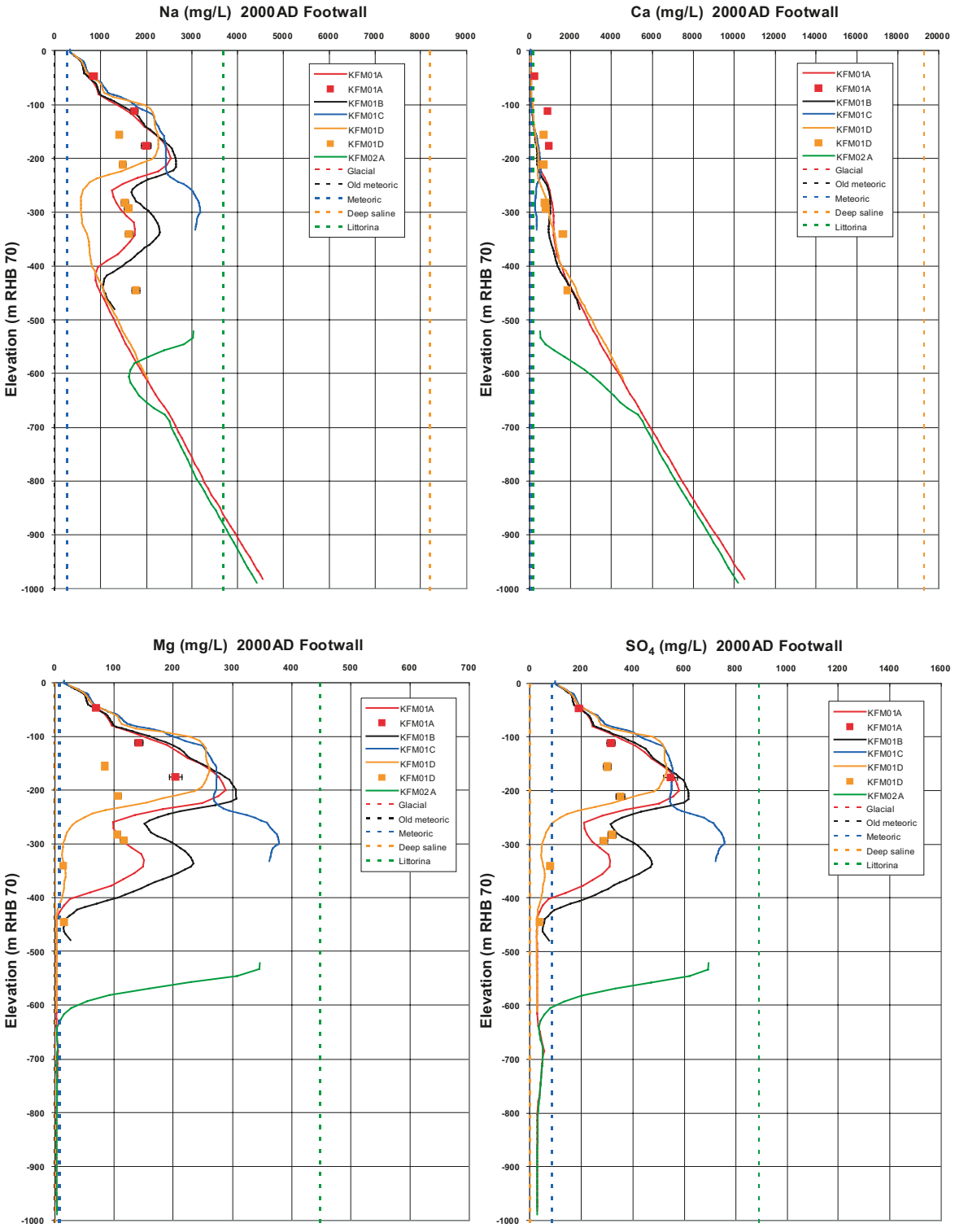

Figure 7-7. *Comparison between the deterministic base model simulation (solid lines) and measured concentrations of Na, Ca, Mg and SO_4 in the fracture system (filled squares) for the first set of boreholes in the footwall of A2. The error bars on the measured data indicate the laboratory analytical error. The dashed lines show the specified concentration of Na, Ca, Mg and SO_4 in the reference waters. (Figure 5-19 in /Follin et al. 2008a/.)*

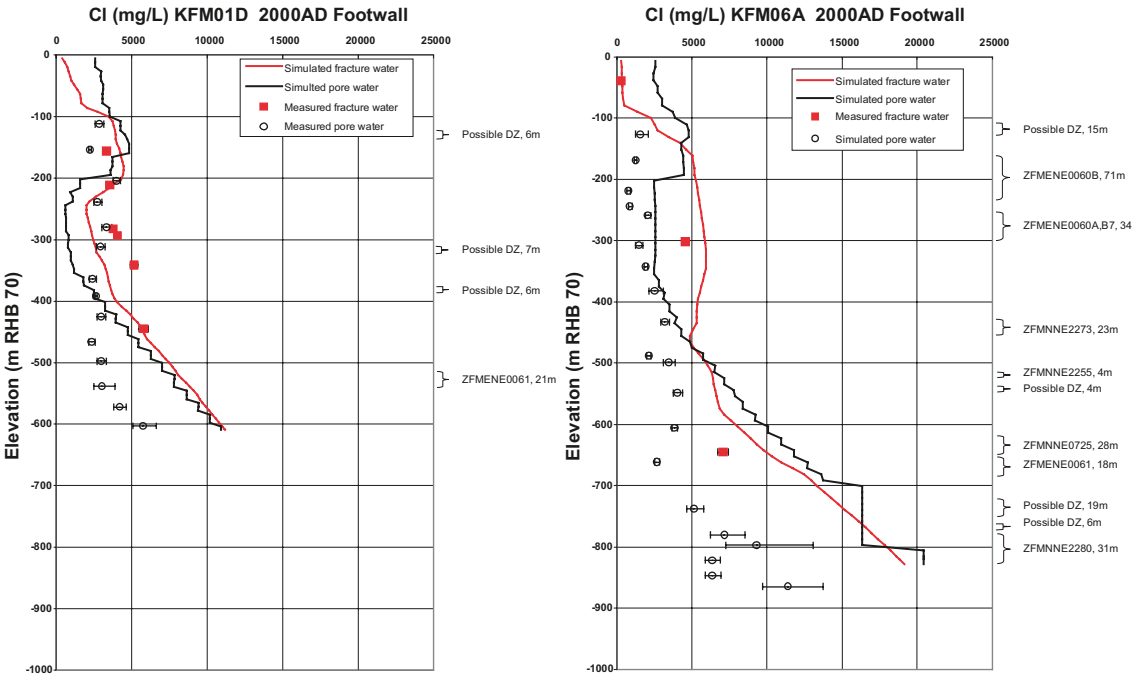

Figure 7-8. *Comparison between the deterministic base model simulation and measured concentrations of Cl in the fracture water and porewater for boreholes KFM01D and KFM06A both in the footwall of A2. The fracture water data are plotted as filled squares and the porewater data are plotted as open circles. The error bars on the fracture data only indicate the laboratory analytical error, while in the porewater they also reflect the uncertainty in the porosity of the rock sample. The red lines show the simulated values in the fracture system, and the black lines show the simulated values in the matrix blocks. (Figure 5-18 in /Follin et al. 2008a/.)*

8 Explorative simulations

8.1 Main characteristics of relevance for the model

Figure 8-1 shows a perspective view of the candidate area towards the south. The regionally significant, ductile and brittle deformation zones with WNW-NW strike, i.e. Forsmark (FDZ), Eckarfjärden (EDZ) and Singö (SDZ), border the candidate area and run more or less perpendicular to the regional hydraulic gradient. Zones A2 and ENE0060 are local major deformation zones. Zone A2 dips gently to the south and splits the bedrock within the candidate area into two parts. The south-eastern part is referred to as the hanging wall bedrock and the north-western part as the footwall bedrock to zone A2. Zone ENE0060 dips steeply and strikes parallel to the regional hydraulic gradient. It divides the target volume in the footwall bedrock into two parts.

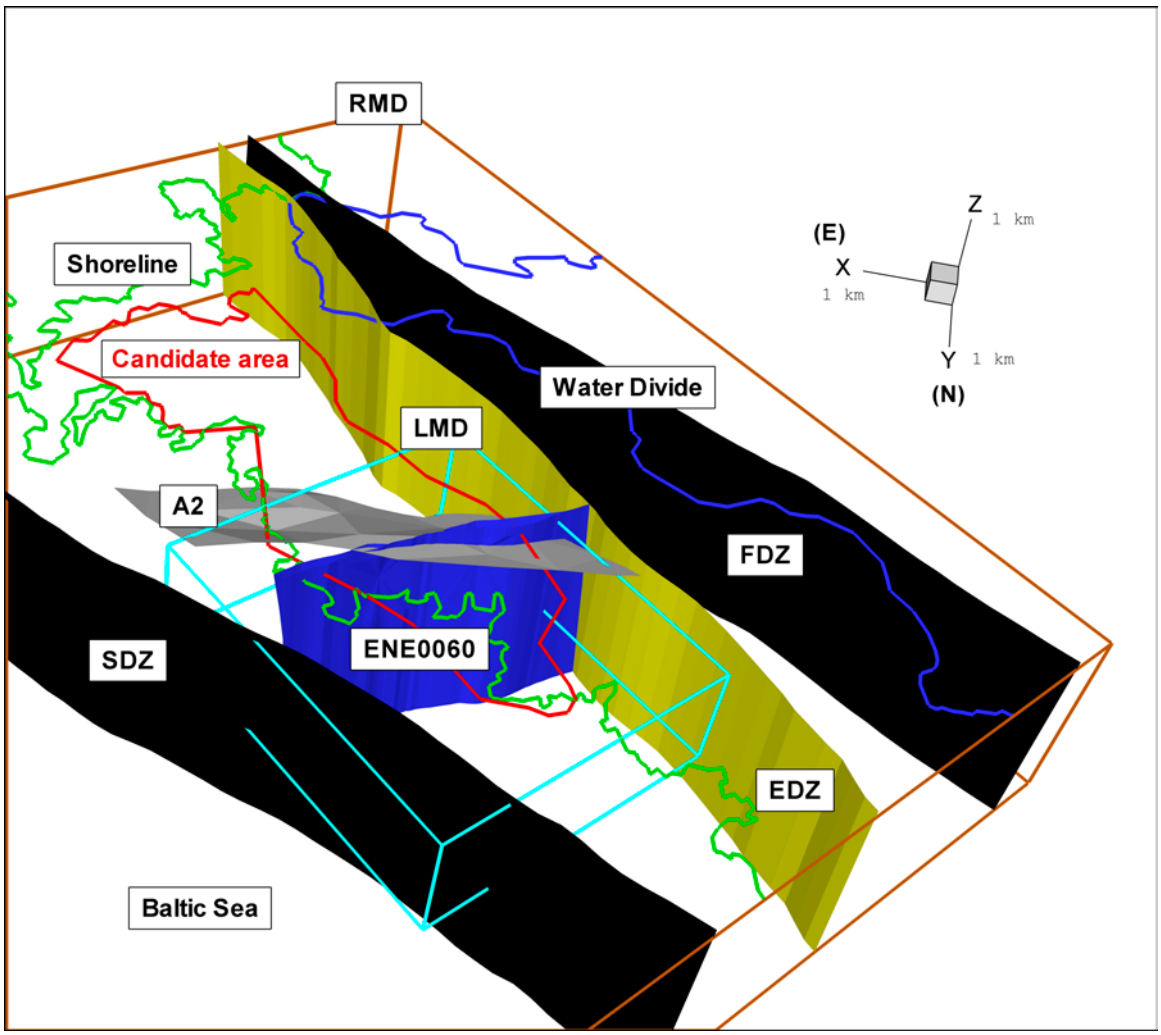

Figure 8-1. *A perspective view towards south showing the candidate area, the local model domain (LMD), the south-western part of the regional model domain (RMD). The regionally significant deformation zones Forsmark (FDZ), Eckarfjärden (EDZ) and Singö (SDZ) border the candidate area. The remaining zones, A2 and ENE0060, are local major deformation zones. The solid blue line indicates the nearest regional topographical water divide.*

The strike of the steep WNW-NW zones is parallel to the main principal stress (σ_{1H}), whereas the strike of zone ENE0060 is parallel to the second principal stress (σ_{2h}). More important, zone A2 is at a high angle to the minimum principal stress (σ_{3v}) (cf. Figure 7-10 and Table 7-2). The A2 zone is far more transmissive and less hydraulically heterogeneous than zone ENE0060. The three regional zones are not nearly as well investigated as the zones inside or close to the candidate area. The data gathered in the three regional zones, together with the data from local major deformation zones with similar orientations and located closer to the candidate area, suggest that steeply dipping zones with a WNW-NW strike may have noteworthy in-plane transmissivities, yet less significant relative to the in-plane transmissivities of gently dipping zones such as zone A2. The hydraulic investigations carried out in the deterministically modelled deformation zones reveal both a significant decrease in the in-plane transmissivity with depth and a considerable in-plane lateral heterogeneity (channelling).

The hydraulic investigations carried out in the fracture domains suggest that the frequency of water-conductive fractures varies significantly in space. Data suggest that there is less than one flowing fracture per hundred metres below c 400 m depth within the target volume, which is located in the footwall bedrock. In contrast, the uppermost c 150 m of bedrock inside the target volume is considerably more fractured, with more than 30 flowing fractures per hundred metres. In addition, the near-surface bedrock between the deterministically modelled deformation zones within the target volume contains discrete sub-horizontal fractures/sheet joints, many of which have high in-plane transmissivities and extends tens to hundreds of metres. Here, the hydraulic gradient is low due to the flat topography and the pronounced structural-hydraulic anisotropy. The strong contrast in the structural-hydraulic properties with depth within the target volume creates a hydraulic phenomenon that causes a short circuit in the near-surface flow system, which may contribute to a slow transient evolution of fracture water and porewater hydrochemistry at depth, although the slow evolution is mainly due to the very low permeability at these depths.

8.2 Visualisations for interpretation of hydrochemistry

Figure 8-2 shows a 2D cross section parallel to the shoreline with chloride concentrations for the *deterministic base model simulation*. The blue line is a regional water divide, which is used as the upstream flow boundary (cf. Figure 1-9). The black arrows indicate the directions of the resultant Darcy fluxes in the plane of the 2D cross section. The directions of the Darcy fluxes vary, but the mean direction is essentially perpendicular to the cross section and points towards the shoreline, i.e. parallel with the topographic gradient. The red lines shows forward as well as backward flowpaths for 100 particles starting at the intersection between zone A2 (grey shade) and the 2D cross section. The majority of the backward flowpaths recharge locally at different places downstream the regional water divide. The forward flow paths stay close to zone A2 or follow the “sheet joint features”. In summary, Figure 8-2 suggests that the groundwater flow system inside the target area is heterogeneous and to a large extent structure-controlled.

Figure 8-3 shows simulated concentrations of Cl and $\delta^{18}O$ in the plane of the 2D cross-section shown in Figure 8-2 (shown in the reversed direction). By the same token, Figure 8-6 shows concentrations of TDS and mixing proportions of the reference waters discussed in section 7.4. The differences seen between the footwall and the hanging wall to zone A2 are due to structural-hydraulic differences between the two bedrock segments and to the differences these cause regarding the initial conditions at 8000 BC. It is noted that the pictures shown in Figure 8-3 through Figure 8-6 represent the *deterministic base model simulation*. The effect of varying the properties of the hydrogeological DFN model and the lateral deformation zone heterogeneity is discussed in section 9.2.3.

The flat topography of the Forsmark area and the recent withdrawal of the Baltic Sea are examples of important factors in determining the surface and near-surface hydrochemistry. Marine remnants in the Quaternary deposits, as well as modern sea water transgressions, are strongly influencing the hydrochemistry, especially in areas at low altitude close to the coast. However, hydrological and chemical observations in the surface water and the shallow groundwater

indicate that there is probably little ongoing discharge of deep saline waters into the superficial freshwater system located above the horizontal sheet joints within the area modelled as a shallow bedrock aquifer. Outside this area, however, there are examples of observations that possibly indicate deep saline signatures in the groundwater at relatively shallow depths in the Quaternary deposits. One such area is Lake Gällsboträsket, which coincides with a depression along the trace line of the Eckarfjärden deformation zone, see Figure 5-2. Here, the concentration of chloride in the discharging brook indicates an influence from deep groundwater of older origin than the Littorina Sea Water (see section 3.17.5 in /Follin et al. 2007c/).

Figure 8-7 and Figure 8-8 shows the predicted present-day spatial distribution of chloride at the surface and at 50 m depth, respectively. Table 8-1 shows the magnitudes of the predicted concentrations together with the ranges of the concentrations measured in the till.

The predictions shown in Table 8-1 were calculated with the *deterministic base model simulation* using a grid size of 20 m. The magnitude of discrepancies in relation to the measured data may perhaps be regarded as acceptable considering the uncertainty of differing support scales between measurements and model. Moreover, the predictions shown in Table 8-1 represent a single realisation of the flow model (i.e. without parameter uncertainty) and the borehole hydrochemical data fluctuates in space and over recordings made at different dates.

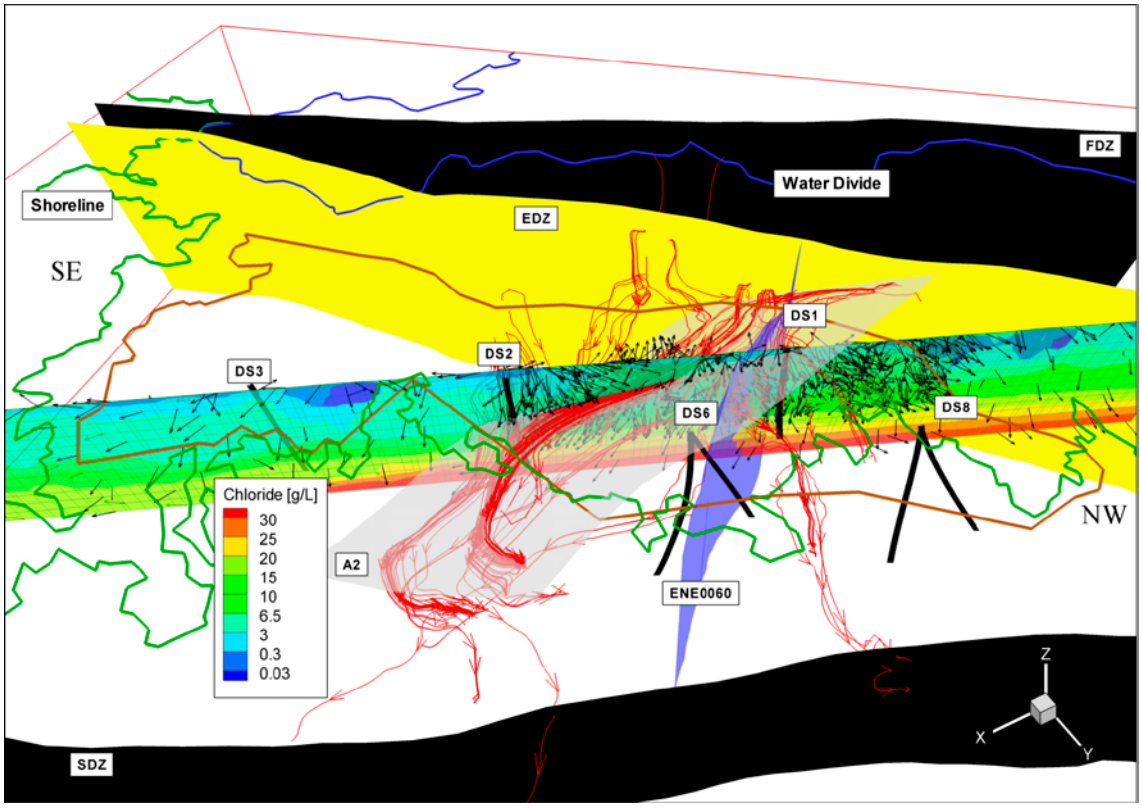

Figure 8-2. *A 1,200 m deep 2D vertical cross section parallel to the shoreline (green line) showing chloride concentrations for the deterministic base model simulation. Black arrows indicate the directions of the Darcy flux along the plane of the cross section. Red lines indicate forward as well ass backward flowpaths for 100 particles starting at the intersection between the 2D cross section and zone A2. The solid blue line is the upstream boundary of the model domain, which coincides with a regional water divide. (Figure 6-10 in /Follin et al. 2008a/.)*

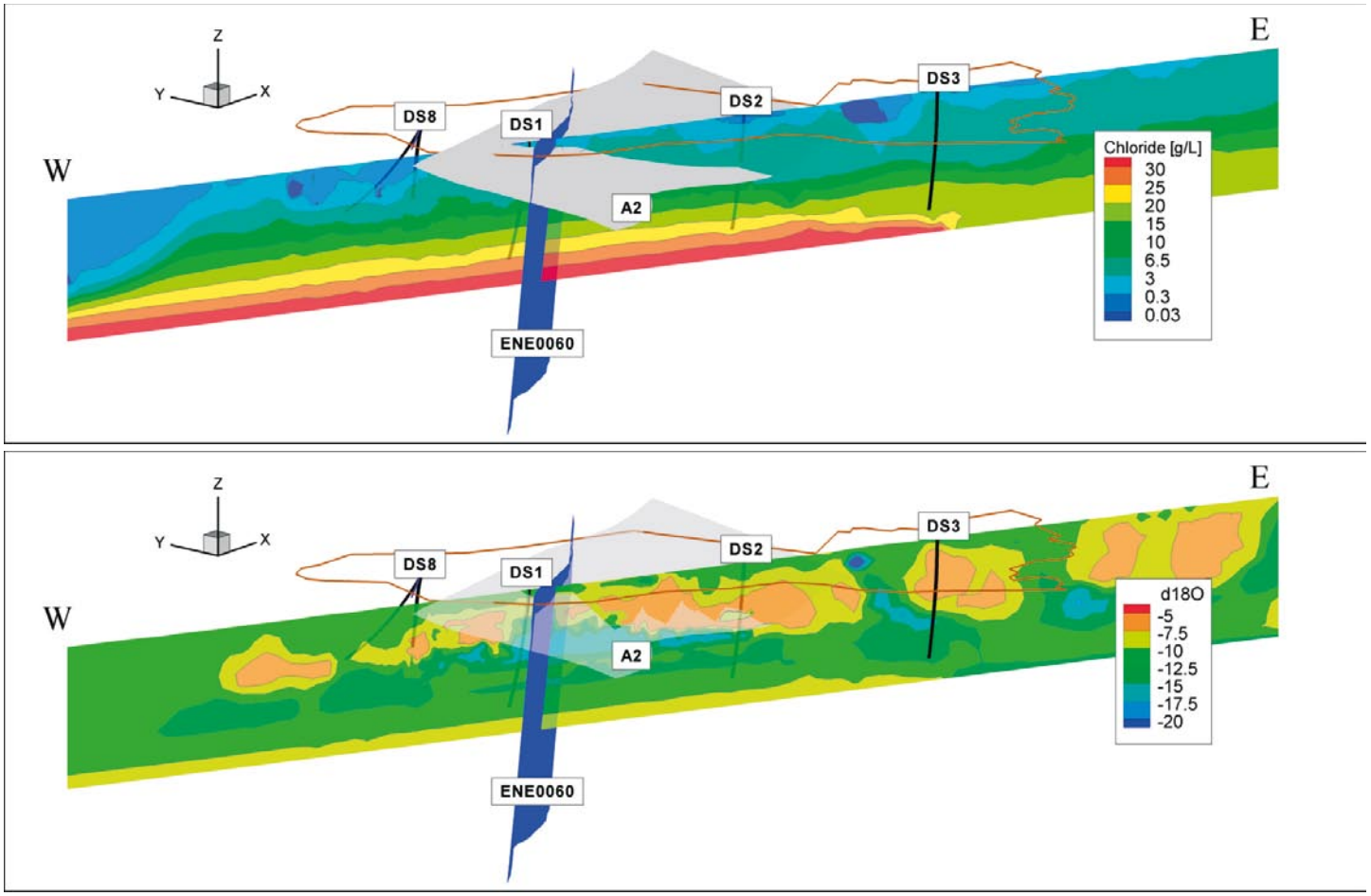

Figure 8-3. *Perspective view towards NE showing simulated concentrations of Cl and $\delta^{18}O$ in the plane of the 1,200 m deep 2D cross-section shown in Figure 8-2 (shown in the reversed direction). The pictures represent the deterministic base model simulation. (Figure 6-11 in /Follin et al. 2008a/.)*

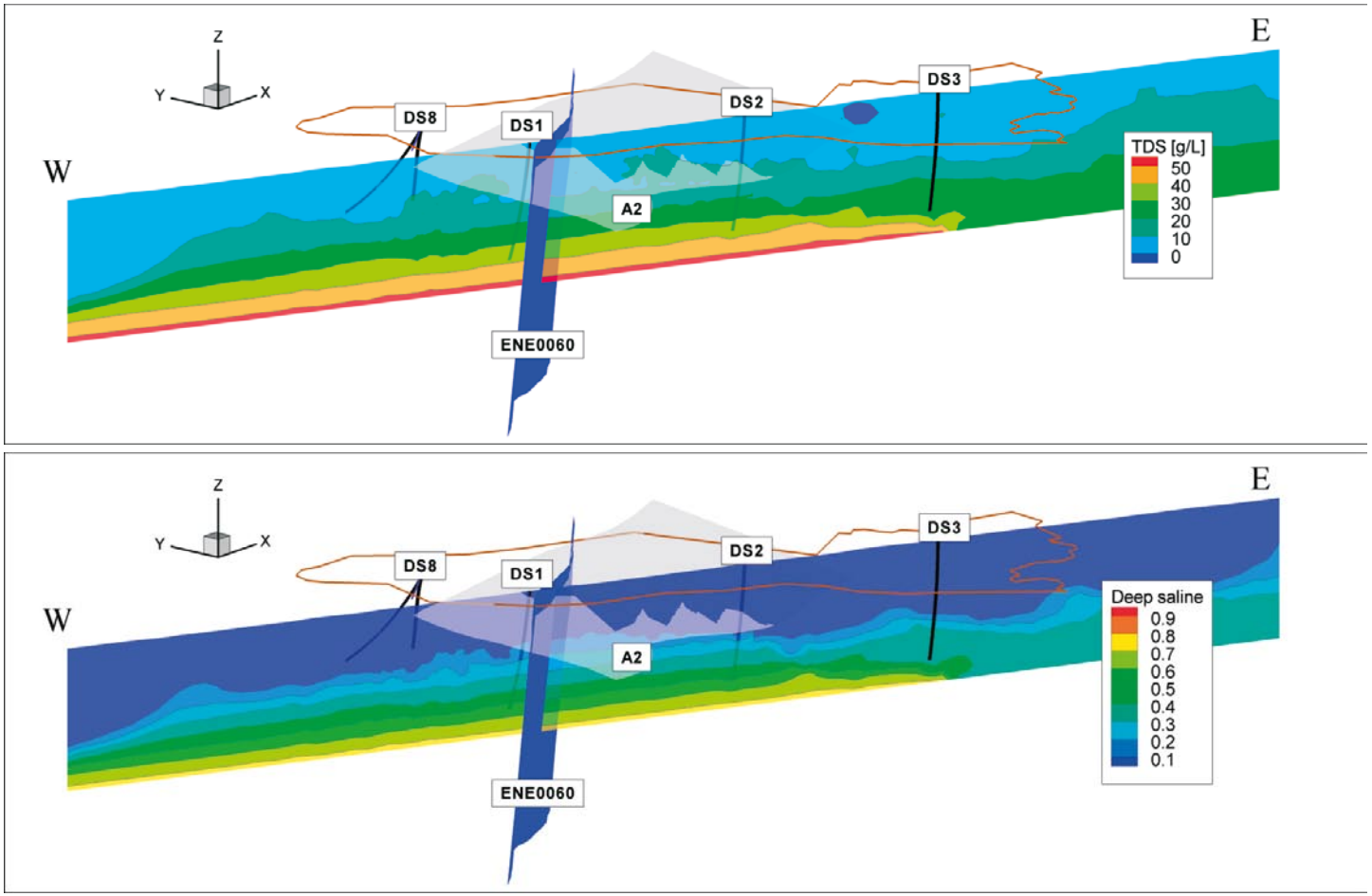

Figure 8-4. *Perspective view towards NE showing simulated concentration of TDS and distribution of Deep Saline Water in the plane of the 1,200 m deep 2D cross-section shown in Figure 8-2 (shown in the reversed direction). The pictures represent the deterministic base model simulation.*

Old Meteoric and Glacial Waters

Holocene Glacial Melt Water

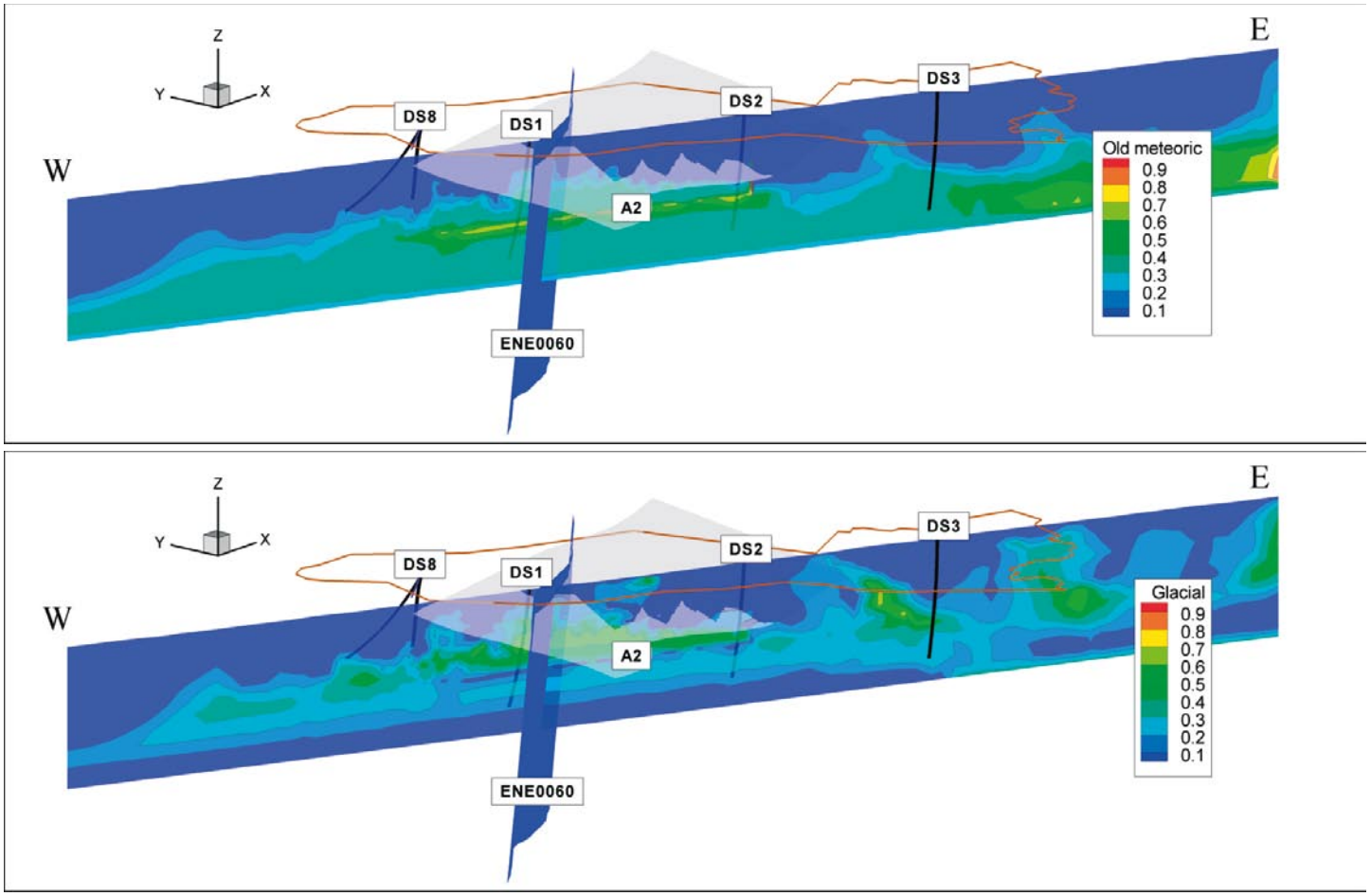

Figure 8-5. *Perspective view towards NE showing simulated distributions of Old Meteoric and Glacial Waters and Holocene Glacial Melt Water in the plane of the 1,200 m deep 2D cross-section shown in Figure 8-2 (shown in the reversed direction) The pictures represent the deterministic base model simulation.*

Littorina Sea Water

Present-day Meteoric Water

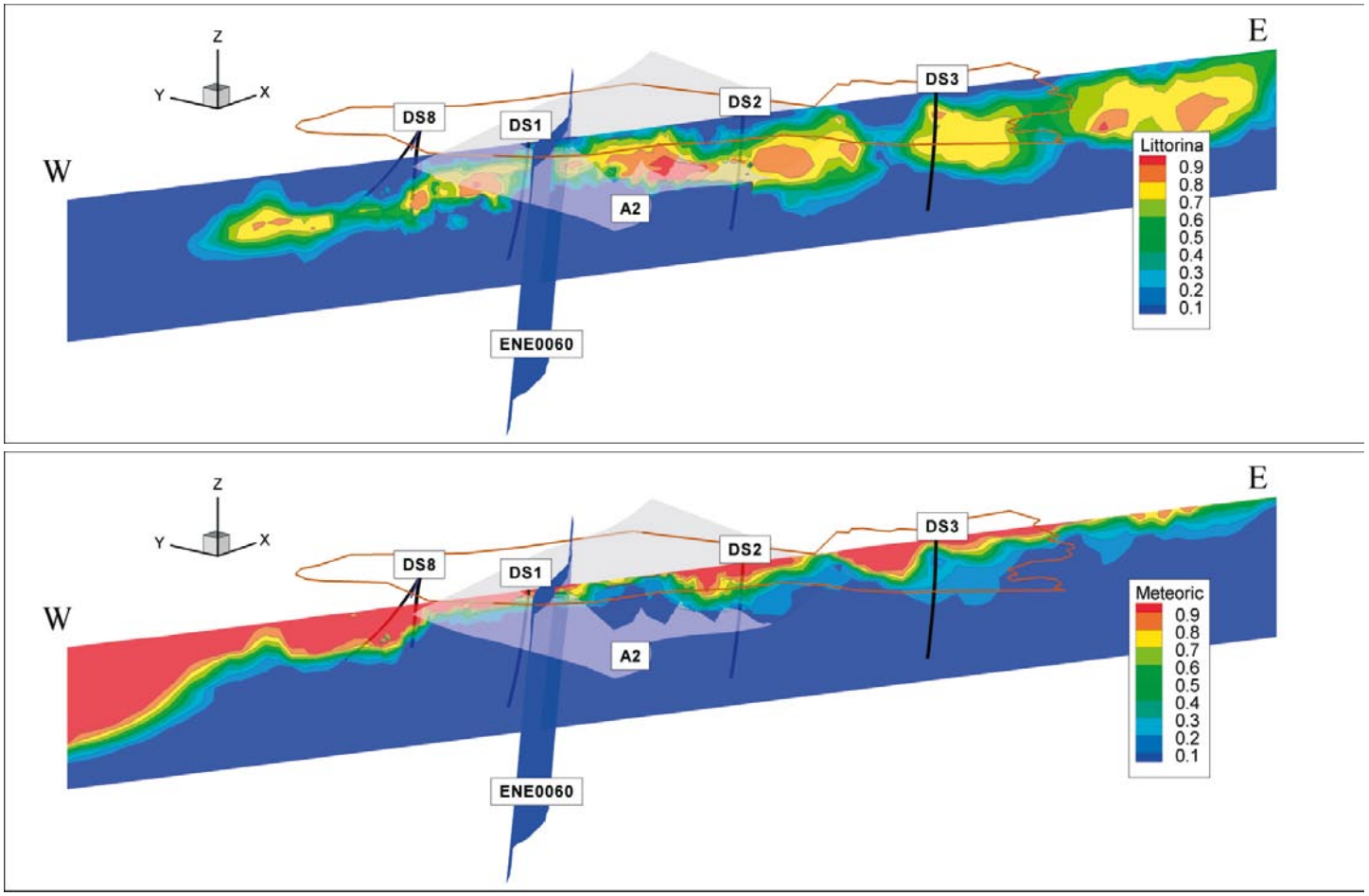

Figure 8-6. *Perspective view towards NE showing simulated distributions of Littorina Sea Water and Present-day Meteoric Water in the plane of the 1,200 m deep 2D cross-section shown in Figure 8-2 (shown in the reversed direction) The pictures represent the deterministic base model simulation.*

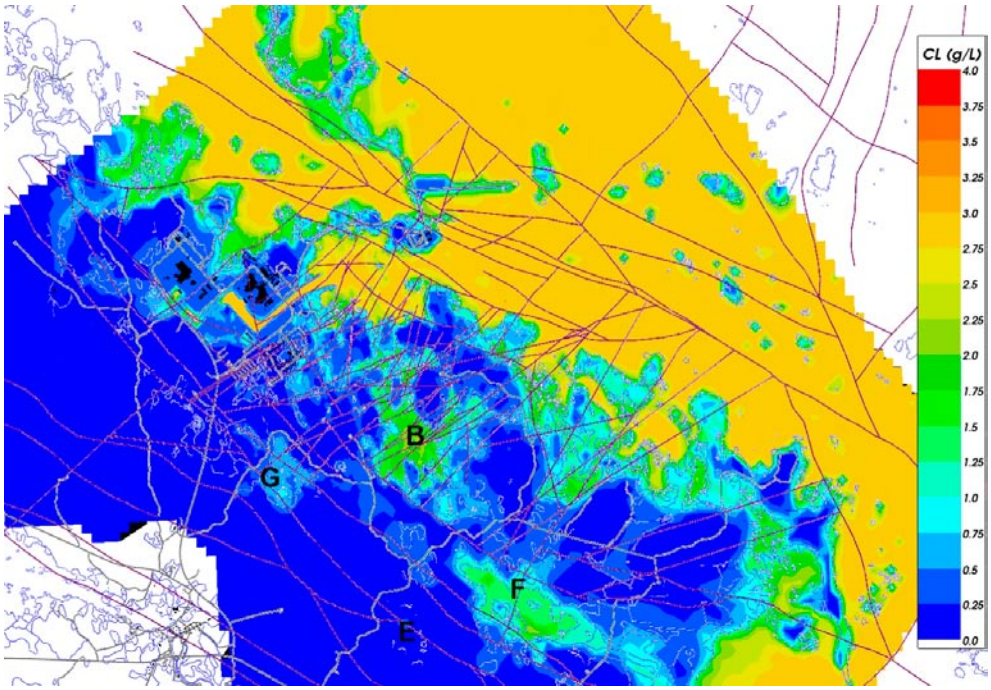

Figure 8-7. *Predicted spatial distribution of chloride at the surface for the deterministic base model simulation. B = Lake Bolundsfjärden, F = Lake Fiskarfjärden, E = Lake Eckarfjärden, G = Lake Gällsboträsket. (Figure 7-1 in /Follin et al. 2007c/.)*

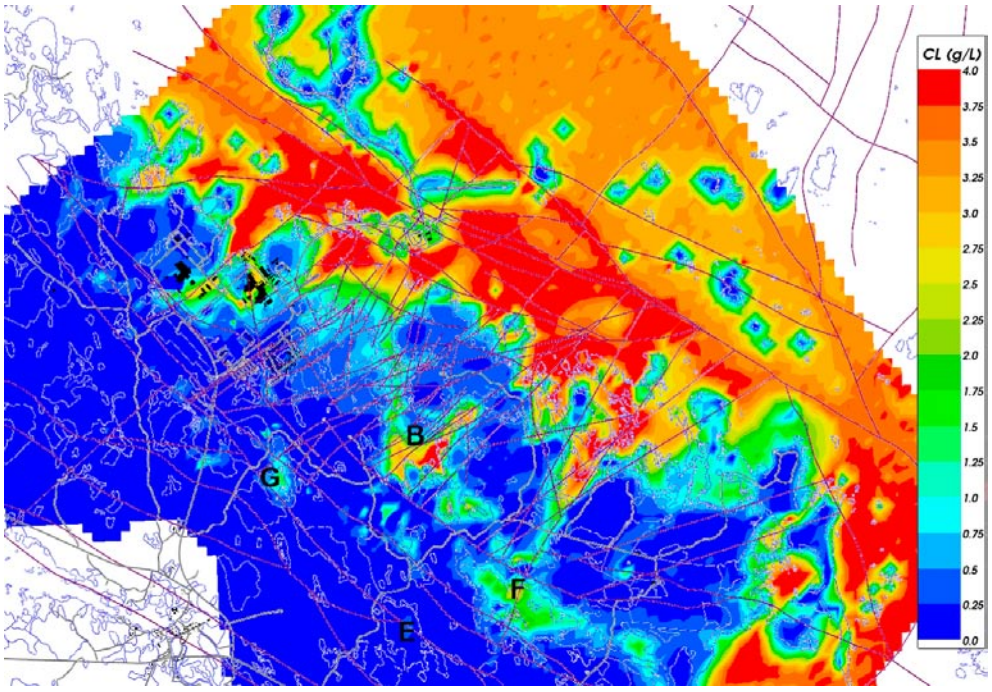

Figure 8-8. *Predicted spatial distribution of chloride at 50 m depth for the deterministic base model simulation in B = Lake Bolundsfjärden, F = Lake Fiskarfjärden, E = Lake Eckarfjärden, G = Lake Gällsboträsket. Data from hydraulic tests and analyses of water compositions in the till below the lakes indicate that the waters sampled below B and F are probably stagnant and of a marine origin (Littorina Sea Water). In contrast, the outflow rate of chloride in the brook that discharges from G suggests an influence of deep saline groundwater. This observation is supported by the chemical signature of the groundwater sampled in the monitoring well SFM0057 located at the edge of the Gällsboträsket. (Figure 7-2 in /Follin et al. 2007c/.)*

Table 8-1. Predicted and measured chloride concentrations (mg/L) in the till layer below the lake sediments in Lake Bolundsfjärden, Lake Fiskarfjärden, Lake Eckarfjärden, Lake Gällsboträsket and the Baltic Sea. Predicted concentrations at 50 m depth below these water bodies are also shown. The predicted concentrations represent the *deterministic base model simulation*. (Table 7-1 in /Follin et al. 2007c/.)

Object	Predicted maximum value of Cl in the till and at 50 m depth	Range of the Cl data in the till	Monitoring well
B ; L. Bolundsfjärden	2,250 / 4,000+	3,520–4,340	SFM0023
F ; L. Fiskarfjärden	2,250 / 2,750	947–1,300	SFM0022
E ; L. Eckarfjärden	250 / 250	277–375	SFM0015
G ; L. Gällsboträsket	1,000 / 1,750	2,160–2,340	SFM0012
Baltic Sea	3,000 / 4,000+	690–3,940	SFM0024, -25, -65, -81

8.3 Visualisations for interpretation of flow and solute transport

Particle tracking is a useful tool for interpretation of groundwater flow paths and calculation of solute transport flow path properties. Figure 8-9 and Figure 8-10 show particle tracks for the *deterministic base model simulation*. The particles were released at 500 m depth within the target volume with one particle starting every 100 m on a regular mesh over an area of about 1.7 km by 1.7 km. There are two distinct types of flow paths followed, one set of shorter flow paths that flow toward the SFR buildings to the north, and a second set of longer flow paths that move downwards before moving to the Baltic Sea to the east.

The shorter flow paths are generally associated with the western side of the release area and travel upward until they encounter the "sheet joint features", then track along these until they discharge around the intersect with the Singö deformation zone, some of which cross the zone. The long flow paths starting in the eastern side of the release area tend to move horizontally or downward, as shown in Figure 8-10, until they encounter the deformation zones that slope gently to the south-east. Again, a number of particles appear to go beyond the Singö deformation zone. These particle-tracking results highlight the importance of the property assignment of the Singö deformation zone in influencing the discharge areas. It should be noted that pumping in the SFR repository was not implemented in the *deterministic base model simulation*.

Figure 8-11 shows another picture of particle tracks for the *deterministic base model simulation* at 2000AD. Here, 447 particles were released at 450 m depth within a sub area located in the centre of the target volume, with one particle starting every 40 m on a regular mesh. One of the particle tracks, #228, is coloured red and the trajectory of this flow path is shown in a perspective view in Figure 8-12, where the different colours represent the structural elements that the particle encounters on its way to the exit point, i.e. fracture domains, deformation zones and sheet joint features. In these two figures, the blue line denotes the shoreline and the greenish polygon the candidate area.

Figure 8-13 shows the hydraulic gradients in the ECPM model along the flow path of particle #228. The gradients are coloured with regard to the structural elements shown in Figure 8-12. Figure 8-14 shows a scatter plot of the hydraulic gradient for particle #228 versus the geometric mean hydraulic conductivity. The dots in the scatter plot are coloured with regard to elevation (m RHB 70).

Figure 8-13 and Figure 8-14 show that the hydraulic gradients along the visualised flow path are low ($2 \cdot 10^{-5}$ to $7 \cdot 10^{-3}$ m/m). The highest values of the hydraulic gradient are found in the proximity of the release position in fracture domain FFM01, where the ECPM hydraulic conductivity is low ($\sim 10^{-11}$ m/s). The lowest values of the hydraulic gradient are found in the proximity of the sheet joint features, where the ECPM hydraulic conductivity is high ($\sim 10^{-4}$ m/s). The correlation between hydraulic gradients and hydraulic conductivity, with decreasing gradient with increasing hydraulic conductivity is expected because, for a given flow path with a given flow,

low-conductive parts require a higher gradient drop than high-conductive parts. However, it is emphasised that Figure 8-13 and Figure 8-14 show results for a single particle only. /Crawford (ed) 2008/ discusses the calculated F-factor and the advective residence time for particle #228 in relation to the transport properties of the ensemble of particles shown in Figure 8-11.

Figure 8-15 shows groundwater flow vs. mid-section elevation for dilution measurements in Forsmark and Figure 8-16 shows the interpreted hydraulic gradients versus mid-section elevation for the same dilution measurements. There is an overall impression that the magnitudes of the calculated hydraulic gradients tend to be too high relative to reasonable topographically-based estimates of the regional hydraulic gradient, which is of the order of c 1%. This viewpoint is supported by gradients obtained in the numerical simulations; see Figure 8-13 for an example.

/Nordqvist et al. 2008/ provides an examination of possible sources of error for the gradient estimation. They conclude that it is likely that gradients tend to be over-estimated. This because the flow convergence correction factor probably often is larger than the commonly assumed value of 2, due to fracture orientation and artificially increased hydraulic conductivity (negative skin) around the borehole (cf. Figure 4-8 in /Follin et al. 2007b/). Of particular importance is the transmissivity values used for estimation of hydraulic gradients and this may be the largest source of error. The transmissivity values used are obtained from different hydraulic test methods (PFL-f, PSS or HTHB). Further, independent of methods, transmissivity values are obtained during a different flow regime (radial flow) than what prevails during the tracer experiments. Reported data are often based on preliminary transmissivity estimates from then available measurements. One may argue that the relatively long-term PFL measurements provide more representative transmissivity estimates for the connected flowing path, and some support for this may also be found in available data (cf. Figure 7-2 in /Nordqvist et al. 2008/). In order to improve the hydraulic gradient estimates, the used transmissivity data should be updated using final transmissivity estimates, and preferably from PFL-f measurements if available.

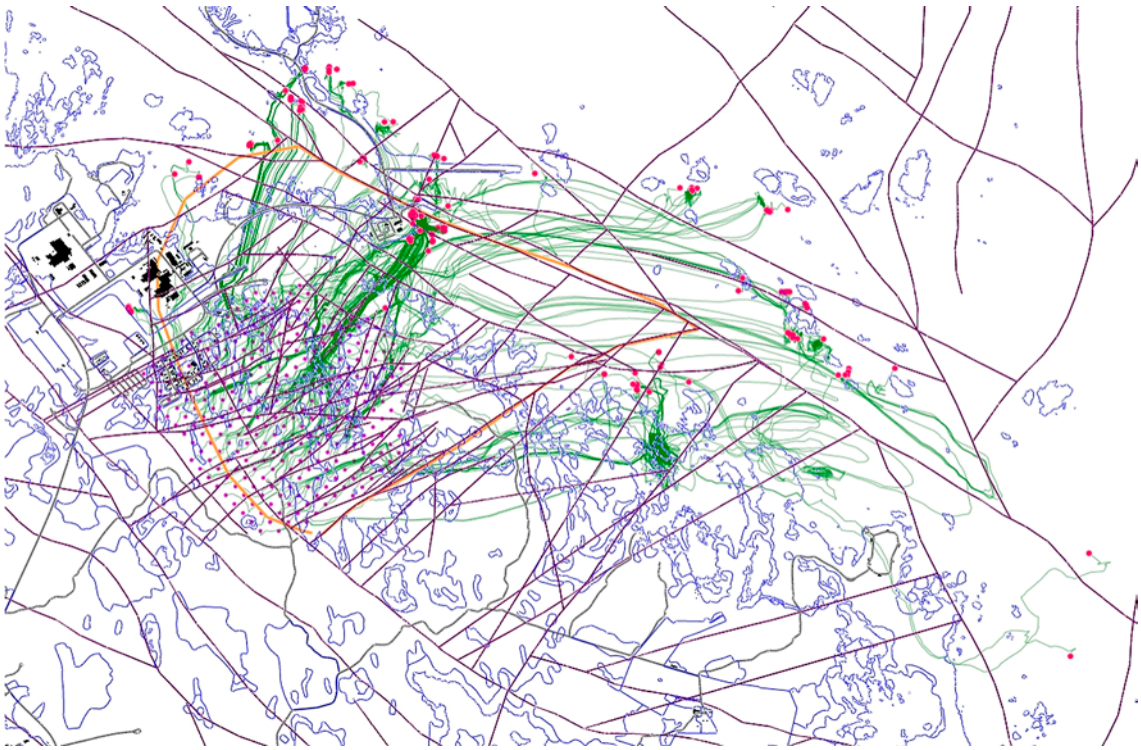

Figure 8-9. *Plane view of the target area with predicted flow paths and exit locations at the surface (red dots) of c 300 particles using the base model simulation in ConnectFlow. The particles were released in a 100 m by 100 m mesh at 500 m depth. The exit locations are marked with red dots. The orange line represents the perimeter of the assumed extent of the shallow bedrock aquifer. (Figure 6-1 in /Follin et al. 2008a/.)*

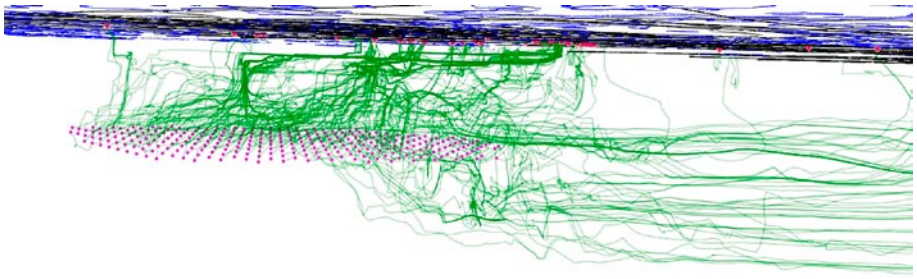

Figure 8-10. *A perspective view through the subsurface towards the north-west showing the impact of the high horizontal transmissivity of the shallow bedrock aquifer on the particle tracking shown in Figure 8-9. (Figure 6-1 in /Follin et al. 2008a/.)*

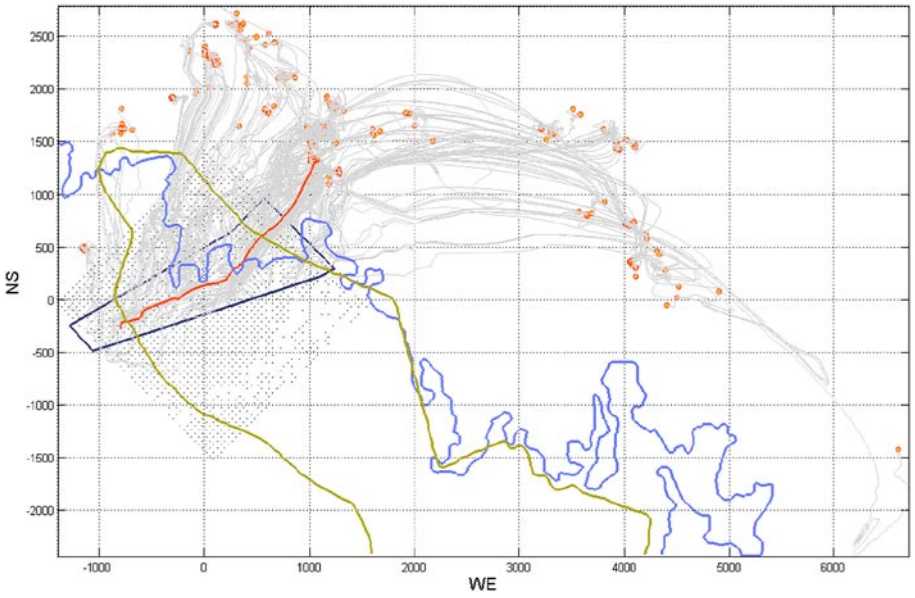

Figure 8-11. *Visualisation of 447 particles released at 450 m depth within a sub area located in the centre of the target volume with one particle starting every 40 m on a regular mesh. One of the particle tracks, #228, is coloured red and the trajectory of this flow path is shown in a perspective view in Figure 8-12. The blue line is the shoreline and the olive green line is the candidate area. (Figure 6-4 in /Follin et al. 2008a/.)*

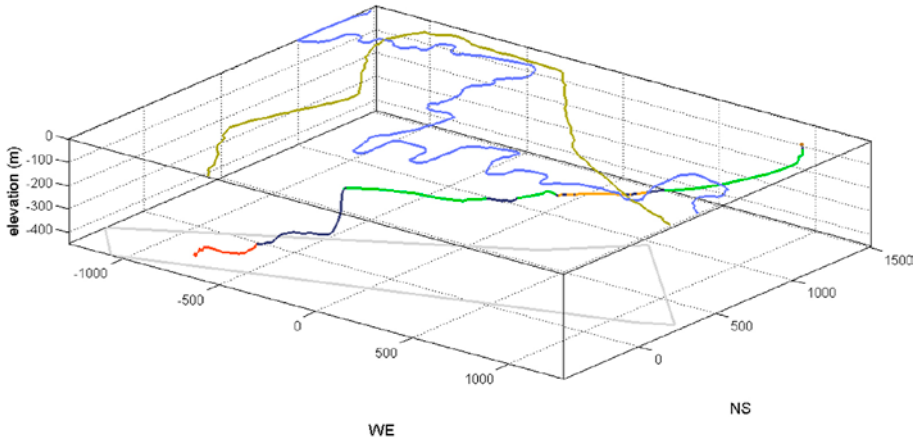

Figure 8-12. *The flow path of particle #228 shown in Figure 8-11 is here coloured with regard to the structural elements that the particle encounters on its way to the exit point, i.e. red for fracture domain FFM01 and yellow for FFM06, blue for various deformation zones, green for different sheet joint features and brown for the Quaternary deposits. The blue line is the shoreline and the olive green line is the candidate area. (Figure 6-5 in /Follin et al. 2008a/.)*

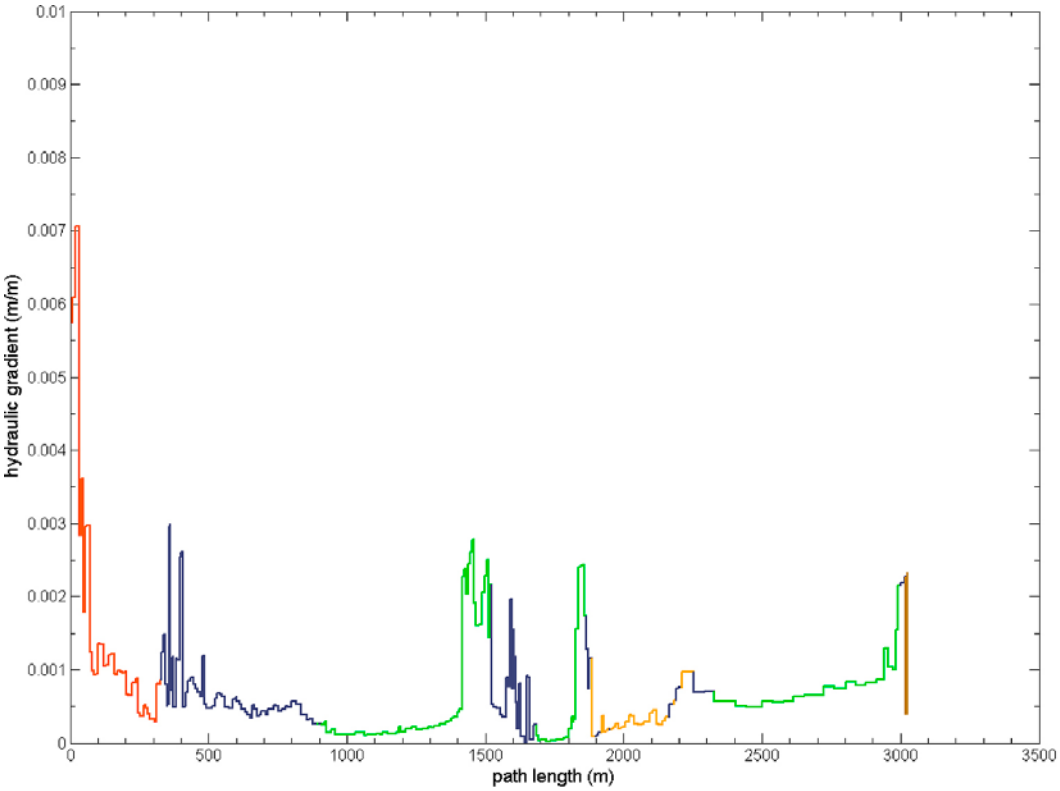

Figure 8-13. *A plot of the hydraulic gradients along the flow path of particle #228 in the ECPM model. The gradients are coloured with regard to the structural elements that the particle encounters on its way to the exit point, cf Figure 8-12. (Figure 6-6 in /Follin et al. 2008a/.)*

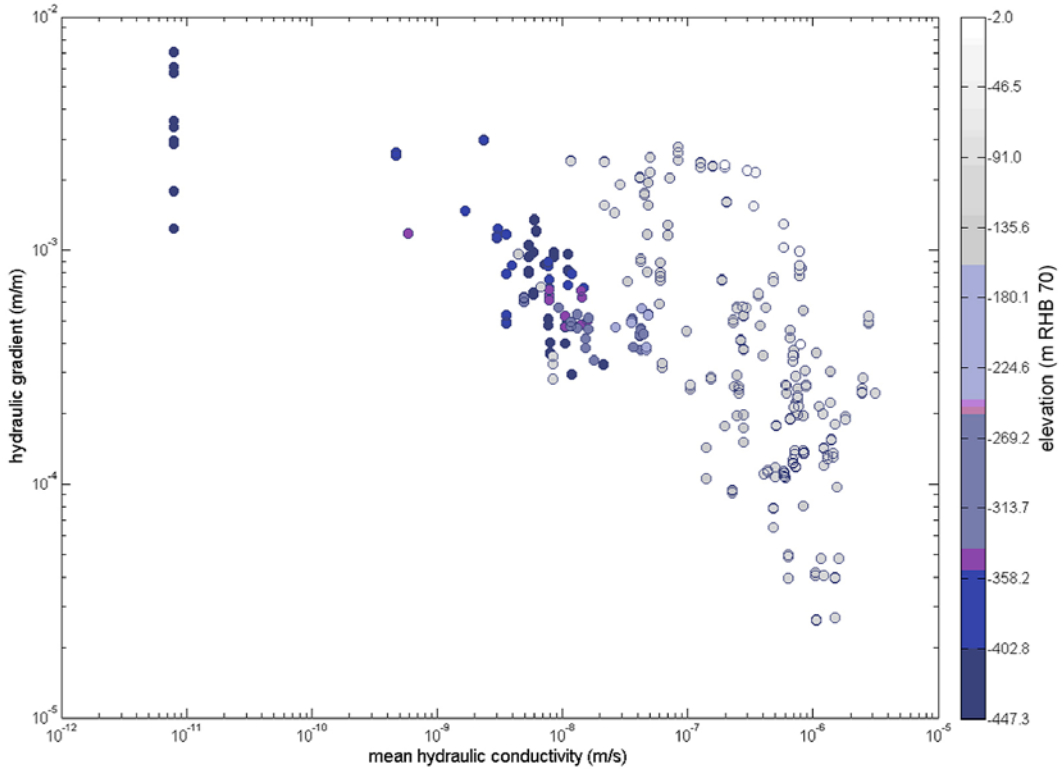

Figure 8-14. *A scatter plot of the hydraulic gradient for particle #228 versus the geometric mean hydraulic conductivity for particle #228. The dots are coloured with regard to elevation (m RHB 70). (Figure 6-7 in /Follin et al. 2008a/.)*

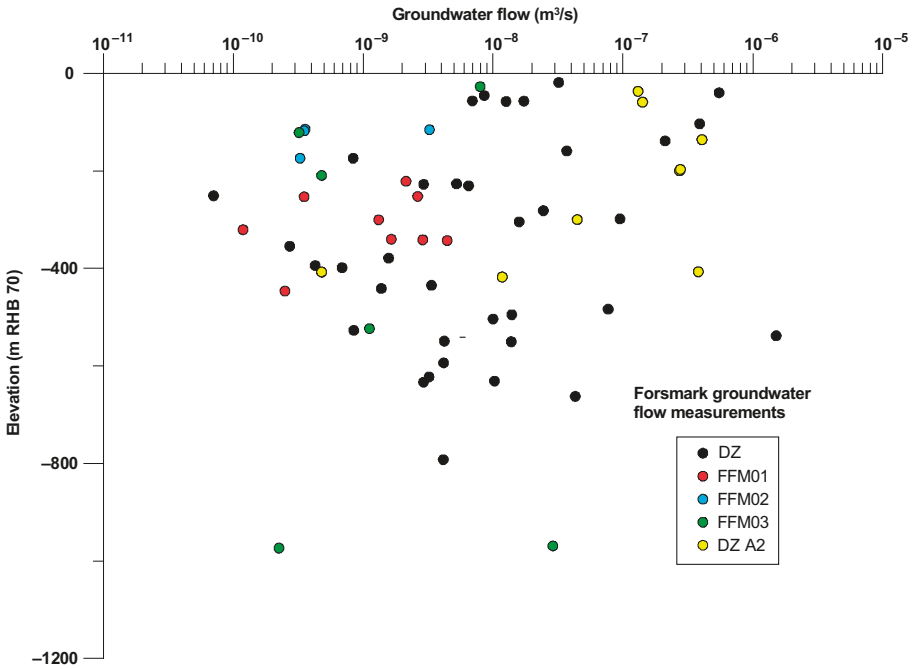

Figure 8-15. *Groundwater flow versus mid-section elevation for dilution measurements in Forsmark. Plotted points are classified into deformation zones and fracture domains. Modified after /Nordqvist et al. 2008/.(Figure 6-8 in /Follin et al. 2008a/.)*

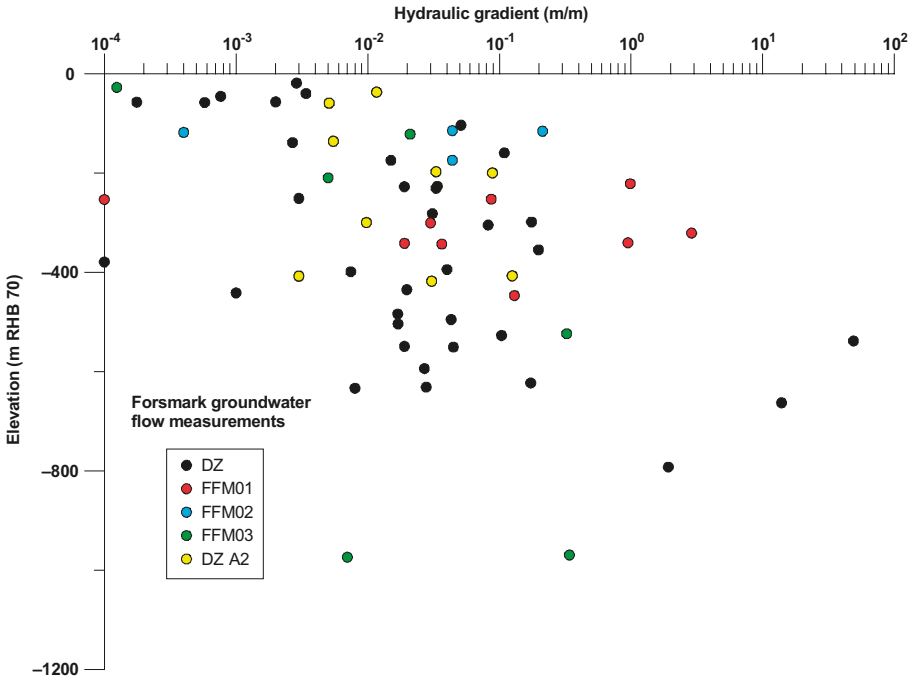

Figure 8-16. *Interpreted hydraulic gradient versus mid-section elevation for dilution measurements in Forsmark. Plotted points are classified into deformation zones and fracture domains. Modified after /Nordqvist et al. 2008/. (Figure 6-9 in /Follin et al. 2008a/.)*

9 Sensitivity to model uncertainties

This chapter aims at assessing the sensitivity of the flow model results presented earlier to some model uncertainties. The overall confidence in the hydrogeological model and remaining uncertainties are discussed in chapter 10 and in /SKB 2008ab/.

9.1 Uncertainties outside the target area

As part of the preliminary site description, a number of uncertainties outside the target area were analysed by performing variant cases to illustrate the sensitivity of the flow model calibration to alternative regional concepts and models. The geometrical uncertainties outside the target area studied in the preliminary site description included different sizes and locations of the flow model domain, different boundary conditions and different deformation zone models. None of these uncertainties, however, was found to have an impact on the migration paths inside the target volume that was greater than the impact of the parameter heterogeneity assumed for the local major deformation zones inside the target area /Follin et al. 2005/.

As previously mentioned, the strong contrasts in the structural-hydraulic properties with depth encountered inside the target volume during stage 2.2 suggest a hydraulic phenomenon that causes a short circuit in the near-surface groundwater flow system. This phenomenon probably contributes to the observed slow transient evolution of fracture water and porewater hydrochemistry at depth, although the slow evolution is mainly due to the very low permeability at these depths. In conclusion, the present-day groundwater flow through the key fracture domains at depth inside the target volume (FFM01 and FFM06) is probably low and the regional surface water divide to the south of the candidate area (Figure 8-1 and Figure 8-2) is envisaged to be a representative upstream boundary for the sake of the objectives of the SDM.

9.2 Uncertainties inside the target area

Figure 9-1 through Figure 9-4 illustrate some of the experiences gained in stage 2.3 (see chapter 7 in /Follin et al. 2008a/ for a fuller description) regarding the influences of the spatial variability (parameter heterogeneity) in the HCD properties ($\sigma_{log(T)} = 0.632$) and the HRD properties (multiple hydrogeological DFN realisations) on the calibration of the *deterministic base model simulation* against Tasks B–D (cf. section 7.1).

9.2.1 Interference test data

The role of spatial heterogeneity in determining the distribution of drawdown resulting from the year 2006 interference test in HFM14 was assessed by ten realisations of the spatial variability both with the HCD and HRD. Figure 9-1 shows the variation in predicted drawdown across the ten realisations in the form of a bar and whisker plot to indicate the median, 25/75 percentiles, minimum and maximum for each monitoring interval. For boreholes with about 300 m of HFM14 the drawdowns vary by about 2–4 m, and about 1 m with about 800 m of HFM14. These variations are likely to result primarily from the spatial variability with zone A2. Further than 800 m, the effect of the boundary condition at the Baltic Sea has strong control, and the variations are only a few decimetres at most.

Figure 9-1 does not suggest that spatial variability within HCD or HRD leads to significantly different conclusions compared to the calibrated *deterministic base model simulation*. For many of the monitored intervals at distance less than 800 m, the measured drawdown falls within the simulated variations, which may indicate that heterogeneity within zone A2 and other zones are the cause of the variations in drawdown distribution. Further away, spatial variability is less important, and improved simulation results may require consideration of issues such as the connections between deformation zones and boundary conditions.

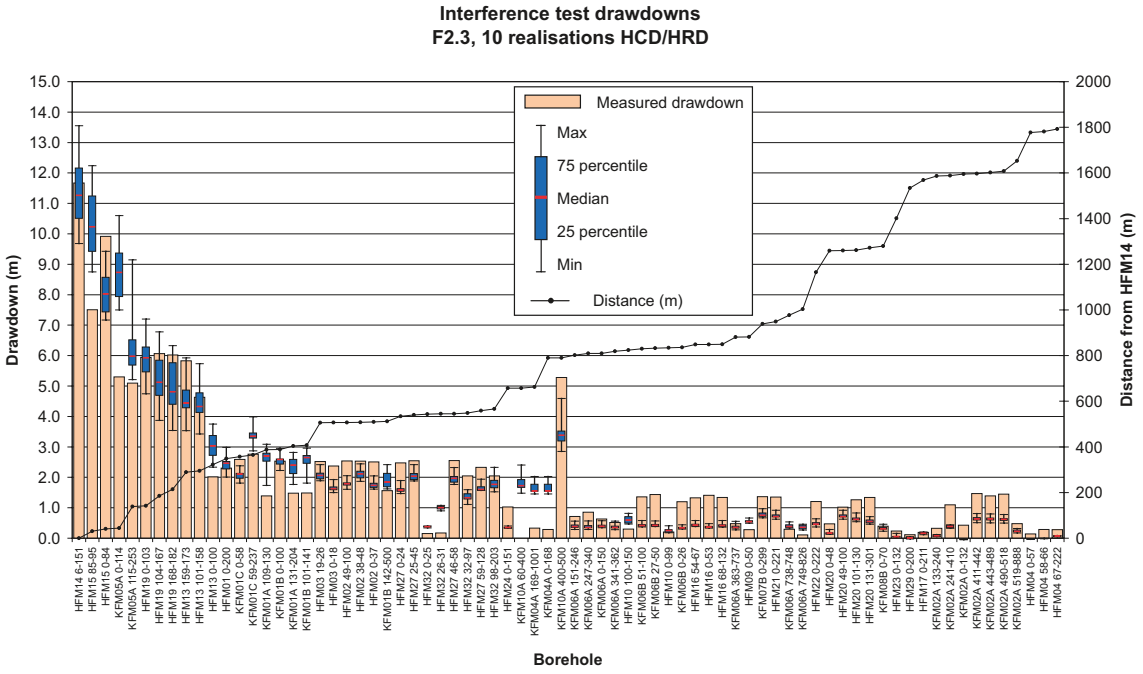

Figure 9-1. *Box-and-whisker statistics of ten stochastic model simulations showing the sensitivity of model calibration against the 2006 interference test in HFM14 to heterogeneous properties in the HCDs and HRDs. (Figure 7-2 in /Follin et al. 2008a/.)*

9.2.2 Groundwater levels

The distribution of steady state natural groundwater levels shows very little sensitivity to heterogeneity of the HCD and HRD as demonstrated by Figure 9-2. The blue bars show the median, minimum and maximum between realisations. The variations are typically only a few decimetres. It suggests that the distribution of steady state groundwater levels is mainly governed by the top surface boundary conditions and the properties of the HSD controlling the amount of infiltration through the top surface. The sensitivity cases that focussed on variants of the amount of potential infiltration available to recharge the saturated zone and hydraulic properties of the HSD are reported in section 7.5.2 in /Follin et al. 2008a/.

Figure 9-1 demonstrates that model calibration against transient interference test data (Task B) is more sensitive to parameter heterogeneity in the bedrock hydraulic properties than is model calibration against mean (steady state) groundwater levels (Task C) shown in Figure 9-2.

9.2.3 Hydrochemistry profiles

The effects of spatial variability on predictions of the main hydrochemical species considered are estimated in Figure 9-3 and Figure 9-4. Here, the simulations of palaeo-hydrogeology for ten realisations of the HCD and HRD properties are shown in red for Cl, Br/Cl, $\delta^{18}O$ and HCO_3 with a solid line to show the mean, and dashed lines to show the minimum and maximum prediction at each depth over the realisations.

The results from the ten realisations are compared with the *deterministic base model simulation* and measured data for KFM01D and KFM06A, which contain samples from both the fracture water and porewater. In a sense, these plots indicate the limit to which we should expect any individual simulation, such as the *deterministic base model simulation*, to predict the measured data. The prediction of Cl and HCO_3 are relatively stable between realisations, suggesting models should be expected to give quite close approximation to the data for these species, whereas Br/Cl and $\delta^{18}O$ vary more between realisations, especially for KFM01D. It is interesting that the *deterministic base model simulation* over-predicted glacial water in KFM01D, while a number of the stochastic realisation give a much better prediction. Overall, the envelope

of realisations captures much of the sampled data and shows that the few shortcomings in the prediction of the *deterministic base model simulation* may be explained by property heterogeneity. Potentially, one could use the hydrochemistry results to identify simulations that give further improvements to the matching.

9.3 Sensitivities in particle tracking

Two main questions were considered with regards to particle tracking for a release from an approximation of the D1 repository layout /SKB 2005c/:

- How sensitive are the exit locations to spatial heterogeneity in the HCD and HRD and are the exit locations predicted by the *deterministic base model simulation* representative?
- How much do the properties of the Singö zone affect the discharge area, for example making it less conductive or a barrier to flow?

The first of these issues was addressed by comparing the set of exit locations predicted by the ten stochastic sensitivity cases which have spatial heterogeneity within the HCD and are based on different realisations of the Hydro-DFN model used to derive the spatially varying HRD properties. Around 300 particle tracks were calculated for each of the ten realisations to give an ensemble of exit locations which is compared with the exit locations for the *deterministic base model simulation* in Figure 9-5. This confirms that the *deterministic base model simulation*, which uses deterministic HCD properties, gives a consistent prediction of the main discharge areas, which is not unexpected since the exit locations are largely controlled by the deterministically modelled geological structures, i.e. HCD. Heterogeneity does not disperse the exit locations to any radical degree.

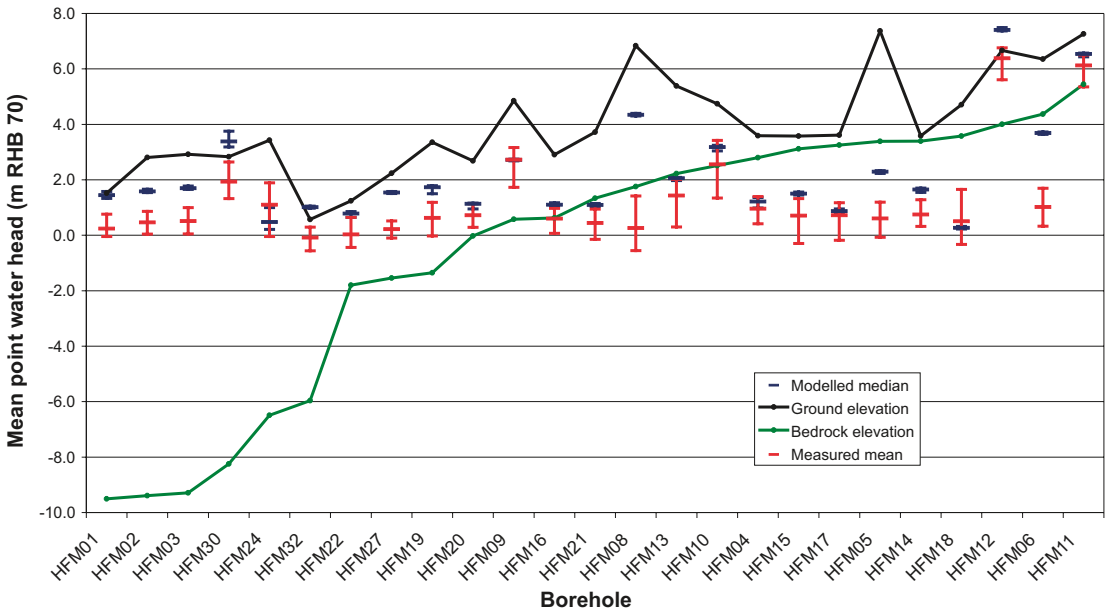

Figure 9-2. *Plot of ten realisations (blue) showing the sensitivity of model calibration against groundwater levels measured in the percussion-drilled boreholes (red) to heterogeneous properties in the deformation zones and in the fracture domains. The boreholes are ordered by increasing bedrock elevation. The simulated data are plotted as median groundwater levels with error bars to show the range between the minimum and maximum values. The measured data are plotted as mean groundwater levels with error bars to show the range of the diurnal recordings over time. The simulated groundwater levels in the boreholes within the target volume are on the average c 0.7 m higher than the corresponding measured levels. (Figure 7-7 in /Follin et al. 2008a/.)*

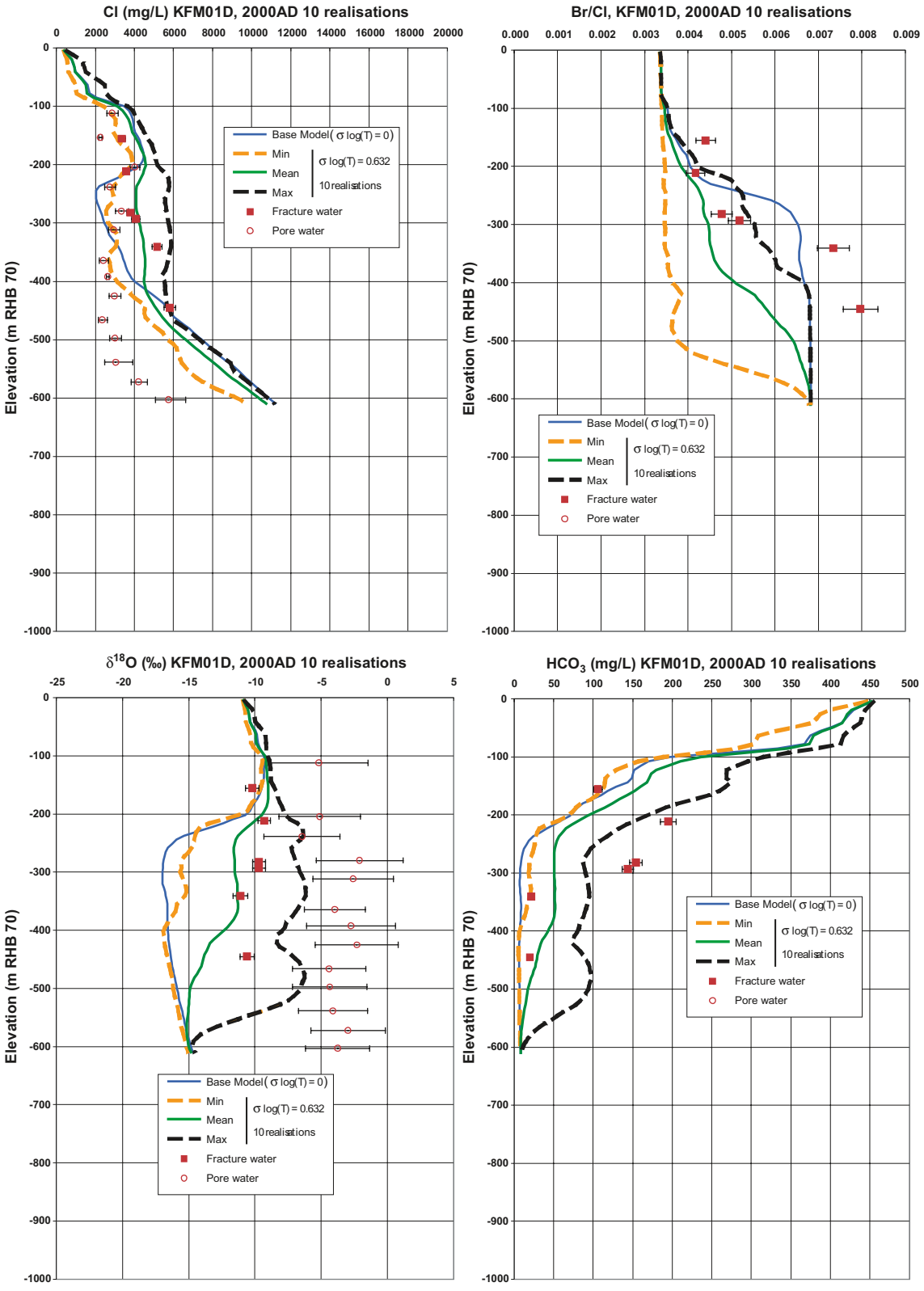

Figure 9-3. *Uncertainties in predictions of different hydrochemical components in KFM01D associated with heterogeneity in transmissivity. The blue line represents the deterministic base model simulation. The green line represents the mean of ten realisations. The dashed lines show the minimum and maximum in these realisations. The field data are shown by points. Note the greater variability in $\delta^{18}O$ vis-à-vis Cl, and the differences between fracture water $\delta^{18}O$ and porewater $\delta^{18}O$. These differences are a very strong indication that the matrix porewater in the target volume has been isolated for a very long time. (Figure 7-8 in /Follin et al. 2008a/.)*

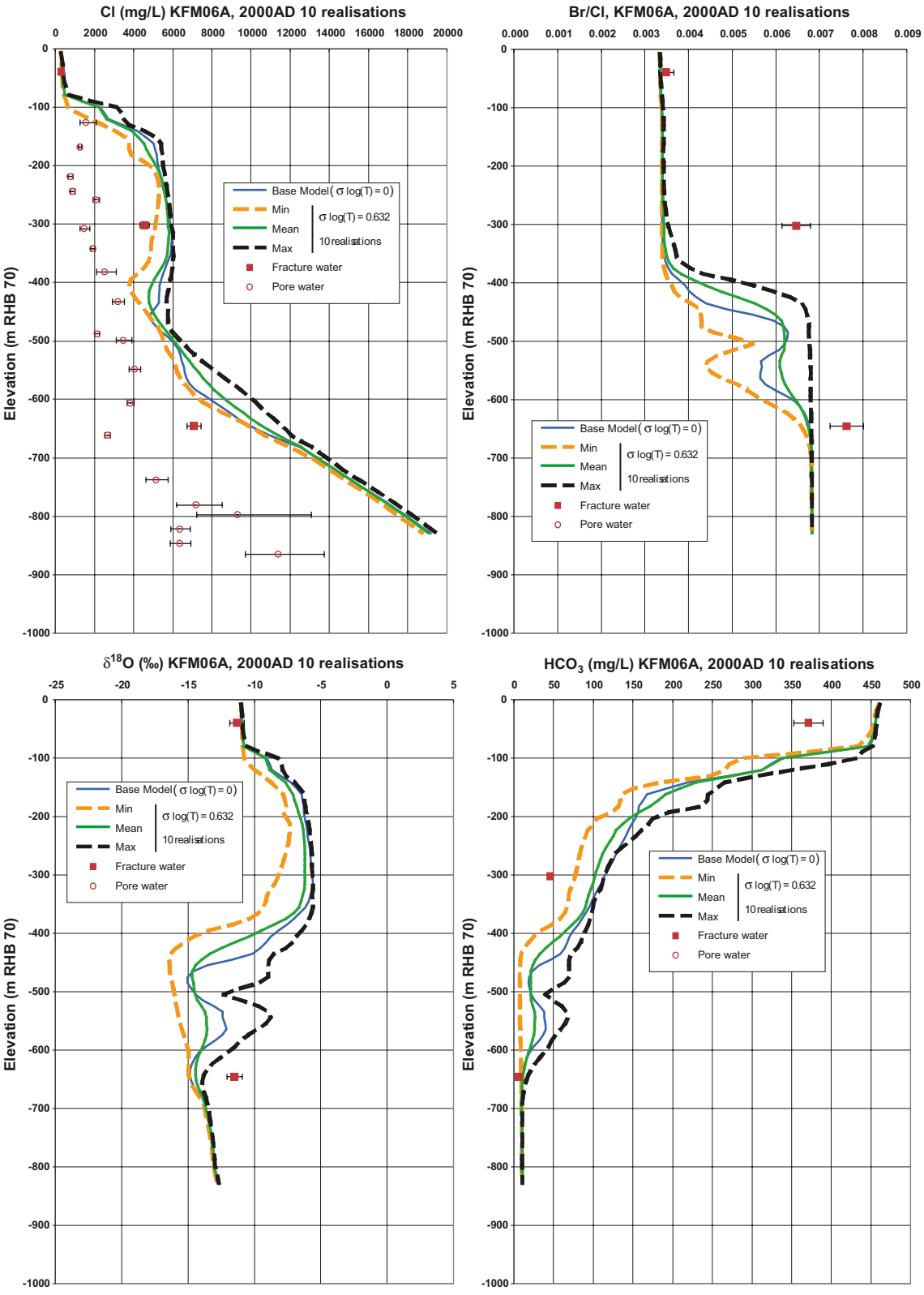

Figure 9-4. *Uncertainties in predictions of different hydrochemical components in KFM06A associated with heterogeneity in transmissivity. The blue line represents the deterministic base model simulation. The green line represents the mean of ten realisations. The dashed lines show the minimum and maximum in these realisations. The field data are shown by points. (Figure 7-9 in /Follin et al. 2008a/.)*

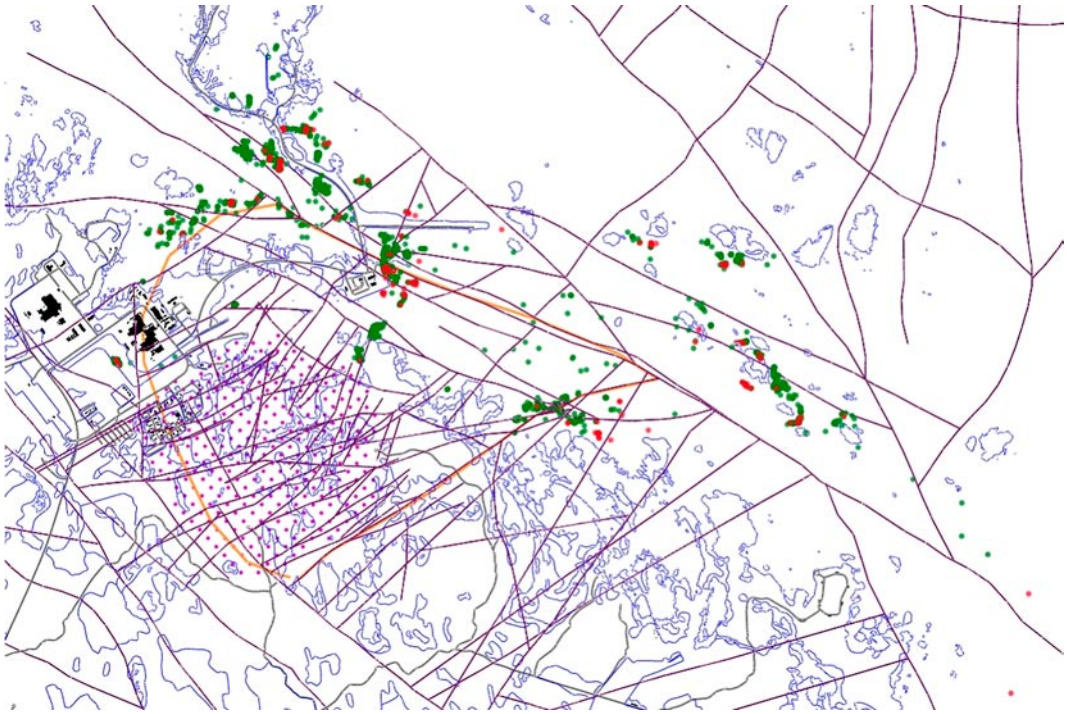

Figure 9-5. *Plan view of the target area with predicted flow paths and exit locations of c 300 particles for the deterministic base model simulation (red dots) and from the ensemble of ten realisations of spatial heterogeneity in HCD and HRD (green dots). The particles were released in a 100 m by 100 m mesh at c 500 m depth using an approximation of the D1 repository layout. (Figure 7-10 in /Follin et al. 2008a/.)*

In terms of individual exit locations, the average variation in particle exit location for the same start point between the stochastic realisations and the *deterministic base model simulation* is 1.2 km. Therefore, heterogeneity can have a significant effect on the fate of an individual particle, but the numbers and positions of key discharge areas are quite stable.

Figure 9-5 confirms the importance of the Singö deformation zone to discharge locations around the peninsula where the SFR buildings are located. Two variants were made with a reduced transverse hydraulic conductivity through the Singö deformation zone to act as a partial barrier to flow beyond the zone. However, in doing this there was also the consideration of what property to use at the intersection between the WNW Singö deformation zone and other steeply dipping ENE deformation zones or sub-horizontal sheet joint features. Since evidence of the drawdown from the SFR repository is thought to have been witnessed in part of the target area, it was decided to have the sheet joint features penetrate the Singö deformation zone. This means that particles could still pass through the Singö deformation zone in some localised areas. Figure 9-6 shows the results of reducing the transverse conductivity of the Singö deformation zone by a factor 1/10 and 1/100. Interestingly, 1/10 decrease reduced the length of particle tracks to the east, but had less effect around the SFR repository. A reduction of 1/100 shortens the paths more dramatically with most particles discharging around the outcrop of Singö or the immediate area around the SFR repository.

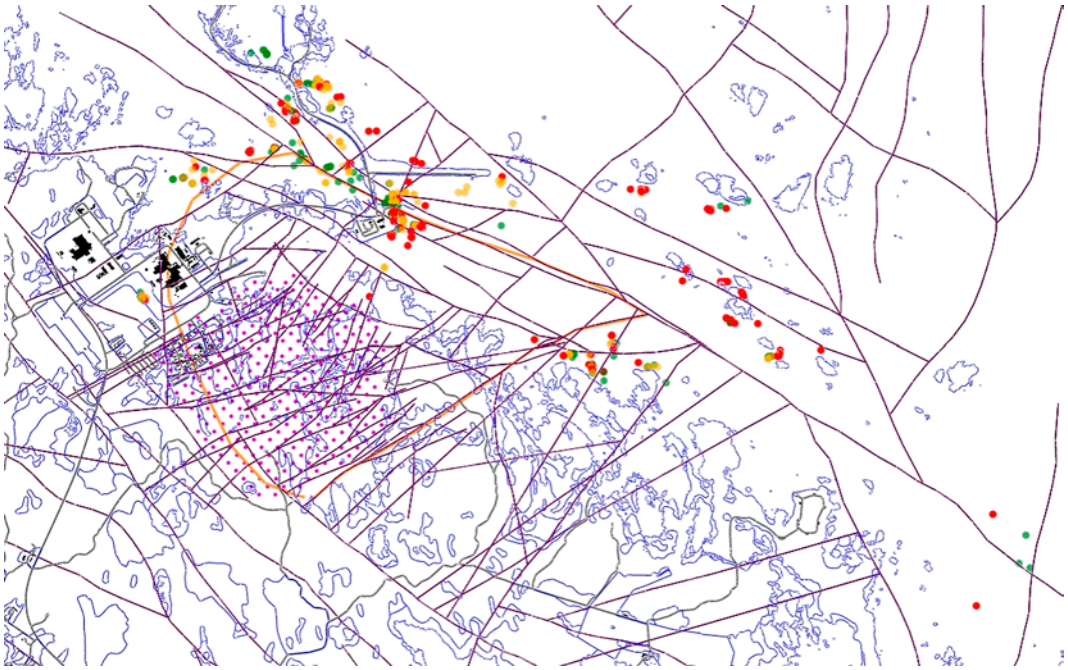

Figure 9-6. *Plan view of the target area with predicted flow paths and exit locations of c 300 particles for the deterministic base model simulation (red dots), for the sensitivity case with a 1/10 transverse hydraulic conductivity through the Singö zone (orange), and for the sensitivity case with a 1/100 transverse hydraulic conductivity through the Singö zone (green). The particles were released in a 100 m by 100 m mesh at 500 m depth using an approximation of the D1 repository layout. (Figure 7-11 in /Follin et al. 2008a/.)*

10 Discussion and conclusions

10.1 Summary of the bedrock hydrogeological model

The bedrock in the Forsmark area has been thoroughly characterised with both single-hole and cross-hole (interference) tests. Constant-head injection tests and difference flow logging pumping tests have been used in parallel to characterise the fracture properties close to the boreholes, and interference tests have been used for larger-scale studies. The overall experience from these investigations is that spatial variability in the structural geology significantly affects the bedrock hydrogeology and associated hydraulic properties at all depths. There is a considerable depth trend in deformation zone transmissivity and in the conductive fracture frequency in the bedrock between the deformation zones, where the uppermost part of the bedrock is found to be significantly more conductive than the deeper parts. In conclusion, the strong contrasts in the structural-hydraulic properties with depth encountered inside the target volume suggest a hydraulic phenomenon that causes a short circuit of the near-surface groundwater flow system. The short circuit phenomenon probably contributes to the observed slow transient evolution of fracture water and porewater hydrochemistry at repository depth, although the slow evolution is mainly due to the very low permeability at these depths.

The left picture in Figure 10-1 illustrates the water yield capacity of a percussion-drilled borehole penetrating a geological structure at c 40 m depth within the target volume. In contrast, the right picture suggests that the bedrock at repository depth within the target volume contains a low frequency of open (broken) fractures. Indeed, the groundwater flow is found to be close to the percolation threshold in a large part of the north-western part of the candidate area. The spatial extent of these two observations was hypothesised in modelling stage 2.2. The hypothesis was not falsified by means of the new boreholes, single-hole hydraulic tests and interference tests conducted in modelling stage 2.3.

Figure 10-1. *Two key features of the bedrock in the target area at Forsmark. Left: High water yields are often observed in the uppermost c 150 m of the bedrock. Right: The large number of unbroken drill cores gathered at depth support the observation of few flowing test sections in the deeper bedrock. (Figure 3-24 and Figure 3-34 in /Follin et al. 2007c/.)*

10.1.1 Hydraulic characteristics of hydraulic conductor domains (HCD)

The following hydrogeological model has been suggested for the deterministically modelled deformation zones:

- The geological division of the deterministically modelled deformation zones into major sets and subsets is useful from a hydrogeological point of view. Most of these structural entities are steeply dipping and strike WNW-NW, NNW and NNE-NE-ENE; one is gently dipping (G).
- All deformation zones, regardless of orientation (strike and dip), display a substantial decrease in transmissivity with depth. The data suggest a contrast of c 20,000 times in the uppermost one kilometre of the bedrock, i.e. more than four orders of magnitude. Hydraulic data below this depth are lacking.
- The lateral heterogeneity in transmissivity is also substantial (a few orders of magnitude) but more irregular in its appearance.
- The highest transmissivities within the candidate area, regardless of depth, were found among the gently dipping deformation zones. The gently dipping zones are at a high angle to the minimum principal stress (σ_{3v}) but also sub-parallel to both the first (maximum, σ_{1H}) and second principal stresses (σ_{2h}). The steeply dipping deformation zones that strike WNW and NW are sub-parallel to the azimuth of σ_{1H} and have, relatively speaking, higher mean transmissivities than steeply dipping deformation zones in other directions, which are sub-parallel to the azimuth of σ_{2h}.

10.1.2 Hydraulic characteristics of the hydraulic rock domains (HRD)

The following hydrogeological model has been suggested for the fractured bedrock between the deterministically modelled deformation zones:

- The geological division of the bedrock between the deterministically modelled deformation zones into fracture domains is useful from a hydrogeological point of view.
- The conductive fracture frequency (CFF) shows very strong variations with depth, and a discrete network model for conductive fractures within the target volume is adopted that is split into three layers; above 200 m depth, between 200 and 400 m depth, and below 400 m depth.
- The hydraulic character of the fracture domains is dominated by the gently dipping (HZ) fracture set, and with only a small contribution from the steeply dipping NS and possibly NE fracture sets. However, the depth trend in fracture transmissivity for the fracture domains is not as conclusive as for the deformation zones.
- The sparse number of steeply dipping flowing features at depth within the target volume suggests that fractures associated with the gently dipping HZ fracture set may be fairly long (large) in order to form a sufficiently connected network.
- Available hydrogeological (structural-hydraulic) data do not falsify the hypothesis that the size and intensity of *potentially flowing fractures* can be approximated through the use of a *single* power-law relationship, i.e. a tectonic continuum. Figure 10-2 shows a NW-SE cross-section of a tectonic continuum realisation that is based on the hydrogeological DFN model parameters shown in Appendix C. The *connected open fractures* shown in Figure 10-2 are coloured by fracture domain.

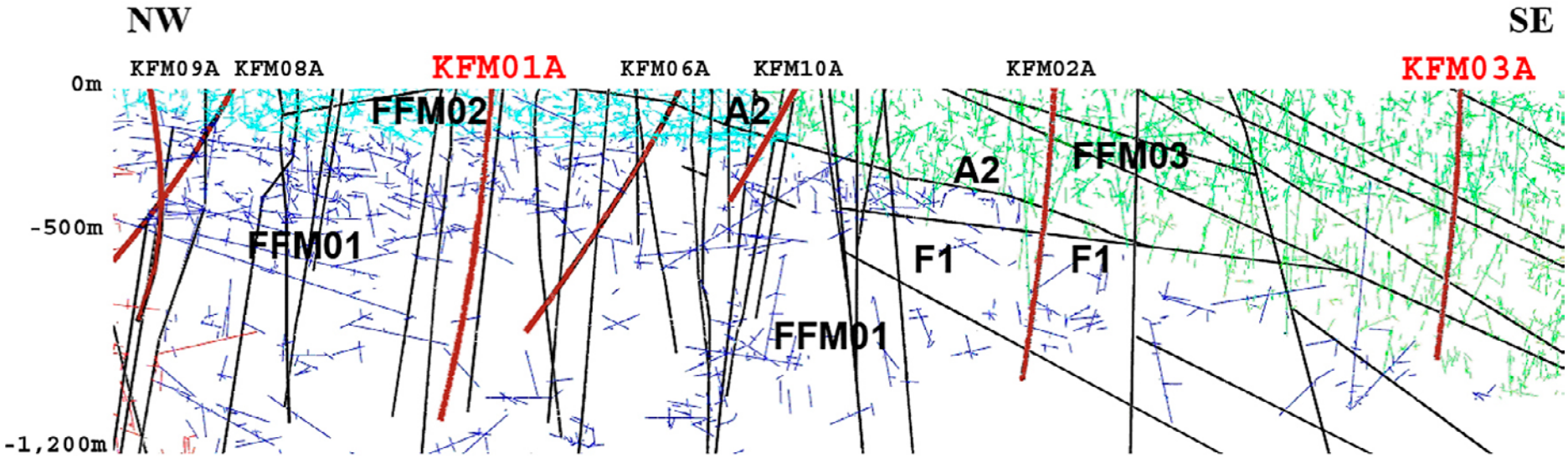

Figure 10-2. *One example of a realisation of the hydrogeological DFN model showing connected open fractures, coloured by fracture domain, in a NW-SE cross-section. The highlighted boreholes, KFM01A and KFM03A, are located in the footwall and the hanging wall of zones A2–F1, respectively. The deterministically modelled deformation zones are shown in black and grey, respectively. The effect of the low connectivity below 400 m depth in fracture domain FFM01 is apparent. (Figure 5 in /Follin et al. 2008b.)*

10.1.3 Hydrogeological characteristics of the target volume

The cross-section cartoon in Figure 10-3 summarises the key components of the conceptual model of the bedrock hydrogeology in the target volume at Forsmark. The flow at repository depth in fracture domains FFM01 and FFM06 is probably channelised in the sparse network of connected fractures, **D**, which is dominated by two fracture sets, HZ and NE. The HZ fracture set is interpreted to be longer and probably more transmissive than the NE set. **D** connects to **A** and **C**, where **A** represents the steeply dipping NNE-ENE deformation zones, which are abundant but hydraulically heterogeneous, and **C** represents the intensely fractured fracture domain FFM02, which lies on top of **D**. The groundwater flow in **C** is dominated by the HZ fracture set, which occurs with a high frequency. More importantly, **C** is intersected by several extensive, horizontal fractures/sheet joints, **B**, which can be *very* transmissive. **B** and **C** and the outcropping parts of **A** probably form a shallow network of flowing fractures. The network is interpreted to be highly anisotropic, structurally and hydraulically. Together with **D**, which is close to the percolation threshold, the network creates a hydrogeological situation that is referred to as a shallow bedrock aquifer on top of a thicker bedrock segment with aquitard type properties.

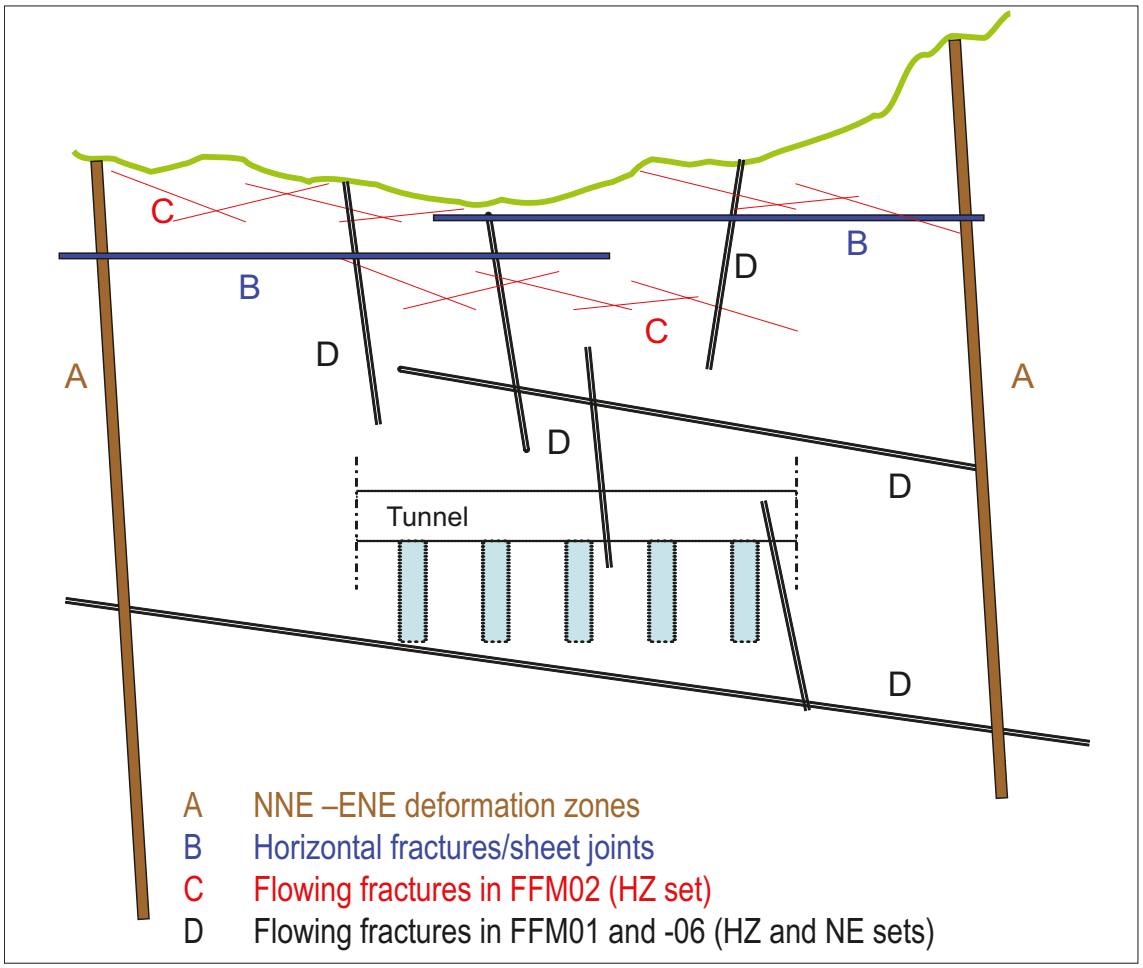

Figure 10-3. *A 2D cartoon facing NE that summarises the hydrogeological conceptual model of the bedrock within the target volume at Forsmark. (Modified after Figure 3-34 in /Follin et al. 2007c/.)*

10.2 Confirmatory testing

10.2.1 Conceptual modelling

The conceptual modelling conducted in stage 2.2 /Follin et al. 2007bc/ invoked three important hypotheses that were addressed in stage 2.3 /Follin et al. 2008a/ by means of complementary field investigations (hydraulic tests).

Transmissivity for deformation zones of different orientation: The field investigations carried out suggest that the gently dipping deformation zones that occur predominantly in the hanging wall bedrock of zones A2 and F1 are the most transmissive at each elevation. The steeply dipping deformation zones that strike WNW and NW was hypothesised in stage 2.2 to come in second place as far as transmissivity is concerned. The steeply dipping deformation zones that strike ENE and NNE occur in the footwall bedrock mainly. These zones can occasionally also be fairly transmissive, but a main characteristic, as it appears from data, is that they are on the average the least transmissive but at the same time significantly more heterogeneous laterally than the other categories of deformation zones. The validity of this hypothesis may be constrained to the upper 400–500 m of bedrock, however.

The hypothesis was tested in stage 2.3 by means of single-hole hydraulic tests in the new boreholes KF08D, KFM11A, KFM12A, HFM34, HFM36 and HFM37 (see Figure A-1 and Figure A-2 in Appendix A). These boreholes, except for KFM08D, intersect the regionally significant, ductile and brittle Singö and Forsmark deformation zones that border the tectonic lens and the candidate area. In contrast, KFM08D intersect a series of zones inside the target area that strike NNE-ENE.

Character of fracture domain FFM06: Fracture domain FFM06 is one of three fracture domains within the so-called target area, the other being FFM01 and FFM02. Due to lack of boreholes and hydraulic data in FFM06, it was hypothesised in stage 2.2 that this fracture domain has the same hydrogeological (structural-hydraulic) properties as inferred from the tests run in fracture domain FFM01. This hypothesis was tested in stage 2.3 by means of single-hole hydraulic tests in the new borehole KFM08D.

Extent of horizontal sheet joints: It was assumed in stage 2.2 that the sheet joints encountered in the target area follow the undulations of the bedrock surface, implying that some of them do not outcrop but stay below the bedrock surface as this dips under the Baltic Sea. The horizontal extent of the sheet joint was assumed to form a triangle bounded to the northeast by the Singö deformation zone, (WNW0001), to the southeast by the NE0062A deformation zone, and to the west by the expression of the sheath fold structure in rock domains 32 and 44. This hypothesis was tested hydraulically in stage 2.3 by means of an interference test conducted at the new percussion-drilled borehole HFM33 drilled on the peninsula close to the SFR buildings.

The results from the hydraulic tests carried out in stage 2.3 do not falsify or contradict any of these hypotheses, hence none of them should be rejected. In fact, the hypotheses are all supported by new evidence, which strengthens the overall credibility in the conceptual model developed in stage 2.2.

10.2.2 Numerical modelling

The primary objective of the numerical modelling carried out in stage 2.3 /Follin et al. 2008a/ was to address the sensitivity of the calibrated *deterministic base model simulation* developed in stage 2.2 /Follin et al. 2007c/ to parameter uncertainty. A comprehensive set of uncertainties were quantified to each of the model elements, HCD, HRD and HSD, as well as boundary conditions both in terms of their effects on the model calibration processes and in predictions of discharge areas for groundwater flow through the repository candidate volume. The results from the numerical modelling and the sensitivity tests carried out may be summarised as follows:

Transient, large-scale cross-hole (interference) tests

Sensitivity studies confirm that the large-scale cross-hole (interference) test carried out in stage 2.2 – 21 days of pumping in borehole HFM14 – has primarily helped inform the large-scale hydraulic properties of the major A2 deformation zone as well as its connection to the sheet joints (called cage features in the numerical model), and the top surface boundary conditions. Other important results from the HFM14 interference test are that heterogeneity in the hydraulic properties of the HCD and the cage features may account for some of the variability in the magnitude of drawdowns for bedrock boreholes less than c 800 m away from HFM14, that 50–100 m is an appropriate integral scale for this heterogeneity, and that the HSD and/or uppermost bedrock is very anisotropic; the transient simulations indicated a ratio of the horizontal to vertical hydraulic conductivity, K_h:K_v, of 100:1 or 1,000:1.

Steady state, average groundwater levels

The steady state model of the measured natural groundwater levels in the uppermost part of the bedrock is relatively insensitive to structural-hydraulic heterogeneity and bedrock properties in general. The groundwater levels are rather governed by the top surface boundary conditions, i.e. amount of potential infiltration, and the hydraulic properties of the HSD. Generally, the results are improved as the horizontal hydraulic conductivity of HSD is increased, or vertical hydraulic conductivity is decreased, confirming that high degrees of anisotropy in the HSD and/or uppermost bedrock seem to characterise the site.

Hydrochemical data in deep boreholes

Sensitivities of the predictions of the hydrochemical conditions at depth to heterogeneity in the structural-hydraulic properties demonstrated that the predictions of Cl and HCO_3 are relatively stable between realisations and so these species should be matched to a relatively high degree, as is the case for the *deterministic base model simulation*. There is a higher degree of variability in the predictions of Br/Cl and $\delta^{18}O$ between realisations, which also varies between boreholes. Overall, the envelope of realisations captures much of the sampled data and shows that the few shortcomings in the predictions of the *deterministic base model simulation* may be explained by heterogeneity in the structural-hydraulic properties. Potentially, one could use the hydrochemical results to identify simulations that give further improvements to the matching. The greater variability in $\delta^{18}O$ vis-à-vis Cl and the differences between fracture water $\delta^{18}O$ and porewater $\delta^{18}O$ are very strong indications that the matrix porewater in the target volume has been isolated for a very long time.

Particle tracking

Sensitivity studies considering the role of structural-hydraulic heterogeneity on discharge locations for the repository target volume corroborate that the *deterministic base model simulation* gives a consistent prediction of the main discharge areas, confirming that the deterministically modelled geological structures are the dominant control on groundwater pathways, and that hydraulic heterogeneity does not disperse the exit locations to any major extent. Exploratory simulations considering the Singö deformation zone as potential barrier to flow emphasise the importance of this zone for controlling the ultimate fate of any release.

10.3 Confidence and some remaining uncertainties

Model calibration is non-unique in that different combinations of parameter settings may achieve equally good and plausible matches to the test data. In the process of calibrating the numerical model against single-hole hydraulic tests, cross-hole tests, natural point water head measurements and hydrochemical data samples, a number of lessons were learnt in terms of the key features, processes and parameters required to mimic the observed behaviour of the

hydrogeological system. Sensitivities to various features and parameters had to be considered to find one or more ways to honour the field data. This prompted relatively few changes to the initial implementation of the conceptual model and the changes made were within the reasonable ranges of parameter uncertainty. Three uncertainties that affect the modelling of the hydrogeological conditions inside the target volume are described below.

10.3.1 Groundwater levels in the shallow bedrock aquifer

The ConnectFlow model used a simplistic representation of the near-surface hydrogeological system and aimed at matching the average groundwater levels of time series data in different boreholes with a steady state flow model as one of three calibration tasks. Although the magnitude and direction of the modelled gradient between the Quaternary deposits and the uppermost bedrock in the ConnectFlow model is in accordance with the monitoring data, the absolute values of the simulated average groundwater levels are too high, c +0.7 m of mean difference for both the percussion-drilled boreholes and the monitoring wells *within* the target volume. In comparison, the results reported from the MIKE SHE model, which used a detailed representation of the near-surface hydrogeological system and models the time series data on a diurnal basis, suggest that the low groundwater levels measured in the uppermost part of the bedrock cannot be matched unless there is a continuous sink somewhere in the bedrock. That is, without a continuous sink in the bedrock, the downward hydraulic gradients between the Quaternary deposits and the uppermost bedrock are not as pronounced in the MIKE SHE model as they are in the field measurements (and in the ConnectFlow model). In fact, the simulated hydraulic gradients locally point upwards in the MIKE SHE model unless there is a continuous sink in the bedrock. (It is noted that it is the groundwater levels in the bedrock that are affected by a sink in the bedrock in the MIKE SHE model. The simulated groundwater levels in the Quaternary deposits model are independent of whether or not there is a sink in the bedrock in the MIKE SHE model.)

There are two examples of sinks in the uppermost bedrock not far form the target area, none of which that can be turned off, however. The stronger of these sinks is the abstraction of drainage water in the SFR repository. The SFR repository is located below the Baltic Sea and is reached by two tunnels, which cross the Singö deformation zone. The drainage water is abstracted at two pump stations. The first pump station is located after the crossing of the Singö deformation zone (88 m depth; 1.2 L/s) and the other is located below the bottom of the SFR repository (140 m depth; 4.8 L/s) /Follin et al. 2008a/. The other example of a sink is the lowering of the groundwater level beneath the three nuclear power reactors, which are located northwest of the target area. The pumping under the reactors is not continuous (c. 20 m depth; c 1–2 L/s of intermittent pumping /Follin et al. 2008a/).

The simulations carried out with the MIKE SHE model suggest that a continuous abstraction of drainage water in the SFR repository affects the on-shore groundwater levels in the uppermost part of the bedrock within the target volume. It is noted that the calibrated MIKE SHE model is based on the ConnectFlow model with two main exceptions: 1) the horizontal hydraulic conductivity, K_h, was increased ten times in the part of the model describing the sheet joints only, and 2) the vertical hydraulic conductivity, K_v, was decreased ten times in the uppermost 200 m of bedrock throughout the entire model domain.

The results obtained from the single-hole geological interpretation and hydraulic testing of borehole KFM11A, which investigates the Singö deformation zone, together with the interference test data obtained from the interference test at borehole HFM33 during the fall of 2007, suggest that the Singö deformation zone is hydraulically heterogeneous and has a very low transverse transmissivity in the surroundings of the SFR buildings, i.e. there are no hydraulic responses observed in boreholes HFM34, HFM35 and KFM11A while pumping in borehole HFM33. The crossing of the two SFR tunnels could provide a possibility for a hydraulic interference through the Singö deformation zone, but the tunnels cross through the zone in close proximity to borehole HFM34, which did not respond to the pumping in borehole HFM33.

In contrast to the pumping in HFM33, the abstraction of drainage water in the SFR repository has a strong impact (metres to tens of metres) on the groundwater levels in the monitoring network in the bedrock in the proximity of the repository, including HFM34 (c. 3 m) and HFM35 (c. 5.5 m), which are located at a distance of c 500 m from the SFR repository, see Figure 5-22. Furthermore, the monitoring of groundwater levels in KFM11A that began at the end of 2007 indicates that all monitoring intervals on both sides of the Singö deformation zone respond to the abstraction of drainage water in the SFR repository. For instance, the uppermost monitoring section in KFM11A (0–130 m borehole length) has a groundwater level of c two metres below the datum and the bottommost monitoring section in KFM11A (711–850 m borehole length) has a groundwater level of c seven metres below the datum. The estimated transmissivities of these two bedrock intervals are $8 \cdot 10^{-6}$ m^2/s and $1 \cdot 10^{-6}$ m^2/s, respectively.

In conclusion, the prevailing situation with fairly low groundwater levels in the shallow bedrock within the target area may partly be caused by the pumping in the SFR repository. However, no definite conclusions on this issue can be drawn based on existing data. The ConnectFlow model assumes that the Singö deformation zone is heterogeneous, but the model is not calibrated for a scenario where there is a continuous sink in the bedrock in the SFR repository. However, exploration simulations, with the pumping in the SFR repository included in the calibrated ConnectFlow model, confirm that the hydraulic properties of the shallow bedrock aquifer system reported in the SDM are credible and adequate for further modelling, because the differences between measured and simulated groundwater levels decrease when the pumping in the SFR repository is incorporated. That is, even if the abstraction of drainage water in the SFR repository is an uncertain boundary condition that may affect the natural groundwater levels, the hydraulic stresses (drawdowns) induced by the cross-hole tests run in the target area apparently are sufficiently strong to allow for a fair calibration of the hydraulic properties.

10.3.2 Compartmentalised fracture networks at repository depth

The hydraulic description of the less fractured bedrock between the deformation zones is focussed on the conductive fracture frequency (CFF) of continuously flowing fractures. This means that the connected fracture network situations were regarded as more important for the hydrogeological DFN modelling and the groundwater flow modelling in the site description than disconnected (compartmentalised) networks. The role of compartmentalised networks, if any, needs to be addressed in the safety assessment. Their existence can only effectively be determined from detailed scale measurements e.g. carried out from tunnels at repository depth.

10.3.3 Evaluation of PFL-f transmissivity data

It is important to recollect what is actually measured with the PFL-f tests. For each PFL-f transmissivity value identified, the change in flux (inflow) and head (drawdown) after several days of pumping relative to conditions prior to pumping are calculated. A transmissivity value is interpreted for each PFL-f test based on Thiem's equation /Thiem 1906/ and an assumed value of the radius of influence to borehole radius ratio (R_0 / r_w) = 500. The choice of 500 reflects that tests are performed over several days, and hence should represent an effective transmissivity of the whole fracture intersected, and possibly adjoining parts of the network, but the choice of 500 is otherwise arbitrary. Consequently, the interpreted values of transmissivity should not be viewed as necessarily the transmissivity of individual fractures, or the transmissivity of the fracture local to the borehole intersect. They are more indicative of the effective transmissivity over a larger scale. This remark influences the way the PFL-f data are used in the hydrogeological DFN modelling as explained in the present report, see section 2.3.4.

10.3.4 Concluding remark

The present report is intended to summarise the hydrogeological conditions and the hydraulic properties of the bedrock at Forsmark and to give the information essential for demonstrating understanding. There is a good understanding of the overall hydrogeology inside the target volume and the confidence in the developed models is high. The remaining uncertainties concern predominantly the structural-hydraulic conditions outside this volume. These are identified and described in /SKB 2008a/.

11 References

Andersson J, Ström A, Almén K-E, Ericsson LO, 2000. Vilka krav ställer djupförvaret på berget? Geovetenskapliga lämplighetsindikationer och kriterier för lokalisering och platsutvärdering. SKB R-00-15, Svensk Kärnbränslehantering AB.

Andersson J, 2003. Site descriptive modelling – strategy for integrated evaluation. SKB R-03-05, Svensk Kärnbränslehantering AB.

Andersson J-E, Nordqvist R, Nyberg G, Smellie J, Tirén S, 1991. Hydrogeological conditions in the Finnsjön area. Compilation of data and conceptual model. SKB TR-91-24, Svensk Kärnbränslehantering AB.

Bath A, Lalieux P, 1999. Technical summary of the SEDE Workshop on the use of hydrogeochemical information in testing groundwater flow models. In: Use of hydrogeochemical information in testing groundwater flow models, Technical summary and proceedings of an NEA Workshop, Borgholm, Sweden, 1–3 September 1997 (organised by the NEA Co-ordinating Group on Site Evaluation and Design of Experiments for Radioactive Waste Disposal (SEDE)). OECD/NEA, Radioactive Waste Management, pp. 13–30.

Berggren M, 1998. Hydraulic conductivity in Swedish bedrock estimated by means of geostatistics. Thesis report series 1998:9, Royal Institute of Technology, Stockholm.

Bosson E, Berglund S, 2006. Near-surface hydrogeological model of Forsmark. Open repository and solute transport applications – Forsmark 1.2. SKB R-06-52, Svensk Kärnbränslehantering AB.

Bosson E, Gustafsson L-G, Sassner M, 2008. Numerical modelling of surface hydrology and near-surface hydrogeology at Forsmark, Site descriptive modelling, SDM-Site Forsmark. SKB R-08-09, Svensk Kärnbränslehantering AB.

Crawford J (ed), 2008. Bedrock transport properties Forsmark. Site descriptive modelling, SDM-Site Forsmark. SKB R-08-48, Svensk Kärnbränslehantering AB.

Dershowitz W, Winberg A, Hermanson J, Byegård J, Tullborg E-L, Andersson P, Mazurek M, 2003. Äspö Task Force on modelling of groundwater flow and transport of solutes. Task 6c. A semi synthetic model of block scale conductive structures at the Äspö HRL. Äspö Hard Rock Laboratory, International Progress Report IPR-03-13, Svensk Kärnbränslehantering AB.

DHI Software, 2008. MIKE SHE – User manual. DHI Water & Environment, Hørsholm, Denmark.

Follin S, Stigsson M, Svensson U, 2005. Regional hydrogeological simulations for Forsmark – numerical modelling using DarcyTools. Preliminary site description Forsmark area – stage 1.2. SKB R-05-60, Svensk Kärnbränslehantering AB.

Follin S, Johansson P-O, Levén J, Hartley L, Holton D, McCarthy R, Roberts D, 2007a. Updated strategy and test of new concepts for groundwater flow modelling in Forsmark in preparation of site descriptive modelling stage 2.2. SKB R-07-20, Svensk Kärnbränslehantering AB.

Follin S, Levén J, Hartley L, Jackson P, Joyce S, Roberts D, Swift B, 2007b. Hydrogeological characterisation and modelling of deformation zones and fracture domains, Forsmark modelling stage 2.2. SKB R-07-48, Svensk Kärnbränslehantering AB.

Follin S, Johansson P-O, Hartley L, Jackson P, Roberts D, Marsic N, 2007c. Conceptual model development and numerical modelling using ConnectFlow, Forsmark modelling stage 2.2. SKB R-07-49, Svensk Kärnbränslehantering AB.

Follin S, Hartley L, Jackson P, Roberts D, Marsic N, 2008a. Conceptual model development and numerical modelling using ConnectFlow, Forsmark modelling stage 2.3. SKB R-08-23, Svensk Kärnbränslehantering AB.

Follin S, Stephens M B, Laaksoharju M, Nilsson A-C, Smellie J A T, Tullborg E-L, 2008b. Modelling the evolution of hydrochemical conditions in the Fennoscandian Shield during Holocene time using multidisciplinary information. *Applied Geochemistry*, 23(7), 2004–2020.

Forsman I, Zetterlund M, Rhén I, 2004. Correlation of Posiva Flow Log anomalies to core mapped features in Forsmark (KFM01A to KFM05A). SKB R-04-77, Svensk Kärnbränslehantering AB.

Forssman I, Forsmark T, Rhén I, 2007. Forsmark site investigation. Correlation of Posiva Flow Log anomalies to core mapped features in KFM02B, -08D and -11A. SKB P-07-128, Svensk Kärnbränslehantering AB.

Fox A, La Pointe P, Hermanson J, Öhman J, 2007. Statistical geological discrete fracture network model, Forsmark modelling stage 2.2. SKB R-07-46, Svensk Kärnbränslehantering AB.

Fox A, La Pointe P, Hermanson J, Öhman J, 2008. Erratum to R-97-46, Dec. 2008, Svensk Kärnbränslehantering AB.

Gentzschein B, Levén J, Follin S, 2006. A comparison between well yield data from the site investigation in Forsmark and domestic wells in northern Uppland. SKB P-06-53, Svensk Kärnbränslehantering AB.

Glamheden R, Fredriksson A, Persson L, Röshoff K, Karlsson J, Bohlin H, Lindberg U, Hakami H, Hakami E, Johansson M, 2007. Rock mechanics Forsmark, Site descriptive modelling Forsmark stage 2.2. SKB R-07-31, Svensk Kärnbränslehantering AB.

Glamheden R, Lanaro F, Karlsson J, Wrafter J, Hakami H, Johansson M, 2008. Rock mechanics Forsmark, Modelling stage 2.3. Complementary analyses and verification of the rock mechanics model. SKB R-08-66, Svensk Kärnbränslehantering AB.

Gokall-Norman K, and Ludvigson J-E, 2006. Hydraulic interference test in borehole HFM14. Forsmark site investigation, SKB P-06-196, Svensk Kärnbränslehantering AB.

Hartley L J, Holton D, 2004. ConnectFlow (Release 8.0). Technical summary document, Serco Assurance Report SA/ERRA C/TSD02V1.

Hartley L J, Hoch A R, Cliffe K A, Jackson C P, Holton D, 2004a. NAMMU (Release 8.0). Technical summary document, Serco Assurance Report SA/ENV/0626.

Hartley L J, Holton D, Hoch A R, 2004b. NAPSAC (Release 8.0). Technical summary document, Serco Assurance Report SA/ERRA-N/TSD02V1.

Hartley L J, Cox I, Hunter F, Jackson C P, Joyce S, Swift B, Gylling B, Marsic N, 2005. Regional hydrogeological simulations for Forsmark – numerical modelling using ConnectFlow, Preliminary site description Forsmark area – stage 1.2. SKB R-05-32, Svensk Kärnbränslehantering AB.

Hartley L J, Hoch A, Jackson C P, Joyce S, McCarthy R, Rodwell W, and Marsic N, 2006. Groundwater flow and transport modelling during the temperate period for the SR-Can assessment – Forsmark sub-area – version 1.2, SKB R-06-98, Svensk Kärnbränslehantering AB.

Hedenström A, Sohlenius G, 2008. Description of the regolith at Forsmark. Site descriptive modelling, SDM-Site Forsmark. SKB R-08-04, Svensk Kärnbränslehantering AB.

Hedenström A, Sohlenius G, Strömgren M, Brydsten L, Nyman H, 2008. Depth and stratigraphy of regolith at Forsmark. Site descriptive modelling, SDM-Site Forsmark. SKB R-08-07, Svensk Kärnbränslehantering AB.

Hedin A, 2008. Semi-Analytic Stereological Analysis of Waste Package/Fracture Intersections in a Granitic Rock Nuclear Waste Repository. *Mathematical Geosciences*, DOI 10: 008-9175.

Hoch A R, Jackson C P, 2004. Rock-matrix diffusion in transport of salinity. Implementation in ConnectFlow. SKB R-04-78, Svensk Kärnbränslehantering AB.

Jackson C P, Hoch A R, Todman S, 2000. Self-consistency of a heterogeneous continuum porous medium representation of a fractured medium. *Water Resourc. Res.*, 36(1), 189–202.

Johansson P-O, Werner K, Bosson E, Berglund S, Juston J. 2005. Description of climate, surface hydrology, and near-surface hydrogeology. Preliminary site description Forsmark area – version 1.2. SKB R-05-06, Svensk Kärnbränslehantering AB.

Johansson P-O, 2008. Description of surface hydrology and near-surface hydrogeology at Forsmark. Site descriptive modelling, SDM-Site Forsmark. SKB R-08-08, Svensk Kärnbränslehantering AB.

Johansson P-O, Öhman J, 2008. Presentation of meteorological, hydrological and hydrogeological monitoring data from Forsmark. Site descriptive modelling, SDM-Site Forsmark, SKB R-08-10. Svensk Kärnbränslehantering AB.

Juston J, Johansson P-O, 2005. Analysis of meteorological data, surface water level data, and groundwater level data. Forsmark site investigation. SKB P-05-152, Svensk Kärnbränslehantering AB.

Juston J, Johansson, P-O, Levén, J, Tröjbom, M, Follin, S, 2007. Analysis of meteorological, hydrological and hydrogeological monitoring data. Forsmark – stage 2.1. SKB R-06-49, Svensk Kärnbränslehantering AB.

Laaksoharju M, Wallin B (eds.), 1997. Evolution of the groundwater chemistry at the Äspö Hard Rock Laboratory. Proceedings of the second Äspö International Geochemistry Workshop, June 6–7, 1995. SKB International Co-operation Report ISRN SKB-ICR-91/04-SE. ISSN 1104-3210 Stockholm, Sweden.

Laaksoharju M, Skårman C, Skårman E, 1999. Multivariate Mixing and Mass-balance (M3) calculations, a new tool for decoding hydrogeochemical information. *Applied Geochemistry*, 14(7), 861–871.

Laaksoharju M, Smellie J, Tullborg E-L, Gimeno M, Hallbeck L, Molinero J, Waber N, 2008. Bedrock hydrogeochemistry Forsmark. Site descriptive modelling, SDM-Site Forsmark. SKB R-08-47, Svensk Kärnbränslehantering AB.

La Pointe P, Olofsson I, Hermanson J, 2005. Statistical model of fractures and deformation zones for Forsmark: Preliminary site description Forsmark area – version 1.2. SKB R-05-26, Svensk Kärnbränslehantering AB.

Lusczynski NJ, 1961. Head and flow of ground water of variable density. Journal of Geophysical Research, 66 (12), pp. 4247–4256.

Munier R, Stenberg L, Stanfors R, Milnes A, Hermanson J, Triumf C-A, 2003. Geological Site Descriptive Model. A strategy for the model development during site investigations. SKB R-03-07, Svensk Kärnbränslehantering AB.

NEA/OECD, 1993. Palaeohydrogeological methods and their application, Proceedings of a NEA workshop, Paris, 9–10 November 1992, Co-ordinating Group on Site Evaluation and Design of Experiments for Radioactive Waste Disposal – SEDE.

Nordqvist R, Gustafsson E, Andersson P, Thur P, 2008. Groundwater flow and hydraulic gradients in fractures and fracture zones at Forsmark and Oskarshamn. SKB R-08-103, Svensk Kärnbränslehantering AB.

Olofsson I, Simeonov A, Stigsson M, Stephens M, Follin S, Nilsson A-C, Röshoff K, Lindberg U, Lanaro F, Fredriksson A, Persson L, 2007. Site descriptive modelling Forsmark, stage 2.2. A fracture domain concept as a basis for the statistical modelling of fractures and minor deformation zones, and interdisciplinary coordination. SKB R-07-15, Svensk Kärnbränslehantering AB.

Painter S, 2006. Effect of single-fracture aperture variability on field-scale transport. SKB R-06-25, Svensk Kärnbränslehantering AB.

Rhén I, Forsmark T, Hartley L, Jackson P, Roberts D, Swan D, Gylling B, 2008. Hydrogeological conceptualisation and parameterisation, Site descriptive modelling SDM-Site Laxemar. SKB R-08-78, Svensk Kärnbränslehantering AB.

Rhén I, Smellie J, 2003. Task force modelling of groundwater flow and transport of solutes. Task 5 summary report. (ISSN 1404-0344) SKB TR-03-01, Svensk Kärnbränslehantering AB.

Rhén I, Follin S, Hermanson J, 2003. Hydrogeological Site Descriptive Model. A strategy for the model development during site investigations. SKB R-03-08, Svensk Kärnbränslehantering AB.

SKB, 2000. Samlad redovisning av metod, platsval och program inför platsundersökningsskedet (FUD-k), Svensk Kärnbränslehantering AB.

SKB, 2002. Forsmark – site descriptive model version 0. SKB R-02-32, Svensk Kärnbränslehantering AB.

SKB, 2004. Preliminary site description Forsmark area–version 1.1. SKB R-04-15, Svensk Kärnbränslehantering AB.

SKB, 2005a. Preliminary site description Forsmark area – version 1.2. SKB R-05-18, Svensk Kärnbränslehantering AB.

SKB, 2005b. Preliminary safety evaluation for the Forsmark area. Based on data and site descriptions after the initial site investigation stage. SKB TR-05-16, Svensk Kärnbränslehantering AB.

SKB, 2005c. Forsmark site investigation. Programme for further investigations of geosphere and biosphere. SKB R-05-14, Svensk Kärnbränslehantering AB.

SKB, 2005d. Hydrogeochemical evaluation for Forsmark model version 1.2. Preliminary site description of the Forsmark area. SKB-R-05-17. Svensk Kärnbränslehantering AB.

SKB, 2006a. Site descriptive modelling Forsmark stage 2.1. Feedback for completion of the site investigation including input from safety assessment and repository engineering. SKB R-06-38, Svensk Kärnbränslehantering AB.

SKB, 2006b. Hydrogeochemical evaluation of the Forsmark site, model stage 2.1 – issue report. SKB R-06-69, Svensk Kärnbränslehantering AB.

SKB, 2008a. Confidence assessment Forsmark, Site descriptive modelling, SDM-Site Forsmark. SKB R-08-82, Svensk Kärnbränslehantering AB.

SKB, 2008b. Site description of Forsmark at completion of the site investigation phase, SDM-Site Forsmark. SKB TR-08-05, Svensk Kärnbränslehantering AB.

Stephens MB, Fox A, La Pointe P, Simeonov A, Isaksson H, Hermanson J, Öhman J, 2007. Geology Forsmark. Site descriptive modelling Forsmark stage 2.2. SKB R-07-45, Svensk Kärnbränslehantering AB.

Söderbäck B (ed), 2008. Geological evolution, palaeoclimate and historical development of the Forsmark and Laxemar-Simpevarp areas. Site descriptive modelling, SDM-Site. SKB R-08-19, Svensk Kärnbränslehantering AB.

Streltsova T D, 1988. *Well testing in heterogeneous formations*. Exxon Monograph. John Wiley and Sons**.**

Thiem G, 1906. *Hydrologische Methoden*. J M Gebhardt, Leipzig.

Teurneau B, Forsmark T, Forssman I, Rhén I, Zinn E, 2007. Forsmark site investigation. Correlation of Posiva Flow Log anomalies to core mapped featuresin KFM01D, -07C, -08A, -08C and -10A. SKB R-07-127, Svensk Kärnbränslehantering AB.

Wikberg P, 1998. Äspö Task Force on modelling of groundwater flow and transport of solutes. SKB progress report HRL-98-07, Svensk Kärnbränslehantering AB.

Appendix A

A – Drill sites, boreholes and investigations

The candidate area and its drill sites

Figure A-1 illustrates the candidate area with its twelve drill sites (DS). The candidate area is approximately 6 km long and 2 km wide. Figure A-2 presents detailed maps of the drill sites. There are 25 core-drilled and 38 percussion-drilled boreholes in the bedrock at Forsmark. Some of the boreholes belong to data freeze 2.3. The boreholes in mind are the deep, core-drilled boreholes referred to as KFM02B, KFM08D, KFM11A and -12A, located at drill sites 2, 8, 11 and 12, respectively, and the shallow, percussion-drilled boreholes denoted by HFM33–38. The information from these four plus six boreholes was for most parts not available in stage 2.2 at the time of the bedrock hydrogeological modelling reported in /Follin et al. 2007bc/, but was used for hypotheses testing and model verification purposes in stage 2.3, see /Follin et al. 2008a/.

Single-hole hydraulic bedrock investigations

Table A-1 lists the boreholes with regard to the geological information acquired at the time of the different data freezes. Table A-2 lists which of the cored boreholes that were investigated with the Posiva Flow Log (PLF) unit and the Pipe String System (PSS) unit, respectively. All percussion-drilled boreholes are investigated with the HTHB unit (combined pumping and impeller flow logging) except those with a very poor yield. The data from the single-hole hydraulic tests were used to parameterise the HCD and the HRD, cf Figure 2-1 and Task A in Figure 2-2.

Table A-1. List of cored and percussion-drilled boreholes with regard to the different data freezes in Forsmark.

Data freeze	No. of core drilled boreholes	KFM-hole	No. of percussion drilled boreholes	HFM-hole
1.1 *2003-04-30*	1	KFM01A	8	HFM01–08
1.2 *2004-07-31*	5	KFM02A–05A KFM01B	11	HFM09–19
2.1 *2005-07-29*	4	KFM06A–07A KFM03B, -06B	3	HFM020–22
2.2 *2006-09-30*	11	KFM08A–10A KFM06B–09B KFM01C, KFM07C–08C KFM01D	10	HFM23–32
2.3 *2007-03-31*	4	KFM11A–12A KFM02B KFM08D	6	HFM33–38
All	25	KFM01A–12A KFM01B–03B KFM06B–09B KFM01C, KFM07C–08C KFM01D, -08D	38	HFM01–38

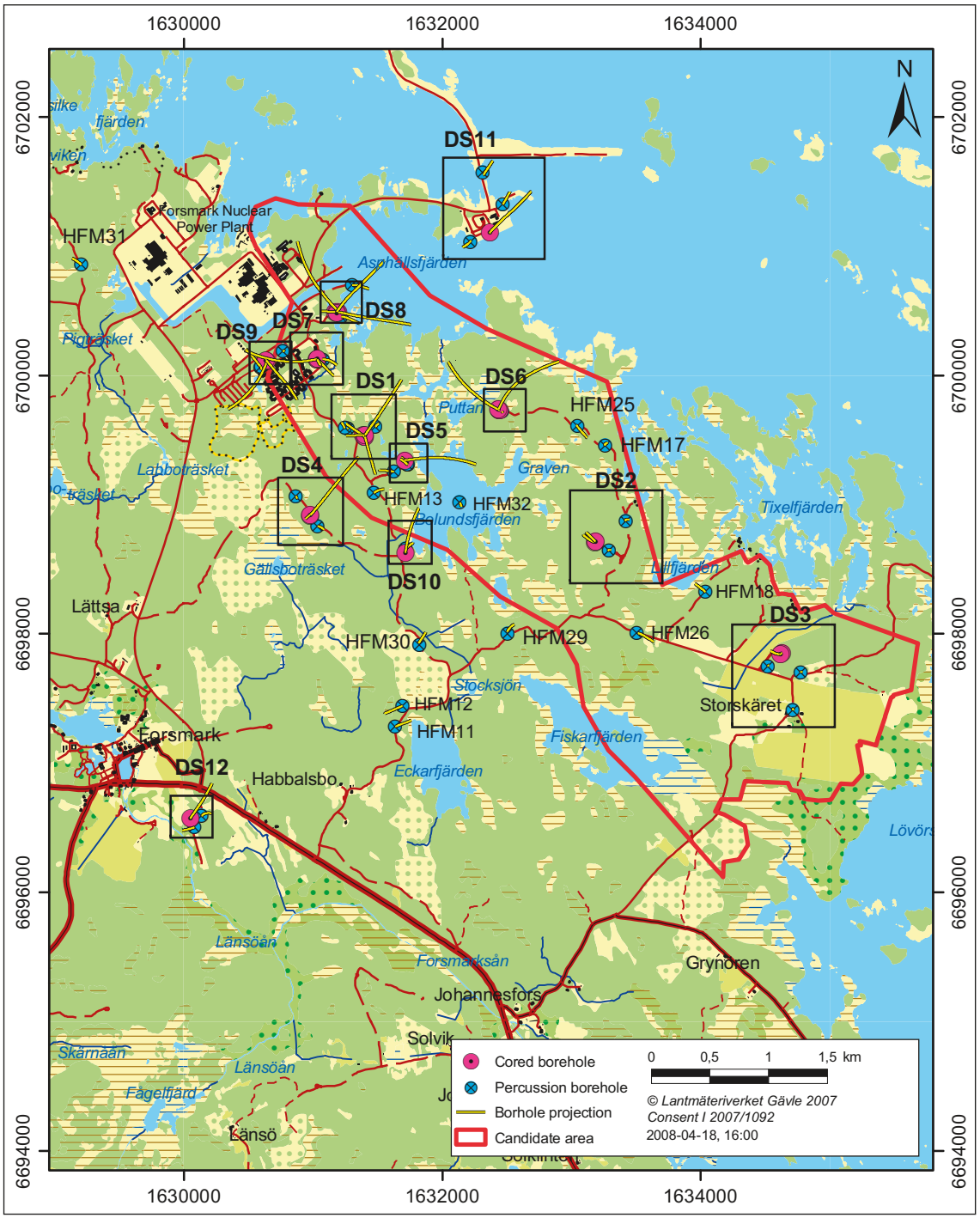

Figure A-1. *All telescopic, conventionally core-drilled and percussion-drilled boreholes produced during the site investigation at Forsmark 2002–2007. The projection of the boreholes on the ground surface due to their inclination is also shown. Some of the boreholes belong to data freeze/model stage 2.3. The boreholes in mind are the deep, core-drilled boreholes referred to as KFM02B, KFM08D, KFM11A and -12A, located at drill sites 2, 8, 11 and 12, respectively, and the shallow, percussion-drilled boreholes denoted by HFM33–38. The information from these four plus six boreholes was for most parts not available at the time of the bedrock hydrogeological modelling /Follin et al. 2007bc/, but was used for verification purposes /Follin et al. 2008a/.*

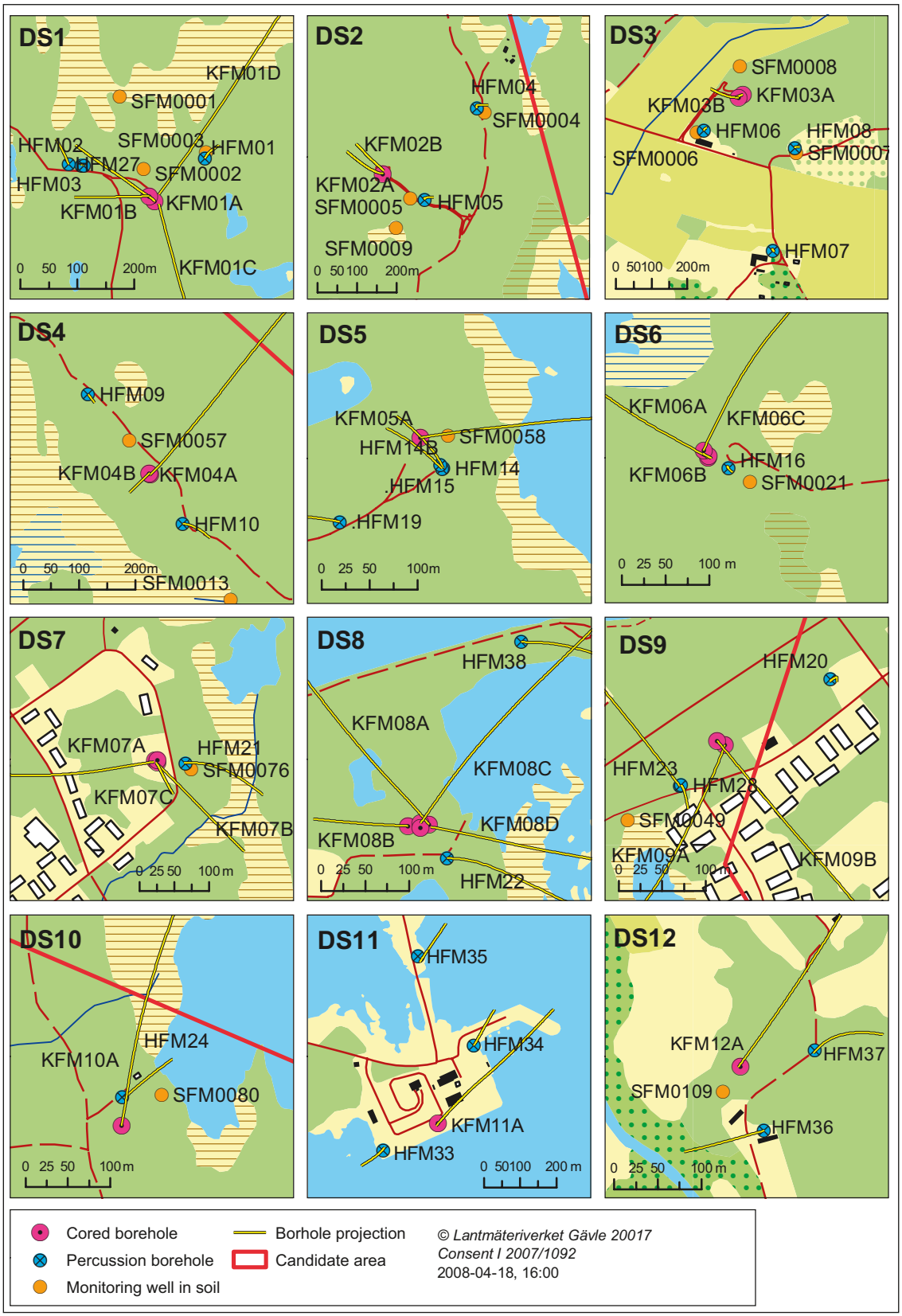

Figure A-2. *Detailed maps of each drill site that show the location and projection of core- and percussion-drilled boreholes. Boreholes in the Quaternary deposits at or close to the drill sites are also included.*

Table A-2. List of PFL and PSS tests, cf Table A-1.

Data freeze	No. of PFL tested boreholes	Tested boreholes KFM-hole	No. of PSS tested boreholes	Tested bore-holes KFM-hole
1.1 *2003-04-30*	1	KFM01A	0	–
1.2 *2004-07-31*	4	KFM02A–05A	3	KFM01A–03A
2.1 *2005-07-29*	2	KFM06A–07A	6	KFM04A–07A KFM03B, -06B
2.2 *2006-09-30*	5	KFM08A, -10A KFM07C–08C KFM01D	8	KFM08A–09A KFM07B–09B KFM01C, -06C KFM01D
2.3 *2007-03-31*	3	KFM11A KFM07C KFM08D	7	KFM10A–12A KFM02B KFM07C–08C KFM08D
All	15	KFM01–08A KFM10A–11A KFM02B KFM07C–8C KFM01D, -08D	24	KFM01A–12A KFM02B–03B, KFM06B–09B KFM01C, KFM06C–08C KFM01D, -08D

Cross-hole hydraulic bedrock investigations

Table A-3 shows completed, ongoing and upcoming pumping tests with the potential to reveal hydraulic properties in the bedrock between adjacent boreholes; that is, cross-hole investigations (interference tests). The most important interference test for the numerical modelling carried out in the work reported here is the interference test conducted in year 2006 in HFM14 /Gokall-Norman and Ludvigson 2006/. The data from this interference test are used for the confirmatory testing task referred to as Task B in Figure 2-2. The interference tests conducted during 2007 were used for hypotheses testing and model verification purposes.

Quaternary deposits and surface water hydrological investigations

Table A-4 lists the different kinds of near-surface single-hole investigations carried out at the Forsmark area with regard to the five data freezes 1.1–2.3. All together, about 70 boreholes (SFM-holes) were drilled in the Quaternary deposits. About 60 of these are terrestrial and ten are marine/lacustrine; that is, drilled through the sea/lake sediments into the underlying till. So-called BAT filter tips were used to collect hydrogeological data in low-permeable sediments such as silt, gyttja and clay. Table A-5 lists the number of BAT tests, slugtests and pumping tests conducted. The hydraulic measurements carried out in the boreholes in the Quaternary deposits are summarised in /Johansson et al. 2005/ and /Johansson 2008/. The properties deduced for hydrogeological modelling of the Quaternary deposits in modelling stages 1.2 and 2.2 are reported in /Bosson and Berglund 2006/ and /Bosson et al. 2008/, respectively. The surface runoff in the brooks, the surface water levels in the lakes and in the sea, and the groundwater levels in the boreholes drilled in the Quaternary deposits as well as in the bedrock are continuously monitored using SKB's hydrological monitoring system (HMS). Figure A-3 shows the network of boreholes used for monitoring the groundwater levels in the Quaternary deposits. Figure A-4 shows the location of stand pipes used for surface water level measurements in the lakes and in the sea. Figure A-5 shows the location of the discharge gauging stations used to monitor the runoff in the brooks.

The hydrological time series data gathered are analysed and reported in /Juston and Johansson 2005, Johansson et al. 2005, Juston et al. 2007, Johansson and Öhman 2008/. The diurnal variations in the monitoring data were modelled in stage 1.2 by /Bosson and Berglund 2006/ and in

model stage 2.2 by /Bosson et al. 2008/. The findings are summarised in /Johansson 2008/. The surface/near-surface modelling was made with the MIKE SHE code /DHI Software 2008/.

Mean values of the groundwater level measurements carried out in the Quaternary deposits and the percussion-drilled boreholes are used for the confirmatory testing task referred to as Task C in Figure 2-2.

Hydrochemical investigations

The hydrochemical programme encompassed the following constituents:

- major cations and anions (Na, K, Ca, Mg, Si, Cl, HCO_3^-,SO_4^{2-}, S^{2-}),
- trace elements (Br, F, Fe, Mn, Li, Sr, DOC, N, PO_4^{3-}, U, Th, Sc, Rb, In, Cs, Ba, Tl, Y and REEs),
- stable isotopes (^{18}O, ^{2}H, ^{13}C, ^{37}Cl, ^{10}B, ^{34}S),
- radioactive-radiogenic isotopes (^{3}H, ^{226}Ra, ^{228}Ra, ^{222}Rn, ^{238}U, ^{235}U, ^{234}U, ^{232}Th, ^{230}Th and ^{228}Th),
- microbes, gases and colloids.

The hydrochemical programme in the bedrock and in the Quaternary deposits was carried out in the same boreholes as the hydrogeological investigations.

The hydrochemistry available for the confirmatory testing task referred to as Task D in Figure 2-2 (palaeo-hydrogeology-hydrogeochemistry) was delivered in Excel format in January 2007. Besides fracture water chemistry the database includes porewater hydrochemistry of fresh rock samples.

Table A-3. List of pumping tests in the bedrock intended to function as interference tests.

Data freeze	Pumped borehole	Duration	Target of investigation
1.1 *2003-04-30*	HFM01 HFM02	7 hr 6 hrs	Connectivity between horizontal sheet joints and A2
1.2 *2004-07-31*	HFM11	4 hrs	Eckarfjärden deformation zone
2.1 *2005-07-29*	HFM16 HFM16 HFM18 KFM04A KFM02A	4 hrs 1 day 2 days 5 days 8 days	– A2 – A2 – A4 in hanging wall of A2 – Extent of A2 to southwest – A3 in hanging wall of A2
2.2 *2006-09-30*	HFM01 HFM14	3 weeks 3 weeks	Connectivity between horizontal sheet joints and A2
2.3 *2007-03-31*	–	–	–
Posterior 2.3 2007-12-31	KFM02B HFM14 HFM33	8 weeks 12 weeks 2 weeks	– Tracer transport properties in A2 at repository depth – Tracer transport properties in A2 near surface – Connectivity of horizontal sheet joints across Singö deformation zone and Asphällsfjärden

Table A-4. List of completed boreholes, BAT filter tips and stand pipes for groundwater (GW) levels and hydraulic conductivity (K) with regard to the different data freezes (DF) in Forsmark.

Type of installation	DF 1.1	DF 1.2	DF 2.1	DF 2.2	DF 2.3	Total
Monitoring wells for GW levels and K on land	32	13	3	10	2	60
Monitoring wells for GW levels and K below surface water	6	3	–	1	–	10
BAT filter tips for pore pressure and K	3	–	–	7	–	10
BAT filter tips for water sampling	3	–	–	7	–	10
Stand pipes for lake water levels	3	3	–	–	–	6
Stand pipes for sea water levels	2	–	–	–	–	2

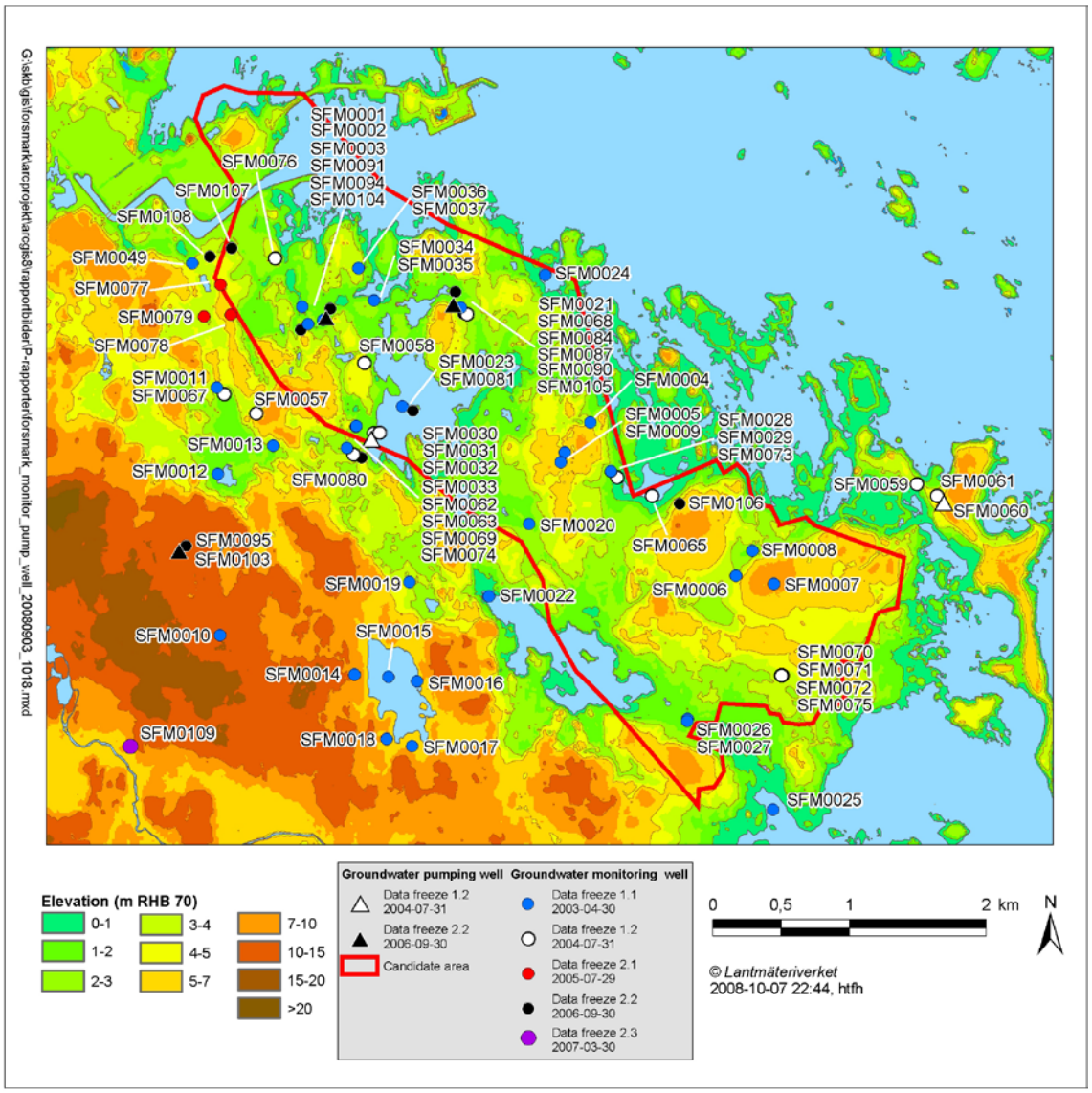

Figure A-3. *Elevation map showing existing boreholes in the Quaternary deposits at Forsmark. (Figure 2-6 in /Johansson 2008/.).*

Table A-5. List of completed single-hole slug tests and pumping tests in Quaternary deposits with regard to the different data freezes (DF) in Forsmark.

Type of installation	DF 1.1	DF 1.2	DF 2.1	DF 2.2	DF 2.3	Total
BAT tests	3	–	–	7	–	10
Slug tests	36	12	–	11	–	59
Pumping tests	–	2	–	3	–	5

Figure A-4. *Locations of the surface water level gauges. (Figure 2-4 in /Johansson 2008/.)*

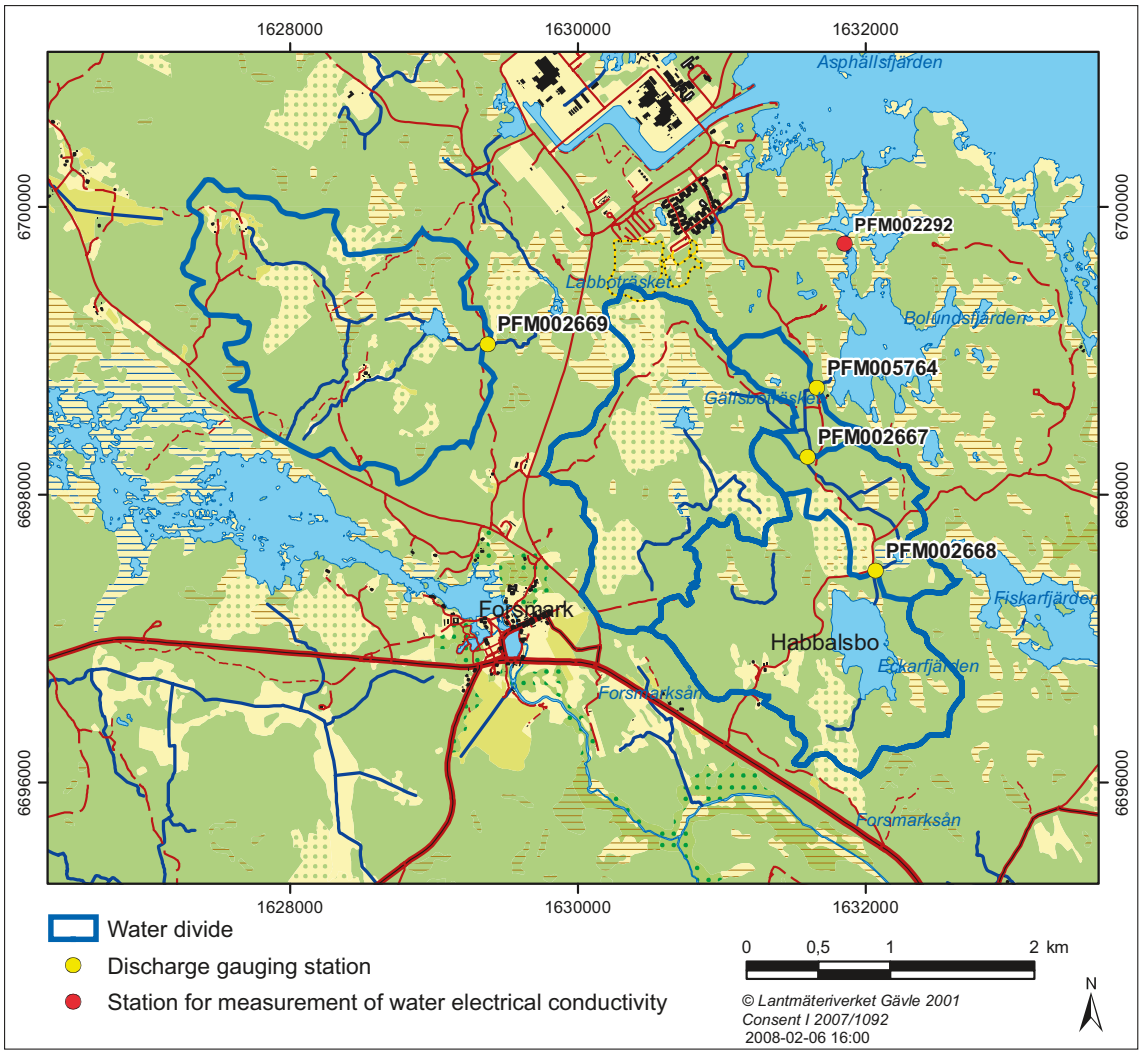

Figure A-5. *Locations of discharge gauging stations. (Figure 2-5 in /Johansson 2008/.)*

Appendix B

B – Table of SKB reports that describe the primary data archived in Sicada and used for parameterisation of hydraulic domains

Specifications of quality-assured data that were available for use in the site descriptive bedrock hydrogeological modelling at Forsmark are compiled in Table B-1 together with a summary of the application of these data in the analytical and modelling work. For simplification and traceability reasons, Table B-2 lists all the SKB reports referred to in Table B-1.

Table B-1. Available hydrogeological data of the bedrock and the Quaternary deposits and their handling in Forsmark SDM-Site bedrock hydrogeological modelling.

Available data Data specification	Ref	Usage in SDM-Site Analysis/Modelling
Single-hole data from core-drilled boreholes in the bedrock		
Double-packer injection tests (PSS)		
KFM01A	P-04-95	Lumped characterisation of rock fracture transmissivities in terms of different test section length transmissivities (5 m, 20 m and 100 m).
KFM01C	P-06-165	
KFM01D	P-06-195	
KFM02A	P-04-100	
KFM02A – re-measurement after hydraulic fracturing	P-05-145	
KFM03A	P-04-194	
KFM03B	P-04-278	
KFM04A	P-04-293	
KFM05A	P-05-56	
KFM06A and 06B	P-05-165	
KFM06C	P-06-23	
KFM07A	P-05-133	
KFM07B	P-06-86	
KFM08A	P-06-194	
KFM08B	P-05-235	
KFM08C	P-07-06	
KFM09A	P-06-52	
KFM09B	P-06-122	
KFM10A	P-07-31	
KFM11A	P-07-177	
KFM12A	P-07-121	
Difference-flow logging (PFL)		
KFM01A	P-03-28 P-04-193	Detailed characterisation of individual rock fracture transmissivities in terms of high-resolution test section length transmissivities (0.1 m).
KFM01D	P-06-161	
KFM02A	P-04-188	
KFM02B	P-07-83	
KFM03A	P-04-189	
KFM04A	P-04-190	
KFM05A	P-04-191	
KFM06A	P-05-15	
KFM07A	P-05-63	
KFM07C	P-06-247	
KFM08A	P-05-43	
KFM08C	P-06-189	
KFM08D	P-07-84	
KFM10A	P-06-190	
KFM11A	P-07-85	

Available data Data specification	Ref	Usage in SDM-Site Analysis/Modelling
Single-hole data from percussion-drilled boreholes in the bedrock		
Pumping tests and impeller flow logging		
HFM01, HFM02, HFM03	P-03-33	Characterisation of superficial rock fracture transmissivities in terms of borehole specific capacity and cumulative flow logging.
HFM04, HFM05	P-03-34	
HFM06, HFM07, HFM08	P-03-36	
HFM09, HFM10	P-04-74	
HFM11, HFM12	P-04-64	
HFM13, HFM14, HFM15	P-04-71	
HFM16	P-04-65	
HFM17, HFM18, HFM19	P-04-72	
HFM20, HFM21, HFM22	P-05-14	
HFM24, HFM32	P-06-96	
HFM25, HFM26	P-06-139	
HFM23, HFM27, HFM28	P-06-191	
HFM29, HFM30, HFM31	P-06-192	
HFM33, HFM34, HFM35	P-06-193	
HFM36, HFM37, HFM38	P-07-22	
Cross-hole (interference) data from boreholes in the bedock		
HFM01, HFM02, HFM03	P-03-35	Characterisation of the hydraulic contact between boreholes presumably intersected by a swarm of connected fractures forming a transmissive deformations zone.
HFM11, HFM12	P-04-200	
HFM18, KFM03A	P-04-307	
HFM16, KFM02A	P-05-78	
	P-05-37	
KFM04A, HFM10, HFM13, HFM19, HFK252	P-05-186	
HFM01	P-05-236	
KFM02A, KFM03A	P-06-09	
HFM14, KFM05A	P-06-140	
HFM14 – 2006	P-06-196	
HFM14 – 2007	P-07-228	
HFM33	P-07-229	
Correlation of structural, hydraulic and hydrogeochemical data in the bedrock		
KFM01A, KFM02A, KFM03A, KFM04A, KFM05A	R-04-77	Correlation of Posiva Flow Log anomalies to core mapped features.
KFM06A, KFM07A	P-06-56	
KFM01D, KFM07C, KFM08A, KFM08C, KFM10A	P-07-127	
KFM02B, KFM08D, KFM11A	P-07-128	
HFM16, KFM02A	Sicada Field note Forsmark 437	Hydraulic responses during drilling of HFM16.
KFM03A	P-04-96	Hydraulic evaluation of pumping activities prior to hydrogeochemical sampling – indications of upconing.
KFM02A, KFM03A, KFM04A	P-05-21	Comparison of measured EC in selected fractures – indications of upconing.
KFM01B, HFM01, HFM02, HFM03, KFM01A	P-04-135	Hydraulic responses during drilling of KFM01B.
HFM14	P-06-188	Hydraulic responses during pumping in HFM14
HFM01-22	P-06-53	Statistical comparison with SGU's Archive of Wells
KFM06A	P-06-54	A comparison between standard well test evaluation methods used in SKB's site investigations and the Generalised Radial Flow concept.

Available data Data specification	Ref	Usage in SDM-Site Analysis/Modelling
Laboratory data on core samples		
KFM01D	P-07-162	Characterisation of rock matrix permeability.
Near-surface hydrogeological data		
Inventory of private wells	R-02-17	Description of available hydro-geological information. Comment: No attempt is made to infer hydraulic parameters from capacity data.
Data on installed groundwater monitoring wells, abstraction wells and BAT filter tips	P-03-64 P-04-136 P-04-138 P-04-139 P-06-89	Description of QD type and depth to bedrock, basis for groundwater level measurements and hydraulic tests.
Hydraulic conductivity of Quaternary deposits	P-03-65 P-04-136 P-04-138 P-04-140 P-04-142 P-06-224 R-08-08 R-08-09	Basis for assigning hydraulic conductivity of Quaternary deposits in conceptual and quantitative models.
Groundwater levels in near-surface bedrock and in Quaternary deposits	R-05-06 P-04-313 P-05-152 P-05-245 R-06-49 P-06-263 P-07-113 R-08-08 R-08-09 R-08-10	Conceptual and descriptive modelling, and calibration of quantitative models.
Supplemenatry information and models		
SFR	R-98-48 R-99-08, R-02-14, R-01-02	General description, conceptual and quantitative modelling. Basis for assigning transmissivity data to some of the deterministically treated deformation zones.
Finnsjön	TR 91-24, TR 92-07, TR 92-33, TR 99-18	General description, conceptual and quantitative modelling. Basis for assigning hydraulic conductivity and kinematic porosity data to the bedrock outside fracture domains FFM01-06.
Previous site descriptive models versions 0, 1.1 and 1.2 and stage 2.1	R-02-32, R-04-15, R-05-18, R-06-38	General description, conceptual and quantitative modelling.

Table B-2. Reports in SKB's P-, R- and TR- series that are mentioned in Table B-1.

P-03-28 **Rouhiainen P, Pöllänen J.** Forsmark site investigation. Difference flow logging of borehole KFM01A.

P-03-33 **Ludvigson J-E, Jönsson S, Levén, J.** Forsmark site investigation. Pumping tests and flow logging. Boreholes KFM01A (0-100 m), HFM01, HFM02 and HFM03.

P-03-34 **Ludvigson J-E, Jönsson S, Svensson T.** Forsmark site investigation. Pumping tests and flow logging. Boreholes KFM02A (0-100 m), HFM04 and HFM05.

P-03-35 **Ludvigson J-E, Jönsson S.** Forsmark site investigation. Hydraulic interference tests. Boreholes HFM01, HFM02 and HFM03.

P-03-36 **Källgården J, Ludvigson J-E, Jönsson S.** Forsmark site investigation. Pumping tests and flow logging. Boreholes KFM03A (0-100 m), HFM06, HFM07 and HFM08.

P-03-64 **Johansson P-O.** Forsmark site investigation. Slug tests in groundwater monitoring wells in soil.

P-03-65 **Werner K, Johansson P-O.** Forsmark site investigation. Slug tests in groundwater monitoring wells in soil.

P-04-64 **Ludvigson J-E, Jönsson S, Jönsson J.** Forsmark site investigation. Pumping tests and flow logging. Boreholes HFM11 and HFM12.

P-04-65 **Ludvigson J-E, Jönsson S, Hjerne C.** Forsmark site investigation. Pumping tests and flow logging. Boreholes KFM06A (0-100m) and HFM16.

P-04-71 **Ludvigson J-E, Jönsson S, Jönsson J.** Forsmark site investigation. Pumping tests and flow logging. Boreholes HFM13, HFM14 and HFM15.

P-04-72 **Ludvigson J-E, Källgården J, Hjerne C.** Forsmark site investigation. Pumping tests and flow logging. Boreholes HFM17, HFM18 and HFM19.

P-04-74 **Ludvigson J-E, Källgården J, Jönsson J.** Forsmark site investigation. Pumping tests and flow logging. Boreholes HFM09 and HFM10.

P-04-95 **Ludvigson J-E, Levén J, Jönsson S.** Forsmark site investigation. Single-hole injection tests in borehole KFM01A.

P-04-96 **Ludvigson J-E, Jönsson S, Levén J.** Forsmark site investigation. Hydraulic evaluation of pumping activities prior to hydro-geochemical sampling in borehole KFM03A – Comparison with results from difference flow logging.

P-04-100 **Källgården J, Ludvigson J-E, Jönsson J.** Forsmark site investigation. Single-hole injection tests in borehole KFM02A.

P-04-135 **Levén J, Ludvigson J-E.** Forsmark site investigation. Hydraulic interferences during the drilling of borehole KFM01B. Boreholes HFM01, HFM02, HFM03 and KFM01A.

P-04-136 **Johansson P-O.** Forsmark site investigation. Undisturbed porewater sampling and permeability measurements with BAT filter tips. Soil sampling for porewater analyses.

P-04-138 **Werner K, Lundholm L, Johansson P-O.** Forsmark site investigation. Drilling and pumping test of wells at Börstilåsen.

P-04-139 **Werner K, Lundholm L.** Forsmark site investigation. Supplementary drilling and soil sampling, installation of groundwater monitoring wells, a pumping well and surface water level gauges.

P-04-140 **Werner K.** Forsmark site investigation. Supplementary slug tests in groundwater monitoring wells in soil.

P-04-142 **Werner K, Lundholm L.** Forsmark site investigation. Pumping test in wells SFM0074.

P-04-188 **Rouhiainen P, Pöllänen J.** Forsmark site investigation. Difference flow logging in borehole KFM02A.

P-04-189 **Pöllänen J, Sokolnicki M.** Forsmark site investigation. Difference flow logging in borehole KFM03A.

P-04-190 **Rouhiainen P, Pöllänen J.** Forsmark site investigation. Difference flow logging in borehole KFM04A.

P-04-191 **Pöllänen J, Sokolnicki M, Rouhiainen P.** Forsmark site investigation. Difference flow logging in borehole KFM05A.

P-04-193 **Rouhiainen P, Pöllänen J, Ludvigson J-E.** Forsmark site investigation. Addendum to Difference flow logging in borehole KFM01A.

P-04-194 **Källgården J, Ludvigson J-E, Hjerne C.** Forsmark site investigation. Single-hole injection tests in borehole KFM03A.

P-04-200 **Jönsson S, Ludvigson J-E, Svensson T.** Forsmark site investigation. Hydraulic interference tests. Boreholes HFM11 and HFM12.

P-04-278 **Hjerne C, Jönsson J, Ludvigson J-E.** Forsmark site investigation. Single-hole injection tests in borehole KFM03B.

P-04-293 **Hjerne C, Ludvigson J-E.** Forsmark site investigation. Single-hole injection tests in borehole KFM04A.

P-04-307 **Gokall-Norman K, Svensson T, Ludvigson L-E, Jönsson S.** Forsmark site investigation. Hydraulic interference test. Boreholes HFM18 and KFM03A.

P-04-313 **Nyberg G, Wass E, Askling P, Johansson P-O.** Forsmark site investigation. Hydro monitoring programme. Report for June 2002 – July 2004.

P-05-14 **Jönsson J, Hjerne C, Ludvigson J-E.** Forsmark site investigation. Pumping tests and flow logging. Boreholes HFM20, HFM21 and HFM22.

P-05-15 **Rouhiainen P, Sokolnicki M.** Forsmark site investigation. Difference flow logging in borehole KFM06A.

P-05-21 **Ludvigson J-E, Levén J.** Forsmark site investigation. Comparison of measured EC in selected fractures in boreholes KFM02A, KFM03A and KFM04A from difference flow logging and hydrogeochemical characterization – Analysis of observed discrepancies in KFM03A.

P-05-37 **Rouhiainen P, Sokolnicki M.** Forsmark site investigation. Difference flow logging in borehole KFM02A during pumping in HFM16.

P-05-43 **Sokolnicki M, Rouhiainen P.** Forsmark site investigation. Difference flow logging in borehole KFM08A.

P-05-56 **Gokall-Norman K, Ludvigson J-E, Hjerne C.** Forsmark site investigation. Single-hole injection tests in borehole KFM05A.

P-05-63 **Sokolnicki M, Rouhiainen P.** Forsmark site investigation. Difference flow logging in borehole KFM07A

P-05-77 **Gustafsson E, Nordqvist R, Thur P.** Forsmark site investigation. Groundwater flow measurements in boreholes KFM01A, KFM02A, KFM03A, KFM03B and SWIW tests in KFM02A, KFM03A.

P-05-78 **Gokall-Norman, Ludvigson J-E.** Forsmark site investigation. Hydraulic interference test. Boreholes HFM16, HFM19 and KFM02A.

P-05-133 **Gokall-Norman K, Svensson T, Ludvigson.** Forsmark site investigation. Single-hole injection tests in borehole KFM07A.

P-05-145 **Svensson T, Ludvigson J-E, Hjerne C.** Forsmark site investigation. Single-hole injection tests in borehole KFM02A, re-measurements after hydraulic fracturing.

P-05-152 **Juston J, Johansson P-O, 2005.** Analysis of meteorological data, surface water level data, and groundwater level data.

P-05-165 **Hjerne C, Ludvigson J-E, Lindquist A.** Forsmark site investigation. Single-hole injection tests in boreholes KFM06A and KFM06B.

P-05-186 **Gokall-Norman K, Ludvigson J-E, Jönsson S.** Forsmark site investigation. Hydraulic interference test. Boreholes KFM04A, HFM10, HFM13, HFM19 and HFK252.

P-05-235 **Lindquist A, Ludvigson J-E, Svensson T.** Forsmark site investigation. Single-hole injection tests and pressure pulse tests in borehole KFM08B.

P-05-236 **Gokall-Norman K, Ludvigson J-E, Jönsson S.** Forsmark site investigation. Hydraulic interference test in borehole HFM01.

P-05-245 **Nyberg G, Wass E.** Forsmark site investigation. Hydro Monitoring Program. Report for August 2004-July 2005.

P-06-09 **Gokall-Norman K, Ludvigson J-E, Jönsson S.** Forsmark site investigation. Hydraulic interference test. Boreholes KFM02A and KFM03A.

P-06-23 **Lindquist A, Ludvigson J-E, Gokall-Norman K.** Forsmark site investigation. Single-hole injection tests in borehole KFM06C.

P-06-52 **Lindqust A, Ludvigson J-E, Harrström J, Svensson T.** Forsmark site investigation. Single-hole injection tests in borehole KFM09A.

P-06-53 **Gentzschein B, Levén J, Follin S.** A comparison between well yield data from the site investigation in Forsmark and domestic wells in northern Uppland.

P-06-54 **Follin S, Ludvigson J-E, Levén J. Follin S, Ludvigson J-E, Levén J, 2006a.** A comparison between standard well test evaluation methods used in SKB's site investigations and the Generalised Radial Flow concept

P-06-56 **Forssman I, Zetterlund M, Forsmark T, Rhén I.** Correlation of Posiva Flow Log anomalies to core mapped features in Forsmark in KFM06A and KFM07A.

P-06-86 **Gokall-Norman K, Lindquist A, Ludvigson J-E, Gustavsson E.** Forsmark site investigation. Single-hole injection tests and pressure pulse tests in borehole KFM07B.

P-06-89 **Werner K, Lundholm L, Johansson P-O.** Forsmark site investigation. Supplementary drilling and soil sampling, and installation of groundwater monitoring wells, pumping wells and BAT filter tips.

P-06-90 **Gustafsson E, Nordqvist R, Thur P.** Forsmark site investigation. Groundwater flow measurements and SWIW test in borehole KFM08A.

P-06-96 **Jönsson S, Ludvigson J-E.** Forsmark site investigation. Pumping tests and flow logging. Boreholes HFM24, HFM32.

P-06-122 **Gustavsson E, Ludvigson J-E, Gokall-Norman K.** Forsmark site investigation. Single-hole injection tests in borehole KFM09B.

P-06-139 **Jönsson S, Ludvigson J-E.** Forsmark site investigation. Pumping tests and flow logging. Boreholes HFM25, HFM26.

P-06-140 **Lindquist A, Ludvigson J-E.** Pumping tests and flow logging in borehole HFM14 and pumping test in KFM05A (0 – 114 m).

P-06-161 **Väisäsvaara J, Leppänen H, Pekkanen J.** Forsmark site investigation. Difference flow logging in borehole KFM01D.

P-06-165 **Gustavsson E, Ludvigson J-E, Hjerne C, Florberger J.** Forsmark site investigation. Single-hole injection tests in borehole KFM01C.

P-06-188 **Lindquist A, Wass E.** Forsmark site investigation. Groundwater flow measurements in conjunction with the interference test with pumping in HFM14.

P-06-189 **Väisäsvaara J, Leppänen H, Pekkanen J, Pöllänen J.** Forsmark site investigation. Difference flow logging in borehole KFM08C.

P-06-190 **Sokolnicki M, Pöllänen J, Pekkanen J.** Forsmark site investigation. Difference flow logging in borehole KFM10A.

P-06-191 **Jönsson S, Ludvigson J-E.** Forsmark site investigation. Pumping tests and flow logging. Boreholes HFM23, HFM27 and HFM28.

P-06-192 **Lindquist A, Ludvigson J-E.** Forsmark site investigation. Pumping tests and flow logging. Boreholes HFM29, HFM30 and HFM31.

P-06-193 **Gustavsson E, Jönsson S, Ludvigson J-E.** Forsmark site investigation. Pumping tests and flow logging. Boreholes HFM33, HFM34 and HFM35.

P-06-194 **Walger E, Hjerne C, Ludvigson J-E, Harrström J.** Forsmark site investigation. Single-hole injection tests and pressure pulse tests in borehole KFM08A.

P-06-195 **Florberger J, Hjerne C, Ludvigson J-E, Walger E.** Forsmark site investigation. Single-hole injection tests in borehole KFM01D.

P-06-196 **Gokall-Norman K, Ludvigson J-E.** Forsmark site investigation. Hydraulic interference test in boreholes HFM14.

P-06-224 **Alm P, Gebrezghi M, Werner K.** Forsmark site investigation. Supplementary hydraulic tests in Quaternary deposits.

P-06-247 **Väisesvaara J, Pekkanen J, Pöllänen J.** Forsmark site investigation. Difference flow logging in KFM07C.

P-06-263 **Nyberg G, Wass E.** Forsmark site investigation. Hydro Monitoring Program. Report for August 2005–September 2006.

P-07-06 **Harrström J, Hjerne C, Ludvigson J-E.** Forsmark site investigation. Single-hole injection tests in borehole KFM08C.

P-07-22 **Walger E, Jönsson S, Ludvigson J-E.** Forsmark site investigation. Pumping tests and flow logging. Boreholes HFM36, HFM37 and HFM38.

P-07-31 **Walger E, Hjerne C, Ludvigson J-E.** Forsmark site investigation. Single-hole injection tests in borehole KFM10A.

P-07-52 **Thur P, Nordqvist R, Gustafsson E.** Forsmark site investigation. Groundwater flow measurements and SWIW tests in borehole KFM01D.

P-07-83 **Väisäsvaara J, Pöllänen J.** Forsmark site investigation. Difference flow logging in borehole KFM02B.

P-07-84 **Kristiansson S.** Forsmark site investigation. Difference flow logging in borehole KFM08D.

P-07-85 **Väisäsvaara J, Pekkanen J.** Forsmark site investigation. Difference flow logging in borehole KFM11A.

P-07-113 **Nyberg G, Wass E.** Forsmark site investigation. Hydro monitoring program. Report for October 2006 – March 2007.

P-07-121 **Harrström J, Svensson T, Ludvigson J-E.** Forsmark site investigation. Single-hole injection tests in borehole KFM12A.

P-07-127 **Teurneau B, Forsmark T, Forssman I, Rhén I, Zinn E.** Forsmark site investigation. Correlation of Posiva Flow Log anomalies to core mapped featuresin KFM01D, -07C, -08A, -08C and -10A.

P-07-128 **Forssman I, Forsmark T, Rhén I.** Forsmark site investigation. Correlation of Posiva Flow Log anomalies to core mapped features in KFM02B, -08D and -11A.

P-07-162 **Vilks P, 2007.** Rock matrix permeability measurements on core samples from borehole KFM01D.

P-07-177 **Harrström J, Svensson T, Ludvigson J-E.** Forsmark site investigation. Single-hole hydraulic tests in borehole KFM11A.

P-07-228 **Gokall-Norman K, Ludvigson J-E.** Forsmarks site investigation. Hydraulic interference test in borehole HFM14, summer of 2007.

P-07-229 **Gokall-Norman K, Ludvigson J-E.** Forsmarks site investigation. Hydraulic interference test in borehole HFM33, autumn 2007.

R-98-48 **Axelsson C-L, 1998.** Data for calibration and validation of numerical models at SFR Nuclear Waste Repository.

R-99-08 **Stigsson M, Follin S, Andersson J.** On the simulation of variable density flow at SFR, Sweden.

R-01-02 **Holmén J G, Stigsson M.** Modelling of future hydrogeological conditions at SFR.

R-02-17 **Ludvigson J-E.** Brunnsinventering i Forsmark.

R-02-14 **Axelsson C-L, Ekstav A, Lindblad Påsse A**. SFR – Utvärdering av hydrogeologi.

R-02-32 **SKB.** Forsmark – site descriptive model version 0.

R-04-15 **SKB.** Preliminary site description Forsmark area – version 1.1.

R-04-77 **Forsman I, Zetterlund M, Rhén I.** Correlation of Posiva Flow Log anomalies to core mapped features in Forsmark (KFM01A to KFM05A).

R-05-06 **Johansson P-O, Werner K, Bosson E, Berglund S, Juston J.** Description of climate, surface hydrology, and near-surface hydrogeology. Preliminary site description Forsmark area – version 1.2.

R-05-18 **SKB.** Preliminary site description Forsmark area – version 1.2.

R-06-38 **SKB.** Site descriptive modelling Forsmark stage 2.1. Feedback for completion of the site investigation including input from safety assessment and repository engineering.

R-06-49 **Juston J, Johansson P-O, Levén J, Follin S.** Analysis of meteorological, hydrological and hydrogeological monitoring data. Forsmark - stage 2.1.

R-08-08 **Johansson P-O.** Description of surface hydrology and near-surface hydrogeology at Forsmark. Site descriptive modelling, SDM-Site Forsmark.

R-08-09 **Bosson E, Gustafsson L-G, Sassner M.** Numerical modelling of surface hydrology and near-surface hydrogeology at Forsmark. Site descriptive modelling, SDM-Site Forsmark.

R-08-10 **Johansson P-O, Öhman J, 2008.** Presentation of meteorological, hydrological and hydrogeological monitoring data from Forskmark, Site descriptive modelling, SDM-Site Forsmark.

TR-91-24 **Andersson J-E, Nordqvist R, Nyberg G, Smellie J, Tirén S.** Hydrogeological conditions in the Finnsjön area. Compilation of data and conceptual model.

TR-92-07 **Geir J E, Axelsson C-E, Hässler L, Benabderrahmane A.** Discrete fracture modelling of the Finnsjön rock mass: Phase 2.

TR-92-33 **Ahlbom K, Andersson J-E, Andersson P, Ittner T, Ljunggren C, Tirén S.** Finnsjön study site. Scope of activities and main results.

TR-99-18 **Gylling B, Walker D, Hartley L.** Site-scale groundwater flow modelling of Beberg.

Appendix C

C – On the use of the tectonic continuum working hypothesis at Forsmark

Objective

The purpose of this appendix is to address the question if the data and methodology employed in the hydrogeological DFN modelling work /Follin et al. 2007b/ are consistent with those used in the geological DFN modelling work /Fox et al. 2007/. We focus on the derivation of the so-called r_0-fixed size-intensity model as a means demonstrate the conceptual similarities and differences in the two works carried out.

Definition

All size-intensity model variants considered in the geological DFN modelling work are based on the assumption of a power-law feature size probability density function. The tectonic continuum invokes that the frequency of features of different sizes can be approximated through the use of a *single* power-law relationship, i.e. a straight line. The tectonic continuum hypothesis is a working hypothesis, the validity of which can be tested by plotting the numbers of observations of different types of discrete features (fractures, lineaments, deformation zones) versus their characteristic sizes on a log-log plot. Assuming that the discrete features can be described as circular discs of radius r, the power-law feature size probability density function, $f(r)$, may be written as:

$$f(r) = \frac{k_r r_0^{k_r}}{r^{k_r+1}} \tag{C-1}$$

where $r_0 > 0$ and $k_r > 0$. r_0 is often referred to as the location parameter and k_r as the shape parameter (or the scaling exponent). The values of these parameters of the power-law density function may vary between fracture orientation sets. Hence, the lumped probability density function may not plot as a straight line.

If $P_{32}[r \geq r_0]$ denotes the feature surface area per unit volume of rock of all features greater than the location parameter, the feature surface area per unit volume of rock in the size interval $[r_1, r_2]$ may be written as (cf. Eq. (3-11) in /Fox et al. 2007/):

$$P_{32}[r_1, r_2] = P_{32}[r \geq r_0]\left(\frac{(r_1)^{(2-k_r)} - (r_2)^{(2-k_r)}}{(r_0)^{(2-k_r)}} \right) \tag{C-2}$$

The corresponding number of features per unit volume of rock, $P_{30}[r_1, r_2]$, may be approximated as (modified after Eq. (5) in /Hedin 2008/):

$$P_{30}[r_1, r_2] = \frac{P_{32}[r \geq r_0] r_0^{(k_r-2)} (k_r - 2)}{\pi\ k_r} (r_1^{-k_r} - r_2^{-k_r}) \tag{C-3}$$

In the geological DFN modelling work, r_2 was set to 564 m regardless of model variant. r_2 m corresponds to a circular disc with the same surface area as a square of side length L = 1,000 m, cf Figure 2-3. That is, features with visible trace lengths greater than 1,000 m, where modelled as deterministic deformation zones in the SDM.

The r_0-fixed model variant

The uncertainty analysis section of the geological DFN modelling work (cf. p. 213 in /Fox et al. 2007/) describes a model variant for fracture domains FFM01 and FFM06 where r_0 and r_1 were both set to about half the nominal diameter of the core-drilled boreholes (0.039 m). This assumption was in due time denoted as the r_0-fixed model variant in the SDM (cf. section 5.6.4

in /SKB 2008b/). In conclusion, the values of k_r for fracture domains FFM01 and FFM06 shown in Table 5-3 and Table 5-4 in /Fox et al. 2007/, respectively, were derived based on the assumptions that $r_0 = r_1 = 0.039$ m and $r_2 = 564$ m (cf. Eq. (5-2) in /Fox et al. 2007/), i.e.:

$$k_r = 2 - \frac{\ln(P_{32}[r \geq 0.039]/P_{32}[r \geq 564])}{\ln(0.039/564)} \quad \text{(C-4)}$$

The r_0-fixed model variant employs the tectonic continuum working hypothesis. The assumption that $r_0 = 0.039$ m is identical with the assumption considered in the hydrogeological DFN modelling work. However, the values of k_r derived in /Follin et al. 2007b/ were not based on an estimation of the fracture surface area per unit volume of rock of large features, but based on a connectivity analysis of the frequency of *potentially flowing features* (*open features*) observed in the boreholes, see section 6.2.

Consistency checks

The frequency of *open features* handled in the hydrogeological DFN modelling work can be conceived as a fraction (subset) of the frequency of *all features* handled in the geological DFN modelling work. The envisaged relationship between the associated power-law density functions is illustrated in Figure 2-4. Figure 2-4 implies that completely sealed features exist only among the small features, i.e. fractures, whereas large features, e.g. deformation zones, are all heterogeneous with regard to flow, i.e. more or less partly open. Figure 2-4 shows also the conceived intensity of *connected open fractures*, e.g. *continuously flowing fractures*. The so called *PFL-f fractures* are imagined to be a subset of the latter category, see Figure 6-3.

There is a clear variation in the occurrence of steeply dipping lineaments and deformation zones with WNW-ESE to NW-SE strike as well as in the occurrence of gently dipping deformation zones at Forsmark /Stephens et al. 2007/. For instance, the intensity of large, steeply-dipping structures with WNW-ESE to NW-SE strike is much higher in the bedrock outside relative to that inside the tectonic lens, which hosts the candidate and target areas, cf Figure 1-5 and Figure 1-6. The spatial variability in the intensity of large structures in different directions is illustrated in Figure C-1, which shows the traces of the dominating steeply dipping deformation zones within the local model domain, cf Figure 3-5. FFM01 coincides approximately with the part of the candidate area shown in Figure C-1. The spatial variability between the three feature orientation sets, NS, NE and NW, is readily seen in this figure.

The spatial variability in the intensity of large structures impacts on the geological DFN modelling work which uses the intensity of lineament and deformation zone traces as pivot point in the probability density plot shown in Figure 2-4 /Fox et al. 2008/. In effect, the fracture size models derived in the geological DFN modelling work /Fox et al. 2007/ are not readily compared with those derived in the hydrogeological DFN modelling work /Follin et al. 2007b/, a conclusion that affects the attempt to demonstrate the notion of subsets shown in Appendix C in /Follin et al. 2007c/.

/Fox et al. 2007/ did not subdivide the lineaments and deformation zone traces by fracture domain; the only subdivision made was by orientation set. /Fox et al. 2008/ describe the difficulties encountered if one tries to honour the spatial variability in the intensity of the lineaments and deformation zone traces by fracture domain. /Fox et al. 2008/ also state that the approach taken leads to lower k_r values (higher intensities of large features) of the different feature orientation sets than observed in Figure C-1. In conclusion, the k_r values derived in the geological DFN modelling work are not fracture domain specific as suggested in Table 5-3 and Table 5-4 in /Fox et al. 2007/.

By plotting the intensities of all feature orientation sets combined versus feature size rather than the feature set specific intensities, the impact of spatial variability in the intensity between the different feature orientation sets and fracture domains may be reduced. The different graphs in Figure C-2 through Figure C-4 show the values of $P_{32}[r_1, r_2]$ of all sets combined for one

hydrogeological DFN realisation of the three depth intervals in fracture domain FFM01: above 200 m depth, between 200 and 400 m depth and between 400 and 1,000 m depth. The red and blue graphs represent the intensity of all sets combined of *open fractures* and *connected open fractures*, respectively. By the same token, the green graphs represent the intensity of all sets combined of *all* fractures as provided by Table 5-3 in /Fox et al. 2008/).

Discussion and conclusions

Figure C-2 through Figure C-4 indicate a reasonable agreement with regard to the envisaged relationship shown in Figure 2-4. The threshold value of r below which $P_{32,cof} \neq P_{32,open}$ is highlighted in Figure C-5, which shows the ratio of the intensity of *connected open fractures* to *open fractures* as a function of feature size for different depth intervals in fracture domain FFM01.

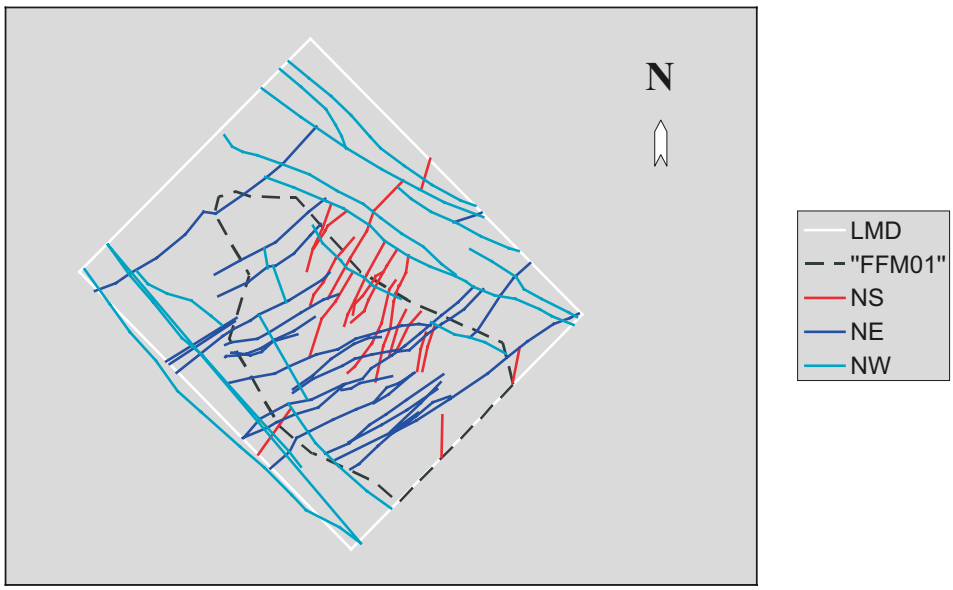

Figure C-1. *Illustration of the traces of the dominating steeply dipping feature orientation sets within the local model domain (LMD). Fracture domain FFM01 coincides approximately with the shown part of the candidate area (dashed line). (Modified after Figure 3-5.)*

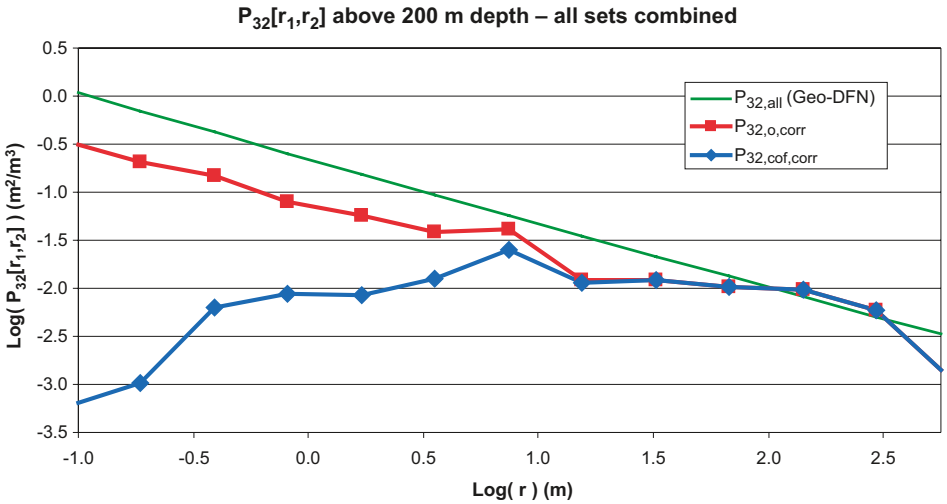

Figure C-2. *Feature intensity $P_{32}[r_1, r_2]$ as a function of feature size above 200 m depth in fracture domain FFM01. The green, red and blue graphs represent the intensity of all features (a), open features (o) and connected open features (cof), respectively.*

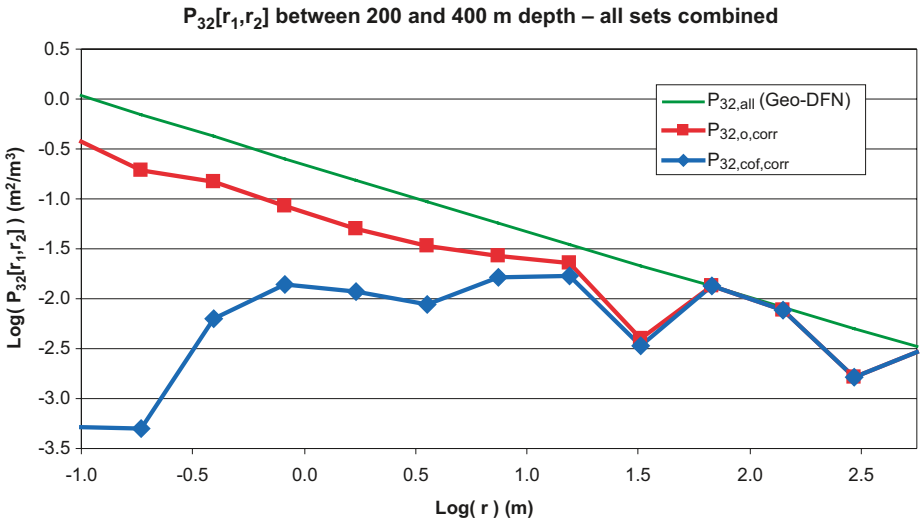

Figure C-3. *Feature intensity $P_{32}[r_1, r_2]$ as a function of feature size between 200 to 400 m depth in fracture domain FFM01. The green, red and blue graphs represent the intensity of all features (a), open features (o) and connected open features (cof), respectively.*

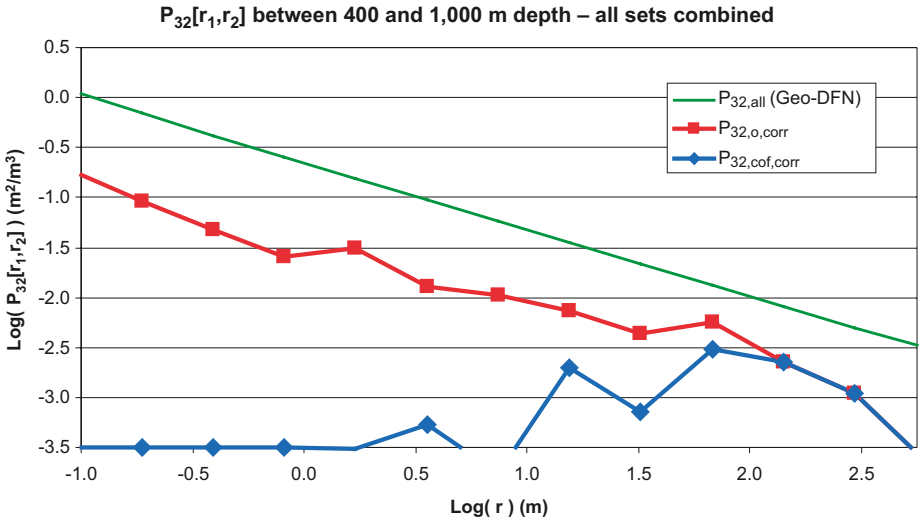

Figure C-4. *Feature intensity $P_{32}[r_1, r_2]$ as a function of feature size between 400 to 1,000 m depth in fracture domain FFM01. The green, red and blue graphs represent the intensity of all features (a), open features (o) and connected open features (cof), respectively.*

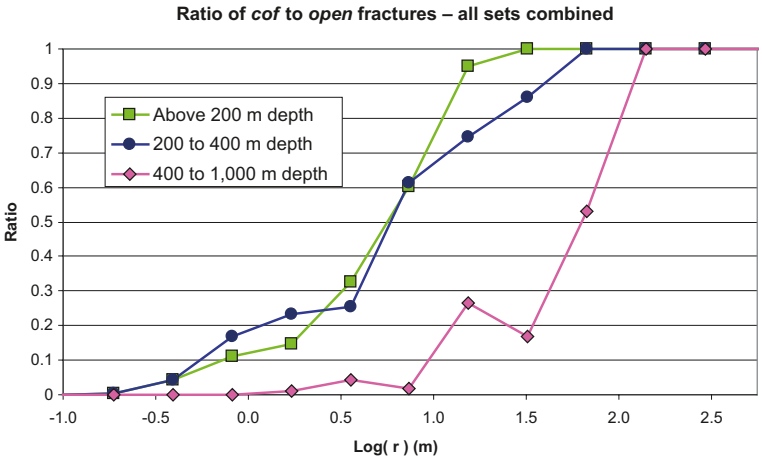

Figure C-5. *Ratio of the intensity of connected open features (cof) to open features (o) as a function of feature size for different depth intervals in fracture domain FFM01.*

Suggested hydrogeological DFN parameters for FFM01–FFM06

The hydrogeological DFN parameters deduced for FFM01 and FFM06 in /Follin et al. 2007b/ are tabulated in Table C-1. The 3D intensities, $P_{32,open}$, represent the Terzaghi corrected linear frequencies of *open fractures*, $P_{10,open,corr}$. Table C-2 and Table C-3 show the parameters deduced for FFM02–FFM05.

Table C-1. Hydrogeological DFN parameters for FFM01 and FFM06 with depth dependency: above –200 m, –200 m to –400 m and below –400 m RHB 70 (Appendix F in /Follin et al. 2007c/).

Fracture domain (m RHB 70)	Fracture set name	Orientation set pole: (trend, plunge), conc. κ	Size model, power-law (r_0, k_r) (m, -)	Intensity, ($P_{32,open}$), valid size interval: (r_0, 564 m) (m^2/m^3)	Transmissivity model constants (Table 2-2)
FFM01 > –200	NS	(292, 1) 17.8	(0.038, 2.50)	0.073	Semi-correlated: (a,b,σ) = (6.3 · 10^{-9}, 1.3, 1.0); Correlated: (a,b) = (6.7 · 10^{-9}, 1.4); Uncorrelated: (μ, σ) = (–6.7, 1.2)
	NE	(326, 2) 14.3	(0.038, 2.70)	0.319	
	NW	(60, 6) 12.9	(0.038, 3.10)	0.107	
	EW	(15, 2) 14.0	(0.038, 3.10)	0.088	
	HZ	(5, 86) 15.2	(0.038, 2.38)	0.543	
FFM01 –200 to –400	NS	As above	As above	0.142	Semi-correlated: (a,b,σ) = (1.3 · 10^{-9}, 0.5, 1.0); Correlated: (a,b) = (1.6 · 10^{-9}, 0.8); Uncorrelated: (μ, σ) = (–7.5, 0.8)
	NE	As above	As above	0.345	
	NW	As above	As above	0.133	
	EW	As above	As above	0.081	
	HZ	As above	As above	0.316	
FFM01 < –400	NS	As above	As above	0.094	Semi-correlated: (a,b,σ) = (5.3 · 10^{-11}, 0.5, 1.0); Correlated: (a,b) = (1.8 · 10^{-10}, 1.0); Uncorrelated: (μ, σ) = (–8.8, 1.0)
	NE	As above	As above	0.163	
	NW	As above	As above	0.098	
	EW	As above	As above	0.039	
	HZ	As above	As above	0.141	

Table C-2. Hydrogeological DFN parameters for FFM02 (Appendix F in /Follin et al. 2007c/).

Fracture domain (m RHB 70)	Fracture set name	Orientation set pole: (trend, plunge), conc. κ	Size model, power-law (r_0, k_r) (m, -)	Intensity, ($P_{32,open}$), valid size interval: (r_0, 564 m) (m^2/m^3)	Transmissivity model constants (Table 2-2)
FFM02 > –200	NS	(83, 10) 16.9	(0.038, 2.75)	0.342	Semi-correlated: (a,b,σ) = (9.0 · 10^{-9}, 0.7, 1.0);
	NE	(143, 9) 11.7	(0.038, 2.62)	0.752	
	NW	(51, 15) 12.1	(0.038, 3.20)	0.335	Correlated: (a,b) = (5.0 · 10^{-9}, 1.2);
	EW	(12, 0) 13.3	(0.038, 3.40)	0.156	
	HZ	(71, 87) 20.4	(0.038, 2.58)	1.582	Uncorrelated: (μ, σ) = (–7.1, 1.1)

Table C-3. Hydrogeological DFN parameters for FFM03, FFM04 and FFM05 with depth dependency above and below –400 m RHB 70. Transmissivity is increased by a factor 2 for FFM04 (Appendix F in /Follin et al. 2007c/).

Fracture domain (m RHB 70)	Fracture set name	Orientation set pole: (trend, plunge), conc. κ	Size model, power-law (r_0, k_r) (m, -)	Intensity, ($P_{32,open}$), valid size interval: (r_0, 564 m) (m^2/m^3)	Transmissivity model constants (Table 2-2)
FFM03 > –400	NS	(292, 1) 17.8	(0.038, 2.60)	0.091	Semi-correlated: (a,b,σ) = (1.3 · 10^{-8}, 0.4, 0.8);
	NE	(326, 2) 14.3	(0.038, 2.50)	0.253	
	NW	(60, 6) 12.9	(0.038, 2.55)	0.258	
	EW	(15, 2) 14.0	(0.038, 2.40)	0.097	Correlated: (a,b) = (1.4 · 10^{-8}, 0.6);
	HZ	(5, 86) 15.2	(0.038, 2.55)	0.397	
					Uncorrelated: (a,b) = (–7.2, 0.8)
FFM03 < –400 m	NS	As above	As above	0.102	Semi-correlated: (a,b,σ) = (1.8 · 10^{-8}, 0.3, 0.5);
	NE	As above	As above	0.247	
	NW	As above	As above	0.103	
	EW	As above	As above	0.068	Correlated: (a,b) = (7.1 · 10^{-9}, 0.6);
	HZ	As above	As above	0.250	
					Uncorrelated: (μ, σ) = (–7.2, 0.8)

References

Follin S, Levén J, Hartley L, Jackson P, Joyce S, Roberts D, Swift B, 2007b. Hydrogeological characterisation and modelling of deformation zones and fracture domains, Forsmark modelling stage 2.2. SKB R-07-48, Svensk Kärnbränslehantering AB.

Follin S, Johansson P-O, Hartley L, Jackson P, Roberts D, Marsic N, 2007c. Conceptual model development and numerical modelling using ConnectFlow, Forsmark modelling stage 2.2. SKB R-07-49, Svensk Kärnbränslehantering AB.

Fox A, La Pointe P, Hermanson J, Öhman J, 2007. Statistical geological discrete fracture network model, Forsmark modelling stage 2.2. SKB R-07-46, Svensk Kärnbränslehantering AB.

Fox A, La Pointe P, Hermanson J, Öhman J, 2008. Erratum to R-07-46, Dec. 2008, Svensk Kärnbränslehantering AB.

Hedin A, 2008. Semi-Analytic Stereological Analysis of Waste Package/Fracture Intersections in a Granitic Rock Nuclear Waste Repository. In: Mathematical Geosciences, DOI 10: 008-9175.

SKB, 2008b. SDM-Site Site description of Forsmark at completion of the site investigation phase, SDM-Site Forsmark. SKB R-08-05, Svensk Kärnbränslehantering AB.